REACTION AND COKING KINETICS OF n-HEPTANE CATALYTIC REFORMING

---The Development of A New Vibrational Microbalance and Its Application for *In Situ* Determination of Catalytic Reforming Reaction and Coking Kinetics

by

Ke Liu

A dissertation submitted to the Graduate Faculty in Engineering in partial fulfillment of the requirements for the degree of Doctor of Philosophy, The City University of New York

1995

This manuscript has been read and accepted for the Graduate Faculty in Engineering in satisfaction of the dissertation requirement for the degree of Doctor of Philosophy.

9/15/95
Date

Professor David S. Rumschitzki
Chair of Examining Committee

9/15/95
Date

Professor Gerard G. Lowen
Executive Officer

Dr. Shun C. Fung

Dr. Teh C. Ho

Professor Reuel Shinnar

Professor Herbert Weinstein

Professor Robert Graff

Supervisory Committee

The City University of New York

Abstract

REACTION AND COKING KINETICS OF n-HEPTANE CATALYTIC REFORMING

--The Development of A New Vibrational Microbalance and Its Application for *In Situ* Determination of Catalytic Reforming Reaction and Coking Kinetics

by

Ke Liu

Adviser: Professor David S. Rumschitzki; Co-advisers: Drs. Shun C. Fung and Teh C. Ho

In order to gain an understanding of the coking processes of a reforming catalyst and of how the reforming reactions interact with coking, this thesis reports experiments on the model system of n-heptane reforming over a Pt-Re/Al_2O_3 catalyst in a temperature range of 733 K < T < 799 K and pressure range of 207 kPa < P < 1034 kPa in a multi-outlet fixed bed reactor and a novel vibrational microbalance reactor.

We have found that the bulk of catalyst coke in n-heptane reforming derives from C5 naphthene intermediates (alkyl-cyclopentanes). This motivated the development of a simple, five-lump kinetic model for the reforming reactions that includes one lump for the potent coke-forming C5 naphthenes, to provide a precursor profile along the bed. Armed with knowledge of the precursor and how its concentration varies in space, we use methyl- and ethyl-cyclopentane as model C5 naphthenes, focused on determining the kinetics of coke formation: $\frac{dC_k}{dt} = e^{-\alpha C_k} P_{C5N}\left(\frac{\kappa_1}{P_{H_2}} + \frac{\kappa_2}{P_{H_2}^2}\right)$ where C_k is the catalyst coke content, α, κ_1 and κ_2 are the parameters. This work proposes a new multi-layer coking

model and a coking mechanism to explain the data measured. The multilayer model, together with the site-coverage concept, strongly suggests a catalyst deactivation mechanism.

This work then unifies the newly proposed reforming and coking mechanisms. First, the deactivation mechanism deriving from the coking study predicts the decay of the reforming model's rate constants. Second, the measured (or predicted) C5 naphthene profile predicts the coke profile. These results form a rather complete, consistent picture of reforming reaction and coking for n-heptane reforming system.

In addition we found that in the absence of hydrocarbon feed, flowing hydrogen can strip a portion of the coke even in our temperature/pressure range. The kinetics of this process suggests the identification of removable with new, low molecular weight coke, and we construct a mechanism based on this identification.

Finally, it has been possible to carry out these sensitive experiments only because we, together with R&P Company, developed a novel microbalance system. This system accurately measures the time evolution of both the coke amount and the composition of the gas phase in contact with the catalyst simultaneously, under realistic conditions. This microbalance works by sensing how a change in mass affects the balance's natural vibrational frequency. It alleviates the problem of severe feed gas by-passing that conventional gravimetric microbalances encounter by virtue of a new flow-through design.

ACKNOWLEDGMENT

I heartily thank my mentor, Professor David S. Rumschitzki, and my co-mentors, Drs. Shun C. Fung and Teh C. Ho of Exxon's Corporate Research Laboratories, for their excellent guidance, great help, deep involvement, encouragement and patience throughout the course of this research. Association with people of their scientific reasoning and organizing ability has provided perhaps the greatest learning experience for this author. Their vast experience, exemplary approach to research, never-ending enthusiasm, and personal integrity will long be remembered. I am deeply indebted to them not only for their intelligent and patient guidance, but also for their inspirational dedication to research, great human understanding and for the excellent art of developing even the hidden talents of graduate students. Finally, I benefited greatly from their excellent cooperation in providing this great opportunity to do this research.

I am very thankful to George Gamble and Greg Springstun of Exxon for their assistance on the experimental work.

Professors Reuel Shinnar, Herbert Weinstein and Robert Graff are greatly appreciated for serving on my supervisory committee.

Exxon Research and Engineering Company and the Presidential Young Investigator Award (to DSR) are especially acknowledged for the financial support of this project.

I also wish to express my appreciation to R&P Co. and Dave Hassel for working with us in the development of their technology for our application.

Finally, I owe special gratitude to my wife, Lan Ma, who cheerfully took over many of my duties at home, especially taking care of our lovely baby Angela Liu, and who also provided cheerfulness and understanding that made this effort worthwhile. Naturally, I owe special thanks to my father Xicheng Liu and my mother Sumei Zhang for their moral support.

CONTENTS

List of Tables

List of Figures

Chapter 1. INTRODUCTION

1.A. Catalytic Reforming

Catalytic reforming is a key petroleum refining process that produces high-octane blending stocks for motor fuel and high-value aromatic hydrocarbons such as benzene, toluene, and xylenes for the petrochemical industries from more saturated C_6-C_{10} hydrocarbon feeds. These feeds are usually olefin-free naphtha with a boiling range of 355-450 K that contain roughly 10-20 wt% aromatics, 20-50 wt% naphthenes, and 40-70 wt% paraffins. Hydrogen is also a valuable reforming product and, in most refineries, the 80-1,500 standard cubic feet hydrogen yield per barrel of oil feed is the source of all or part of the hydrogen used for the refinery's hydrotreating processes. Due to environmental regulations that prohibit lead antiknock compounds in gasoline, almost all automobile fuels used today other than ethanol are formulated around high-octane bases that result from catalytic reforming (Gates et al., 1979, and Sinfelt, 1981).

The development of catalytic reforming since its beginnings in 1940 has been a story of catalyst development. This reaction, initially using chromium and molybdenum oxides catalysts has relied on bifunctional platinum-based catalysts since the early 1950s. From 1953 to 1967, platinum impregnated on a slightly chlorinated cubic γ-alumina support was the most widely used bifunctional monometallic reforming catalyst. However, since Chevron Research announced its rhenium promoted Pt/Al_2O_3 catalyst in 1969 (Kluksdahl, 1969), a large number of bimetallic or multimetallic catalysts have been patented, and some have been put into commercial practice.

Many types of reactions occur in catalytic reforming. At typical reaction conditions, the dehydrogenation reactions are by far the fastest, being at least an order of magnitude

faster than all other reactions (Clem, 1977). The most important reactions are those that produce high octane products, such as the conversion of naphthenes and paraffins to aromatics and the isomerization and hydrocracking of paraffins. The reactions of naphthenes to aromatics are very fast and selective in comparison with the reactions of paraffins. Since paraffins make up a large fraction (20-70 wt%) of the feed and since they are also the lowest octane components, a large incentive exists to selectively convert them to aromatics.

Because the overall reforming process is highly endothermic, typically 600-1200 KJ per kilogram of feed treated, the catalytic reforming process generally consists of three to four fixed-bed reactors in series. Reheat furnaces between the reactors make up the large endothermic heat of the reaction. Since the rates of the various reactions involved are vastly different from each other, the catalyst is not distributed evenly among the reactors. On the average, the first reactor contains only 10-15% of the catalyst, enough to ensure the dehydrogenation of most of the naphthenes. In contrast, there is three to four times as much catalyst in the last reactor in order to bring about paraffins dehydrocyclization. To maintain a uniform hydrogen partial pressure, part of the hydrogen produced recycles back to the reactors. Average operation pressure is between 689 and 4134 kPa. Operation temperatures at the catalyst bed inlets are usually in the range of 728-810 K with bed ΔT as great as 93 K. The H_2/Hydrocarbon (mol) ranges from 3 to 6 and weight hourly space velocity (WHSV) ranges between 1 and 3.

Over 50 years of reforming experience has established certain facts about the thermodynamics and kinetics of these reactions. The main points are:

(1). An increase in reaction temperature thermodynamically shifts the equilibrium of the main reaction in the desired direction. Unfortunately it also accelerates the rate of the side reactions and the net result is a lower product yield.

(2). A lower pressure favors a higher yield of aromatics but causes more rapid coke formation on the catalyst. An increase in hydrogen pressure, which is thermodynamically unfavorable for aromatics formation, decreases the coking rate of the catalyst, and thereby increases its life.

As the reforming reaction proceeds, the activity of any reforming catalyst gradually declines, thus leading to a decrease in both octane number and hydrogen yield. To compensate for this decline, refiners must gradually increase the average operating temperature. Unfortunately, as we have just seen, this also brings about an increase in the rate of side reactions (cracking and hydrogenolysis) that have high activation energies; the result is a loss in both reformate and hydrogen yields. In practice, the plant must be shut down periodically for regeneration of the catalyst to restore its activity through controlled coke combustion and readjustment of the catalyst's chloride level (Frank and Martino, 1982). In a more recent version of the process, the catalyst circulates between the reactors and the regenerator, making it possible to operate under stricter conditions which are close to those at the start of the run (Sutton, et al., 1972; Cha, et al., 1973).

Deactivation of catalysts by coke deposition is ubiquitous in oil refining as well as in some petrochemical processes. Despite its scientific and industrial importance, catalyst deactivation due to coking in reforming has received relatively little attention (Frank and Martino, 1982). Several groups have studied the deactivation mechanism and coke deposition on reforming catalysts. Some have attempted to ascertain which of the two functions, metal or acid, controls the deactivation behavior of the reforming catalyst. However, despite these efforts, many contradictory claims exist in the literature (Froment et al., 1987; Shum, 1984; Butt and Sachtler, 1984). Due to the extremely long experiments and the highly accurate and stable instruments required for a reliable coking

kinetics study, adequate data for *in situ* coke formation under *realistic* reaction conditions are simply not available.

At our disposal for mechanistic studies are Fung's four outlet fixed bed reactor (described in Chapter 3) together with a temperature-programmed oxidation device for coke analysis. In addition, we have developed a novel vibrational microbalance which is particularly useful for carrying out experiments to refine our models for both reforming and coking and to distinguish them from existing ones. We also believe that it is an ideal tool for observing catalyst coking behavior as a function of reforming conditions. Chapter 3 describes the microbalance in detail.

1.B. General Goals and Approach

The present study is an in depth experimental investigation with concomitant modeling of the mechanism, kinetics, and coking of a model paraffin reforming system. The overall goal is to develop a better understanding of the chemistry and kinetics of catalytic reforming and of reforming catalyst coking. What distinguishes this work is our conviction that a detailed appreciation of the inexorable intertwining of the reforming chemistry with the kinetics of catalyst coking is essential for proper perspicuity pertaining to these processes. It is the centrality of this connection that motivates the work below aimed at identifying the predominant coke precursors from amongst the reforming reaction participants; to ascertain their rates of production and destruction in the course of the reforming; and to determine their kinetic roles in coking. The last chapter completes the circle by combining the coking model with that of the reforming chemistry to predict both the coking profiles from measured or predicted precursor concentration profiles and the evolution of the concentrations of reforming products over catalyst coking time scales.

Such ambitious goals oblige a careful choice of model system and ample assurance of the adequacy of the experimental apparatus.

Since the rhenium-promoted catalyst boasts much better activity and selectivity maintenance than the conventional platinum catalyst, particularly at low pressures, most commercial reformers now use the Pt-Re/Al_2O_3 catalyst. As such, it is the logical choice for all of our experiments. In addition, a better understanding of the bifunctional rhenium-promoted bimetallic catalyst may lead to the development of an even more active, selective, and stable catalyst.

We choose the reforming of n-heptane as a representative model system for commercial reforming. It falls within the C_6-C_{10} range of typical reformer feeds and its reactions are representative of those of C_8 and C_9 paraffins (Sinfelt, 1963). The heavier normal paraffins are expensive to obtain at high enough purity for analytical work, and the analysis of their reaction products is quite complex. Accordingly, the kinetic analysis of n-hexane reforming would seem to be the simplest choice. However, hexane's reactions are not representative of C_7-C_9; it reacts primarily to form isohexanes with a poor selectivity to aromatics compared with C_7-C_9 paraffins. Sinfelt (1963) has shown that the reactions of n-heptane are much more representative for reforming of typical C_6 to C_{10} naphtha paraffins than those of n-hexane.

The literature abounds with kinetics studies of n-heptane reforming. Unfortunately, most of these are limited to near atmospheric pressures and differential conversions. The regime of practical interest is one involving the higher conversions achieved in industrial reactors and over time scales typical of catalyst coking. Due to the extremely long experiments and the complicated modeling required for a high-conversion study of n-heptane reforming, extensive data over a wide range of conditions subject to catalyst

deactivation are not yet available. Fung and Querini (1993) have presented some data of this type over a narrower range of operating conditions, showing coke and reaction product profiles along a fixed bed reactor. One focus of this study will be to acquire such data over a much wider range of conditions and to use it as an impetus for mechanistic and kinetic modeling.

Microbalances of various forms have played an important role in studies of catalyst deactivation and of coking kinetics (Dumez and Froment, 1976; Mieville, 1986 and Biswas, et al.,1987) for over a decade. However, the conventional gravimetric microbalance must often operate at atmospheric pressures and encounters mass transfer problems because a large but unmeasurable portion of the feed gases bypasses the catalyst sample; thus the true space velocity and gas composition that the catalyst experiences remains unknown. As a result, it is not possible to obtain intrinsic reaction and coking kinetic parameters at the intended or known reaction conditions. Additionally, such balances are incapable of directly measuring a small weight change below 1% due to significant buoyancy and drag effects when the carrier gas switches to feed gas (Biswas et al., 1987). Thus, in order to obtain reliable coking kinetic data, we have had to develop a new type of reactor, a vibrational microbalance, capable of continuous, accurate monitoring of the coking rate at known space velocity and gas composition (Fung, et al., 1994). This data will allow determination of a coking pathway and reaction kinetic that are consistent with the ample, accurate data taken under realistic conditions.

In summary, the specific objectives of this thesis are:

1. to develop a new type of vibrational microbalance reactor system for the *in situ measurement* of the reaction kinetics and catalyst coking rate under realistic reaction conditions (Chapter 3);

2. to determine the major coke precursor for paraffin reforming with the newly developed microbalance reactor system and to gain a better understanding of the fundamentals of catalyst deactivation (Chapter 3);

3. to develop a reaction network and an associated kinetic model to describe the catalytic reforming of n-heptane over a commercial Pt-Re/Al_2O_3 catalyst (Chapter 4)

4. to develop a coking kinetic model to predict coke formation and to use it as a building block towards a mechanism for Pt-Re/Al_2O_3 reforming catalyst deactivation (Chapter 5);

5. to use the coking model to arrive at a model for catalyst deactivation and to use it to predict the time evolution of the reforming reaction product concentrations over catalyst coking time scales (Chapter 7);

6. to use a knowledge of the relatively easily measurable or predictable (Chapter 4) precursor concentration profile in a fixed bed reactor to predict the coke profile (Chapter 7).

In the course of our experiments, we found that switching from a hydrocarbon feed to pure hydrogen at otherwise reaction conditions partially decokes the catalyst. As a result, two added goals are:

7. to experimentally investigate the hydrogen decoking phenomena, including an experimental investigation of its kinetics and a TPO analysis of the coke before and after decoking, to determine what type of coke is affected (Chapter 6) and;

8. to develop a hydrogen decoking kinetics model which may lead to a better understanding of the role of H_2 in catalytic reforming (Chapter 6).

Chapter 2 surveys the paraffin reforming literature and the coking literature. Chapter 7, in addition to describing specific goals 5 and 6, provides an outlook for future work.

Chapter 2. LITERATURE SURVEY

2.A. n-Heptane Reforming: Reaction Mechanisms

The catalytic reforming of n-heptane takes place through a complex set of coupled reactions which involves over 70 chemical species, as identified by gas chromatography. In order to develop a kinetic model for n-heptane reforming in which one can realistically measure the rate parameters, one has to lump the species and reactions. For instance, one can lump the species involved as n-heptane, isoheptanes, aromatics, C5 naphthenes and cracking products; one can classify reactions as paraffin dehydrocyclization, isomerization and hydrocracking. To construct a proper lumped reaction network of n-heptane reforming, one needs information on reaction pathways and kinetics.

The individual reactions of n-heptane have been the subject of numerous mechanistic studies. Until 1977, most of these studies were carried out at atmospheric pressure over the Pt/Al_2O_3 catalyst or over metal oxides and supported metal oxides, such as Cr_2O_3 and Cr_2O_3/Al_2O_3. It is known that the reforming reaction mechanism can be strongly dependent on the catalyst and the experimental conditions (Haensel, 1961). Davis (1971) has shown that at low pressures, coking of the active sites occurs rapidly and is highly sensitive to hydrogen partial pressure. This in turn greatly affects catalyst selectivity. Nix and Weisz (1964) and Tanatarov et al. (1975) have shown that low pressures favor metal site poisoning. On the basis of these studies, the following review will emphasize kinetic studies performed near commercial conditions, that is, temperature: 728-810 K; pressure: 517-4134 kPa; H_2/hydrocarbon (mol) ratio: 3-6, and weight hourly space velocity: 1-3.

2.A-1. n-Heptane Dehydrocyclization

Fundamental information on n-heptane dehydrocyclization, the formation of a cyclic or aromatic compound from n-heptane with the associated release of hydrogen, is relatively scarce. It is thus no surprise that the mechanism of n-heptane dehydrocyclization has been and continues to be a source of controversy in the literature. In contrast, dehydrocyclization data of fundamental significance are available for n-hexane and n-octane. This review therefore includes all the pertinent data on paraffin dehydrocyclization.

Several workers (Lyster, et al., 1964; Hettinger, et al., 1955) have observed heptenes in the reaction products of n-heptane reforming. These are thought to be intermediates in cracking and isomerization reactions. However, the literature contains no conclusive evidence that a vapor phase olefin intermediate is required prior to the cyclization of n-heptane. Christoffel et al (1975) conclude that vapor phase olefins are not intermediates in the reforming of n-hexane to benzene over the Pt/Al_2O_3 (no chloride) catalyst. They compare the dehydrocyclization products of n-hexane with those of 1-hexene and of 2-methylpentane with those of 2-methylpentene. In both cases, they observed slower rates of ring closure with the olefins. Usov et al.(1974) conclude that the dehydrocyclization to aromatics and the dehydrogenation to olefins are parallel reactions based on their study of the dehydrocyclizations of n-heptane and of n-octane at low pressures.

The existence of both C_5 ring and C_6 ring intermediates has been postulated for n-heptane dehydrocyclization. Both have been observed in the vapor phase (Rohrer, et al., 1962; Lyster, et al., 1964; Hettinger, et al., 1955). Davis (1973) studied ring closure using n-heptane labeled with ^{14}C in the 1 and 4 positions over a non-acidic Pt/Al_2O_3 catalyst. He concluded that the mechanism involved direct six-carbon ring closure based on the amount of ^{14}C in the methyl position. However, his use of non-acidic alumina would

prevent the dehydroisomerization to toluene of any C_5 rings formed. For n-octane dehydrocyclization, the distribution of the four C_8 aromatics can give valuable information about the mechanism of the ring closure reaction. Most of the work on octane aromatization indicates that the key pathway is C_6-ring closure. Clem (1977) and Ramage et al. (1987) proposed that both C_5- and C_6-ring closure exist in n-heptane dehydrocyclization. Levitskii (1973) in an octane reforming study observed mainly xylene and ethylbenzene which are the only products expected from C_6-ring closure at 506-2026 kPa pressures. Vlasov et al. (1970) observed some m-xylene and p-xylene in n-octane aromatization at atmospheric pressure. However, they demonstrated by using xylene and alkylcyclopentane as feeds that the observed m- and p-xylene came from the isomerization of n-octane prior to dehydrocyclization.

Most authors assume that the dehydrocyclization of isoheptanes proceeds via the same mechanism as n-heptane ring closure. However, the isoheptanes have fewer combinations of six carbon atoms in a row and the rate of ring formation is relatively slow. Lyster (1964) observed that the dehydrocyclization rates of 3-methyl hexane and 2,4 dimethylpentane were 90% and 22%, respectively, of that of heptane. Sinfelt and Rohrer (1963) found that the ring formation rate of 3-methyl hexane was 70% of that of n-heptane and the rate of 2,2,4-trimethylpentane was 25-30% of that of n-octane. By comparing toluene yields from the methylhexanes over acidic versus low-acidity catalysts, Usov et al. (1974) found that 50-75% of the toluene formed by six-carbon ring closure. The fraction formed by five-carbon ring closure increased with increasing temperature and conversion and was greater for 2-methyl hexane than for 3-methyl hexane.

Marin and Froment (1982) did not detect cyclohexane in their reforming experiment of n-hexane on a Pt/Al_2O_3 catalyst. Moreover, the methylcyclopentane-to-benzene ratio decreased with increasing n-hexane conversion, from 16000 to the equilibrium ratio of

0.55. On the basis of this observation, they pointed out there was no six-carbon ring closure, and methylcyclopentane is the intermediate of the n-hexane dehydrocyclization. Sun et al. (1992) also proposed that there is no direct six-carbon ring closure in either n-hexane or n-heptane dehydrocyclization.

Many researchers have found that C_6-ring intermediates, once formed, react rapidly and selectively on metal sites to form toluene (Pacheco and Petersen, 1983; Trimpont and Froment, 1986; Hettinger, et al., 1955; Sinfelt, et al., 1960). The C_5-ring does not react as rapidly or as selectively as the C_6-ring. Hettinger et al. (1955) found that ring isomerization limited the aromatization of dimethylcyclopentane and that this rate was approximately equal to the rate of iso/normal paraffin isomerization. By contrast, methylcyclohexane dehydrogenation was seven times as fast as dimethyl-cyclopentane dehydrocyclization.

2.A-2. Paraffin Isomerization and Cracking

Paraffin isomerization is a dual-site reaction associated mainly with the acid sites of the reforming catalyst. Sterba et al. (1976) and Svajgl (1972) showed that reducing the chloride content of the catalyst base decreases its activity for isomerization, and that as long as the Pt content is in excess of 0.1 wt%, the isomerization activity is independent of the metal component (Sinfelt et al., 1963). In their studies of heptane isomerization, Haensel and Donaldson (1951) and Sinfelt et al. (1962) found that 70-95% of the C_7 isomers were 2- and 3-methylhexanes, the balance being dimethylpentanes. This agrees reasonably well with equilibrium predictions.

The rate of isomerization is about twice that of dehydrocyclization. Krane et al. (1959) and Henningsen and co-workers (1970) also observed factors of three and five, respectively, for the ratio of isomerization to dehydrocyclization rate.

The generally accepted mechanism for n-heptane isomerization involves dehydrogenation to form an olefin on a metal site, followed by isomerization via a carbenium ion mechanism on an acid site, and finally hydrogenation of the olefin isomer on a metal site.

It is also generally accepted that n-heptane cracking occurs by a carbenium ion mechanism on acid sites (Sinfelt, 1973; Sterba and Haensel, 1976); it involves initial dehydrogenation on a metal site followed by carbenium ion cracking of the olefin on an acid site and a final step of hydrogenation of the resulting cracked products on a metal site. The predominant products of carbenium ion cracking are C_3 and C_4 olefins resulting from carbon-carbon scission near the center of the heptane molecule. The cracking of iso-heptane also seems to occur by a carbenium ion mechanism. Sinfelt and Rohrer (1963) found that the rate of cracking of 3-methyl hexane is 20% to 30% greater than that of n-heptanes. Froment et al. (1988) claimed that one can neglect the cracking of n-heptane in comparison with the cracking of isoparaffins and that there is no observable distinction between the hydrocracking rates of the single-branched and the multi-branched isoheptanes.

Hettinger et al. (1955) have shown that the ratio of hydrocracking to dehydrocyclization for isoheptane is 1.5, as compared with 0.8 for n-heptane. This is because tertiary carbenium ions are more stable than secondary carbenium ions; thus isoparaffins should have higher cracking rates than normal paraffins.

2.A-3. n-Heptane Reforming Reaction Scheme

Kugelmans (1977), Blue and Nix (1976), McHenry (1960), and Mahoney (1974), all have proposed a reaction network for n-heptane reforming over the Pt/Al_2O_3 catalyst. Excluding low- concentration intermediates, one can represent this network by

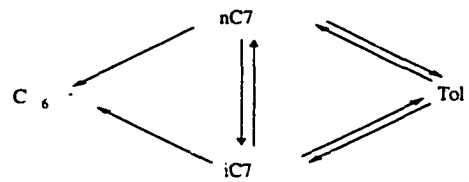

nC7: n-heptane; iC7: iso-heptane; Tol: toluene; C_6-: cracking products

Surprisingly, though, there have been relatively few attempts determine the kinetics of n-heptane reforming over the $Pt\text{-}Re/Al_2O_3$ catalysts. The works of Clem (1977) and Trimpont and Froment(1986,1988) have given the most detailed information on these kinetics over both Pt/Al_2O_3 and $Pt\text{-}Re/Al_2O_3$ catalysts.

Clem (1977) proposed the following reaction scheme as a basis for a kinetic model of the n-heptane reforming for both $Pt\text{-}Re/Al_2O_3$ and Pt/Al_2O_3 catalysts.

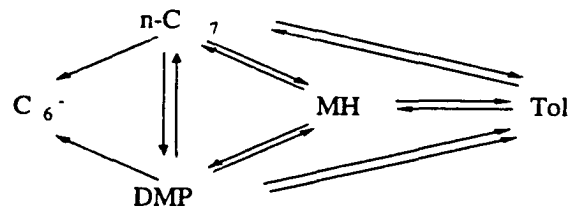

Reaction network for catalytic reforming of
C 7 hydrocarbons proposed by Kenneth R. Clem
MH: methylhexanes,
DMP: dimethylpentanes +3-ethylpentane

Basically, Clem considers all possible reversible reactions in n-heptane reforming. As a result, the model contains far more parameters than the data can accurately and uniquely determine.

Froment and co-workers (1987, 1988) report that direct six-carbon ring closure is absent in n-heptane reforming over both Pt/Al_2O_3 and $Pt\text{-}Re/Al_2O_3$ catalysts at 723 K, 1050 kPa and a molar hydrogen-to-hydrocarbon inlet ratio of 20. Sun et al. (1992) reached a similar conclusion for the $Pt\text{-}Sn/Al_2O_3$ catalyst for the temperature range of 733--773 K and the pressure range of 800-1200 kPa. Froment's group (1987,1988) proposed the following n-heptane reforming scheme:

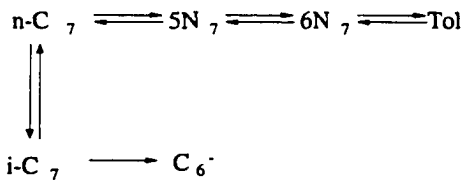

Reaction network for catalytic reforming of C_7 hydrocarbons proposed by Froment et al.

As one can see, this mechanism neglects the dehydrocyclization of isoheptanes and the cracking of n-heptane.

Mobil researchers have developed a reforming kinetic model (Ramage et al., 1980, 1987) for industrial feedstocks. The key to successfully developing this model was to properly define a small set of species lumps and a minimum number of reactions between them. A thorough understanding of the chemistry, thermodynamics, and catalyst deactivation was necessary to reduce the problem to such a manageable level without much loss in accuracy. The lumped reaction network for C_7 hydrocarbons proposed by Ramage et al. takes the form:

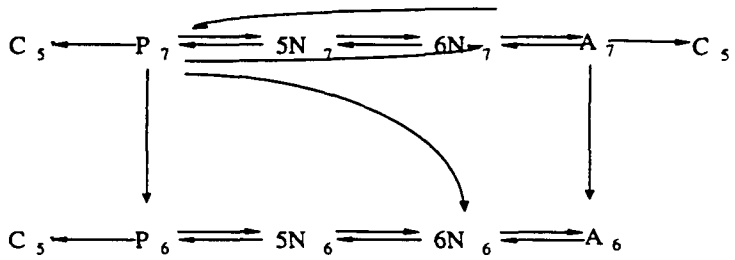

C 7 Hydrocarbons Reforming Lump Reaction network, 5N and 6N, Cyclopentane and Cyclohexane Naphthenes, P, Paraffins, A, Aromatics, C5-, Pentane and Lighters.

Since normal paraffins and iso-paraffins give significantly different octane numbers, it is important to segregate these into two distinct species lumps. Sun et al. (1992) subsequently modified the Mobil model by doing precisely this.

From the above literature review, one sees that the n-heptane reforming reaction network has been and continues to be a source of controversy in the literature. The prior work cited is mostly limited to differential conversion studies of the reaction mechanism. A few groups (Froment et al., 1987, 1988 and Clem, 1977) have conducted experiments at higher conversions. From their proposed reaction scheme, they formulated a set of differential equations for the time rates of change of the concentration of the various lumps. They then solved them by numerical integration and compared the solutions with data to simultaneously determine both the surface reaction rate constants and the adsorption equilibrium constants. However, the reaction rate constants so determined depend on the proposed reaction scheme and multiple rate constants determined from the experiments using only n-heptane as feed are highly suspicious. For almost any choice within a fairly wide range of reaction schemes, the computer will give a set of rate constants that minimizes the RMS difference between the experimental data and model's predictions. So only comparing limited experimental data that are not targeted to isolate

individual reactions with a model's predicted values is not enough to discriminate between models; this point will be discussed in detail in chapter 4.

2.B. Mechanisms and Models for Coke Buildup

2.B-1. General Features

The three most important practical properties of a heterogeneous catalyst are its activity, selectivity and stability (or lifetime). Although it is the aspect that most often defines the viability of a process, the lifetime of a catalyst has been the subject of very few detailed studies. In the oil refining and petrochemical industries, catalyst deactivation due to carbonaceous deposits is a common occurrence. These strongly adsorbed carbonaceous deposits form from large polynuclear aromatic structures, apparently through polymerization and condensation. Structurally, they are pseudographitic or aromatic in nature, with hydrogen-to-carbon ratios that depend on the specific conditions of their formation. To make up for the decrease in activity resulting from coking, the operators gradually increase the reactor temperature. Thus brings about not only a large increase in the rate of side reactions, but also an increase in the operating costs. Obviously, reducing the rate of coke formation is of paramount importance. One can assess the difficulties in bringing about such an improvement by considering that under the normal reforming operating conditions, only one atom of carbon out of 200,000 activated by the catalyst is transformed into a non-desorbable deposit of coke (Frank and Martino, 1982).

The literature contains several coke buildup mechanisms (Zhrove, 1980; Myers, 1961; Bortkevich, 1975). They all involve an initial step of dehydrogenation and the formation of unsaturated species on metal sites. These unsaturated species then are able to migrate, either via the gaseous phase or through the adsorbed phase, to the acid sites of

the catalyst where they form dimeric or polymeric species. Coking of bifunctional catalysts is the accumulation of coke on both the metal and on the support. Temperature-programmed oxidization (TPO), for example, can often distinguish between the coke deposited on the metallic surface versus that on the support.

All the current mechanisms derive from propositions that Myers et al. posited as early as 1961. These propositions, for the most part, merely follow from the consideration of the influence of hydrogen pressure, acidity and the nature of the hydrocarbons being treated. No specific study of the reactions involved in coking seems to have been undertaken. Such a study is difficult to carry out; after all, coke represents only a few parts per million of the reaction products under realistic conditions (Frank and Martino, 1982) and thus such a study would require experiments of at least hundreds of hours in duration. A few studies emphasize the role of the Diels-Adler reaction, either in the adsorbed phase (Zhorov and Panchenkov, 1980) or in the gaseous phase (Bortkevich, 1975), and the role of polymerization reactions at higher temperatures (Cooper and Trimm, 1980).

Analyses of the reaction effluents (Frank and Martino, 1982) have shown the presence of dehydrogenated species. Some of these species happen to be reaction intermediates of the desired products, but others are too dehydrogenated to be able to evolve toward these products. Instead, one assumes that they polymerize to coke. The concentrations of these highly dehydrogenated intermediates are linked directly to the reactor's temperature and hydrogen pressure. Finally, it is normal to find desorption products in the gaseous phase which can later dimerize (Frank and Martino, 1982).

One can represent coke accumulated on a reforming catalyst by $n(CH_x)$, where the hydrogen-to-carbon ratio x ranges 0.5 to 1; the coke that accumulates on the metal sites is typically less dehydrogenated than that on the acid sites. A number of studies have used IR

spectroscopy to examine the chemical nature of the coke (Best and Wojciechowski, 1977; Eisenbach and Gallei, 1979). Irrespective of the catalyst used or the nature of the coking agent, the results in all instances show the regular presence of aromatic C-H bonds, methyl groups and aromatics rings. The extraction of coke with various organic solvents after dissolution of the inorganic matrix, permits the chemical analysis of coke and confirms its polyaromatic nature (Eisenbach and Gallei, 1979; Magnoux, et al., 1984). X-ray diffraction studies have shown that coke deposits comprise a pseudo-graphitic phase with large crystals (250 A^{o}) and an amorphous phase located on small clusters of 10 to 15 A^{o} (Espinat, 1982).

In conclusion, coke deposition is a complex reaction that results partly from the production of coke precursors and partly from their destruction. Unsaturated reaction intermediates such as monocyclic diolefins (e.g. cyclopentadienes) form first, mainly at the platinum sites. It then appears that these initial foulant precursors can desorb from the platinum and migrate to the acid sites where they adsorb reversibly. Just how this migration occurs is not clear, but gas-phase transfer is one possibility (Myers, 1961). These precursors can then polymerize to form polycyclic compounds that have several double bonds per molecule. The usual supposition is that this latter process is the rate-limiting step, since it should be slower than both the platinum-catalyzed reactions and the diffusion processes that transfer the precursors to the acid sites. Thus, through polymerization, dehydrogenated species produced by the metal function lead to the accumulation of coke either on the metal or on the support. Such coke precursor producing reactions take place preferentially on metal sites or on the most acidic sites of the support, such as those responsible for hydrogenolysis and cracking.

2.B-2. Deactivation and Coke Buildup

Although there have been numerous studies of the deactivation of bifunctional metallic-acid catalysts by coke deposition, the interpretations of the results sometimes diverge. Butt (1972,1988) and Franck and Martino (1985) have written thorough reviews of this field.

Modeling industrial catalytic processes requires a knowledge of the kinetics both of the main reaction and of the catalyst deactivation since they most likely couple with each other, albeit at different time scales. Coke deposition is one of the most important causes of catalyst deactivation during the normal operation of naphtha reforming (Frank and Martino,1985). Various studies have dealt in a general way with the kinetics of deactivation by coke deposits (Butt, 1972; Beeckman and Froment, 1979; Wolf and Petersen, 1977). Others have focused on the initial deactivation of model reactions, such as the dehydrogenation of methylcyclohexane (Jossens and Petersen, 1983,1984), n-pentane isomerization (Froment, et al., 1975), C_7 hydrocarbon reforming (Trimpont and Froment, 1988), or the reforming of various C_6 hydrocarbons (Cooper and Trimm, 1980). It has thus been possible to detect changes in the coking mechanism with temperature (Cooper and Trimm, 1980), to account for the coke concentration profiles along the catalyst bed (Fung and Queeni, 1993; Bortkevich, et al., 1975), to examine coking phenomena specific to the low coke regime (Jossens and Petersen, 1982), and even to connect the coke concentration and the coking rate to the concentration of what may be the most potent coke precursors, especially cyclopentanic naphthenes and indenes (Zhorov and Panchenkov, 1980). However, except for a few studies (Myers, et al., 1961; Bortkevich, et al., 1975), the reforming literature has provided little insight into the mechanism and kinetics of the coking process itself. We shall attempt to begin to fill this niche.

In a seminal paper, Voorhies (1945) first described the coke amount as a function of time-on- stream during catalytic cracking in both fixed and fluidized beds. Specifically, he proposed that

$$C_k = Bt^n \qquad (2\text{-}1)$$

where C_k is the weight percent carbon on the catalyst, t the time on stream, A a constant depending on feedstock, reaction conditions and reactor type, and n an exponent with a value close to 0.5. Perhaps the most remarkable observation that Voorhies made was that the amount of coke formed on the catalyst after a given time interval appeared to be independent of the hydrocarbon feed rate. His interpretation was that, although the reaction mixture was changing as it passed through the reactor, the products formed were gasoline and gases which tended to carbonize more than the feed. For the feeds used in his study, there appeared to be a fortuitous balance between the two classes of products to give a coke formation tendency that was the same as that of the feed. This happenstance makes it relatively easy to predict the amount of coke formation but exceedingly difficult to interpret the coking process in a fundamental manner. Despite this obvious shortcoming, this so-called Voorhies' correlation has found wide use in coking kinetics studies, and most of the literature still presents coking kinetic data in the form of equation (2-1).

Voorhies recognized that Eq. (2-1) derives from a differential equation of the form

$$\frac{dC_k}{dt} = \frac{A}{C_k^{-(n-1)/n}} \quad \textit{which for } n = \tfrac{1}{2} \textit{ gives} \quad \frac{dC_k}{dt} = \frac{A}{C_k} \qquad (2\text{-}2)$$

One can arrive at Eq. (2-2) by heuristically arguing that the coke present acts as a diffusion barrier to further coke formation. Mieville (1991) investigated the coking kinetics of reforming in a thermo-gravimetric microbalance reactor and obtained the following coking rate expression:

$$r_{c_k} = A \cdot \frac{P_{feed}^{0.75}}{P_{H_2} C_k} \exp(^{-37,000}/_{RT}) \qquad (2\text{-}3)$$

The inverse relationship of the coking rate to the coke formed is the same as the Voorhies equation. Either of the following three mechanisms can rationalize Eq.(2-3):

1.) Diffusion control through a coke barrier;
2.) A second-order reaction with the formation of the surface species being the controlling step for coke formation; or
3). A polymerization propagation rate constant that depends on the amount of coke present.

The inverse relationship in Eq (2-3) corresponds to $n = 0.5$. But it is not always the case that $n = 0.5$, as Eberly et al. (1966) and Rudershausen and Watson (1954) have shown. Also, the high activation energy of coking observed by Mieville would suggest that any explanation based solely on diffusion is incorrect. Despite this, one cannot entirely dismiss diffusion because the high activation may be the result of physical changes on the catalyst surface. Another problem with the inverse relationship is that at the very beginning of the run, $C_k = 0$. This leads to an infinite coking rate, which is obviously unphysical.

Trimpont and Froment (1988) propose that coke deposition in C_7 reforming mainly originates from an intercondensation between diolefinic naphthenes and toluene. The most important intercondensations would be between toluene (Tol) and C_7 cyclopentadienes ($N_7^{2=}$) and between toluene and methylcyclohexadienes ($MCH^{2=}$). Since the coke content is not zero at the inlet of the bed, they reason that coke deposition must also originate from the feed, n-heptane, or from species, such as n-heptenes or n-heptadienes that are in equilibrium with n-heptane. Thus the third contribution to coke formation in Trimpont and Froment's proposed coking kinetic model originates from n-heptenes ($nP_7^{=}$) and accounts for the parallel coke deposition observed with n-heptane as the feed stock, i.e., for the coke content measured at the reactor inlet. On the basis of the above assumptions and analyses, they propose the following coking reaction schemes (for cokes C_{pj}, j=1,2,3) and coking kinetics model for n-heptane reforming on a sulfided Pt/Al_2O_3 catalyst:

Coking pathways:

$$Tol + 5N_7^{2=} \rightarrow C_{P_1}$$

$$Tol + MCH^{2=} \rightarrow C_{P_2}$$

$$n\text{-}P_7^{=} \rightarrow C_{P_3}$$

Coking Kinetics:

$$R_{Co} = k_{C1}\frac{P_{Tol}P_{5N7}}{P_{H_2}^2} + k_{C2}\frac{P_{Tol}P_{MCH}}{P_{H_2}^2} + k_{C3}\frac{P_{nC7}}{P_{H_2}} \qquad (2\text{-}4)$$

The data presented by Zhorov and Panchenkov (1980) in Table (2-1) show the relative coke-forming tendencies of different hydrocarbons. It is evident that the main contributors to coke formation on this chart are alkycyclopentadienes, alkylaromatics (C_8 and higher) and polycyclic hydrocarbons.

On the basis of prior studies (Bakulin, 1975; Allan, 1966; Myers and Lang, 1961), Zhorov and Panchenkov (1980) assumed that the most probable intermediate products in coke formation are alkylcyclopentadienes, indenes, and aromatic hydrocarbons with

unsaturated side chains. As in a few previous studies (Fung and Querini, 1993; Myers, et al., 1961; Barbier, et al., 1990), we shall show that appreciable quantities of alkylcyclopentanes and indan form as a result of the C5-dehydrocyclization of paraffinic and heavy aromatic hydrocarbons in catalytic reforming. In the main reaction, paraffins form five-membered naphthenes (C5N) and aromatics (A). Zhorov and Panchenkov assumed that coke forms solely from five-membered naphthenes and alkylaromatics. They lump all the possible intermediate products of the coke formation process into the following groups: alkylcyclopentenes and alkycyclopentadienes (AP), indenes and aromatics with unsaturated side chains (IU), and polycyclic hydrocarbons (PH). The resulting lumped kinetic scheme for coke formation takes the form

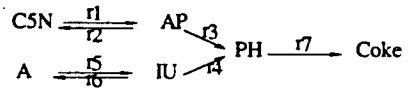

The coking kinetic model based on this scheme is:

$$r_7 = \left[\frac{k_{1_0}}{P_{H_2}^{a_0}}\exp\left(\frac{-E_{1_0}}{RT}\right)\right]C_{C_5N} + \left[\frac{k_{2_0}}{P_{H_2}^{a_0}}\exp\left(\frac{-E_{2_0}}{RT}\right)\right]C_A \qquad (2\text{-}5)$$

Zhorov and Panchenkov's (1980) analysis of the rate constants k_{10} and k_{20} reveals that at low temperatures the five-membered naphthenes are the main coke contributor, while at higher temperatures, because of the high activation energy E_{20}, aromatic hydrocarbons predominate. It should be pointed out that Zhorov and Panchenkov obtained this kinetic model by regressing of rather limited set of experimental data taken over a Pt/Al_2O_3 catalyst. To extend this model to bimetallic catalysts might require substantial revision.

Unfortunately, no systematic studies of coking kinetics with rhenium-promoted bimetallic catalysts exists, and hence this will be the focus of our study.

Table 2-1 Coke Yields in Reforming Various Hydrocarbons
(773 K, 101 kPa, WHSV = 2, H2/HC = 4, run length = 5 h)

Feed Hydrocarbon	Coke Yield (wt%)	Feed Hydrocarbon	Coke Yield (wt%)
n-Hexane	3.5	Benzene	0.3
n-Nonane	4.1	Ethylbenzene	2.3
Cyclohexane	0.1	Indan	25
1,2-Dimethylcyclohexane	2.1	Methylcyclopentane	13
Methylcyclopentene	37	Cyclopentadiene	67

In Chapter 4, we will suggest and experimentally substantiate a scheme for the inter-conversions of n-paraffins, isoparaffins, five-membered naphthenes and aromatics. As evident from Table 2-1, theoretically, all of these hydrocarbon groups contribute to some degree to catalyst deactivation.

The above literature review demonstrates the heavy reliance of early work on various empirical time-on-stream correlations. While these in general have been useful and are still used in many instances, they ignore the chemistry of coke formation. Subsequent work has begun to pay attention to coke formation chemistry by trying to identify significant foulant precursors (Froment et al., 1988; Appleby et al., 1962; Zhorov and Panchenkov, 1980). Such identification provides a basis for proposing possible coke formation mechanisms in terms of carbenium ion chemistry (Appleby et al., 1962). It is

also crucial for the development of realistic kinetic networks, such as the multiplet fouling model of Pacheco and Petersen (1983) and the coking kinetic model of Zhorov and Panchenkov (1980). Despite these efforts, the chemistries of coke formation and foulant deposition are not completely understood. Perhaps the prime reason for this is that it is very difficult to carry out coking kinetics measurement *in situ*. To this end, we have developed a novel vibrational microbalance reactor system that makes it possible to do *in situ* coking kinetic measurements under realistic condition. By feeding different hydrocarbons to the microbalance, one can systematically determine the major coke precursors in paraffin reforming. This will provide us with much needed information about the fundamentals of coke formation chemistry and kinetics (see Chapter 3 and 5).

Chapter 3. CATALYST DEACTIVATION AND MAJOR COKE PRECURSOR IN n-HEPTANE REFORMING

—The Development of a New Vibrational Microbalance and Its Application

The goal of this thesis is to gain a more fundamental understanding of the processes of coke formation in n-heptane reforming over a supported Pt-Re/Al_2O_3 catalyst and of their kinetics. Naturally, one hopes that insights gained through the study of this model system will be somewhat more general, carrying over to the problem of catalyst coking, in general, and of reforming catalyst coking, in particular. The understanding of the deactivation of a reforming catalyst is important not only for the future development of more stable catalysts, but also for the operation and control of a commercial reformer and its catalyst regeneration process.

The first step in a fundamental look at catalyst coking is the determination of the precursor species that go on to form coke. Aside from its theoretical value for the understanding of the coking process, knowledge of the major coke precursor would have an important practical impact. Since it is very difficulty to monitor the coke formation *in situ* in a commercial reformer, but it is quite easy to monitor the gas phase composition along the catalyst bed by GC, it would be extremely useful to answer the question: Can one calculate the coke amount at any time and position of the catalyst bed simply by monitoring the gas phase coke precursor concentration on-line? The answer requires the identification of the precursor followed by quantitative coking kinetics research that the qualitative experiments below motivate. That is, once the major precursor is known, one can run experiments with those precursor(s) to focus on the reactions turning the precursor to coke and their kinetics. This chapter focuses on the experimental determination and proof of the

major coke precursors in our model n-heptane reforming system. The remaining part of this program constitutes the subject of the later chapters of this thesis.

To carry out the work in this chapter and, in fact, in this entire thesis, we have at our disposal an integral fixed bed reactor with four gas outlets along the bed, a new vibrational differential microbalance reactor for simultaneous *in situ* coke measurement and gas phase composition determination and a temperature programmed oxidation (TPO) device for the detailed analysis and classification of the coke on downloaded catalyst particles. Below we begin by describing the experimental apparatus and operating parameters (section 3A). Section 3B discusses some general trends — such as the effects of T, P and WHSV on catalyst coking and on the concentrations of various reforming intermediates. It concludes by noting an interesting correlation between the coke formation and the amount of C5 naphthenes (C5N) present under those conditions. Section 3C then embarks on an analysis which tracks the profiles of the coke amount, of the time-averaged C5N concentration and of the catalyst activity, all as functions of position along the pseudo steady fixed bed reactor. Note that this tracking is both substantive (coke amount) and functional (quantitative measure of catalyst activity). Finally, in section 3D, we present microbalance data which, together with the previous data, constitute a package of very strong and varied evidence that C5N's are the major coke precursors in our system.

3A. Experimental Methods

3.A-1. The Multi-outlet Fixed Bed Reactor System

The experimental equipment used for this research is located in the Corporate Research Laboratories of Exxon Research and Engineering Co. in Clinton, New Jersey, and its detailed description appears elsewhere (Fung, et al., 1991; Querini and Fung, 1993).

The equipment consists of a liquid and gas feed system, a multioutlet fixed bed reactor, process control instruments, and analytical instruments. A schematic diagram of the multi-outlet reactor system appears in Figure 3-1. The reactor is fabricated from a 1.27 cm OD stainless steel tubing with an ID of 1.02 cm. It has four outlets along its wall, which permit sampling of the gas at four bed heights, corresponding to four different space times for a given flow rate and catalyst packing. In this way one can amass conversion versus space time data for the kinetic analysis, by either changing the catalyst loading in different sections or by varying the feed rate or both. A computer-controlled stream selection valve automatically connects one of the outlet to the gas chromatography (GC) sample coil. A needle valve upstream of the stream selection valve drops the pressure of outlet stream to atmospheric pressure and controls its flow rate to the GC sample coil. Heat tracing of the sample stream flow path to 483-543 K ensures that the total product is in the vapor phase. Since the sample stream extracts less than 5% of the total volumetric flow traversing the catalyst bed, there is little change in the space velocity due to the diversion of the sample stream.

A three-zone furnace with independent PC-programmed temperature controls provides the heat input to the reactor. This configuration helps to achieve an isothermal wall profile along the length of the reactor where the catalyst is situated despite the highly endothermic character of the aromatization reaction and the different catalyst loadings in each section. Further, dilution of the catalyst and separation of catalyst sections with inert quartz particles of the same size as the catalyst particles were also used to minimize axial temperature gradients (see Figure 4-11). As a result, the furnace achieves a uniform temperature (less than 2 K variation, as indicated by a multi-point thermocouple) along the reactor's center line over the entire length (about 33 cm) of the catalyst bed during catalyst reduction.

For unattended overnight operation, the reactor system has an automatic alarm system that shuts off the furnace and stops the feed pumps and the hydrogen supply in the event of an abnormal situation, such as loss of temperature or pressure control.

3.A-1.a. Materials

The gases used in this research are house (cylinder) hydrogen of electrolytic grade (99.95%), house helium and nitrogen. The n-heptane liquid feed is analytic pure grade (99 moles%). The bimetallic Pt-Rc/Al_2O_3 catalyst contains 0.3 wt% Pt, 0.3% Re and 0.9 wt% Cl, which has a nitrogen BET specific surface area of 200 m^2/g.

3.A-1.b. Experimental Procedure

We used this multi-outlet integral reactor for all of our kinetic studies at different conversion levels. A typical run's loading consists of a total of five grams of catalyst, diluted to ensure isothermality with quartz particles of a uniform size, in the four catalyst sections above outlet 4. Table 1 shows the different loadings of thc catalyst in the reactor's four sections and the corresponding space velocities. A half inch section of quartz particles separates the sections from each other to avoid ambiguity in the amount of catalyst attributed to each section. We vary the conversion either by changing the feed rate for a given catalyst loading distribution or by changing the catalyst loading of different sections for a given overall feed rate. The reforming conditions for n-heptane on the Pt-Re/$A1_2O_3$ catalyst are similar to those in commercial units. Specifically, experimental temperatures are 733 K, 750 K, 772 K, 783 K and 794 K at 517 kPa. At each temperature, three runs totaling 12 space velocities constitute the kinetic data. Experiments at 207 kPa, 345 kPa, 517 kPa and 1034 kPa at 750 K provide the total pressure-dependence of the kinetics. To

keep the number of manipulated variables small, we fix the hydrogen-to-hydrocarbon mole ratio in all experiments at three, which is a typical value for a commercial reformer.

Table 3-1. Catalyst Loading and Corresponding Space Velocities of Different Sections. 12 Weight Hour Space Velocities (WHSV) in 3 Runs; Total Catalyst Loading: 5 g.

Outlet Number	4	3	2	1	4	3	2	1	4	3	2	1
WHSV (g/hr-gcat.)	2	4	10	110	6	14	26	120	8	18	57	133
Section Catalyst Loading (g)	2.5	1.5	0.91	0.09	2.85	1.0	0.9	0.25	2.8	1.5	0.4	0.3

Catalyst pre-reduction serves to remove adsorbed water from the catalyst surface and to reduce catalyst metals to their proper valence state. Fung et al. (1992) have described this catalyst pretreatment. After loading, heating the catalyst from room temperature to 789 K at 3 K/min. under 2000 cc/min. of hydrogen and maintaining this temperature for eight hours reduces the catalyst *in situ*. A gradual, three hour cooling of the reactor to 643 K precedes the introduction of the n-heptane reactor feed. A subsequent slow, three hour heating of the reactor brings it to run temperature. From the time the reactor reaches 700 K, the GC begins to analyze samples from the different reactor exits at about 100 minute intervals.

It should be pointed out that we neither presulfide the catalyst nor add sulfur to the feed during the run. On-oil time begins at the moment the reactor attains the pre-selected reaction temperature.

At the end of the run, one stops the liquid feed, cools the reactor to 643 K over three hours and maintains this temperature for five hours in hydrogen flowing at 430 cc/min. This procedure strips the reversibly adsorbed hydrocarbons off the catalyst, so as not to contribute to the temperature program oxidation (TPO) signal during the analysis of the catalyst coke. Following the 643 K hydrogen stripping, the reactor cools to room temperature under flowing hydrogen.

After the termination of the run, one discharges the catalyst in discrete sections without mixing so as to be able to compare the coke content of each section with the activity measurements described below. The amount of catalyst above outlet 1 is labeled section 1, the catalyst between outlets 1 and 2 is section 2, and so on.

3.A-2. A New Vibrational Microbalance

3.A-2.a. Introduction

The thermogravimetric analyzer (TGA) microbalance (Lin et al., 1983; Dean and Dadyburjor 1988) allows continuous catalyst bed weight measurement while the catalyst-promoted reactions proceed. It has long played an important role in catalyst coking and decoking kinetics studies (Dumez and Froment, 1976, Mieville, 1986 and Biswas et al., 1987). However, the conventional thermo-gravimetric microbalance has a number of limitations. Since a large but unmeasurable portion of the feed gases bypasses the catalyst

bed (see Figure 2), it can determine neither the true space velocity nor the actual reaction conditions that the catalyst bed experiences, and the intrinsic reaction kinetics remain inaccessible due to these poorly defined conditions. TGAs can suffer external diffusion problems. Thin layers (1-2 particles deep) of catalyst particles (Biswas, et al., 1987) and high flow rates and/or recycle can minimize such problems, but the necessarily large particle sizes (0.07 ~ 0.1 cm, —the flow in the TGA can blow finer particles out of the basket) are likely to encounter internal diffusion limitations for fast reactions such as hydrogenation. Finally, TGAs are not accurate for small weight changes below 1% because of significant buoyancy and drag effects when one switches from carrier gas to feed gases (Biswas et al., 1987).

In this work, we develop a novel inertial microbalance system for high temperature and moderate pressure operation. The major advantage of the new design is that it provides a packed bed of catalyst *through which all the feed gases flow*. It detects changes in the catalyst mass located at the tip of a tapered element by sensing the changes in its vibrational frequency. Because of its inertial design, it can enclose a packed bed of catalyst through which feed vapor flows at considerable rates, without significant flow induced buoyancy and drag effects. This design permits short contact times for operation as a differential reactor and sharp hydrocarbon concentration gradients that are useful in quantifying mass transfer. Our microbalance can measure transient mass gains and losses with a 0.1 s time resolution, permitting the observation of transient adsorption and desorption, and coking and decoking kinetics under realistic conditions.

Patashnick et al. (1980) first reported this TEOM^{R} microbalance as a device to quantify dust particles suspended in air at ambient condition. Recently, Hershkowitz et al. (1993) reported a pulse adsorption study of hydrocarbons on Y-zeolite using a Rupprecht and Patashnick Co. ("R&P" Albany, NY) vibrational microbalance. R&P custom

manufactured our high temperature microbalance and Hershkowitz et al.'s (1993) at about the same time, and it represents the first high temperature, moderate pressure, gram size catalyst loading, highly stable vibrational microbalance available for long-term catalyst deactivation studies under plug-flow conditions. This led to R&P's subsequent development of the "Model 1500 Pulse Mass Analyzer," which also uses mechanical energy and an optical feedback device to oscillate the tapered element at its natural frequency. The flow-through capability and the high sensitivity and stability of the vibrational microbalance make it an ideal general tool for research not only in catalyst coking/decoking kinetics study under realistic conditions but also in:

Absorption/adsorption and desorption studies;

Gas-solid reaction kinetics involving mass gain/loss;

Solvent recovery/destruction analysis;

Desiccant characterization;

Gas density and catalyst pore volume measurements; and

Catalyst characterization and regeneration.

3.A-2.b. MICROBALANCE REACTOR SYSTEM: Design and Operation Principles

The microbalance reactor system consists of a flow-through tapered element oscillating microbalance with an optical sensor unit, a valving control feeding unit, a computer and a product analysis unit. It includes connections for the carrier/sample gas input, purge gas input, and gas output. The valving system allows either a continuous flow or pulse mode operation. Figure 2 shows the diagram of this unit. It can operate at up to 900 K and 514 kPa. The control unit contains the support hardware necessary to perform, record and display real-time measurements with the microbalance optical sensor unit, including temperature and pressure controllers and feedback circuitry to maintain the

oscillation of the tapered element. The product analysis unit contains an HP 5890 GC and a computer with Chrom Perfect software for collecting and processing the GC data. Since the tapered element has to vibrate freely, it is not possible to connect the sample cell outlet directly to the GC for analysis. Therefore, a stainless steel tube houses the tapered element and the system requires an inert gas (He) to purge the space between this outer tube and the tapered element (Figure 2) so that the downstream GC samples the true instantaneous gas composition. The purge is controlled by a mass flow controller to give a highly stable flow.

The microbalance itself is made up of a hollow tapered tube with a material test bed located at its tip. Granular 60/80 mesh (177-250 micron) catalyst particles, held in place by packed quartz wool and an end cap, fill the material test bed. The other end of the tapered element is fixed. As the carrier or sample gas flows through the tapered element and the catalyst bed, the system records changes in the mass of the catalyst as a result of its interactions with the gas stream.

An electronic feedback system maintains the oscillation of the tapered element with the catalyst bed on its end in a clamp-free mode. A feedback circuit uses mechanical energy to drive the tapered glass element to its natural frequency oscillation. This natural frequency is a function of the mechanical properties of the glass, as well as the inertia of the glass and catalyst bed. As this inertia changes, so does the natural frequency. The microbalance detects changes in the mass m of the catalyst by monitoring frequency f changes and using the cantilever beam, mass-spring equation

$$f(m) = \left(\frac{k}{m}\right)^{1/2}, \qquad (3\text{-}1)$$

where f is the natural frequency of the spring-mass system; k is the spring (tapered element) constant; and m is the total oscillating mass (catalyst bed mass + mass deposited or lost + part of the tapered element mass).

The positive feedback amplifier detects the motion of the tapered element and feeds back just enough energy to overcome windage and damping losses to maintain a fixed amplitude of the tapered element's natural frequency oscillation. The materials and mounting used for the tapered element have very small losses, resulting in an oscillating system that has a high mechanical quality (Q) factor (low damping). Mechanical systems with low damping oscillate very easily at their resonant frequencies and are also very sharply tuned at that frequency.

To determine the spring constant k, one adds a known weight to the sample cell, such as the cap, and assumes that k does not change as the mass in the crucible changes. As mentioned above, m consists of several parts. Only one part, the mass being deposited or lost, is of interest. The other parts are constant for a given tapered element or experimental run. Thus, once the k determined, one can calculate the change in mass between time 1 and time 2 as follows:

$$\Delta m = k\left[\frac{1}{f_2^2} - \frac{1}{f_1^2}\right], \qquad (3\text{-}2)$$

where f_1 and f_2 are the natural frequencies of the spring-mass system at time 1 and time 2, respectively. In subsequent experiments, software and hardware provided by R&P count the frequency, calculate the corresponding mass change as Eq.(3-2) as often as once per 0.1 s, display the results on a PC screen and store them on the hard disk. The computer

contains software and two expansion boards that allow for the computation and display of mass and temperature data in graphical and numerical forms. The data files are suitable for use with spreadsheets or other analysis programs.

3.A-2.c. Stability, Sensitivity, Reproducibility and Operation of Microbalance Reactor System

In order to decrease the noise and lower the detection limit of the measurements, the catalyst particles should be tightly packed in the sample cell to insure no movement of the catalyst particles as the tapered element vibrates. Any movement of the catalyst particles will introduce noises to the measured frequency and lower the detection limit of the balance. During catalyst loading, the tapered element is in an inverted, up-right position, i.e., the sample cell at the tip of the tapered element is pointing upward. A quartz wool plug at the bottom of the sample cell prevents the 60/80 mesh (250-177 micron) catalyst particles from falling into the hollow tube and another quartz wool plug between the top of the catalyst particles and the cap provides sufficient compression for holding the catalyst particles firmly in place. The microbalance continuously monitors the coking of the catalyst in term of its mass gain and the on-line GC simultaneously analyzes the gases exiting the catalyst bed. The stability of the balance is excellent. It drifted less than 0.1 wt% in 60 hours as shown in Figure 3-3. This facilitates long-term coking measurements. The sensitivity of the balance depends upon the catalyst loading. We have designed two tapered elements with sample cells to hold about 0.1 and 1 g of catalyst particles for this microbalance. For a vibrating element assembly designed to hold 0.1 gram catalyst, it detects a mass change of 10^{-5} gram, with a time resolution as short as 0.1 second.

Due to the high sensitivity of this balance, the mass of the gases occupying the 'void space' in the catalyst bed (including the internal pores of the catalyst particles) and, to a

much lesser extent due to the shorter distance to the pinned end, the void space in the rest of the hollow tapered element both affect the vibrational frequency of the balance. Upon switching carrier gases, the microbalance can detect changes in mass due to the density difference of the two gases, even when no adsorption or coking occurs. Therefore, one needs to know what fraction of the total cell mass is due to the gas itself, i.e., one has to measure the 'effective volume' (total void space in the tapered element including the sample cell) in each experiment to be able to take this effect into account when switching from an inert gas to a feed gas or when adding a feed gas to a hydrogen stream.

To measure this 'effective volume,' one introduces a step change in the gas density in the tapered element by, for example, switching from one inert gas to another, e.g., from helium to nitrogen and vice versa, while maintaining the same purge gas. This generates a change $\Delta\ m$ in the measured mass from which one can calculate the 'effective volume' Vg from the ideal gas law:

$$V_g = \frac{\Delta m R T}{(M_2 - M_1) P}. \qquad (3\text{-}3)$$

Here M_2 and M_1 are the molecular weights of the inert gases that generate a change $\Delta\ m$ in the measured mass; P is the pressure, T the temperature, and R the ideal gas constant. One determines the actual adsorption and coke deposition amount on the catalyst by subtracting the mass change due to the gas density difference from the measured value.

Figure 3-4 shows the results of experiments done to measure the effective volume of the empty 1 g microbalance's tapered element, when switching from He to N_2 and vice versa. The flow rate of He and N_2 was 300 cc/min. at ambient condition. From the measured mass difference of 0.0023 grams between nitrogen and helium, Eq.(3-3)

determines the 'effective volume' V_g to be 2.34 cc. The estimated volume, based on the physical dimensions of the large sample cell at the tip of the tapered element is 2.1 cc. Therefore, the effective void volume from the rest of the tapered element is about 0.24 cc which is reasonable because the opening of the hollow tube leading to the sample cell is small and this volume is distributed along the tapered element rather then at its tip.

The 'effective volume' of the 0.1 g microbalance's empty tapered element was determined to be 0.47 cc. When one fills the sample cell with 0.17 g of 60/80 mesh non porous quartz (quartz particles are 1.7 times denser than catalyst particles), the effective volume reduces to 0.36 cc. This indicates that the solid volume of the quartz particles is 0.11 cc if one neglects the solid volume of the quartz wool. The measured bulk volume of 0.17 g of the quartz particles is 0.15 cc. The maximum packing density of the bed is 0.11/0.15 = 0.73.

Note the sensitivity of the device to the tiny mass changes due to the density difference of the two gases within the cell volume and the reproducibility displayed in Figure 3-4. This suggests just how sensitive and stable the microbalance is, and this device may even allow measurement of the loss of pore volume due to coking of a porous material *in situ.*

We had found that it is very important to perform this procedure using exactly the same carrier gas flow rate because changing the carrier gas flow rate resulted in a different measured mass change. For instance, with the large sample cell, a decrease in the flow rate from 300 cc/min. to 100 cc/min. at ambient condition led to a 12% reduction in the mass change of the large sample cell upon switching from helium to nitrogen (Figure 3-5). This is probably due to the lower pressure drop, proportional to the lower flow rates. Since the outlet pressures are fixed, a lower pressure drop means a lower pressure upstream in the

microbalance and thus a lower gas density, i.e., total mass, occupying V_g. An order of magnitude estimate confirms this as the likely cause.

Finally, to test the reproducibility of microbalance measurements, we performed two separate coking runs at exactly the same conditions, T = 750 K, P = 207 kPa, H_2/HC = 3.0 and WHSV = 40 with nC_7 feed. The experimental data (not shown) demonstrate that both the coking and the gas phase concentration data are quite reproducible for runs lasting 60 hours. Thus, our newly developed vibrational microbalance has the high sensitivity and the excellent stability and reproducibility necessary for both short- and long-term coking and other kinetics studies.

3.A-2.d. Comparison of Catalyst Performance Between Microbalance and Fixed-Bed Reactor

Recall that the reaction mixture's space velocity and composition in the catalyst bed are inaccessible in a conventional thermogravimetric microbalance (TGA), since a large but unmeasurable portion of the feed gas bypasses the catalyst bed. Therefore, one cannot relate the exit gas conversion to the true activity of the catalyst. To demonstrate that the vibrational microbalance overcomes this problem, we have carried out experiments in both the microbalance and a conventional fixed-bed reactor under the same conditions: 210 kPa, 750 K, H_2/nC_7 = 3 and liquid-weight-hourly space velocity WHSV = 28.

Figure 3-7 compares the exit nC_7 feed gas and toluene concentrations with time as the catalyst deactivates. Within experimental error, toluene yields and unconverted nC_7 fractions for both units are virtually the same during the entire 80-hour run. This indicates that one can determine the activity of the catalyst directly from the exit gas composition from the vibrational microbalance. Therefore, unlike the TGA, the microbalance reactor

system not only permits *in situ* coking kinetic measurement, but also gives reliable reactor gas phase composition, space velocity and thus reaction kinetics data under realistic conditions. It is this fact that allows us to present Figure 3-8 for precisely known space velocities.

Notice that, in contrast to TGA's (Cooper and Trim's, 1980), Figures 3-7 and 3-8 even provide initial coking rate data, since the mass corrections due to gas density change upon introduction of the nC_7 feed are easy to make. We are not nit-picking here. Coke deposition is initially very fast and slows as the catalyst deactivates. n-Heptane conversion decreases from 45 wt% to 25 wt% during the initial period. There is an obvious advantage in being able to observe this regime directly. Previous studies (Querini et al., 1989b, Barbier, et al., 1988) had to separately precoke and test catalysts before using them to study how coke affects catalyst activity and selectivity.

Changes in selectivity show the different toxicities of the coke for the metal and acid functions. Methane selectivity initially displays a large decay and then appears to remain constant. Toluene selectivity decreases monotonically with catalyst coke content. According to Barbier et al. (1982) report, metal function eventually reaches a pseudo steady state for coke content and activity, while acid function deactivates continuously throughout a run. Acid function controls the n-heptane dehydrocyclization reaction after the metal activity reaches a pseudo steady state (Querini, et al., 1989a). Previous studies done with the objective of observing the influence of coke on activity and selectivity were carried out using pre-coked catalyst (Querini et al., 1989b, Barbier, et al., 1988). The obvious disadvantage of these studies is the large number of experiments required to generate and to test the coked catalysts.

3.A-3. Products and Coke Analysis

A Hewlett Packard (HP) 5880 gas chromatography (GC) with a 50 m capillary column coated with crosslinked methylsilicone gum and a flame ionization detector (FID) provides a quantitative analysis of the components in the product. An HP 5890A GC was also used in the microbalance differential reactor for quantitative analysis of the reaction vapors. Here we only introduce the newer HP 5890A since the two GCs are similar. This unit is equipped with an alphanumeric display keyboard to permit convenient definition of the instrument's set points. The inlet system is capable of split or splitless capillary column mode, as well as packed column mode, all connected to a back-pressure regulated flow. The oven temperature programming is possible with three temperature ramps available with the smallest increment being 0.1 degrees per minute. We use liquid nitrogen to lower the oven temperature to 253 K, which is the initial temperature used in all runs. The upper temperature limit for the oven depends on the type of column used and was set for a maximum of 623 K. The GC oven temperature program used here is as follows:

initial oven temperature value 253 K
oven temperature initial time 0 min.
heating rate 4 K/min. to 397 K.
change heating rate to 15 K/min. to 513 K.
stay at final temperature 513 K for 34 minutes.

The FID responds to compounds which produce ions when burned in a hydrogen-air flame. All organic compounds are then suitable for use with this detector. A linear response is obtainable for most organic compounds from the minimum detectable limit through concentrations greater than 10^7 times the minimum detectable limit.

The capillary column used for the separation of the various components in the reaction mixture is an HP-1 column. This column is 25 meters long, 0.2 mm in diameter,

with 0.33 micrometer thick crosslinked methyl silicone film and is most suitable for petroleum components ranging from gases up to heavy gas oil molecules.

An HP integrator measures the GC peak areas. The integrator accepts voltage outputs from the GC instrument, detects and integrates peaks and plots the chromatogram. This information was also transferred to a computer through a compatible interface for further analysis. Both the Chrom Perfect programs and the HP Cals system were used to collect, process and analyze the GC data.

We employ a highly sensitive temperature programmed oxidation (TPO) technique to characterize the coke. Details of the technique appear elsewhere (Fung and Querini, 1992). Figure 3-10 shows a diagram of the modified TPO unit. The unit consists of a modified Altamira Instruments, Inc., model AMI-1 temperature programmed unit and a computer-controlled valving system for selecting and routing the desired gas stream to the sample cell. Without modifications, the AMI-1 apparatus is not suitable for coke analysis since it only has a TCD and does not have a GC column. The idea behind this new detection scheme is to convert CO_2 (produced during coke oxidation), an FID insensitive gas, to CH_4, an FID sensitive gas, in the presence of an oxygen-containing carrier gas. The addition of a smaller reactor filled with Ru catalyst after the sample cell achieves this. In the presence of added hydrogen, the Ru catalyst hydrogenates CO_2 to CH_4 quantitatively. An FID, Model 12-800, manufactured by Gow-Mac Instrument Company can monitor the CH_4 generation rate, which is equal to the coke oxidation rate. An electrometer (Gow-Mac), Model 40-900 controls the FID signal and a computer stores and displays the FID signal as a function of sample temperature. There is no need for a GC column to separate the O_2 and H_2O present in the gas stream coming from the sample cell, since the FID is sensitive to neither O_2 nor H_2O. Thus, both sensitivity and resolution are far superior to

those of a thermal conductivity detector (TCD) which requires a GC column to separate CO_2 from oxygen.

One loads the coked sample, about 10-20 mg, into a U-shaped quartz cell, and places it in a furnace. The coked catalyst, ground, thoroughly mixed, reground and remixed, yields a fine powder that must pass through an 80-mesh screen. A pressure of 138 kPa compresses the fine powder to a 1" diameter pellet, which one then breaks into small particles of 60-80 mesh. During the preparation of the sample, the handler must take care not to introduce any carbon-containing material, such as the oil from the handler's fingers, into the sample. Therefore the preparation and loading of the sample into the sample cell can involve contact with only clean glass, ceramic, and metal surfaces that are free of carbon contaminants.

TPO analyses use 1% O_2/He flowing at 60 cc/min. at room temperature through the sample with sample heating at a rate of 13 K/min. from room temperature to 1043 K. Alternatively, pure helium and 10% H_2 in argon can replace the oxidizing mixture. With this procedure and the standard TPO (using 1% O_2) that follows, it is possible to distinguish the kinds of coke that hydrogasification can strip from the catalyst. A quantitative determination of the types of coke on the catalyst is possible via a calibration run on the TPO unit. There is no need for catalyst pretreatment before TPO. This sampling method gives highly reproducible results.

We also performed the continuous coking and decoking monitoring experiments just described on the tapered element oscillating microbalance (Figure 3-2), which Rupprecht and Patashnick Company manufactured to our specifications (Fung et al. 1994, Patashnick et al. 1980). Section 3.A-2 detailed the microbalance apparatus and technique.

3.B. General Trends: Pressure, Temperature and Space Velocity

3.B-1. The Effects of Pressure

Evaluating the effect of the total gas pressure is one of the principal methods for studying a reaction mechanism, for defining the preferred operating conditions for a catalyst, and for gaining a feel for how the pressure affect the catalyst deactivation.

Clem (1977) studied how the hydrogen and hydrocarbon partial pressures affect overall selectivity, reaction intermediates and byproducts by varying either the hydrogen or heptane partial pressure at constant H_2/nC_7 ratio. Here, we vary the total pressure while holding the H_2/nC_7 ratio and other conditions constant.

Figures 3-11 to 3-15 plot nC_7, iC_7, toluene, C5-naphthene (C5N) and cracked products (C_1-C_6) vs. time for four or five pressures. As the pressure increases, the conversion of nC_7 also increases. At a low pressure (207 kPa) the catalyst deactivates rapidly, and the conversion of nC_7 drops from 80% initially to 40% at 120 hours. At this pressure, the toluene yield is as high as 27% initially and drops to 7% at 120 hours. After the initial transient catalyst deactivation period, the higher the pressure, the more toluene the reaction produces.

Also, higher operation pressures lead to more hydrocracking products produced. The yield of hydrocracking products increases from 10% at 207 kPa to 32% at 1034 kPa. iC_7, on the other hand, seems to go through a maximum at 517 kPa, of 37%, as compared with 20% at 207 kPa.

Finally, and most significantly for this study, Figure 3-14 shows that the reaction produces more C5 naphthenes at the lower pressure. For instance, the total C5 naphthenes concentration increases from 1.2% at 1034 kPa to 5.8% at 207 kPa. Since C5N is the only intermediate or product whose concentration increases with decreasing pressure, it suggest that the more C5N produced might fuel the faster deactivation (see Figure 3-11).

3.B-2. The Effects of Temperature

For paraffin reforming to aromatics, the desirable dehydrocyclization reactions are endothermic, the undesirable cracking reactions are exothermic, while the isomerization reactions are essentially thermal-neutral. The net overall effect of catalytic reforming is endothermic. Commercial catalyst beds consist of three or four reactors in series with reheat furnaces between them. This provides a high reaction rate throughout without an excessively high reactor inlet temperature. As reactor operation proceeds, the catalyst activity gradually decreases. This loss of activity becomes apparent "on the outside" through a drop in the reformate octane number and a decrease in the hydrogen yield. To make up for this decrease and still maintain the same product antiknock qualities, refiners must gradually increase the average reactor operating temperature. On other hand, this rise in temperature brings about a considerable increase in the rate of coking and other side reactions such as, cracking, hydrocracking and hydrogenolysis that have high activation energies. Moreover, there is an upper limit on the temperature in plant operation. So temperature strongly affects both the reforming reactions and the catalyst deactivation.

Figures 3-16 and 3-17 show that the higher the temperature, the faster the deactivation. At 794 K, the conversion of nC_7 drops from 98% initially to 50% at 160 hours' on-oil, but at 733 K, the conversion of nC_7 is relatively stable between 25% and 32% over the same time range. As expected, Figure 3-18 shows that higher temperatures

yield more C_1-C_6 cracking products for a fresh catalyst but they also accelerate the deactivation rate; so, the curves of different temperatures can cross. For example, at 794 K, the cracking products concentration drops from 36% initially to 18% after 160 hours' on-oil, while at 733 K the yield of cracking products (13%) declines slightly over the same period. Figure 3-19 shows that the lower the temperature, the more iC_7 produced. The yield of iC_7 increases from 11% at 794 K to 40% at 733 K. This might be due to a larger amount of iC_7 being hydrocracked at higher temperatures. Finally, Figure 3-20 shows that C5 naphthene yields increase with temperature, e.g., from 1.5% at 733 K to 6.0% at 794 K. Curiously, both the pressure and temperature effects show a qualitative correlation between C5N concentration and the rate of catalyst deactivation (see Figures 3-14 and 3-20). We shall make this correlation quantitative in section 3.C.

3.B-2. The Effects of Space Velocity

The final general operating variable that is easy to control and which strongly affects the catalyst coking is the space velocity. Figures 3-8 and 3-9 show the reactor coke and C5N outputs from the vibrational microbalance, which allow precise adjustment of the gas space velocity through the catalyst, as functions of time for three space velocities at otherwise unchanged reactor conditions, i.e., 60/80 mesh (177-250 μm) particles, 0.3%Pt+0.3%Re/Al_2O_3 catalyst and the same temperature history of the catalyst.

The general conclusion is that lower space velocities result in higher C5N concentration and faster coke build-up and thus faster deactivation in the space velocity regime (28~80) that we have studied. Together with the temperature and pressure effects, this trend is consistent with an increase in the pseudo-steady C5N concentration with faster catalyst coking/deactivation.

3.C. Catalyst Activity and Coking Profiles in a Multioutlet Fixed Bed Reactor

In section 3B, all of the deactivation trends of the reforming catalyst with changes in operating parameters point to a qualitative correlation between C5N concentration and catalyst coking rate. Querini and Fung (1993) inferred this connection from some preliminary data. The work below uses the same multioutlet fixed bed reactor as Querini and Fung and together with their data, presents a quantitative profiles of coke amount, catalyst activity and C5N concentrations along the catalyst bed. As we shall see, the correlation is remarkable. Together with section 3.B's data, they argue for a cause-and-effect conclusion, that C5Ns are the most potent coke precursor in our system, and motivate the detailed studies in section 3.D.

3.C-1. A Simplified Model of Catalyst Deactivation and A Quantitative Measure of Local Catalyst Activity

Figure 3-21 shows that the C5N concentration does not vary much during a 100-hour run. In contrast, the coke builds up over this period, and one can, with a suitable microbalance, quantify its rate. However, in practice, the engineer is interested in the functional deactivation and Szepe and Levenspiel (1970) outline a class of direct phenomenological measures of catalyst activity based on reaction conversion that complement the coking data. We briefly summarize their development as follows.

As a catalyst ages, its ability to promote the reactions decreases. One usually associates the substantive build up of catalyst coke with this functional aging but a direct functional measure is useful and need not be simply proportional to the coke amount. We

adapt the development of Szepe and Levenspiel (1970), Butt and Petersen (1988) and Shum et. al. (1987) of such a measure to our system.

Consider a general catalytic reaction together with a side coking reaction:

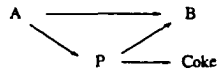

Here, A is the reactant fed to the reactor, B is the product and P is the reaction participant (reactant, intermediate or product), that is the candidate culprit deactivator.

Assume that the main reaction is *q-th* order in the reactant concentration and has separable deactivation kinetics

$$-r_A = ar_{A0} = akC_A^q , \qquad (3\text{-}4)$$

r_{Ao} is the initial, i.e., fresh catalyst, reaction rate and a is the deactivation function (activity) defined as the ratio of the reaction rate $r_A(t)$ at any time t to the initial reaction rate r_{Ao}. If c is the vector of species concentrations, then

$$a = \frac{r_A(t)}{r_{A0}} = a(t,\ c(t,\tau,T)). \qquad (3\text{-}5)$$

Suppose now that the activity depends on the concentration c_{ps}, of a foulant on the catalyst surface. In terms of c_{ps} and the ultimate capacity c_{p0} of catalyst for fouling, one can express the fraction f of the catalyst surface's unused fouling capacity as

$$f = (c_{P0} - c_{Ps})/c_{P0}. \qquad (3\text{-}6)$$

If one pictures the catalyst surface as providing a discrete number of catalyst sites, some or all of which the coke may foul, one can interpret f as the fraction of active sites not covered by the coke. The correspondence is most apt when c_{p0} corresponds to monolayer site coverage.

If the rate of foulant accumulation on the catalyst obeys a power law form of order n (the order of the fouling reaction) or if the fouling reaction involves n active sites, then

$$\frac{df}{dt} = -k_d f^n F(\mathbf{c}(t,\tau,T)). \qquad (3\text{-}7)$$

Suppose that F depends only on the precursor's concentration and that the concentration of the precursor does not change significantly with time during a run. Then $F(\mathbf{c}) = F(c_p(\tau\ ,\ T))$ is constant in time and $a = a(t,\ c_p(\tau\ ,\ T))$ is a function only of time and of the precursor concentration, and is independent of all other concentrations. Integration of Eq. 3-7 yields

$$f = \exp(-K_d t) \qquad \text{for } n = 1 \qquad (3\text{-}8a)$$

$$f = \left[\frac{1}{1+(n-1)K_d t}\right]^{1/n-1} \qquad \text{for } n \neq 1, \qquad (3\text{-}8b)$$

where $K_d = k_d F(c_p(t,\tau\ ,\ T))$.

If the deactivation is due to the site coverage, and m is the number of active sites involved in the controlling step of the main reaction, the relationship between a and f takes the form, $a = f^m$ which, with Eqs. (3-8a, b), yields

$$a = \exp(-mK_d t) \qquad \text{for n= 1;} \qquad (3\text{-}9a)$$

$$a = \left[\frac{1}{1+(n-1)K_d t}\right]^{m/n-1} \qquad \text{for n} \neq 1\ . \qquad (3\text{-}9b)$$

The constitutive equation (3-4) can be used to describe the mass balance in the multi-outlet fixed bed reactor with fluid phase plug flow and uniform, constant volumetric flow rate. In principle, k should be uniform if the main reaction depends only on C_A; on the other hand, $a(t, C_p(t,\tau\ , T))$ changes along the bed τ in a complex manner. However, by hypothesis, $a = a(t, C_p(\tau\ , T))$. Even though C_p varies along the bed in an as yet unknown manner, it is reasonable to assume that C_p and a are continuous everywhere. The integral mean value theorem defines the average value $<a>_i$ of the catalyst activity between outlet i and $i+1$, by the integral (Eq.3-4):

$$\int_{C_{Ai}}^{C_{Ai+1}} \frac{dC_A}{C_A^q} = -k\int_{\tau_i}^{\tau_{i+1}} a\,d\tau = -k < a >_i (\tau_{i+1} - \tau_i), \quad i = 0,\ 1, \cdots,\ b\text{-}1. \qquad (3\text{-}10)$$

The integral mean value theorem assures us that there is at least one point, whose exact position τ_i^* is not specified but which lies between outlets i and $i+1$, at which the activity takes on the value $<a>_i$. At τ_i^*, one can substitute Eq.3-8, Eq.3-9 to obtain the correlations in Table 3-2 for various values of m, n and q.

Table 3- 2. Different Activity Functions and nC_7 Concentration vs. Time Correlations

Parameters: m and n	Activity function, a	Correlations of concentration verse time , q=1	Correlations of concentration verse time , q=0
m=1, n=1	a=exp(-mK_dt)	$\ln\left(\frac{\ln\frac{C_{A,i}}{C_{A,i+1}}}{(\tau_{i+1}-\tau_i)}\right)=\ln k-K_d t$	$\ln(C_{A,i}-C_{A,i+1})=\ln k(\tau_{i+1}-\tau_i)-K_d t$
m=1, n=0	a = 1 - K_dt	$\ln\frac{C_A}{C_{A,i+1}}=k(\tau_{i+1}-\tau_i)-k(\tau_{i+1}-\tau_i)K_d t$	$C_{A,i}-C_{A,i+1}=k(\tau_{i+1}-\tau_i)-k(\tau_{i+1}-\tau_i)K_d t$
m= 1, n=2	a = 1/(1+K_dt)	$\left(\ln\frac{C_A}{C_{A,i}}\right)^{-1}=\frac{1}{k(\tau_{i+1}-\tau_i)}+\frac{1}{k(\tau_{i+1}-\tau_i)}K_d t$	$\frac{1}{C_A-C_{A,i}}=\frac{1}{k(\tau_{i+1}-\tau_i)}+\frac{1}{k(\tau_{i+1}-\tau_i)}K_d t$
m= 2, n=2	a=[1/(1+K_dt)]^2	$\left(\ln\frac{C_A}{C_{A,i}}\right)^{-1/2}=\left(\frac{1}{k(\tau_{i+1}-\tau_i)}\right)^{1/2}+\left(\frac{1}{k(\tau_{i+1}-\tau_i)}\right)^{1/2}K_d t$	$(C_A-C_{A,i})^{-1/2}=\left(\frac{1}{k(\tau_{i+1}-\tau_i)}\right)^{1/2}+\left(\frac{1}{k(\tau_{i+1}-\tau_i)}\right)^{1/2}K_d t$

For a specific catalytic reactor and candidate coke precursor, one can use the data of reactant concentration at the inlet and at each of the outlets as functions of time to test each of the correlation forms in Table 2. If the data in each reactor section obey the same correlation for different operating conditions and yield one k [1] for each set of operating conditions for all reactor outlets, then the $K_d(\tau_i^*)$ parameter is a measure of the local rate of

[1] As detailed in Appendix I, under certain circumstances, k may not represent simply the main reaction rate constant and thus it may depend on bed position τ . Since $a(\tau)$ is non-negative, (3-10) becomes in such a case, $-\int_{C_{A,i}}^{C_{A,i+1}}\frac{dC_A}{C_A^q}=\int_{\tau_i}^{\tau_{i+1}}kad\tau=-<k>'\int_{\tau_i}^{\tau_{i+1}}ad\tau=<k>'<a>_i(\tau_{i+1}-\tau_i)$, $i=0, 1,\cdots, b-1$ where $<>'$ indicates the average with respect to $ad\tau$ rather than with respect to $d\tau$.

catalyst deactivation under the given operating conditions. Note that, in order to carry out this procedure, one must assume that the positions τ_i^* do not change significantly with time. In fact, if the variation of a is not too wild, say monotonic, then one may safely assume that τ_i^* remains near the midpoint of τ_i and τ_{i+1}, for all time.

Let us apply this analysis to n-heptane reforming. Clem (1977) indicates that, with excess hydrogen, all reactions in n-heptane reforming are first order; so $q = 1$. From section 3.B, the C5Ns are the candidate coke precursors P and n-heptane is the reactant A. Moreover, Figure 3-21 shows that the concentration of C5N, the putative coke precursor, is fairly time independent (< 20% variation) at each outlet for the fixed bed runs after the initial transient period. Thus the assumption about F and a that this method invokes are reasonable and we set about to test the data against the various functional forms in Table 3-2.

Figure 3-22 shows the n-heptane concentration as function of run time for each bed outlet. Curve 1 from outlet 1 has an equivalent space velocity of 133 w/w/hr. Similarly, curves 2, 3 and 4 have space velocities of 57, 18 and 8 w/w/hr, respectively. The amount of nC_7 at each outlet increases with on-oil time as the catalyst deactivates. For example, at outlet 3, it increases from 35% to 65% (wt%) during a 100-hour on oil run. The overall catalyst activity drops significantly as the conversion of nC_7 at outlet 3 decreases from 74% to 54% during the initial 20 hrs on oil. Figures 3-23 to 3-25 show the concentrations of toluene, iC_7 and cracking products as functions of time at the four outlets. After 100 hours, the amount of toluene at outlet 4 is about one third of the initial yield on fresh catalyst. Finally, Figure 3-21 shows the corresponding data for the C5Ns, the putative coke precursor.

Figures 3-26 - 3-29 show the correlation results for $m = n = q = 1$ for four long fixed bed reactor runs. The data are such that any of the $q = 1$ entries in Table 3-2 fits the data equally well for most of the measured time span, since $K_d t_{max}$ turns out to be ≤ 0.6. As such, these data can not distinguish amongst these $q = 1$ models and we simply choose $m = n = 1$ for convenience. The excellent correlation that this form affords motivates parameter extraction and examination. We have extensive data of nC_7 concentration versus time at different conditions and all of them fit as well as Figures 3-26 - 3-29.

Table 3-3. K_d, Coke and C5N Concentrations Obtained at Different Space Velocities

T = 750 K, P = 517 kPa, $H_2/nC_7 = 3$

WHSV	2	4	6	8	10	14	18	26	57	110	120	133
Space time min	30	15	10	7.5	6	4.29	3.33	2.31	1.05	0.55	0.50	0.45
$K_d x10^3$	0.41	0.98	1.89	2.0	2.50	2.75	2.69	2.54	2.65	2.24	1.80	1.45
Coke (wt%)	1.87	2.73	3.04	2.59	3.17	3.30	3.17	3.18	2.98	2.92	2.86	2.79
C5N (wt%)	1.0	2.05	2.16	2.4	2.75	2.63	2.65	2.21	1.80	1.02	0.98	0.93
k	4.26	6.36	7.96	9.51	10.5	10.8	12.7	14.2	17.3	18.2	20.5	18.2

The deactivation "parameter" K_d and the main reaction constant k derive from the slopes and intercepts of these plots[2]. Table 3-3 presents the results at different experimental conditions (3 flow rates × 4 exits). Now, one may argue that taking the logarithm twice of almost any monotonic function will provide a plot that looks linear. But, as shown later in Chapter 7, plots for other $q = 1$, $m = 1$ models are also linear and provide similar parameter values. The point here, as we shall see, is that the resulting parameter K_d correlates very well with coke build-up and with the concentration profile of one of the reaction participants.

3.C-2 Comparison of Deactivation, Coke and C5-Naphthene Profiles in a Fixed Bed Reactor

The coke content of each section of the reactor after many (>>20 hrs) hours and its relationship with the gas phase compositions along the bed provide information about the coking mechanism. For example, a series mechanism (reactant → product → coke) would lead to an increasing coke profile along the bed, whereas a parallel mechanism (reactant → product, reactant → coke) would yield a decreasing profile (Froment and Bishoff, 1961, 1962). In more complicated reaction networks, coke deposits may result from a combination of pathways. If the main source of coke deposits is an intermediate compound, the coke profile would exhibit a maximum. In addition, knowledge of the coke profile can greatly improve catalyst regeneration operations. For example, during catalyst regeneration by coke burning, an uneven coke distribution along the catalyst bed can lead to sharp temperature spikes that can sinter the catalyst. With knowledge of the profile, one

[2]Note that the intercept yield values for the main reaction rate constant k which decay monotonically with bed τ. Appendix I modifies the above analysis to show that accounting for the fast, reversible reaction between normal and iso-heptanes can explain this behavior quite well. In that case, k is no longer the main reaction constant k_0 but rather a combination of k_0, the rate constant k_{00} for the lump reaction $iC_7 \rightarrow nC_7$ and the concentration of the isoheptanes.

can avoid such sintering. Reports of coke profiles exist for the following systems: cumene cracking on a zeolite catalyst (Achary, et al., 1990); isomerization of n-pentane on Pt/Al_2O_3 (DePaw and Froment, 1975); naphtha reforming on Pt/Al_2O_3 (Levinter, et al.); and nC_7 reforming on both Pt/Al_2O_3 and $Pt\text{-}Re/Al_2O_3$ catalysts (Fung, et al., 1991, 1993). Butt and Petersen (1988) list other examples.

As described in section 3.A, we determine the coke profile by downloading the catalyst by section at the end of a run, and performing TPO analysis on each section. Figure 3-30 shows the profiles of deposited coke[3], the corresponding time-averaged C5N concentrations and the K_d values obtained from the last section for typical runs from 170 to 240 hours. Remarkably, all three profiles are extremely similar. As we can see, all three profiles exhibit maxima at section 2 or 3 under these experimental conditions. The shape of the coke profile alone indicates that the coke derives from a reforming intermediate. The C5N curve confirms our group's (Querini and Fung, 1993) preliminary profiles for C5N and coke. Finally, the functional measurement K_d shows that the C5N profile tracks both the substantive profile of coke as well as the functional profile of the deactivation rate constant. This again points to C5N as the coke precursor and motivates the quantitative study in section 3.D.

Since our reactor has only four outlets, each circa ~200 hour run provides only four data points for the coke, C5N and K_d profiles. To assemble more data, we also plot the collected coke, C5N and K_d data versus the 12 space velocities corresponding to three

[3]The resulting value represents an average value for the coke content of that section. Again, a mean value theorem argument guarantees (under appropriate continuity assumptions) that some point τ_i^* between τ_i and τ_{i+1} actually has that coke concentration. As with τ_i^*, (see appendix), even though τ_i^* is unknown, we approximate it by the midpoint between τ_i and τ_{i+1}. The same is true for the gas phase concentration in each section.

separate runs in Figure 3-31. All three runs had the same temperature, pressure and H_2/nC_7 mole ratio, but different on-oil times (240, 224 and 170 hours); hence the data in Figure 3-31 are not as smooth as those of Figure 3-30. Nevertheless, the three profiles are still quite similar, and only appear to cross due to the choice of scale.

Furthermore, Froment et al. (Trimpont et al., 1988; Marin and Froment, 1982) have found experimentally that the activity of a Pt/Al_2O_3 catalyst in nC_6 and nC_7 reforming decays exponentially with the amount of coke on the catalyst (C_k). To compare their result with our findings, we performed *in situ* coking experiments by feeding nC_7 to our newly developed microbalance reactor (see Figures 3-7 and 3-32). As these two figures show, after an initial rapid deactivation period of 15~20 hours, the coke amount on the catalyst increases almost linearly with time. Therefore, the deactivation function just derived, $a = \exp(-K_d t) = \exp(\frac{aK_d}{b})\exp(-\frac{K_d}{b}C_k)$ when $C_k = a+bt$ increase linearly with t. This agrees with Froment et al.'s (1988, 1982) empirical correlation.

In summary, our functional deactivation kinetics analysis and measure based on how the reactant (here nC_7) concentration changes with time would seem to provide a quick and simple method for the screening of reaction/deactivation behavior at one level beyond pure empiricism. The only data required in the above analyses are the reactant and candidate precursor concentrations as functions of time, which are relatively easy to get both on laboratory and commercial scales.

3.D. Detailed Differential Microbalance Studies to Determine The Major Coke Precursor in n-Heptane Reforming

Up to this point, we have assembled a battery of evidence pointing qualitatively to C5N as the major coke precursor in n-heptane reforming. This evidence includes pressure,

temperature and space velocity effects on the coking/deactivation rates and the coincidence of fixed bed coke, deactivation rate constant and C5N profiles along the reactor. Unfortunately even these last data are integral in nature and thus may leave some room for doubt. Below we employ the new differential vibrational microbalance with its *in situ* coke measuring and simultaneous reactor gas phase monitoring capabilities to provide our final, most direct and quantitative evidence.

In order to quantitatively determine which of the hydrocarbon groups is the major source of coke and also to test the conjectures/conclusions in the literature, we performed experiments to compare the coking rates of different hydrocarbon feeds in the vibrational microbalance at 207 kPa, 750 K and H_2/HC = 3.0 over 0.3 wt% Pt - 0.3 wt% Re/Al_2O_3 catalyst. Figure 3-32 shows the coking rates of the following feeds: toluene, nC_7, 96% toluene + 4% ethylcyclopentane (ECP), 96% toluene + 4% methylcyclopentane (MCP), 50% toluene + 50% MCP and pure MCP and ECP. MCP and ECP are two of the C5Ns that hexane and heptane reforming generate.

Figure 3-32 shows that the pure MCP and pure ECP feeds produce significant amounts of coke; in fact, much more than pure nC_7 or toluene feeds. This indicates that C5Ns are potent coke precursors in paraffin reforming, and in fact, are much more potent than the feed or product. It is consistent with the multi-outlet fixed bed reactor results and with the conjecture of Zhorov and Panchenkov (1980).

Froment et al. (1988) proposed that the intercondensation between toluene and C_7 cyclopentadienes is responsible for most of the coke in nC_7 reforming. To test this hypothesis, we compare the coking rate of a 50% MCP + 50% toluene mixture feed with the coking rate of pure MCP. If Froment et al. were right, then one would expect the coking rate of a 50/50 MCP/toluene feed to be faster than that of pure MCP. As it turns

out, though, Figure 3-32 shows the opposite is true, and the intercondensation between toluene and C_7 cyclo-pentendienes is not a primary source of coke. In fact, as Figure 5-7 will show, the initial coking rate is linear in the partial pressure of MCP.

At this point, it is natural to conjecture that C5Ns actually account for most of the n-heptane reforming coke. Under the conditions employed, the nC_7 feed produces a total of ~4 wt% C5N at the exit of the microbalance. Also, the coking rate of toluene in Figure 3-32 is very low and almost negligible compared with that of nC_7, MCP or ECP. So, it is easy to test our conjecture by feeding the 4% C5N + 96% toluene into the microbalance and comparing the resulting coking rate with that of pure nC_7. As Figure 3-32 shows, these two are quite similar with either MCP or ECP as the model compounds of C5N. Finally, note that the coking rates of MCP and ECP are almost indistinguishable from each other. This indicates that at least two, and maybe all different C5Ns have similar coking rates. Hence, it is not unreasonable to use the readily available and relatively inexpensive MCP as the model compound for C5N to study coking kinetics.

In view of the coincidence of the C5N concentration and the coking trends with pressure, temperature and space velocity, the confluence of the C5N, coke and deactivation profiles in the fixed bed reactor and the differential microbalance coking studies, we conclude that the catalyst coke in paraffin reforming derives mainly from the C5N intermediates. Moreover, the latter studies show that toluene contributes little to the coke formation and MCP is an adequate model compound of C5N for detailed coking kinetics studies.

Modeling industrial catalytic reforming processes requires a knowledge of both the kinetics of the main reaction and of the side coking reactions that cause catalyst deactivation. If C5Ns are the major coke precursors in paraffin reforming, in general, this

would be very significant. It is easy to do on-line gas product analysis of a commercial reformer to determine, say, how much C5Ns are being formed; on the other hand, it is almost impossible to do on-line coking rate measurement for a commercial reformer. Without an understanding of the coking process, it is also impossible to predict the coke profile of a commercial reformer. However, the identification of C5N as the primary coke precursor and the determination of its coking kinetics (see Chapter 5) hold out the possibility of accurate inference of the state of coking and of the coke profile of an operating commercial reformer, knowledge that is nearly impossible to obtain in any practical "routine" experiment, from the gas-phase monitoring of the C5N concentration. The coke profile is crucial. In order to simulate and control the reforming catalyst regeneration processes, one must know the final coke profile of the reformer which becomes the initial condition of catalyst regeneration model.

There are two obvious questions that remain: 1). Can one predict the amount of coke being formed by measuring the gas phase C5Ns' concentration on-line? If so, can one also use an on-line measured C5Ns' concentration profile to predict the catalyst coke profile? 2). Can one come up with a simple model for the reforming reactions that accurately predicts the C5N profile ? If so, then a combination of this model with a model of coking rates would lead to both coke profile predictions as well as reformer performance predictions over coking time scales. The first part of question 2 is the subject of Chapter 4 while Chapter 5 focuses on question 1. Chapter 7 attempts to combine the models as indicated.

Appendix 3-I:

In this appendix, we consider a modification of the catalyst deactivation measure in section 3.C-1 to account for a fast reversible step involving the main reactant, i.e.,

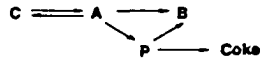

, (3-11)

where C can be an isomer of A. As we shall see, this type of mechanism can explain a situation where the plots dictated in section 3.C-1 are straight but the intercepts, rather than providing a uniform value for k, give k's that vary systematically with τ.

Suppose that C_A and C_B (as well as the other gas phase concentrations are known as functions of t and τ, then C_A varies with τ via a modification of (A) for $q = 1$ by

$$\frac{dC_A}{d\tau} = a(-k_0 C_A + k_{00} C_C) \qquad (3\text{-}12)$$

Here, k_0 is the sum of the rate constants for all of the reactions emanating from A, including the one that produces C. Since $C_C(\tau)$ is known, i.e., measured, one can integrate this equation with $C_C(\tau)$ as a forcing function. Upon rearrangement and use of the mean value theorem as before, one finds

$$\ln\left(\frac{\ln\dfrac{C_A(\tau_i)}{C_A(\tau_{i+1})}}{\tau_{i+1}-\tau_{i+1}}\right) = -K_d(\tau_i^*)t + \ln\left[k_0\{1 - \frac{\ln\left(1+\dfrac{k_{00}}{C_A(\tau=0)}\int_{\tau_i}^{\tau_{i+1}}\exp(-k_0\int_{\tau_i}^{s}ad\tau')a(s)C_c(s)ds\right)}{k_0\exp(-k_d(\tau_i^*)t)(\tau_{i+1}-\tau_i)}\right]. \qquad (3\text{-}13)$$

If the second term on the right of this equation is only a weak function of time, then a plot of the data from each reactor outlet in the form of the left side of this equation vs. t should

give a straight line with slope $-K_d(\tau_i^*)$ and intercept that depends on τ. To see under what conditions the second term on the right is indeed practically independent of time, we resolve the remaining integrals using the mean value theorem.

Since $a = e^{-K_d t}$ and $C_C(t)$ are both non-negative,

$$\begin{aligned}
&\int_{\tau_i}^{\tau_{i+1}} \exp(-k_0 \int_{\tau_i}^{s} a d\tau') a(s) C_c(s) ds = a(\tau_i^{**}) \int_{\tau_i}^{\tau_{i+1}} \exp(-k_0(\tau^*(s)(s-\tau_i)) C_c(s) ds \\
&= a(\tau_i^{**}) C_c(\tau_i^{***}) \int_{\tau_i}^{\tau_{i+1}} \exp(-k_0 a(\tau_i^{+}(s))(s-\tau_i)) ds \\
&\approx a(\tau_i^{**}) C_c(\tau_i^{***}) \frac{1-\exp(-k_0 a(\tau_i^{+*})(\tau_{i+1}-\tau_i))}{k_0 a(\tau_i^{+*})}
\end{aligned} \tag{3-14}$$

where the curved equal sign is approximate because it replaced $\tau_i^+(s)$ by constant τ_i^{+*}. If we presume that all of the mean value theorem τ's are approximately at the midpoint $\bar{\tau}_i$ between τ_i and τ_{i+1}, the second term on the right side of (3-13) reduce to

$$\ln\left[k_0 \{1 - \frac{\ln\left(1 + \frac{k_{00}}{k_0} \frac{C_C(\bar{\tau}_i)}{C_A(\tau=0)} (1-\exp(-k_0 a(\tau_i)(\bar{\tau}_{i+1}-\tau_i)))\right)}{k_0 \exp(-k_d(\bar{\tau}_i)t)(\tau_{i+1}-\tau_i)} \}\right]. \tag{3-15}$$

Now, if $k_0 a(\bar{\tau}_i)(\tau_{i+1}-\tau_i) << 1$ and $\frac{k_{00}}{k_0} \frac{C_C(\bar{\tau}_i)}{C_A(\tau=0)} (1-e^{-k_0 a(\tau_i)(\bar{\tau}_{i+1}-\tau_i)}) << 1$, then expansion of both the logarithm and the exponent to leading order lends to a cancellation of the factors $a(\bar{\tau}_i) = e^{-K_d(\bar{\tau}_i)t}$ and leaves an intercept of

$$\ln\left[k_0 - k_\infty \frac{C_C(\bar{\tau}_i)}{C_A(\tau = 0)}\right]. \qquad (3\text{-}16)$$

Thus if C_C is only a weak function of time and as noted above, the mean value τ_i's are all close to the midpoints of the interval (τ_{i+1}, τ_i), then a plot of (3-13) as suggested above should lead to a straight line whose slope is $-K_d(\bar{\tau}_i)$ and whose intercept is well defined, but depends upon the reactor outlet τ_i in question.

Let us now turn to the problem at hand. It is well known that n-heptane undergoes a fast, reversible reaction with a collection of iso-heptanes, which one may lump into a pseudo-species iC_7. From Figure 3-24, the iC_7 concentration does not vary significantly after the initial transient, particularly when compared with the product species. As such, if one can find a pair of positive constants k_0 and k_{00} such that the twelve intercepts available from the three runs and four reactor outlets at each set of reactor conditions as a function of $C_C(\bar{\tau}_i)$ obey either (3-16) (or 3-15 with t taken as a fixed, average value), one may conclude that it is the $nC_7 \Leftrightarrow iC_7$ reaction that accounts for the monotonic decay of the intercept with τ (Figure 3-33). Figure 3-34 shows that this fit is quite good despite the fact that each k is the result of the intercept of a best-fit line.

Chapter 4. A NEW LUMPED KINETIC MECHANISM FOR n-HEPTANE REFORMING OVER A SUPPORTED Pt-Re CATALYST

Chapter 3 assembled a plethora of experimental evidence that C5 naphthenes are the major coke precursors in n-heptane reforming over supported Pt-Re catalysts at conditions close to those of a commercial reformer. If one accepts the weight of this evidence and would iike to predict coking profiles in operating industrial reactors, it is absolutely necessary to have at one's disposal a kinetics mechanism for n-heptane reforming that is simple, robust and contains C5N as one of its lumps. Moreover, such a model will be useful for a later more complete understanding of the deactivation process. That is, once one has determined the coking kinetics based on experiments with a feed whose only hydrocarbon constituent is the precursor (Chapter 5), one can combine the coking and the reaction models to understand and predict reformer performance over coking time scales, on the one hand, and how the precursor profile predicts the bed's coke profile, on the other. This synthesis is the subject of Chapter 7. Meanwhile, in this chapter, we focus on the reforming reaction mechanisms, valid over time scales short compared with the deactivation time.

As Chapter 2's literature review explained, although much is known about reforming chemistry, there is no general argument as to its kinetic mechanism. We begin with some preliminaries concerning the acquisition and interpretation of kinetic data and then proceed to describe our experiments to determine the relevant reactions and their kinetic rates.

4.A. Experimental Preliminaries

We employed the multi-outlet integral reactor (at varying levels of conversion) for most of our kinetic studies. Certain preliminary studies were necessary before beginning

the bulk of the experimental work. Tests with different sizes of catalyst particles at otherwise constant conditions to check for pore diffusion limitations showed no effect of particle size. Tests with various mass velocities and at otherwise identical reaction conditions to check for external mass transfer limitations revealed none (Clem, 1977).

In undertaking kinetic studies, it is imperative to work with a catalyst that has a relatively stable activity and selectivity and, in addition, to operate in a regime of activity and selectivity that is representative of commercial applications. The reactions themselves that take place on the reforming catalysts often undergo very significant and rapid changes during the early life of the catalyst. Rapid changes in product selectivity, that may last from a few hours or days, depending on the severity of operation, can characterize this initial period. One theory is that the rapid formation of an initial carbon level on the catalyst is responsible for this catalyst "lineout" or "equilibration". Under our operating conditions, the catalyst essentially lined out its activity within 20 hours. Clearly, a systematic kinetic study of the effects of space velocity, temperature, pressure or some other process variable would be difficult because of the rapidly changing nature of the catalyst itself. Despite the fact that, the catalyst continues to change during its entire life, its rate of change slows significantly to a time scale of that is long compared with reforming reaction times after this induction period. One can thus undertake an isolated experimental study of the reforming reactions without considering deactivation only at those times.

In our work, we start each run with fresh catalyst and continue anywhere from 80 hours to 250 hours. With such long experiments, we are able to learn about the lineout period, the long term catalyst deactivation and to safely identify the post-lineout period for our reforming reaction kinetics study. In most cases, the data between hours 20 and 40 are used for parameter evaluation.

4. B. The Development of a Reforming Kinetics Model

As discussed in Chapter 2, there are significant discrepancies among the published reaction networks for nC_7 reforming. Our first task is to implement an experimental program to adequately justify an appropriate reaction network that contains a C5 naphthene lump. Perhaps a safe way to do this, i.e., to investigate the reaction paths that comprise the reaction network over a wide range of conversions, is to use two reactor systems: 1). to vary the feed to the microbalance reactor and 2). to vary the space velocity (or contact time) in an integral reactor at otherwise constant conditions -- and to observe the resulting product distributions.

There is considerable justification for obtaining integral reactor data. First, it can shed light on reaction mechanisms by showing how the yields of certain reaction products and intermediates change with increasing contact time. Such information is not available from most differential reactor studies because of the difficulty encountered in preparing feeds with compositions corresponding to different conversion levels. Due to the complex and sometimes ambiguous, i.e., non-unique data analysis problem one encounters with the integral reactor, though, only a few studies of contact time with the multi-outlets fixed bed reactor exist in the literature. Second, integral data as a function of space time provides a more stringent *tests* of a proposed kinetic model than differential reactor data.

4.B-1. Basic Species, Lumps and Kinetic Trends

The major products of nC_7 reforming are toluene, iC_7 (branched heptane) and cracking products (C_1-C_6). Due to the importance of the C5N contribution to the coke formation, as this thesis shows, it is advantageous to segregate out all of the C5

naphthenes as a separate lump, even though this lump's concentration is generally much lower than the other lumps'. Figures 3-21 to 3-25 show typical concentration changes versus time for different lumps. Note that, the reaction and deactivation essentially decouple after the beginning ~ 20 to 40 hours, because the time scale of catalyst deactivation becomes much larger than that of the main reactions. That is, the reactor is quasi-steady at these times and it is sensible to use only the concentration data after ~20 or 40 hours in kinetic parameter evaluation of a deactivation free reforming model. Figures 4-1 to 4-5 replot these data as reactant and product concentrations versus contact time for 5 temperatures. Both the iC_7 and the C5N lumps show maxima, indicating that they are reaction intermediates. The toluene and C_1-C_6 yields increase monotonically with contact time, indicating that they are end products. Note also that after 10 minutes, iC_7 and nC_7 decline concurrently, which, along with the facts that the iC_7's themselves are roughly in an equilibrium distribution, suggests that their inter-conversion reactions may be much faster than all other inter-lump reactions at these times.

Section 2-A reviews the proposed mechanisms for n-heptane reforming. As noted, these models were the products of varying degrees of insight available at the times of their development into the actual reforming chemistry. However after postulating a reaction network, previous investigators (e.g., Froment et al., 1986, 1988; Clem, 1977) derived all of the rate parameters from the comparison of the integrated model equations with individual integral reactor runs, where the concentrations of all species varied with contact time. Chapter 2 notes that such a method can be very insensitive to changes in network structure and for a particular network can lead to more than one set of parameters that give equivalent RMS deviations. Moreover, it is well known that the requirement that a multistep model kinetically describes the data from a particular experiment can tightly constrain certain parameter values while remaining extremely insensitive to variations in other parameter values. Rather, a proper parameter estimation procedure requires multiple

experiments, each of whose design makes its result sensitive to a particular parameter or to a small subset of the parameters. It is then critical to subject rate constants derived in this way to some consistency checks, e.g., to see if these rate constants, at different temperatures, have reasonable, positive activation energies from straight Arrhenius plots.

Thus we examine the mechanisms proposed below and perform specific experiments that target individual reactions. Each experiment attempts to ascertain if a certain reaction occurs at a relevant rate and if so, what its rate constant is. Only after doing a number of such investigations, do we examine the integral data for nC_7 feed to determine the remaining parameters.

For example, Clem's model (1977) discussed previously (see chapter 2) contains 14 reactions, because it allows almost all possible (reversible) reactions between lumps. By feeding pure toluene and hydrogen to the microbalance, one can test whether or not toluene reacts to nC_7 or iC_7. The result shows that toluene is virtually unreactive at 750 K, 207 kPa, H_2/Tol = 3, and 50 WHSV. This indicates that there are no reverse reactions from toluene to nC_7 and iC_7, that is,

$$\text{Toluene} \xrightarrow{x} nC_7 \text{ or } iC_7.$$

Both Clem's and McHenry's prior networks posit that a dehydrocyclization ring closure of nC_7 and iC_7 produces toluene directly and rapidly. To test this, we run the microbalance using 2-methylhexane, the major iC_7 formed in nC_7 reforming, as the feed at 750 K, 207 kPa, H_2/iC_7 = 3, and 50 WHSV. As Figure 4-6 shows, after the initial catalyst transient period, the major products are nC_7 and cracking products. The almost absence of toluene shows that ring closure of this iC_7 molecule is not important compared to that of nC_7. However, comparison with Figure 4-7 shows that the cracking rate of iC_7 is

comparable to that of nC_7. Froment et al.'s (1987, 1988) model is not consistent with these data.

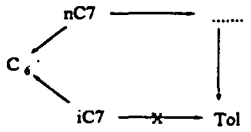

An important question regarding the disagreement between Froment et. al.'s and Mobil's models is: "is the dehydrocyclization reaction i) a direct 6-ring closure; ii) a 5-ring closure to cyclopentane intermediates (C5N) followed by ring expansion to cyclohexane; or, iii) a simultaneous 6-ring and 5-ring closure?" To answer this question, we feed pure ECP and MCP (Figures 4-8 and 4-9) as model compounds of C5N to the microbalance reactor and measure the rate of ring expansion and ring opening in differential operation mode. Aromatics (toluene/benzene) and the normal paraffins (nC_7/nC_6) are the major products of ECP/MCP reforming. Cracking and isoparaffin formation rates are, by comparison, negligible after the initial transient period. In fact they may even require an nC_7 intermediate. It is now a simple matter to calculate the rate constants for the C5N to toluene and C5N to nC_7 reactions from this data. Surprisingly, the rate constant for C5N to toluene measured this way is much smaller than Froment et al.'s (1987,1989) value. This has some critical consequences. Consider the fixed bed reactor data for nC_7 feed in Figure 4-10, after the initial catalyst transient, the reaction C5N $\rightarrow$ toluene with calculated rate constant and C5N concentration shown in the figure and with no other parallel toluene formation pathway is incapable of producing anywhere near the amount of toluene observed even for instantaneous $nC_7 \rightarrow$ C5N rate! This indicates that in addition to 5-ring closure, a simultaneous, direct 6-ring dehydrocyclization also produces aromatics, as shown below.

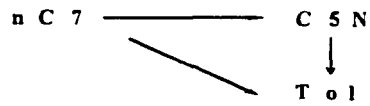

Finally, do we need to include a saturated six carbon ring lump in our nC_7 reforming kinetic scheme? No, because the dehydrogenation of methylcyclohexane (MCH) to toluene is much faster than the other reactions in the network and its concentration is extremely low.

A lumped mechanism for nC_7 reforming that summarized these targeted experiments from both the integral and differential reactors is

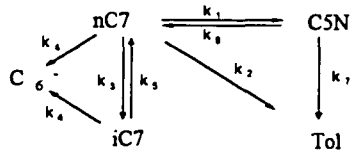

4.B-2. Kinetic Model and Parameter Evaluation

Given a reaction mechanism, the next step is to develop the corresponding kinetics model and then to evaluate the model parameters. This also provides a test, albeit a weak one, of the mechanism itself.

Previous studies (Clem, 1977) and the forms of our traces (Figures 4-1 to 4-5) show that, when, as in our cases, hydrogen is present in large excess, all reaction steps in nC_7 reforming are pseudo first order. Also due to the reactions isothermality, the large excess of hydrogen and the relatively small mole fraction of cracking products, the flow rate

changes only by ~20% from inlet to outlet. Thus the constant density assumption is appropriate. With the same symbol for a species lumps's name representing its concentration, the mass action equations corresponding the above reaction network in a plug flow reactor free of mass transfer effects are:

$$\frac{dnC_7}{d\tau} = -(k_1 + k_2 + k_3 + k_4)\cdot nC_7 + k_5 \cdot iC_7 + k_6 \cdot C5N \qquad (4\text{-}1a)$$

$$\frac{dC5N}{d\tau} = k_1 \cdot nC_7 - (k_6 + k_7)\cdot C5N \qquad (4\text{-}1b)$$

$$\frac{dTol}{d\tau} = k_2 \cdot nC_7 + k_7 \cdot C5N \qquad (4\text{-}1c)$$

$$\frac{diC_7}{d\tau} = k_3 \cdot nC_7 - (K_4 + K_5)\cdot iC_7 \qquad (4\text{-}1d)$$

$$\frac{dC_6^-}{d\tau} = k_4 \cdot nC_7 + k_4 \cdot iC_7. \qquad (4\text{-}1e)$$

Solid-catalyzed reactions occur when molecules from the fluid phase become activated and adsorbed to the surface of the catalyst. The conventional method of treating solid-catalyzed reaction kinetics is based on the Langmuir-Hinshewood models which Hougen and Watson (1947) have thoroughly discussed long ago. These models assume that adsorption occurs on vacant active sites followed by surface reactions and, finally by desorption of the products. To derive the overall pseudo-steady rate of reaction, one selects a surface reaction mechanism and then usually assumes that one of these three steps is rate controlling while the others are almost at equilibrium, i.e., their rate constants

are much larger than that (those) of the controlling step(s). All rate equations derived in this manner have a common form (Yang and Hougen, 1950).

$$\text{rate} = \frac{(\text{kinetic term})(\text{driving force term})}{(\text{adsorption term})^n}$$

where n is a integer, usually 1 or 2, that represents the number of vacant site(s) involved in the reaction; n depends on the particular reaction mechanism. The kinetic term is a group of catalyst-determined constants, that depends only on temperature.

One can interpret the first order rate constants in the model (4-1) as the Langmuir-Hinshelwood kinetic term divided by the adsorption term raised to the appropriate power. The kinetic term, a function of temperature only, is uniform since the reactor temperature profile is nearly isothermal when the catalyst bed is diluted/separated with the same size quartz particles (see Figure 4-11). The adsorption term depends, in principle, on the concentrations of the various species present. However, if one assumes that the H_2/HC mole ratio remains constant throughout the reaction zone, i.e., the number of moles of H_2 and of cracking products C_6- produced are almost equal, and if one also assumes that the adsorption equilibrium constants for all of the hydrocarbons involved are nearly the same, then the adsorption term is uniform as well. In other words, if the following relationship holds for the typical denominator adsorption term, then each of the pseudo first order rate constants will be uniform:

$$[1 + K_{H_2}P_{H_2} + K_{nC_7}P_{nC_7} + K_{C5N}P_{C5N} + K_{Tol}P_{Tol} + K_{iC7}P_{iC7} + K_{C_6^-}P_{C_6^-}]$$
$$= [1 + K_{H_2}P_{H_2} + K_{HC}(P_{NC7} + P_{C5N} + P_{Tol} + P_{iC7} + P_{C_6^-})]$$
$$= [1 + K_{H_2}P_{H_2} + K_{HC}P_{HC}] = \text{uniform when the } H_2/\text{HC ratio is uniform,}$$

where K_{HC} is the common adsorption equilibrium constant for all relevant hydrocarbons. The assumption of similar adsorption properties for these hydrocarbons is not unreasonable (Selman, 1972).

Let us now use the experimental data to evaluate the rate constants at each of five different temperatures. As discussed in 4-B.1, k_6 and k_7 are amenable to direct calculation from differential reactor experiments such as the one in Figure 4-8. This procedure assumes that the rate constants for reactions of ECP are representative of those of all C5Ns. The data in Figures 4-8 and 4-9 support this assertion. Moreover, the mass balance of toluene argument in 4.B-1 yields an estimate of k_2. Next consider the experiment feeding iC_7, Figure 4-6 after the initial transient. Since toluene and C5N are present only in negligible concentrations, the only reactions of our mechanism that can be active in this regime are the exchange reactions between nC_7 and iC_7 and the cracking of iC_7 and nC_7. Since the former reactions are known to be much faster than all other reactions in our mechanism, we include the reaction $nC_7 \rightarrow iC_7$ as well. In fact, it is probably reasonable to assume that this reaction is equilibrated with $iC_7 \rightarrow nC_7$. Moreover, since at a high WHSV of 50, the nC_7 formed does not have enough time to react significantly to tol or to C5N, it is unlikely that it would crack significantly either. Thus, these iC_7 reforming data need only compare with the approximate simplified mechanism

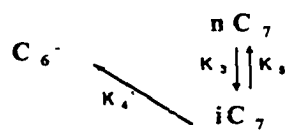

The comparison gives a value for k_4' and at least the ratio of k_3/k_5. Finally, a similar argument for the microbalance run (Figure 4-7) with nC_7/H_2 feed yields an estimate for k_4

and another estimate for k_3/k_5. Before proceeding to the fixed bed nC_7 feed data, let us summarize: we have good values for k_6 and k_7 and reasonable estimates, i.e., rather tight bounds on k_2, the ratio of k_3 to k_5 and k_4'. Moreover, we know from Figures 4-6 and 4-7 that k_4 and k_4' are similar in size. This leaves only k_1 and the magnitude of one of k_3 or k_5 as totally free parameters, with all others either fixed or free to vary only within narrow bands. We take a conservative approach here, preferring to carry over rate constants *bands* from the microbalance differential reactor results to the integral fixed bed reactor analysis rather than actual rate constant *values*. The reasons for this caution are: First, the microbalance run is for a particular iC_7. In contrast, the fixed bed reactor with an nC_7 feed produces a potpourri of iC_7, not just 2-methylhexane (2MH). The rate constants k_5 and k_4' for this mixture, those of interest, should be similar in magnitude to those resulting from the 2MH feed, although not necessarily identical. Second, the microbalance that we use is only capable of running at a total pressure of 207 kPa, as compared with the more relevant value of 517 kPa in the fixed bed. Thus, the theoretical accounting of how P affects species concentrations and the assumed uniform rate-constant-denominator values may not be perfect. Finally, at a WHSV of 30 - 50, the pump delivers 0.05 - 0.08 ml per minute to the microbalance. The imprecision of the pump at these flow rate as well as the fluctuations of this value contribute another source of indefiniteness to the parameter values determined from the differential microbalance data. Thus for all but k_6 and k_7, we carry over rate constant *bands* rather than fixed *values* to the fixed bed data-parameter estimation problem.

Let us finally proceed to the nC_7/H_2-feed integral fixed bed reactor data that Figures 4-1 to 4-6 plot in the form of concentration versus space-time. We used the software package NONLIN to solve the differential equations (4-1) and to estimate the remaining parameters. The program adapts Hartley's modification of the Gauss-Newton method, which minimizes the weighted sum of squares (Metzler, 1969) and the cross products of

the residuals between the observed and calculated conversions, to obtain maximum-likelihood parameter estimates.

At the beginning of the parameter evaluation, we did not assume the same reaction rate constant (k_4 and k_4') for nC_7 and iC_7 cracking. However, even with different initial guesses of the two rate constants, the NONLIN program consistently generated almost identical final values for the two. Hence, in order to reduce the number of fitted parameters, we reran NONLIN assuming that the rate constants of nC_7 and iC_7 cracking are the same, i.e., $k_4 = k_4'$. The model therefore has a total of seven parameters, only two of which are truly free, as compared with 14 in Clem's model. Table 4-1 lists the reaction rate constants so evaluated. Figures 4-1 to 4-5 show that the comparison of the model fits with the experimental data are quite good. A more discriminating test of the model and its parameters is the examination of the Arrhenius plots ($\ln k$ vs. 1/T) for different reaction steps in Figure 4-12. Table 4-1 also lists the activation energies for different reactions. Note how well the rate constants fit the Arrhenius form, i.e., how linear the plots are, and that all yield positive activation energies of reasonable magnitude. The nC_7 dehydrocyclization and cracking have the high activation energies, while the nC_7 isomerization has the lowest activation energy among all the reactions. The activation energies for toluene formation from both C5N and nC_7 are the same for all practical purposes. Also, the activation energies of the reactions $iC_7 \rightarrow nC_7$ and C5N $\rightarrow nC_7$ are comparable, and are much lower than those of dehydrocyclization and cracking. Clearly, these activation energy data give a reasonable and consistent explanation of the experimental effects of temperature in Figures 3-16 to 3-20, i.e., the higher the temperature, the more C5N, toluene and cracking products produced and the less iC_7 formed. This in turn suggests that, the kinetic model and its parameters (activation energies) obtained above are reasonable and can serve as a basis for the simulation and control of nC_7 reforming processes.

Table 4-1. Reaction Rate Constant and Activation Energy Evaluation

Rate Constants	k_1	k_2	k_3	k_4	k_5	k_6	k_7
Reaction T, °K	$nC_7 \rightarrow$ C5N	$nC_7 \rightarrow$ Tol	$nC_7 \rightarrow$ iC_7	$C_7 \rightarrow$ C_6-	$iC_7 \rightarrow$ nC_7	C5N→ nC_7	C5N→ Tol
733	0.376	1.680	7.881	0.939	4.066	1.102	2.769
750	0.685	2.043	7.975	1.367	4.564	1.236	3.729
772	1.207	3.176	8.338	2.653	5.089	1.432	5.013
783	1.600	3.501	8.601	3.089	5.643	1.534	5.920
794	2.010	3.980	8.902	3.400	6.599	1.641	6.896
E, KJ/Mol	132.3	71.7	9.7	108.6	35.7	31.7	71.5

4.B-3. Thermodynamics Considerations

The reaction scheme shows the reactions of $nC_7 \rightarrow C_7$ and $nC_7 \rightarrow$ C5N to be reversible. An independent check of the rate constants determined comes from comparing their values with equilibrium constant estimates from ΔG values based on API-44 free energy data (Rossini, et. al., 1953). Table 4-2 compares the equilibrium constants measured at different temperatures in this study and their literature values. The agreement is embarrassingly good. This further suggests that our model and its kinetic parameters form an adequate representation of both the kinetic and thermodynamics data for this system.

4.C. A Word about Modeling Methods

Let us now illustrate how insensitive a test of a model by fitting the experimental fixed bed data with many undetermined parameters is. Consider our model with $k_2 \equiv 0$, i.e., without the direct C_6-ring closure of nC_7 to toluene. Also, assume there is no direct nC_7 cracking, as Froment et al do. If one uses only the fixed bed data and ignores the microbalance data, NONLIN will find another set of k's to minimize the difference between model solutions and the experimental data. Indeed, Figure 4-13 illustrates that these k values with the corresponding kinetic model provide a fairly good fit of this limited data set. However, this new set of k values is completely different from those shown in Table 4-1. The new k_7 and k_6 do not even come close to describing the ECP - feed differential microbalance reactor data. Moreover, such fits likely give negative activation energies for same reactions. This illustrates how plastic such a process can be: It is dangerous to input a mechanism with many free parameters into a program in order to fit integral reactor data without first doing a series of experiments specifically designed to test the importance and rate of each constituent reaction. No matter what reaction scheme one uses, NONLIN will generate a set of rate constants that minimizes the difference between the experimental data and the model solutions. Simply comparing the experimental data and the model solutions hardly discriminates amongst kinetic models. Thus, experiments that only feed pure nC_7, no matter whether they are differential or integral ones, are not enough for the development of a robust reaction scheme and kinetics model. Unfortunately, many kinetic studies reported in the literature were performed in this manner. Though these kinetic models might correctly predict the experimental data in a certain range, such results are hardly more than curve fitting with meaningless rate constants. There are probably many other equally complex models that could do at least as

Table 4-2. Equilibrium Constant Data Comparison

Rate Constants	k_1 1/hr	k_6 1/hr	K_{16} Measured	K_{16} Calculated	k_3 1/hr	k_5 1/hr	K_{35} Measured	K_{35} Calculated
Temp ^{O}K	$nC_7 \rightarrow$ C5N	C5N$\rightarrow nC_7$	Evaluated in this Work = k_1/k_6	Calculated from Thermodynamics data.	$nC_7 \rightarrow$ iC_7	$iC_7 \rightarrow$ nC_7	Evaluated in this Work = K_3/k_5	Calculated from Thermodynamics Data
733	0.376	1.102	0.224	0.297 (1C2DMCP)	7.881	4.066	1.938	1.539 (2MH) 1.518 (3MH)
750	0.685	1.236	0.554	0.576[a]	7.975	4.564	1.747	1.504 (2MH) 1.500 (3MH)
772	1.207	1.432	0.843	0.748[a]	8.338	5.089	1.639	1.461 (2MH) 1.469 (3MH)
783	1.6	1.534	1.043	1.144 (1C3DMCP)	8.601	5.643	1.524	1.441 (3MH)
794	2.01	1.641	1.225	1.289 (1C3DMCP)	8.902	6.560	1.349	1.422 (2MH) 1.445 (3MH)
E, KJ/Mol	132.3	31.7			9.7	35.7		

(a). Average value of 1-Cis-2-Dimethylpentane (1C2DMCP) and 1-Cis-3-Dimethylpentane (1C3DMCP).
(b). 2MH: 2-methylhexane, 3MH: 3-methylhexane

well in that range. Sometimes, such a model might be useful, but there is hardly a suggestion that it reveals anything about the reaction system. Now, one can never prove that a reaction/kinetics scheme is correct for a complex reaction system, but one can certainly subject it to tests that have the potential to disprove it. By measuring different reaction steps separately and combining the differential and integral methods of experiment and analysis, one might finally approach an adequate kinetics for a complex reaction system, such as nC_7 reforming.

Chapter 5. COKING KINETICS OBTAINED BY FEEDING METHYLCYCLO-PENTANE AS A MODEL COMPOUND OF C5-NAPHTHENES TO THE NEWLY DEVELOPED VIBRATIONAL MICROBALANCE

5.A. Introduction

As noted earlier, it would be very useful to understand and, in fact, to predict the state of coking that an industrial reactor is experiencing during operation. This knowledge would include both the deactivation of the entire catalyst bed as well as the detailed coke profile along the bed. Unfortunately, direct coke measurement *in situ* is not possible because it requires the downloading of the catalyst. All that is easily accessible are samples of the fluid phase. Thus to arrive at the desired information, one needs to develop an understanding of the mechanism and kinetics of the coking process.

As Chapter 2's literature survey indicates, very few coking kinetics studies correlate the coking rate with the actual reaction conditions, such as the partial pressures of hydrogen and of the hydrocarbon, the amount of coke already on the catalyst and the operating temperature. It is manifest that the nature of the coking would depend strongly on the nature of the feed and of the reaction conditions (Cooper and Trim, 1980). However, due to the complexity of the problem, most coking kinetics models thus far have come in the form of Voorhies's correlation, which is nothing more than a power law correlation of the coke amount with time-on-stream (Voorhies, 1945). Others (Beeckman and Froment, 1979; Figoli, et al., 1982; Mieville, 1991;) have gleaned some insight into the kinetics but have not provided an understanding of the origin, nature, or distribution of deposited coke.

In this work, we have set out a program to gain just such an understanding of the coking of a bifunctional reforming catalyst, a complex task (Barbier, et al., 1985). Previous work (Fung and Querini, 1993; Fung, et al., 1994) in our group has suggested, and in chapter 3 we have built a very strong experimental case, that C5 naphthenes are the major source of coke in n-heptane reforming over Pt-Re/Al_2O_3 catalyst. Such knowledge holds out the possibility of predicting how the coke profile in an operating reactor develops with time-on-stream by predicting the amount and distribution of the coke precursor intermediates within the reactor. Of course such a subordinate prediction requires a kinetic model of the reforming reactions that produce the coke precursor. This was the topic of Chapter 4. Alternately, one would like to be able to infer the amount of coke in an operating reactor by continuously *monitoring* the precursor concentration and distribution. A *sine qua non* in both of these approaches is a kinetic understanding of how the precursors generate the coke. Such is the subject of this chapter.

Below, we detail experiments in our newly developed vibrational microbalance to investigate coking kinetics. We feed hydrogen and methylcyclopentane (MCP), the latter as a model compound for C5 naphthenes, into the reactor and study the coking dependence on temperature, on the partial pressures of H_2 and of MCP, and on the amount of coke already on the catalyst. Note that, while MCP itself is not usually present in reformer feeds in significant amounts, the reactions it undergoes are very similar to those of the higher molecular weight cyclopentanes such as dimethylcyclopentanes (DMCPs) or ethylcyclopentane (ECP) that comprise a considerable portion of the naphtha (Selman, 1972). Methylcyclopentane, because it is much more readily available and inexpensive in purified form, is the most convenient model alkyl-cyclopentanes

(C5Ns) to use to investigate the reforming reactions and the coking kinetics that they drive.

Once we have determined an empirical expression for the dependence of the coking rate on the variables just mentioned, we propose a mechanism that relates the coke production and deposition to the catalyst deactivation (rather than simply assuming an activity - coke relationship for coke deposition on active sites only) and a mechanism for the production of coke itself from precursor molecules. Together these models give kinetics that reduce to those observed and are, we believe, at the same time quite reasonable physically. That both of these model components are necessary is well known (Froment and Bischoff, 1961; Wolf and Alfani, 1982).

5.B. Experimental Results and Discussion

5.B-1. General Trends

Figure 5-1 shows typical results of a microbalance-coking experiment. Upon feed introduction, the weight of the catalyst increases sharply (~5 mg) due to the different densities of the hydrocarbon feed and hydrogen gases and due to the initial hydrocarbon adsorption. After this initial increase, we ascribe all further weight changes to coke formation and subtract it from all subsequent total weight gains for the coke data analysis.

From our experiments, it seems that the main parameters influencing the coking rate of a given catalyst in reforming processes are the partial pressures of coke precursor and of hydrogen, the coke amount already on the catalyst and the operating temperature.

Figures 5-2 and 5-3 display the amounts of coke accumulated on the catalyst as functions of time for different partial pressures of MCP and of hydrogen. The experimental results show that increasing the partial pressure of MCP increases coking while hydrogen has the opposite effect. At high hydrocarbon pressures, there are many unsaturated species that are potential coke precursors. Thus, an increasing hydrocarbon concentration increases the rate of coking. A plot of initial coking rates vs. the partial pressure of MCP (Figure 5-7) shows that the order of the coking reaction with respect to P_{mcp} is 1. Some workers have indicated that hydrogen has a negative effect on coking rate, with a negative power of 2 in the range 1-3 MPa (Barbier, et al., 1988). The initial coking rate of our data is indeed consistent with a negative second of coking reaction with respect to P_{H2}. The operating pressure is also an important parameter influencing the coke-fouling of the catalyst. Barbier et al. (1988) have shown that an increasing total pressure with a constant hydrogen/hydrocarbon molar ratio decreases the coking rate. Such a change in the amount of coke deposited parallels the chemical modifications of the coke and the change in the distribution of coke on the metal and on the support. Coke deposited at high pressures is heavier, more dehydrogenated and more graphitic, but less toxic with respect to metallic activity. Figure 5-10 shows the total amount of coke as a function of time for different temperatures.

5.B-2. The Coking Reaction Deactivates Itself

The coking experimental results also show that coke deposition occurs rapidly at first and then more gradually as the coke builds up. Since we operated the microbalance in a differential mode, with the partial pressures and temperatures fixed, the decrease in the rate of coking observed with increasing coke content can only reflect the deactivating effect of coke on the coking reaction itself. That is, the coking reaction deactivates itself

Therefore, the coking kinetic equation must also include a deactivation function ϕ_i multiplying the coking rate that one would have in the absence of coke, i.e.,

$$\frac{dC_k}{dt} = r_0 \cdot \phi_i \ . \qquad (5\text{-}1)$$

Here C_k is the amount of coke per unit weight of catalyst, ϕ_i is the deactivation function for coking, which one determines from experimental coke verse time curves such as Figures 5-2 and 5-3, and r_0 is the initial coking rate at $C_k = 0$, which is a function of temperature and the partial pressures of hydrogen and of the hydrocarbon feed. Since the microbalance maintains these quantities time invariant, r_0 is simply a constant for a given experiment in the microbalance. By assuming different forms of ϕ_i as listed below, substituting them into Eq.(5-1), and integrating the resulting equations, one obtains the following correlations of C_k verse time (t) with r_0 and α as two fitting parameters:

$$C_k = \frac{1}{\alpha}[1 - \exp(-\alpha r_0 t)] \text{ for } \phi_i = 1 - \alpha C_k \qquad (5\text{-}2)$$

$$C_k = \frac{1}{\alpha}\left[1 - \frac{1}{1 + \alpha r_0 t}\right] \qquad \text{for } \phi_i = (1 - \alpha C_k)^2 \qquad (5\text{-}3)$$

$$C_k = \frac{1}{\alpha}[\sqrt{1 + 2\alpha r_0 t} - 1] \text{ for } \phi_i = 1/(1 + \alpha C_k) \qquad (5\text{-}4)$$

$$C_k = \frac{1}{\alpha}[\sqrt[3]{1 + 2\alpha r_0 t} - 1] \text{ for } \phi_i = 1/(1 + \alpha C_k)^2 \qquad (5\text{-}5)$$

$$C_k = \frac{1}{\alpha}\ln[1 + \alpha r_0 t] \qquad \text{for } \phi_i = e^{-\alpha C_k} \qquad (5\text{-}6)$$

In the traditional view, ϕ_i is proportional to the concentration C_* of free active sites. Thus, positing a form for $\phi_i(C_k)$ is equivalent to Cooper and Trim's (1980) and Froment's

(1976) positing the concept of an order of the coking reaction, i.e., $-\frac{dC_k}{dC_\bullet} = \frac{1}{\alpha} C_\bullet^n$ with $n = 0, 1, 2$ etc. and $1/\alpha$ the coking reaction rate constant, to obtain either single or dual site deactivation functions. Note that the deactivation function ϕ_i or, equivalently, $\frac{dC_k}{dC_\bullet}$ is not an explicit function of time-on-stream as in Voorhies' correlation, but only depends on it implicitly via the total coke amount C_k.

A fit of the C_k versus t data according to each of the above $C_k(t)$ expression can provide the deactivation parameter α and the initial coking rate r_0 for the particular model in question for the conditions of the particular experiment. In fact, most of the models (5-2) - (5-6) can fit the data from individual runs. The most robust model should fit the experimental data well, while yielding a reasonable value for r_0 and a model parameter α that is essentially independent of the operating conditions of the different runs. On the basis of this criterion, we find that Eq.(5-6), i.e., the exponential form, outperforms all of the other models.

Table 5-1 lists the α and r_0 values resulting from fitting the coking experimental data for different operating conditions with Eq.(5-6). It shows that r_0 depends on coking conditions. The functional form fits all of the experimental curves reasonably well and yields a relatively minor variation in the value of α, considering the wide range of the conditions.

Froment et al. also report that the exponential deactivation function gives the best fit for a number of processes such as the isomerization of n-pentane (Pauw and Froment, 1975), the dehydrogenation of 1-butene into butadiene (Dumez and Froment, 1976), and the reforming of C_6 and C_7 hydrocarbons (Marin and Froment, 1982; and Trimpont and

Froment, 1986,1988). However, there seems, as yet, to be no physical model for the coking process that gives a reasonable explanation of why $\phi_t = e^{-\alpha C_t}$ fits the deactivation data for so many processes.

Table 5-1. The initial coking rates at different partial pressures of Hydrogen and MCP (T =750 K, P =207 kPa, WHSV = 40)

P_{mcp} ,(kPa)	P_{H2}, (kPa)	r_0,(gcoke/gcat.hr)	1/α, (gcoke/gcat.)
4	155	0.000437	0.0147
21	155	0.002184	0.0169
31	155	0.003523	0.0197
52	155	0.005963	0.0191
69	155	0.009290	0.0177
103	155	0.012957	0.0193
31	103	0.008311	0.0168
31	134	0.004634	0.0163
31	155	0.003523	0.0197
31	176	0.001689	0.0179
31	207	0.000522	0.0159
31	241	0.000327	0.0141

The only attempt at an explanation that we known of is the coking reaction order discussion just mentioned. But, this approach has two problems. First the differential $\frac{dC_k}{dC_\bullet}$ has no clear physical meaning, since the derivative is not with respective to time and thus it is not a rate equation. Second if α were a coking reaction rate constant, one would expect α be an Arrhenius function of temperature with same non-zero activation energy. However, as both our data and the literature data show, α is independent of operating conditions, temperature included. We now propose a new, simple, multilayer coking model which leads to the exponential deactivation function and also explains why α is independent of operating conditions.

5.B-3. Multilayer Coking Model

Figure 5-4 diagrams a new, multilayer coke model:

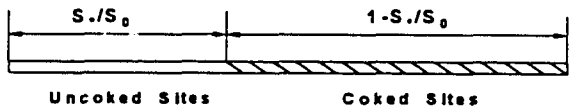

Figure 5-4. Multilayer Coking Model

A fresh catalyst begins with a maximum concentration S_0 of uncoked sites that promote reaction and are susceptible to coking. The uncoked fraction of active sites is S_*/S_0 and the coked fraction is $(1-S_*/S_0)$. The coking of sites (as $C_k \uparrow$) causes the instantaneous concentration S_* of uncoked sites to go down in a manner we shall discuss. As a result,

both the main reaction and the coking reaction will slow as the number of coked sites increases.

Now suppose that a coke molecule forms, presumably on an active site. Suppose further, that rather than automatically depositing itself there, it samples a collection of catalyst sites, both the uncoked and the already totally or particularly coked ones, and then deposits randomly on one of them. The rate dS_*/dt of loss of active sites is proportional to the product of the rate of coking dC_k/dt and the instantaneous fraction S_*/S_0 of sites that are uncoked, i.e.,

$$\frac{dS_*}{dt} = -\beta \frac{S_*}{S_0} \frac{dC_k}{dt} \qquad (5\text{-}7)$$

In Eq.(5-7), β is just a unit conversion from C_k to S_*, and therefore β should be independent of operating conditions including temperature. Note that in this model $C_k + S_* \neq S_0$, since sites already coked can still accept new layers of coke. In fact, this model posits that they take up new coke molecules just as avidly as uncoked sites.

Let $\phi_i := S_*/S_0$. Integration of Eq. (5-7) immediately gives Eq.(5-6) with $\alpha := \beta/S_0$ depending only on the catalyst preparation, which sets S_0, and not on the operating conditions. Although naive, this model explains our empirical findings of Figures 5-2 and 5-3 in the last sub-section.

According to this model's simple view, coke molecules, or at least the products of the rate determining step(s) in coke manufacture, can migrate freely and sample the catalyst surface before depositing. The parameter α does not control the migration, which must only be much faster than deposition, but rather it is a function of the total number S_0

of active sites on the fresh catalyst. A change in catalyst preparation, such as in the amount of platinum on the catalyst could affect S_0 and then change the initial coking rate r_0, which is in principle, also a function of S_0. Figure 5-5 shows coking time traces for three different catalyst platinum loadings in the microbalance and gives the α and r_0 values for each. Note that, the platinum-free catalyst produces very little coke - and, of course, very little reforming products. Both α and r_0 seem, from this limited data, to increase with platinum loading.

This crude picture does not distinguish between metal and acid sites in S_0. One would guess that the number of metal sites increases in proportion to the metal content of the catalyst whereas the acid site number would naturally, be independent of Pt content. That is the total site number $S_0 = s_m S_M + S_A$, S_M = the concentration of metal sites and S_A = the concentration of acid sites. It is likely that the metal sites are more important than the acid sites because the high dehydrogenation capacity of Pt leads to dehydrocyclization of paraffins and subsequent dehydrogenation to unsaturated monocyclic olefin intermediates. These coke precursor would include the alkyl-cyclopentenes, presumably methyl-cyclopentadiene (MCPde) and methyl-cyclopentene (MCPe) (Myers, et al., 1961; Parera, et al., 1984, Barbier, 1986). Indeed, Beltramini et al. (1991) have shown that the selectivity to MCPde and MCPe is enhanced with an increased metal loading. This would correspond to a value of the multiplication factor $s_m >> 1$. Unfortunately, the data are far too scare to evaluate this S_0 relation quantitatively.

If these coke precursors form on the metal sites and, as the model presumes, can migrate to the acid sites (exact mechanism unknown) and sample the catalyst surface before depositing, then one would expect to see both types of sites coked. To examine the type/location of the coke on the catalyst, we performed temperature-programmed

oxidation (TPO) at the end of each run (see Figure 5-6). It is generally accepted that the lower temperature peak (approximately 370 °C) corresponds to coke deposited on, or in contact with the metal site, and the higher temperature peak (approximately 445 °C) is associated with the coke on the acid sites (Fung and Querini, 1992; Beltramini, et al.; 1991, Figoli, et al., 1983; and Barbier, et al., 1980). Figure 5-6 illustrates the plausibility of coke molecule migration by showing that an increased metal content enhances the coke deposition on both type of sites. These results are consistent with those of Beltramini et al.(1991). Barbier (1986) also observed a positive correlation between the metal loading and the extent of coking on the support during the conversion of cyclopentane, cyclohexane, and n-heptane over Pt/Al_2O_3. We can also see from Figure 5-6 that, in fact, *most* of the coke deposits *on the acid sites* for both $Pt\text{-}Re/Al_2O_3$ and Pt/Al_2O_3, while, pure Al_2O_3 does not coke much at all.

5.B-4. A Overall Coking Kinetics Model

Both microbalance and TPO experimental results are consistent with the supposition that coke precursors (MCPde and or MCPe) form on the metal sites due to their dehydrogenation capacity, and then migrate. These alkyl-cyclopent-enes and -adienes, very reactive molecules, can condense with another alkyl-cyclopent -ene and -adiene molecule by a diene-dienophile condensation of the Diels-Alder type to give an indenic structure (Parera et al., 1984; Myers et al., 1961). Lewis acids (Wollweber, 1972), which are present on Al_2O_3 support under reforming conditions (Bakulin, et al., 1974), can catalyze this type of polymerization to polycyclic compounds and eventually to coke.

The dehydrogenation reactions are known to be at least one order of magnitude faster than the other reactions in reforming. It is thus reasonable to assume that the dehydrogenation reaction reaches equilibrium quickly. The reactions' equilibrium constants K_i (i=1,2,...,n) dictate the instantaneous partial pressures (P_1, P_2,...,P_n) of the i-dehydrogenated forms of the hydrocarbon (hydrocarbon)$^{-i}$ which act as the coke precursors on the catalyst and, possibly in particular, on the acid sites. Let P_{mcp} and P_{H2} be the partial pressures of the methylcyclopentane feed and of hydrogen, respectively. Then (Myers et al., 1961),

$$(\text{Hydrocarbon})^{-(i-1)} \xleftarrow[K_i]{\text{metal sites}} (\text{hydrocarbon})^{-i} + H_2 \qquad (i = 1,\ldots,n)$$

with the (Hydrocarbon)$^{-0}$ just the hydrocarbon feed MCP (P_{mcp}) and

$$P_i = \frac{K_i P_{i-1}}{P_{H_2}} \qquad (i=1,\ldots,n) \qquad (5\text{-}8)$$

Some or all of the dehydrogenated forms of the hydrocarbon, may allow polymerization to coke. So, these concentrations, P_i (i=1,...,n) in turn, set the rate of polymerization and hence of the coking. It is well known that there are three basic steps in polymerization: initiation, propagation and termination. If one assumes that the initiation step for the polymerization of P_i is m-th order, with rate constant k_i, and is rate limiting, then,

$$(\text{Hydrocarbon})^{-i} \xrightarrow{k_i} \text{coke} \qquad (i=1,\ldots,n)$$

and the initial coking rate r_0 = polymerization rate is

$$r_0 = \left.\frac{dC_k}{dt}\right|_{C_k=0} = \sum_{i=1}^{n} k_i P_i^{m_i} = \sum_{i=1}^{n} \left(\frac{\prod_j^i K_j}{P_{H2}^i} \right)^{m_i} P_{mcp}^{m_i} \qquad (5\text{-}9)$$

If the m_i turn out to be greater than one, it may be necessary to also consider cross reactions in Eq.(5-9). It is reasonable to assume that the initiation steps for the polymerization of each of the dehydrogenated precursors is of the same order. So, we take $m_i = m$ for $i = 1,...,m$. Let $\kappa_i := k_i \prod_{j=1}^{i} (K_j)^{m_i}$. Then, substituting equations (5-9) and (5-6) into equation (5-1) yields the coking kinetics model

$$r_c = \frac{dC_k}{dt} = \exp(-\alpha C_k) \left(\sum_{i=1}^{n} \frac{\kappa_i}{P_{H_2}^{im}} \right) P_{mcp}^{m}. \qquad (5\text{-}10)$$

Here n and m are integers; again, n represents how many H_2 molecules dehydrogenate from MCP to form the most dehydrogenated major coke precursor. For MCP, n should not be greater than three. So if $n = 1$, the major coke precursors are olefins with only one double bond; if the coke precursors include di-and/or tri- olefins, n is two or three respectively. If one examines the initial rate plots such as Figures 5-7 and 5-8 to determine the orders of the coking reaction with respect to P_{mcp} and P_{H2}, the former will yield m. If the observed order with respect to P_{H2} is 1, 2 or 3, this will indicate that at the operating condition under consideration only the 1-, 2-, or 3- dehydrogenated forms of the hydrocarbon is important as the major coke precursor, i.e., one term in Eq.(5-10) dominates. If, on the other hand, this order turns out to be non-integer, this probably means that more than one dehydrogenated hydrocarbon is contributing significantly to the

coking, i.e., more than one term in Eq.(5-10) is significant. Examination of Figures 5-7 and 5-8 show $m = 1$ and $n = 2$ fit the data extremely well (the data are quite linear). The values $m = 1$, $n = 1$ did not fit well and the corresponding κ value from the hydrogen partial pressure dependence of r_0 was far greater than that from the MCP partial pressure dependence data. With $n = 2$, regressions over the two sets of data give much closer k values. This indicates[1] that the major coke precursors are likely diolefins, rather than mono- or tri-olefins, i.e.,

$$r_c = \frac{dC_k}{dt} = \frac{\kappa_2 P_{mcp}}{P_{H_2}^2} e^{-\alpha C_k}. \qquad (5\text{-}11)$$

In our case, the prodigious coke producers are the methylcyclopetadienes (MCPde) rather than methylclopentene (MCPe), which agrees with previous results (Perera et al., 1984; Barbier, 1986; Beltramini et al., 1991) and (Barbier et al. 1988), the latter, in the range of 1000-3000 kPa.

Parenthetically, we note that we also tried to fit the data with the following Langmuir-Hinshewood model (Froment, !976, 1991; Butt, 1976, 1982).

$$r_c = \frac{dC_k}{dt} = \frac{k_c C_t P_{Hc}}{\left(1 + K_{Hc} P_{Hc} + \sqrt{K_{H2} P_{H2}}\right)^n} \phi \qquad (5\text{-}12)$$

This model gave a rather poor fit for reasonable values of the parameters. If forced to fit our experimental coking data, the model leads to rate parameters, some of which are

[1]Actually, n = 2 ± 0.2 fit the data more or less equally well. Thus even though i = 2 term predominates in Eq.(5-10), it is possible that i = 1 or i = 3 term is not entirely negligible under these conditions. However, since the data do not allow a more precise determination of n, any values of k^1 and k^3 fit from these data would be highly insignificant. Thus, we retain only the i = 2 term in Eq.(5-10).

negative. The Langmuir-Hinshewood approach is based on the competitive adsorption of hydrogen and hydrocarbon species on the catalyst surface. Thus it seems that the hydrogen partial pressure impacts the coking rate mainly by shifting, i.e., reducing the equilibrium concentration of the dehydrogenated coke precursor on the catalyst surface, and not by competitive adsorption. See Chapter 6 for another apparently less important effect of the hydrogen partial pressure.

5.B-5. Effects of Temperature

To compensate for the decline in activity as the catalyst cokes, the operator must gradually increase the temperature in a commercial reformer, which accelerates the rates of parasite reactions, such as coking. Thus the temperature dependence of the coking reactions is quite important.

By fitting the data in Figure 5-10 at different temperatures, we obtain the initial coking rates and the coking rate constants in Table 5-2.

Table 5-2 Coking Rate Constants at Different Temperatures

Temperature, (^{O}K)	Initial Coking Rate, r_0, (gck/gcat.hr)	$1/\alpha$, (gck/gcat.)	Coking Rate Constant, κ_2, (gck/gcat.hr.psi)
733	0.0028	0.0183	0.1890
750	0.00596	0.0191	0.4465
773	0.01313	0.0171	0.8863
793	0.02729	0.0168	1.8421

Since $\kappa_2 = k_3K_1K_2$, appears to be a combination of true rate constants, one would expect it to have an Arrhenius temperature dependence $\kappa_2 = A_o exp(-E/RT)$. The Arrhenius plot in Figure 5-9 yields an apparent activation energy E for the coking reaction of 42.6 kcal/mole and a pre-exponential factor A_o of 1.02 x 10^{12} (gcoke/gcat.hr.psi) for T in the range 733 to 793 K. The value of the activation energy is surprisingly high. It is, however, comparable to the 37 kcal/mole reported by Mieville's (1987) for a reformate feed over a narrow temperature range of 780-789 K. The catalyst in Mieville's experiment was an equilibrated 0.74 wt% Pt on Al_2O_3 which had been regenerated commercially 50 times rather than an active, fresh catalyst with an MCP feed. It is interesting to notice that our activation energy is also close to the 45 Kcal/mol that Zhorov and Panchenkov (1980) report for the coking reaction of aromatics, indenes and aromatics with unsaturated side chains. The high activation process might arise from a change in the catalyst surface itself. Mieville (1987, 1991) argues that higher temperatures change the population of the alumina support's Lewis acid sites, created by dehydroxylation. If these sites are important in coking, the high activation energy might correspond to the dehydroxylation reactions.

The solid curves in Figures 5-2, 5-3 and 5-10 show the comparison of the model's curves and the experimental data for various hydrogen and C5N partial pressures, temperatures and times. For practical purposes, we take the value of α to be the average 56.8 gcat/gcoke of the α values in Tables 5-1 and 5-2.

5.B-6. Robustness of the Model

On the basis of the indicative experiments in Chapter 3 (e.g., Figure 3-32), we concluded that C5Ns were the major coke precursors in paraffin reforming and we based

our coking kinetics studies on the microbalance runs with pure MCP as the hydrocarbon representing all coke precursors, i.e., all C5Ns. It is natural, at this point, to wonder: 1). Can this coking kinetics model predict the coking behavior of other five carbon naphthenes, such as ECP? That is, is there a big difference in coking rates among the alkyl-cyclopentanes? 2). Can this model quantitatively predict the coking data of paraffin (e.g., nC_7) reforming?

The major five-carbon ring naphthenes (C5Ns) that paraffin (nC_7) reforming produces are methylcyclopentane (MCP), ethylcyclopentane (ECP) and the three dimethyl- cyclopentanes (DMCPs). Since cyclopentane is present only in minute amounts in the product, its coking rate does not concern us. We performed coking experiments with nC_7 and ECP, the only seven carbon C5N that was available in purified form, at 750 K, 30 Psi with an H_2/Hydrocarbon ratio of 3. Figure (5-11) shows the excellent agreement between experimental data and the model prediction using kinetic parameters obtained from MCP coking experiments. It also shows that the model can predict the coke buildup for a feed containing 50% MCP in toluene. The prediction of ECP's experimental data is consistent with our suppositions that the conversions of different alkyl-cyclopentanes to the corresponding alkyl-cyclopentadiene proceed at comparable rates and the subsequent polymerization rates are also comparable. The good prediction of the nC_7 coking data based on the concentration of the C5N is also consistent with the assumption used that the bulk of the coke comes from C5N in nC_7 reforming. Thus, it maybe safe to use the coking kinetic model developed in this work to predict the coking behavior of the alkyl-cyclopentane-homologue-reforming as well as of the paraffin reforming. The major point of caution in this explanation is that the hydrocarbon with more carbon atoms may form nontrivial amounts of tri-enes or more highly unsaturated intermediates. As such, they may require more terms in Eq.(5-10).

It is pertinent to make a point regarding the coking tendency of different C5N compounds. Myers et al. (1961) report that methylcyclopentane aged the catalyst only one-tenth as rapidly as cyclopentane, which suggests that alkyl-cyclopentanes do not produce as high a concentration of harmful intermediates as cyclopentane does. This may be because a drain-off isomerization reaction to a 6-membered ring at the acid sites followed by dehydrogenation to benzene or alkylbenzenes at the metal sites (Mills, et al., 1953) is available to alkyl-cyclopentanes but not to cyclopentane itself. For example, if the rate of methylcyclopentane conversion to benzene is faster than to methylcyclopentadiene, then methylcyclopentane processing might well lead to a much lower methylcyclopentadiene concentration than one finds of cyclopentadiene from cyclopentane processing. (Since our data show) If this hypothesis is true for all relevant alkyl-cyclopentanes, our coking kinetics model would explain the radically different catalyst aging rates for cyclopentane and the alkyl-cyclopentanes. Of course, proof of this hypothesis, that the overall conversions of different alkyl-cyclopentanes to the corresponding alkyl-cyclopentadienes are similar and hence the coking rates of different alkyl-cyclopentanes might also be similar if they have similar polymerization rates, would require a significant experimental study.

5.C. Conclusions

In this chapter, we use our newly developed microbalance system with an MCP feed as a model compound of C5N to develop a new coking kinetics model

$$r_c = \frac{dC_k}{dt} = \frac{\kappa_2 P_{mcp}}{P_{H_2}^2} \exp(-\alpha C_k)$$

where $\kappa_2 = 1.02 \cdot 10^{12} \exp(\frac{-42.6}{RT})$ and α=56.8 gcat./gcoke. This model can predict coke levels in alkyl-cyclopentanes and n-heptane reforming after any given time-on-stream for a wide variety of operating variables, i.e., temperature, C5N and hydrogen partial pressures. Our proposed multi-layer coking model leads to a coking rate that decays exponentially and the coking mechanism leads to a coking kinetics that is first order in MCP and negative second order in hydrogen for the microbalance operating range.

Chapter 6. HYDROGEN DECOKING KINETICS

6.A Introduction

In this chapter, we conduct an experimental investigation leading to a kinetic model for another aspect of the coking system, the partial decoking of reforming catalysts with hydrogen. From previous chapters, one can see that hydrogen plays an important role in the coking of reforming catalysts. First, high hydrogen pressures lower the concentration of the coke precursors, thus slowing down the coking rate. Second, hydrogen inhibits the dehydrogenation reactions leading to coke formation. Third, hydrogen hinders the reaction from a reversible to an irreversible coke by an "ensemble effect" (Sachtler and Somorjai, 1983; Jothimurugesan, et al., 1985). Finally, hydrogen plays another role that has not yet been well understood: it can remove some of the deposited coke from the catalyst. It is the last point that we pursue in this chapter.

We stumbled on this later effect when the hydrocarbon feed to the microbalance shut off automatically over a weekend in the middle of a long run. What we found the next Monday, Figure 6-1, was that the catalyst coke content decreased during the period of pure hydrogen feeding. After finding some scatted literature about this effect, we decided to study it more carefully. Let us begin with a brief literature review.

6.B. Literature Review

To understand the mechanism of hydrogen decoking proposed in the literature, one must be cognizant of the prevailing views of the roles of acid and metal sites in coking. In light of the deactivation processes due to coking, it is important to know which of the two functions, metal or acid (Al_2O_3), controls the deactivation behavior of

the reforming catalyst. Many contradictory claims exist in the literature (Shum, et al., 1984). Some works have shown that coking occurs in two stages -- attainment of a quasi-steady state by initial rapid deposition on the metal sites, followed by a slower deposition on the acid sites (Figoli, et al., 1982, 1983; Barbier, et al., 1985a, b). Figoli et al. (1982) and Parera et al. (1983) report that the amount of coke on the metal site after two hours on-oil (lineout) remains virtually constant throughout the reformer cycle and depends strongly on the hydrogen partial pressure. On the other hand, long term coke builds up (up to ~30 wt%) and deactivation occur on the alumina's acid sites (Figoli, et al., 1983). Edgar (1983), Sinfelt (1983) and Sachtler (1984) have shown that, relative to Pt/Al_2O_3, the $Pt\text{-}Re/Al_2O_3$ catalyst has a higher tolerance to the coke deposition that occurs on alumina after the initial coke deposition on the metal sites. As for the metal's role, Shum et al. (1984) show that the metal site controls the dehydrocyclization (the major octane improvement) activity of the catalyst, contrary to Gates et al.'s (1979) theory. Sinfelt (1981) observes that, though the activity of Pt/Al_2O_3 after the initial transient period is higher than that of $Pt\text{-}Re/Al_2O_3$, the former has a much lower dehydrocyclization activity after a long time on oil.

The majority of the prior work on carbon gasification uses temperatures above 650°C, which are considerably higher than typical reformer temperatures (450 ~ 550°C). Very few studies are concerned with Pt-catalyzed coke (Biswas et al., 1987). Further work on model systems has helped shed some light on the detailed role played by transition metals in coke gasification (Katzer,1980). All these prior works give only a qualitative information on the gasification mechanism for carbon deposited on transition metals.

The following diagram summarizes the model for hydrogen decoking that emerges from many of the previous studies (Olander and Balooch, 1979; Rewick et al., 1974; Baker et al., 1980):

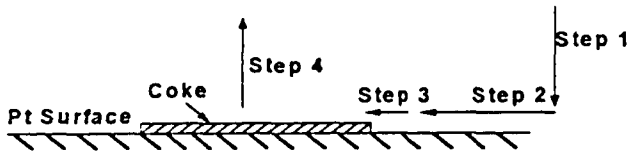

Step 1 Adsorption and dissociation of H2 into atomic hydrogen.

Step 2 Surface migration of atomic hydrogen to coke

Step3 Surface migration of atomic hydrogen onto coke via carbon bridges, (Boudart et al.,1970)

Step4 Metal catalyzed reaction of coke with atomic hydrogen to give methane.

The model assumes that non-catalytic (in the absence of any transition metal) decoking is extremely slow (Katzer, 1980). The first step is hydrogen dissociation on the metal site. Coke covers the metal surface of a platinum-containing catalyst to an extent that only 1-20 percent of the platinum surface sites remain available for chemisorption and dissociation of hydrogen molecules (Davis and Somorjai, 1983). Trim (1985) suggests that the coke then reacts with the dissociated hydrogen. In the slow catalytic gasification process, the low site availability does not adversely affect the overall rate because the rate of hydrogen dissociation is much faster than the intrinsic gasification rate. However, in the case of the faster catalytic hydrogenation of reversible coke, the mode of hydrogen supply, i.e., dissociation of molecular hydrogen or subsequent hydrogen transfer to reversible coke, controls the rate of coke removal (Davis and Somorjai, 1983). The hydrogen transfer reaction is 5-10 times slower than molecular hydrogen dissociation at 300-400 °C. The notion that hydrogen transfer reactions may be important in reforming catalysts is not new. Thomson and Webb (1976) and Gardner and Hansen (1970) both argue that a hydrogen transfer mechanism provides a general

explanation for the patterns of catalytic activity displayed by metal catalysts in olefin hydrogenation reactions. However, these studies do not report the crucial experiments required to distinguish the kinetics of direct hydrogenation and hydrogen transfer.

At different temperatures, different steps may be rate controlling (Bernardo and Trimm, 1979). Rewick et al. (1974) show that the rate determining step for carbon gasification in the range of 700 - 900°C is hydrogen dissociation; in this regime, the reaction is equilibrium limited (Balooch and Olander, 1975; Tomita and Tamai, 1972). Rewick et al.(1974) observe that the hydrogen dissociation and methane formation rates do not balance at lower temperatures, suggesting that another step may be rate limiting. At yet lower temperatures (~300°C) where catalyzed hydrogasification occurs at a negligible rate, Rebell et al. (1964) find that surface migration, rather than hydrogen dissociation, controls the hydrogen uptake. Hence, in terms of the existing model, the rate limiting step for catalyzed coke hydrogasification at typical reforming temperatures (450-550°C) should be either surface migration or the actual gasification reaction. The latter is more likely because surface diffusion across the metal/coke interface is generally fast and leads to interfacial equilibrium (Olander, 1979). Moreover, the hydrogasification rate depends strongly on the amount of deposited coke (Wood and Wise, 1969; Figueiredo and Trimm, 1975; Nishiyama and Tamai, 1976).

As for decoking kinetics, Biswas et al. (1987) did initial coke deposition (1 hour) and removal experiments on the metal site of a Pt-Re/Al_2O_3 catalyst in a standard TGA microbalance. Unfortunately, their data shed little light on the coking and decoking of reforming catalysts due to their short time coking and the considerable measurement errors resulting from significant buoyancy and drag effects of the atmospheric TGA. Also, the atmospheric pressure limitation precluded a partial pressure dependence study.

The mechanism and kinetics of hydrogen decoking on the Pt-Re/Al_2O_3 reforming catalyst are thus ripe for study.

The literature indicates that hydrogen removes only metal-site coke and the quantity of metal-site coke depends on hydrogen partial pressure (Figoli, et al., 1982; Parera, et al., 1983). Below, we investigate this point further with our newly developed microbalance and TPO units to check if this is indeed the case. We shall discuss and interpret our results on the basis of the coking mechanism and the multilayer coking model proposed in Chapter 5.

6.C. Experiments, Results and Discussion

6.C-1. Experiments

The *In situ* hydrogen decoking studies employ our newly developed vibrational microbalance. Chapter 3 and one of our previous papers (Fung, et al., 1994) described the design, development and operation of the microbalance in detail. To perform the decoking experiments, one first needs to generate a sample of coked catalyst. We use methyl-cyclopentane and n-heptane to precoke a bimetallic Pt-Re/Al_2O_3 catalyst, with an N_2 BET surface area of 190 m^2/g and containing 0.3 wt% Pt, 0.3 wt% Re, and 0.9 wt% Cl. The catalyst comes in the form of 1/16" diameter by 0.5" length extrudates. We crushed and sieved the particles and retained the 60-80 mesh (177 - 250 μm) fraction for the microbalance studies. In all the coking experiments, we loaded the fresh catalyst into the microbalance cell and pretreated it overnight with the same hydrogen flow rate (88cc/min. at room temperature) and the same temperature program as in Chapter 3.

The total pressure for all the experiments is 207 kPa (30 Psi) and the weight hourly space velocity (WHSV) is 40~50 g/gcat.hr. Coking experiments were carried out at varying partial pressures of hydrogen and hydrocarbon and temperatures. Once the coking experiment is complete, we stop both the hydrocarbon and hydrogen feeds and turn on the helium flow to strip the physically adsorbed hydrocarbon from the catalyst surface. We then adjust the hydrogen and helium flow rates according to the desired hydrogen partial pressure and collect decoking data under hydrogen (or hydrogen + helium) flow and otherwise reforming conditions for about 30 hours. Thus, we collect both coking and decoking kinetic data with the same catalyst loading. In this way, we need to neither load and download the catalyst nor to heat up and cool down the system. The decoking experiments use various coked catalyst samples, generated under various coking conditions. However, as the data below show, the coking conditions do not seem to affect the measurement of the hydrogen decoking kinetic data.

6.C-2. Results and Discussion

As pointed out in Chapter 5, metal-catalyzed dehydrogenation produces the precursors for the coke that deposit on both metal and acid sites. The literature theorizes that hydrogen removes only metal-site coke (Figoli, et al. 1982, 1983), which is only a small fraction of the total coke. If this were truly the case, metal activity could be recovered by hydrogen decoking. The recovered metal site activity would then produce far more coke precursors, due to its rejuvenated dehydrogenation activity, than it could in its coked state. Paradoxically, this would then *increase* its coking potential when one restarts the hydrocarbon feed after hydrogen decoking and, in the long term, lead to a higher total coke content than if one had never decoked the catalyst, because the enhanced precursor population would coke not only the decoked metal sites, but also the acid sites. Let us explain. From the MCP coking data shown in Chapter 5 (Figures 5-

1 to 5-5), it takes about 10 ~ 20 hours for the coking curve to become linear, i.e., for the metal-site coke to reach its quasi-steady state level, since the metal sites control the dehydrogenation of MCP. But during this period, much more coke accumulates on the acid support than would during the same amount of time in the linear regime. Thus, again, if hydrogen removed only metal site coke, then hydrogen decoking would *speed up* the subsequent coking process and a protocol with hydrogen decoking would ultimately produce more coke than the one without hydrogen decoking.

In order to test the theory that the metal sites control the overall catalyst coking rate, we did coking experiments with catalysts of different metal loadings. Figure 6-2a shows the coking rates of these catalysts with MCP feed and otherwise reforming conditions. Figure 6-2b shows the corresponding TPO spectra for the coked catalysts downloaded at the end of the microbalance runs. From Figures 6-2a and 6-2b, Al_2O_3 alone produces little coke, but the addition of a small amount of Pt results in a significant increase in the coke produced. The more Pt loaded on the Al_2O_3, the stronger the dehydrogenation (metal) activity, and thus -- the faster the coking rate and the more coke accumulates. This is consistent with the theory that the metal activity controls the coking process of alumina-supported bifunctional reforming catalysts. Therefore, if hydrogen removes only the metal coke, the net effect of the hydrogen decoking could be to increase the metal activity, which in turn would speed up the overall coking rate.

Next to test if hydrogen stripping really speeds up the coking process, we carry out the following experiment: In a microbalance coking run, we stop the hydrocarbon feed at 10 hours and let pure hydrogen flow through the coked catalyst for 10 hours at 750 K. After decoking, we feed hydrocarbon for another 36 hours, followed by a second 10 hour hydrogen decoking period, followed by a third hydrocarbon feed period which lasts until the end of the run. Figure 6-3 shows the coking and decoking data for this

run. One sees that the coking rates before and after hydrogen decoking are close to each other. That is, once the decoked amount recovers, the coking process proceeds as if it had never been decoked, i.e., the hydrogen decoking does *not* speed up the overall coking process. This suggests that decoking does *not* preferentially strip metal coke. This prompted us to conduct a detailed TPO study to characterize and to compare the catalyst's coke before and after the decoking.

We conducted several microbalance runs by stopping the MCP feed at different coking times. These runs provide us with coked catalyst samples corresponding to 1 hour, 2.5 hour and 100 hours of precoking. Specifically, the experimental procedure is as follows. After stopping the MCP and hydrogen feed, one cools the catalyst under He flow, picks out some of the coked catalyst for TPO analysis and reloads the rest of the catalyst for hydrogen decoking of up to ~ 30 hours. One then does the TPO analysis on the coked catalyst samples generated before and after hydrogen decoking. Figures 6-4 to 6-6 show the TPO spectra for these catalyst samples. It is generally accepted that the low temperature peak corresponds to coke deposited on, or in contact with, the metal site, and the high temperature peak corresponds to the coke on the acid site (Fung and Querini, 1992, 1994; Beltramini, et al., 1991; Figoli, et al., 1983 and Barbier, et al., 1980). Note that as time proceeds, the proportion of the total coke that is metal coke falls sharply, leading to the acid coke's peak far overshadowing the metal coke's peak even at 2.5 hours. This is because the metal coke seems to be approaching a bounded steady value whereas the acid coke continues to accumulates. Figure 6-4 clearly shows that hydrogen removes both metal and acid cokes. Figures 6-5 and 6-6 show that even when most of the coke is long term acid coke, the acid coke partially strips. This gives direct experimental support of the above argument.

To arrive at a rational explanation for these data, one can discusses the nature of the coke that the hydrogen removes in terms of the multilayer coking model in Chapter 5. According to this model, fresh coke can cover previously deposited coke and can continue to polymerize during the coking process. Eventually, newborn coke will cover it as well. One may then posit that the removable coke is simply the still-exposed, fresh, low molecular weight coke, irrespective of whether it resides on the metal or the acid sites.

This picture is consistent with the TPO results in Figures 6-4 to 6-6: Hydrogen removes most of the initial coke (1 hour); in contrast, only a small fraction of long term (100 hours) coke is removable. The microbalance results in Figure 6-3 indicate that hydrogen can remove most of the initial 10-hour coke. But as the coking process proceeds, this fresh coke continuously polymerizes to larger coke molecule and becomes harder and increasingly less removable. Notice also from Figure 6-3 that, for the same hydrogen decoking period (10 hour), the absolute amounts of removable coke at coking times of 10 and 50 hours are almost the same. This indicates that the total amount of (fresh) removable coke does not change appreciably with coking time after a short initial build up. We suspect that this is because the fresh coke is an intermediate, rather than a final product and its concentration quickly becomes steady. That is: $\text{Precursor} \xrightarrow{k_a} \text{Fresh Coke} \xrightarrow{k_b} \text{Final Coke}$. The formation and conversion of the fresh coke quickly achieve comparable rates, thus leading to an apparent constancy of the removable coke amount. Since the amount of final coke increases with time, the fraction of the removable coke (fresh coke/final coke) decreases with time.

In summary, both TPO and microbalance experiments indicate that, as the coking time increases, the fraction of the removable coke decreases. All of our data support our conjecture that rather than removing exclusively metal-site coke, hydrogen decokes the

fresh, low molecular weight coke, irrespective of whether it resides on metal or acid sites. Moreover, this conclusion is consistent with, and was in fact, suggested by the coking mechanism and the multilayer coking model proposed in Chapter 5.

6.D. Hydrogen Decoking Kinetics Model

To develop a hydrogen decoking kinetics model, we perform microbalance hydrogen decoking experiments and measure the hydrogen decoking rates at different hydrogen partial pressures. We also do hydrogen decoking experiments at different temperatures to determine the decoking activation energy.

Figures 6-7 - 6-10 show coke removal by hydrogen for up to ~45 hours under various hydrogen partial pressures. All of these runs precoke the catalyst by feeding methyl-cyclopentane at 750 K, for the various hydrogen and MCP partial pressures, WHSVs and times listed in Table 6-1. After stopping the MCP and hydrogen feed, helium introduction strips the physically adsorbed hydrocarbons for 10 hours. Following this, the helium flow stops and hydrogen flow at the rate of 75 cc/min. begins. The total amount of coke removed as weight percent of catalyst appears in Table 6-1.

Even after 45 hours (Figure 6-7), the decoking curve has not yet leveled off, but the hydrogen decoking rate does decrease as the amount of coke on the catalyst decreases. This is consistent with the supposition that the gasification reaction is the rate limiting step at typical reforming temperatures. The amount of the hydrogen-removable coke is only 0.2 ~ 0.6 wt%, compared with a total of 3.6 ~ 6.6 wt% coke on the catalyst. This indicates that hydrogen decoking is a very slow process and only a small fraction (~5 - 8.5%) of the long time coke is removable this way within a reasonable time range.

Table 6-1 Precoking and Decoking Conditions

T=750 K

Figure	P_{H2}	P_{mcp}	H_2/MCP	WHSV	Precoking Time	Removing P_{H2}	Coke Removed
	kPa	kPa			hr	kPa	wt%
6-7	155	103	1.5	50	58	207	0.56
6-8	155	20.6	7.5	40	160	103	0.20
6-9	103	4.5	22.9	40	35	158	0.26
6-10	155	52	3	50	62	207	0.39

Table 6-2, shows that the quantity of removable coke correlates with the hydrogen partial pressure of the decoking experiment and the hydrogen-hydrocarbon ratio (H_2/MCP) of the coking experiment: The higher the decoking hydrogen partial pressure, the more coke it removes. Also the higher the H_2/MCP, ratio (i.e., the higher the partial pressure of hydrogen during the precoking period), the less reversible, i.e., the less removable, is the coke formed. Finally, methane is the only detectable off-gas product in the microbalance runs.

From these data, one would like to cull a kinetic model of hydrogen decoking for the range of operating conditions under consideration. Let us begin with the coking scheme from the last section:

$$P \rightarrow NC \rightarrow FC \qquad (6\text{-}1)$$

where P is the precursor, NC is the new or fresh coke and FC is the final, unremovable coke. The decoking hydrogasification process has the following stoichiometry:

$$CH_x + \left(2 - \frac{x}{2}\right) H_2 \xrightarrow{K_h} CH_4 \qquad (6\text{-}2)$$

where consistent with the last section CH_X represents the new coke only and, in principle, $0 < x < 4$. Since the coke is a poly-ring compound, though, all the available data suggests $0.5 < x < 1$. Thus the total coke $C_k = C_{NC} + C_{FC}$, and during the stripping process, C_{FC} is time independent. C_{FC} is simply the final coke after hydrogen decoking for an infinite amount of time, or simply $C_{FC} = C_\infty$. As will be seen, the kinetics of the hydrogasification can reasonably be considered to be first order with respect to the driving force $C_{NC}=C_k-C_\infty$. Then the rate of disappearance of NC during the hydrogen decoking in the microbalance in the absence of diffusion limitation is:

$$\frac{d(C_k - C_\infty)}{dt} = -K_h \cdot P_{H2} \cdot (C_k - C_\infty) \qquad (6\text{-}3)$$

where t is the decoking time, K_h the hydrogen decoking rate constant, and P_{H2} the hydrogen partial pressure. The initial condition is $C_0 = C_{NC}(t=t_o) + C_{FC}$, where C_0 is a function of the precoking conditions (temperature, coking time, partial pressures of hydrocarbon and hydrogen, etc.). Integration of Eq. (6-3) yields

$$C_k = C_\infty + (C_0 - C_\infty) \cdot \exp[-K_h \cdot P_{H2} \cdot (t - t_0)] \qquad (6\text{-}4)$$

Eq.(6-4) is a two-parameter (K_h and C_∞) model. We shall test Eq.(6-4) against the data in Figures 6-7 ~ 6-10 and in Table 6-2 by regressing C_k vs. t data from time t_o onward.

If Eq. (6-3) holds, not only should the curves fit the data, but K_h should be independent of P_{H2}, i.e., only be a function of temperature. Figures 6-8 to 6-10 show satisfactory agreement between the model fits and the experimental data for the hydrogen decoking experiments at different partial pressure of hydrogen. Table 6-2 summarizes the fitting parameters for five different runs. One sees that K_h is nearly constant over a wide range of hydrogen partial pressures.

Table 6-2. Hydrogen Decoking Rate Constants Measured at Different Hydrogen Partial Pressures at T=750 K

Decoking P_{H2}, kPa	Coking H_2/MCP	Coking Time(hr)	C_0, g/g-cat.	Decoking P_{H2}, kPa	$\frac{1}{K_h P_{H_2}}$	$K_h.10^3$ l/hr.kPa	C_∞ g/g-cat.	$\left(\frac{C_t - C_\infty}{C_t}\right)$
207	1.5	58	0.0661	207	12.45	0.389	0.0605	8.46
207	3.0	60	0.0592	207	12.76	0.379	0.0553	7.08
189	3.33	55	0.0426	189	13.27	0.398	0.0399	6.36
158	3.33	24	0.0363	158	16.69	0.380	0.0343	5.59
103	7.5	160	0.0382	103	24.46	0.395	0.0362	5.18

Figure 6-11 is a plot of the product $K_h P_{H2}$ that derives from each data fit vs. P_{H2}. The best fit value for K_h is $0.383*10^{-3}$ $hr^{-1}kPa^{-1}$ at 750 K as shown in Figure 6-11. Moreover, K_h is independent of the initial coke level C_0. These results indicate that the decoking reaction is first order and that Eq. (6-3) adequately models the long term hydrogen decoking experimental data.

To measure the activation energy of the hydrogen decoking reaction, we do experiments at four different temperatures, 750, 773, 788 and 793 K, while keeping the

hydrogen partial pressure fixed at 207 kPa. The data in Figures 6-12 to 6-14 yield the K_h values for the different temperatures listed in Table 6-3.

Figure 6-15 is the Arrhenius plot for the hydrogen decoking rate constant, from which the activation energy turns out to be 9.2 kcal/mol. This value is in the range of diffusion-limited processes. As such, it is conceivable that some fresh, removable coke reside beneath older coke and the retain product must diffuse out. However, aside from the fact that we have no direct evidence of this, it would seem that were this the case, the diffusion path, and hence the rate of coke removal, would change with increasing coke build-up. This, however, does not appear to be the case. See Fig. 6-2. In summary, the hydrogen decoking rate at our experimental temperature range is slow. The low activation energy suggests that hydrogen has to "fish" for the relatively small amount of fresh coke.

Table 6-3. Hydrogen Decoking Rate Constants Measured at Different Temperatures

Temperature, K	$1/K_h.P_{H2}$	K_h*10^3 (1/hr/kPa)
750	12.76	0.383
773	10.97	0.441
788	9.465	0.511
793	9.052	0.534

6.E. Conclusions

1). The Al_2O_3 support (without metal sites) produces little coke. The metal sites, due to their dehydrogenation activity, control coke formation. The higher the metal activity the faster the rate of coking and the more coke produced.

2). Hydrogen can remove both the metal coke and the acid coke.

3). Hydrogen appears to remove only the new coke which is freshly formed at the temperature and pressure of our experiments. Coke that has been "cooked" for a long time becomes virtually unremovable by hydrogen. As time proceeds, the fraction of removable coke declines as the amount of removable coke remains steady and that of unremovable cokes grows. The multilayer coking model from Chapter 5 suggests these effects.

4). The kinetics of coke hydrogasification is first order with respect to both the concentration of new coke and the hydrogen partial pressure. The activation energy is 9.2 kcal/mol over the temperature range of 733 K to 783 K.

Chapter 7. COKE PROFILE PREDICTION AND THE ACTIVITY MODEL

7.A. Introduction

As pointed out at the outset, this research aims to develop a quantitative understanding of the chemistry and kinetics of reforming and of reforming catalyst deactivation for the model system of n-heptane reforming over an alumina-supported Pt-Re catalyst. Chapter 3 determined the reforming reaction participant lump, the C5 naphthenes, that acts as the major precursor for catalyst coke in the system. Chapter 4 developed a kinetic model for the reforming process in question that includes this precursor lump and allows prediction of its concentration along the fixed catalyst bed. Chapter 5 combined experiment with theory to provide a coking model that gives the local rate of catalyst coking as a function of the local concentration, i.e., the partial pressures of hydrogen and of the coke precursor. The philosophy of this work has been that the chemistry and kinetics of the main reaction and of the coking reactions are intimately connected and that an adequate understanding of one requires deciphering how the other interacts with it. In particular, to understand the main reaction properly, one should be able to account for how the rates of its major reactions change over time scales characteristic of catalyst aging. To claim to understand the coking, one should also be able to predict coke profiles as functions of on-oil time and of bed position based upon the knowledge of the precursor profile. Thus, in this Chapter, we complete the circle by combining the coking model (Chapter 5) with the reforming kinetics model (Chapter 4) to answer both of these expectations. We also connect the primitive activity measures of Chapter 3 with the more detailed coking kinetics of Chapter 5 and investigate their consistency. Finally, it is important to note that when hydrocarbon is present in the feed, the rate of hydrogen decoking of Chapter 6 is insignificant relative to

the coking processes and thus does not contribute significantly to the overall picture in the presence of the hydrocarbon feed. Let us begin with the prediction of the coke profile in the multioutlet fixed-bed reactor.

7.B. Coke Profile Prediction

Can one use the coking kinetics model in Chapter 5, based on the coking behavior of MCP in the microbalance, and a knowledge of the partial pressures of C5N and H_2 for each section of the bed to predict the nC_7 reforming coke profile in the integral multioutlet reactor? Before answering this question, let us consider a few facts about the experiment.

Due to their designs, the microbalance operates at a maximum total pressure of 241 kPa, while the multi-outlet reactor operates at 517 kPa in most experiments. MCP is used as feed in the microbalance. Therefore, C5N partial pressure can range from 3.62 to as high as 103.4 kPa in the microbalance. n-Heptane is fed into the multi-outlet reactor. Thus, low C5N partial pressure in the range of 1.31 to 3.58 kPa is experienced in the reactor. The H_2 partial pressure varies between 103.4 to 241.3 kPa in the microbalance but maintains approximately at 387.7 kPa everywhere along the bed in the multi-outlet reactor due to the a H_2/hydrocarbon ratio of 3 being employed. Thus, the H_2 partial pressure and, in particular P_{H_2}/P_{MCP}, is much larger in the reactor than in the microbalance. Recall, in Chapter 5's development of the coking model, the term $\kappa_2/P_{H_2}^2$ dominates κ_1/P_{H_2} and was the only term retained in Eq. (5-10) as shown in Eq. (5-11). In the reactor, however, the much higher P_{H_2} might make the two terms comparable and thus permit (and require) determination of κ_1. Moreover, at even higher P_{H_2} one would expect the κ_1/P_{H_2} term to dominate.

To see if this is indeed the case, we attempted to use Eq.(5-11) directly to predict the multioutlet reactor's coke profile. As expected, while qualitatively predicting the observed (via TPO) coke profile, Eq. (5-11) systematically underestimates the coke amount. On the other hand, integration of Eq.(5-11) for time invariant P_{MCP} and P_{H_2} with 2 replaced by a phenomenological parameter N yields

$$C_k = \frac{1}{\alpha}\ln\left(1+\frac{\alpha P_{MCP}}{P_{H_2}^N}\kappa_N t\right) \tag{7-1}$$

and a fit of the reactor coke profiles yields a best value of N ~ 1.75. This again argues that both the $i = 1$ and $i = 2$ terms in Eq.(5-10) contribute significantly at reactor hydrogen pressures, i.e., both MCPe and MCPde are important coke precursors here. Returning now to Eq.(5-10) for $n = 2$, we have

$$\begin{aligned} r_0 &= k_1 P_{MCPe} + k_2 P_{MCPde} = \frac{k_1 K_1 P_{MCP}}{P_{H_2}} + \frac{k_2 K_1 K_2 P_{MCP}}{P_{H_2}^2} \\ &= \frac{\kappa_1 P_{MCP}}{P_{H_2}}\left(1+\frac{\kappa_2/\kappa_1}{P_{H_2}}\right) \qquad \text{where } \kappa_2 = k_2 K_1 K_2, \quad \kappa_1 = k_1 K_1 \end{aligned} \tag{7-2}$$

Combination with $\phi = e^{-\alpha C_k}$ as in Eq.(5-11) and integration for time invariant P_{H_2} and P_{mcp} yields

$$C_k = \frac{1}{\alpha}\ln\left(1+\alpha\frac{\kappa_1 P_{MCP}}{P_{H_2}}\left(1+\frac{\kappa_2/\kappa_1}{P_{H_2}}\right)t\right). \tag{7-3}$$

α and κ_2 are already known from the low P_{H_2} microbalance regime. This leaves κ_1 as the only unknown parameter in Eq. (7-3). The reactor data include GC-determined P_{H2} and P_{MCP} for each section of the bed, and end-of-run TPO analysis of the coke in each section. Thus, the fixed-bed coke data for these runs and Eq.(7-3) lead to the κ_1 estimates in Table 7-1. The average value of κ_1 is 0.025 (gcoke/gcat.hr). Figure 7-1

compares coke amount calculated from Eq.(7-3) by using the average κ_1 with the measured coke profiles. Figure 7-1 shows that the predicted overall coke profile tracks the measured coke profile for the whole bed including section 1's coke data. Since section 1 accounts for only the first 5% of the catalyst bed, a low prediction for the coke in this small part does not affect the overall coke profile prediction in Figure 7-1.

Table 7-1[1]. Evaluation κ_1 and Prediction of Coke Profile
T=750 K, P_{H2}=387.7 kPa

Section Numbe	Space Time (min)	Bed%	P_{C5N} (kPa)	On-oil Time (h	Coke measure by TPO (g/gcat.)	Coke Predicte by Mode (g/gcat.)	κ_1 (g/gcat.hr	αr_0
1	0.45	1.5	1.30	170.3	0.0279	0.0186	0.0696	0.0061
1	0.50	1.7	1.27	224.3	0.0286	0.021	0.0557	0.0060
1	0.55	1.8	1.32	240.5	0.0292	0.0221	0.0519	0.0062
2	1.05	3.5	2.32	170.3	0.0298	0.0245	0.0424	0.0093
2	2.31	7.7	2.85	224.3	0.0318	0.0305	0.0285	0.0135
3	3.33	11	3.43	170.3	0.0317	0.0293	0.0317	0.0162
3	4.29	14	3.40	224.3	0.033	0.0329	0.0256	0.0161
2	6.00	20	3.56	240.5	0.0317	0.0345	0.0194	0.0168
4	7.50	25	3.10	170.3	0.0259	0.0281	0.0201	0.0147
4	10.0	33	2.79	224.3	0.0304	0.0302	0.0257	0.0132
3	15.0	50	2.65	240.5	0.0273	0.0305	0.0182	0.0125
4	30.0	100	1.30	240.5	0.0187	0.0219	0.0162	0.0061
Averag							0.025*	0.011

* Section 1's data neglected, average of the nine data points based from reactor sections 2, 3 and 4 (see discussion in text).

[1]Table 7-1 lists coke data for three reactor runs with different space velocities and run times (170, 224 and 240 hours). In analyzing the coke data from the microbalance, we subtract the initial, sharp weight increase (~0.6 wt%), due to adsorption and density change, from all subsequent total weight gains. We do the same here, i.e., subtract this amount (0.6 wt%) from the TPO coke to obtain the C_k for estimating k^1 with Eq.(7-3).

The variation of the κ_1 values in Table 7-1 requires comment. First, since N~1.75, the $P_{H_2}^2$ term in Eq.(7-3) still dominates. Thus, extraction of κ_1 from such data is rather inaccurate and small errors in the data can lead to large errors in the calculated κ_1 values. This can easily lead to a variation of a factor of two in the determination of κ_1 from data of different runs or different exit ports. Conversely, the predicted coke values are not very sensitive to the precise value of κ_1 in that a factor of two change in κ_1 does not change the prediction by more than a few percent. Nevertheless, it is important to note that the κ_1 values based on coke data of section 1 are higher than those obtained based on the coke data of other sections. This may very well be because the coked catalyst samples from section 1 might be contaminated. In typical runs, we loaded only 0.09 to 0.3 g catalyst into section 1. When discharging the catalyst, the reactor is vertical (up and down), with section 1 catalyst being unloaded first. In most cases, one has to tap the reactor with a hammer to discharge the coked catalyst. During this process, either a small amount of soft coke that had formed in section 2 or even a small bit of coked catalyst from section 2 can drop down into section 1. Since section 1 only has a very small amount of catalyst to begin with, this can lead to an enormously percentage error in the TPO-measured coke amount for section 1. That is why we did not use section 1's coke data to evaluate average κ_1 as shown in Table 7-1. It also explains why with this average κ_1, the predicted coke amounts of section 1 are lower than the TPO measured data in Figure 7-1. Since other sections contain much more catalyst than section 1, the percentage change due to such contamination is small and, in any case, one can always pick the coked catalyst particles located in middle of this section while unloading the catalyst for subsequent TPO analysis. Thus, the contamination possibility for these sections is much less than section 1. In fact, it is impossible to contaminate section 4, since there is no coked catalyst above it.

Thus, the identification of C5N as the major coke precursor and the development of its coking mechanism and kinetics provide a powerful tool for predicting the coke profile in a reformer by simply monitoring gas phase C5N's concentration on-line. This is a significant accomplishment, since the coke profile is a important initial condition for the simulation model of the reforming catalyst's regeneration process. Moreover, to the best of our knowledge, there are no models in the literature that can predict the coke profile. In practice, one might not want to open holes, along the commercial fixed bed reformer to monitor the C5N concentration profile. In principle the models of Chapter 4 can provide this profile for a given on-oil time. Even though this profile should vary slowly as a function of on-oil time, a reasonable coke prediction would require knowledge of how it evolves. Moreover, one would like to know how the reactor's performance degrades with on-oil time. To these ends, we extend the multilayer coking model of Chapter 5 to predict the time evolution of free, uncoked surface sites. If the reforming reaction is surface site dependent, then this should lead to a prediction for the on-oil-time variation of the reaction intermediates (C5N) and products which one can compare with experiment.

7.C. Activity Model

We now investigate what the multilayer coking model of Chapter 5 predicts for the time evolution of the uncoked surface sites. This will lead to predictions for how the reformer performance evolves over coking time scale. Recall the multilayer coking model relates the time rate of change of the number density $S_\bullet$ of uncoked sites to the rate $\frac{dC_k}{dt}$ of coke production by

$$\frac{dS_\bullet}{dt} = -\alpha S_\bullet \frac{dC_k}{dt} \qquad (5\text{-}7)$$

Integrating Eq.(5-11) gives $e^{-\alpha C_k} = (1+\alpha r_0 t)^{-1}$ or $\frac{dC_k}{dt} = \frac{r_0}{1+\alpha r_0 t}$. Inserting this into Eq.(5-7) and integrating for a time invariant P_{H_2} and P_{mcp} gives

$$s = \frac{S_a}{S_0} = e^{-\alpha C_k} = \frac{1}{1+\alpha r_0 t}. \qquad (7\text{-}4)$$

For reaction models that introduce deactivation due to site coverage, the activity of the corresponding rate constant k_i decays according to $k_i = k_i(t=0)s^p$, where p is the number of surface sites involved in the reaction. In section 7.C-1 we shall make just such a test while in section 7.C-2 we shall compare Eq.(7-4) with the primitive activity measure defined in Chapter 3.

7.C-1. Can This Activity Model Predict The Time Evolution of The Reaction Network Developed in Chapter 4?

As just noted, the multilayer coking model predicts that if a reforming catalyst deactivates due to site coverage by coke, then the reaction rate constant at any time k_i(t) should follow

$$k_i(t) = k_i(t=0)s = \frac{k_i(t=0)}{(1+\alpha r_0 t)} \qquad \text{for } p = 1. \qquad (7\text{-}5)$$

To use Eq. (7-5) to predict any time's reaction rate constants, one has to know α, r_0 and a set of rate constants at a certain time t_0. Chapter 4 determines the reforming reaction rate constants $k_i(t=40)$ at 40 hours' on-oil; Chapter 5 finds α to be 56.8, and the initial coking rate $r_0 = \frac{\kappa_1 P_{C5N}}{P_{H_2}}(1+\frac{\kappa_2/\kappa_1}{P_{H_2}})$ is easy to determine for any run with prescribed P_{H_2} and P_{C5N} since we have just found κ_1 and κ_2 in the last section. Table 7-1 lists the r_0 varies along the catalyst bed for three runs discussed in section 7-B. Since the C5N

partial pressure changes along the bed, so does r_o, but the variation of r_o is at most ±50% from the mean. To simplify the problem, we apply the average value of αr_0 listed in Table 7-1 into Eq. (7-5) to predict the time evolution of the reaction rate constants.

We have described the experiments in Table 1 previously (see Chapter 3). These experiments feed nC_7 into the fixed bed reactor for up to 200 hours at each of 12 space velocities and five temperatures. Chapter 4 develops a kinetic model with 5 lumped species. The experiment keeps track of the time evolution of each of these lumps for each space velocity, i.e., exit, for each temperature. In Chapter 4 we detail, for each temperature at t = 40 hours, the procedure for evaluating the rate constants. It involves combining the results of a number of microbalance experiments to determine or to tightly bound most of the rate constants and then inputs the reactor's different on-oil time's concentration versus space time data into the NONLIN program to obtain the remaining rate constants, all at the corresponding on-oil time.

With k_i(t=40), one can use Eq. (7-5) to predict the reaction rate constants at any time. The lines in Figure 7-2 represent the model-predicted reaction rate constants from time 0 to 200 hours.

We would now like to input different lump's concentration versus space time data at t = 70, 100 and 130 hours, respectively to the NONLIN program as in Chapter 4, to determine the reaction rate constants at each of these times and to compare them with these predictions. Recall that Chapter 4 used pure ECP feed data to determine k_6 and k_7. Unfortunately, due to cost constraints, we do not have long-time ECP feed data to measure k_6 and k_7 at long on-oil times; thus, there are no long-time data for these two rate constants. We evaluate the other five rate constants at long times in two ways. One way assumes that these two rate constants' decays obey Eq. (7-5). Thus, one can

calculate any time's k_6 and k_7 with Eq. (7-5) and input these two predicted rate constants with tight bounds for k_1 - k_5 into NONLIN program to find other five rate constants at the corresponding time, as in Chapter 4. The other way is simply to input the c vs. τ data for a particular longer time — without making any assumption as to what k_6 and k_7 are. We then let the NONLIN program blindly search all seven rate constants at once with the provision that the initial guess for each k_i is its value at the last time and its value is allowed to vary at most by 50% from that value. We found that the five rate constants k_1 to k_5 obtained by both methods are quite close, even if the k_6 and k_7 values end up being different. The symbols in Figure 7-2 are the results for k_1 to k_5 obtained by the first method. Clearly the activity model proposed here predicts the evolution of all the reaction rate constants extremely well. That is, the reforming kinetics model (Eq. 4-1) in Chapter 4, with rate constant that vary with on-oil time, can predict the reformer's product profile (5 lumps: iC7, nC7, Tol, C5N and cracking products) at any on-oil time. This suggests that the proposed multilayer coking model is a good model, not just for the coking but also for the deactivation of the paraffin reforming system. Furthermore, with the predicted C5N profile, one can also predict the coke profile along the catalyst bed at any time. This completes the overall kinetics package for n-heptane reforming; it allows prediction of both the product and coke profiles at any time and position along the catalyst bed.

7.C-2. How Does The Activity Deriving from The Multilayer Coking Model Compare with Chapter 3's Primitive Activity Measure?

Before developing the multilayer coking model, we used a primitive, phenomenological activity model $a = e^{-K_d t}$, adapted from the literature, to analyze the n-heptane conversion data in Chapter 3. At that time our goal was to get a qualitative picture of how the activity varied with space time τ and on-oil time t. Now with our

more sophisticated understanding of the multilayer coking model, we find the deactivation function $s = \frac{1}{1+\alpha\sigma_0 t}$ in Eq.(7-5). Do the two models agree? Do they agree quantitatively? If not, then why was the earlier model adequate? Finally, does the latter model add to our understanding of the former?

Let us begin with the question, do they agree functional form? From Taylor's Theorem with or without remainder,

$$e^{-K_d t} = \frac{1}{e^{K_d t}} = \frac{1}{1+K_d e^{K_d \xi} t} \qquad (0<\xi<t)$$
$$= \frac{1}{1+K_d t+(K_d t)^2/2+0(K_d t)^3} \qquad (7\text{-}6)$$

For values of t such that $K_d t << 1$, one can neglect terms beyond the linear term in the denominator and find agreement with Eq.(7-4) for the identification $K_d = \alpha\sigma_0$. Phrased according to the remainder theorem, $\alpha\sigma_0 = K_d e^{K_d \xi}$, where, in principle $\xi = \xi(t)$ with $0 < \xi < t$. For $K_d t$ not large with respect to one, ξ should be a weak function of t and one can use this later identification of $\alpha\sigma_0$ for ξ a constant. From Chapter 3, we see that $K_d \le 3\times10^{-3}/hr$ and, for the runs discussed there, $t \le 200$ hr. Thus $K_d t \le 0.6$ and as a result, all of the activity models in Table 3.2, are equivalent for the data analyzed there. Only much longer time data ($\ge$ 2000 hours) of the Chapter 3 type, or the microbalance experiments of Chapter 5 could reasonably distinguish them[2].

To verify that Eq.(7-4) reduces to the models in Chapter 3 for the multi-outlet fixed bed data considered there, we check that the K_d from Chapter 3 satisfies K_d (or $K_d e^{K_d \xi}$, for some $0 < \xi < t_{run}$, t_{run} being the on-oil time of the run, or K_d^* if we refit the

[2]On the other hand, one can construct an argument similar to that in appendix I of Chapter 3 to explain the variation of the apparent main reaction constant k with τ for any of those models -- so that basic reasoning should be activity-model independent.

data in Chapter 3 to the model $a = \frac{1}{1+K_d^* t}$) proportional to r_0, i.e., to P_{C5N}. Figure 7-3a shows that both K_d and K_d^* plots are reasonably linear, especially considering that each K_d or K_d^* value is itself a best fit of many data to a phenomenological equation. Figure 7-3b shows that K_d^* also qualitatively tracks the coking and C5N profiles. So, it appears that the activity function $e^{-K_d t}$ reduces to a form equivalent to $\frac{1}{1+\alpha r_0 t}$ when $K_d t << 1$ as in Chapter 3, but is much more accurate over a wider range of times for our model system. It is still an open question as to whether these forms are the appropriate ones for other systems. To address this, consider Shum et al's (1987) n-hexane reforming data over a catalyst similar to ours in a single-outlet reactor. Using the same K_d-analysis for their single-outlet reactor as we did for each of the four outlets of our fixed bed system, they found that they required two parameters, a short-time K_d value and a long-time K_d value, to fit their data (see Figure 7-4a taken from Shum et al, 1987). If indeed the form Eq.(7-4) is more appropriate for their system as well, then it should fit both their short- and long-term data with a single αr_0 parameter value. Figure 7-4 shows that for $\alpha r_0 = 0.0095$, this is in fact the case, where we have read the data as accurately as we could from Shum et al's figure.

Before concluding that the two models agree, though, there are two final points. The first, is that such agreement would require the y-intercept in Figure 7-3a to be zero, particularly for the K_d^* plot. This does not seem to agree with the data. The second point is that one can perform a more precise check on the possible equivalence under discussion. In section 7.B, we found the parameter values for κ_1 and k^2 which allow an evaluation of $\alpha r_0 = \alpha \frac{\kappa_1 P_{C5N}}{P_{H_2}} (1 + \frac{\kappa_2 / \kappa_1}{P_{H_2}})$ that is independent of the K_d or K_d^* fit of the reactant nC_7 concentration versus time data. The values of K_d and K_d^* determined previously and of αr_0 from this calculation all appear in Table 7.2.

Table 7-2 K_d, K_d^* and αr_0 Obtained at Different Space Velocities

T = 750 K, P = 517 kPa, H_2/nC_7 = 3

WHSV	2	4	6	8	10	14	18	26	57	110	120	133
Space tim	30	15	10	7.5	6	4.29	3.33	2.31	1.05	0.55	0.50	0.45
$K_d \times 10^3$	0.41	0.98	1.89	2.0	2.50	2.75	2.69	2.54	2.65	2.24	1.80	1.45
$K_d^* \times 10^3$	0.71	0.94	2.19	2.4	2.79	2.61	3.76	3.66	3.34	3.14	2.58	2.16
$\alpha r_0 \times 10^3$	6.1	12.5	13.2	14.7	16.8	16.1	16.2	13.5	8.3	6.2	6.0	6.1

A quick perusal of these data shows that rather than αr_0 equaling K_d or K_d^*, it is systematically larger, varying from 2 to more than 10 times the latter values. The discrepancy does not lie in the difference in the functional forms, since the K_d^* fit has removed this (minor) difference.

The answer to this riddle is that although $a = \frac{1}{1+K_d^* t}$ and Eq.(7-4) are the same functional forms, they derive from very different models. The activity in Chapter 3 derives solely from reactant, i.e., n-heptane, conversion versus time data. As such it is just a qualitative measure of the activity in a reaction system as complex as n-heptane reforming, which contains reactions that not only consume, but also produce n-heptane. That it is a valid qualitative measure is a result of what we learned in Chapter 4 --that the sum of the rates of the reactions that consume n-heptane, all of which are first order, is a few times larger than the rates of the reactions that produce it.

The activity model Eq.(7-4), on the other hand, is the result of a mechanistic model of coke deposition on the catalyst surface. As such, the appropriate comparison is not with the qualitative activity model of Chapter 3, but rather with the activity or activities that one can infer, once one has established a mechanism for the main reaction, by seeing how each of the main reaction rate constants decays over coking/deactivation time scales. This comparison as shown in Section 7.C-1, turns out to be quantitatively excellent for, in fact, all of the main reaction's rate constants.

Thus, in the absence of an established detailed mechanism for the main reaction, one relies on the phenomenological activity models in Szepe and Levenspiel (1987; although, one might want to include an explicit dependence on the coke amount in the expression for *da/dt* — their equation (15) or (19) — to distinguish it from the concentrations of the main reaction participants) as we did in Chapter 3. However, when such a mechanism exists, it facilitates the calculation of much finer activity measures. In our case, these measures for each reaction would have led to a single αr_0 measure that, as Figure 7-5 shows, indeed tracks the measured coke profile. Since, in our case, αr_0 is proportional to P_{C5N}, both track the coke precursor concentration profile equally well.

7-D. Recommendations for Future Work

a). Different total pressure coking kinetics.

b). Dimethyl-cyclopentane reforming reaction and coking kinetics.

c). Comparison of commercial feed with the results obtained with the model compound nC_7.

d). Coke regeneration kinetics with the vibrational microbalance.

e). Comparison of reaction and coking kinetics of different catalysts, such as sulfided catalysts, nickel, etc.

f). Check if the multilayer coking model can predict the coking/deactivation behavior of other reaction (catalyst) systems.

Multi-outlet Fixed Bed Reactor with On-line GC Analysis

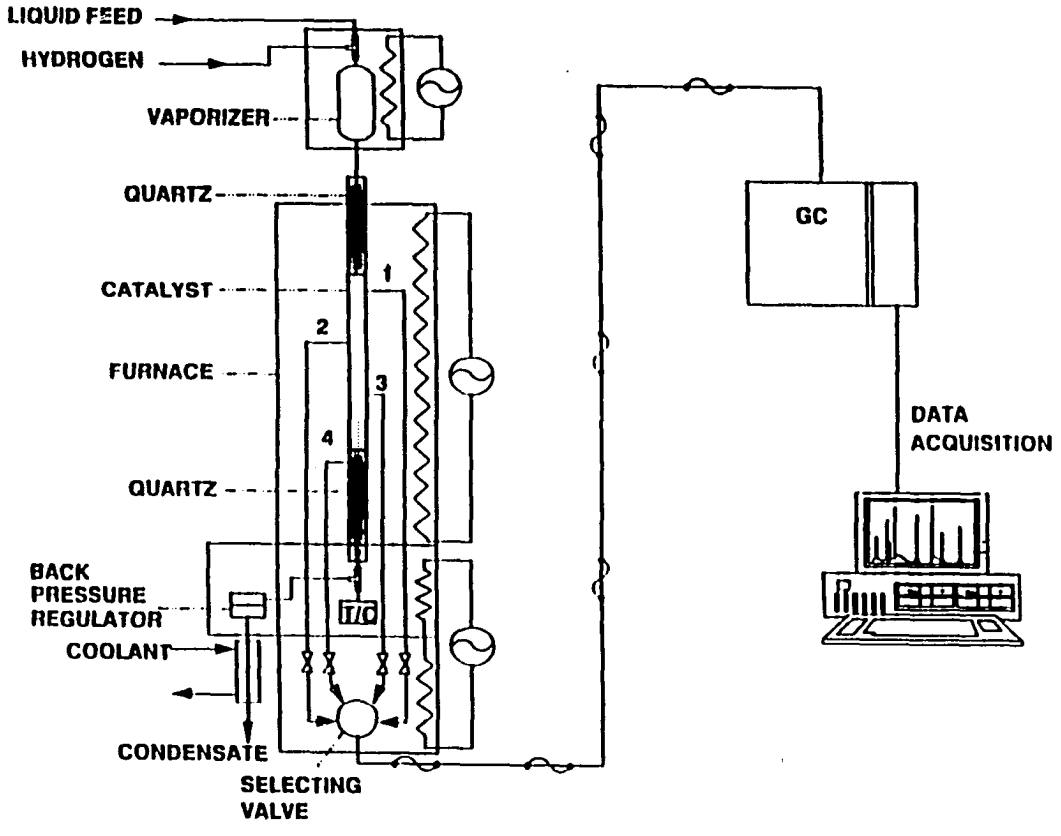

Figure 3-1

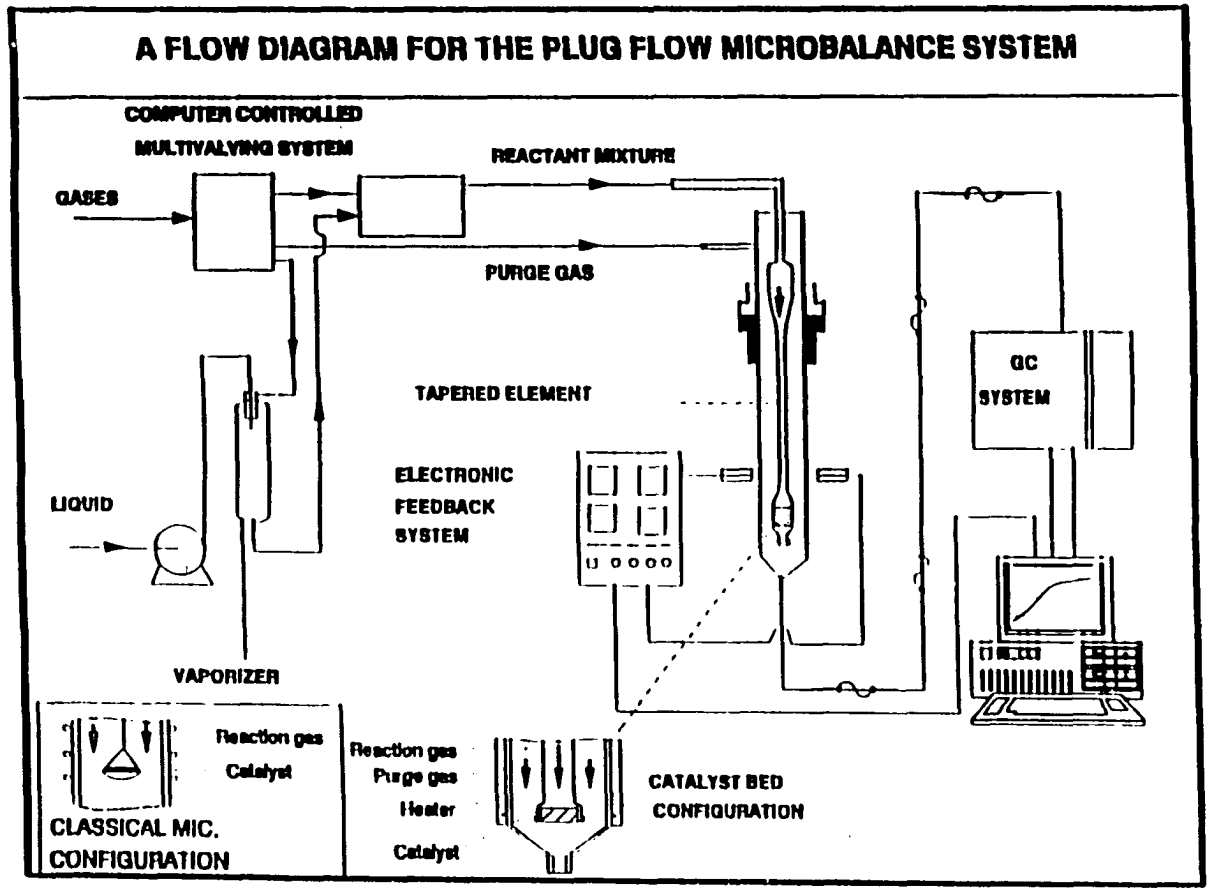

Figure 3-2

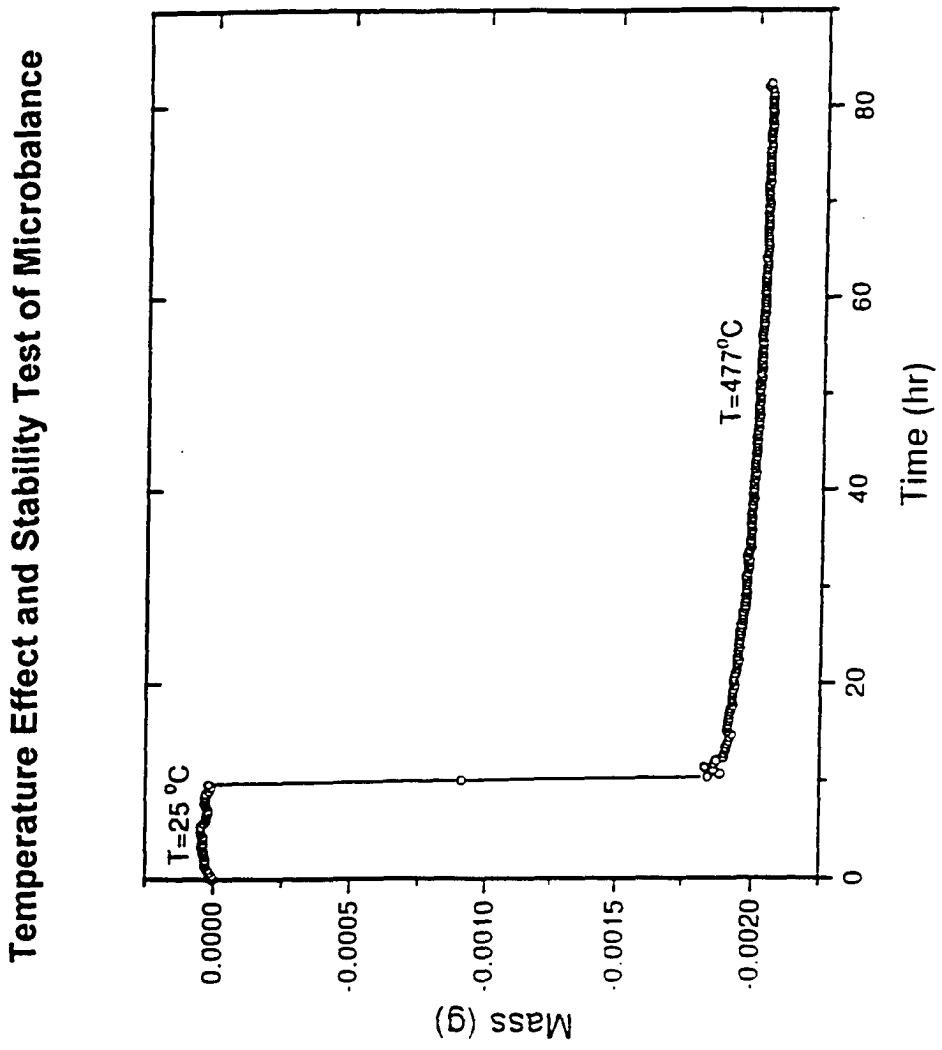

Figure 3-3

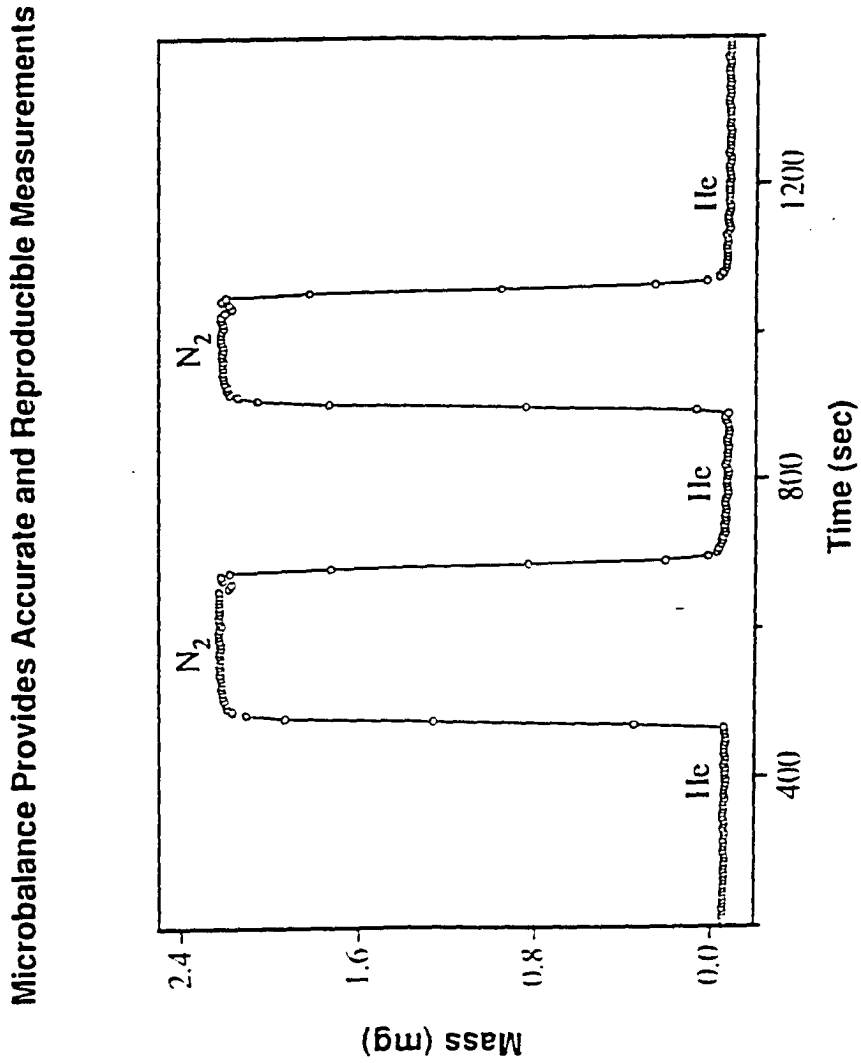

Figure 3-4

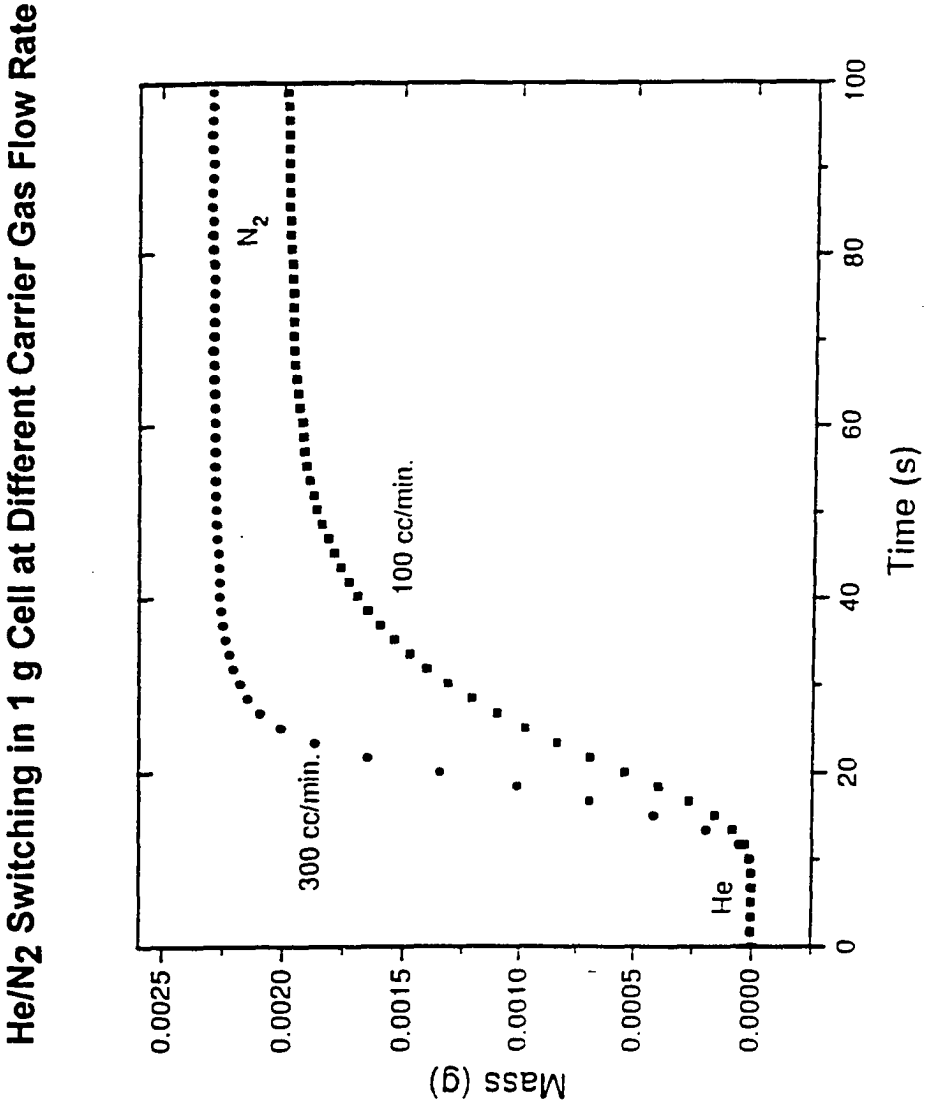

Figure 3-5

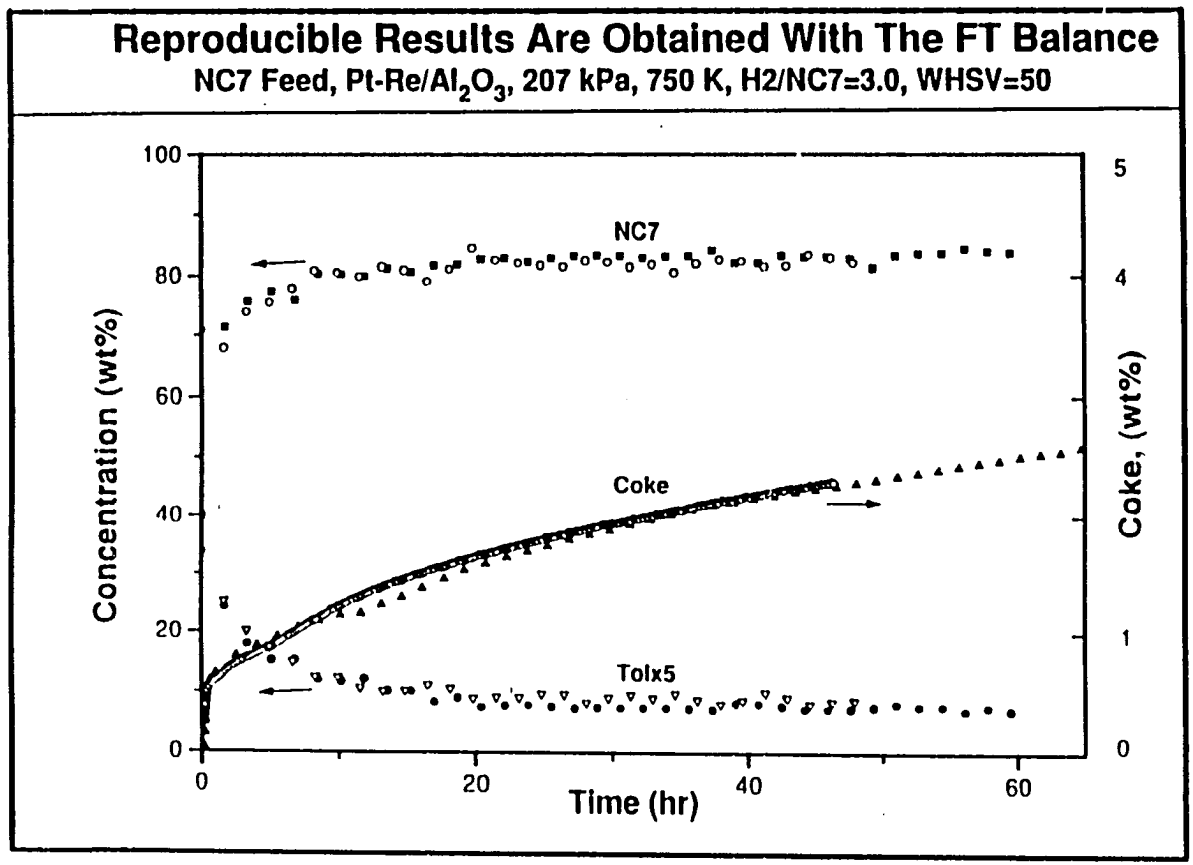

Figure 3-6

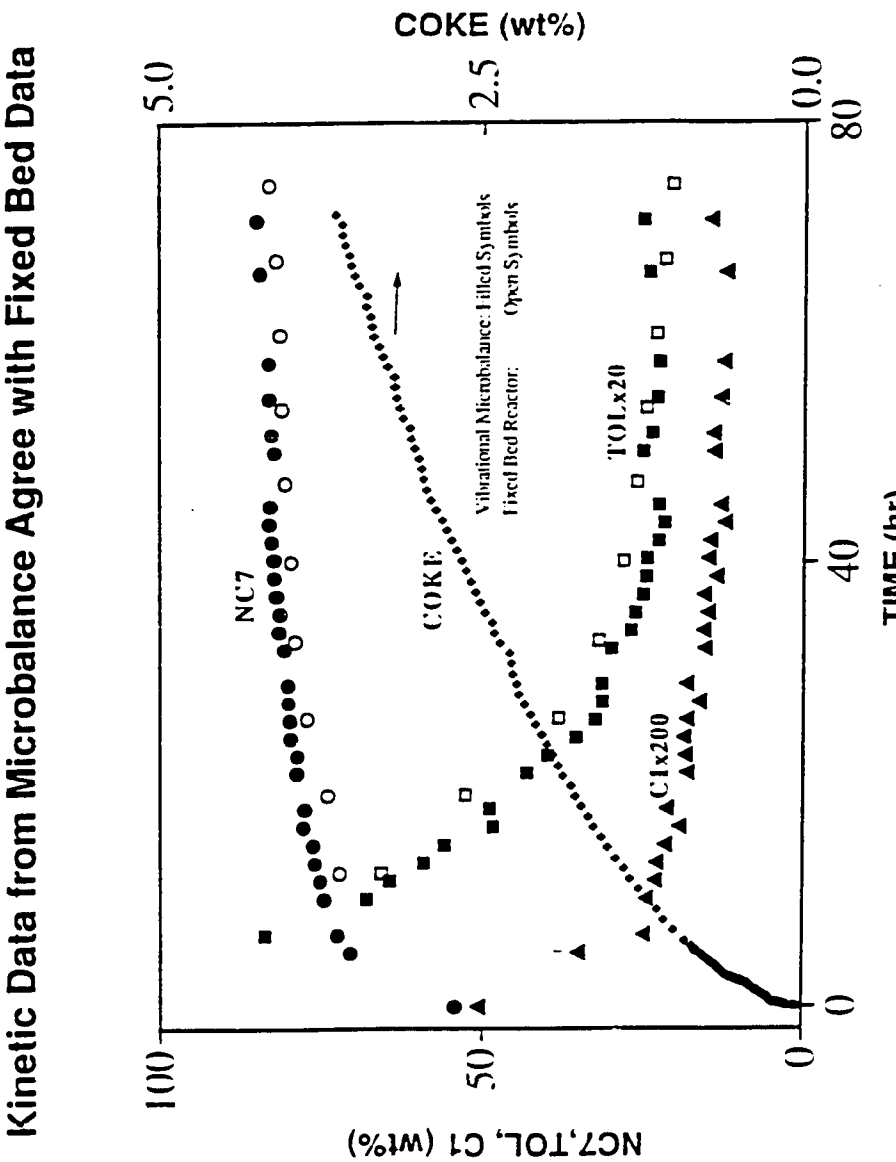

Figure 3-7

Faster Coking Rate at Lower Space Velocity

207 kPa, 750 K, H_2/HC=3.0

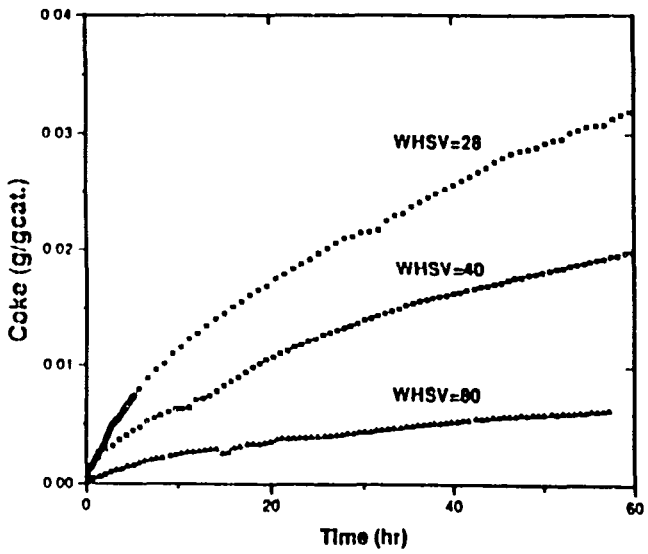

Figure 3-8

More C5N Produced at Lower Space Velocity

207 kPa, 750 K, H_2/HC=3.0

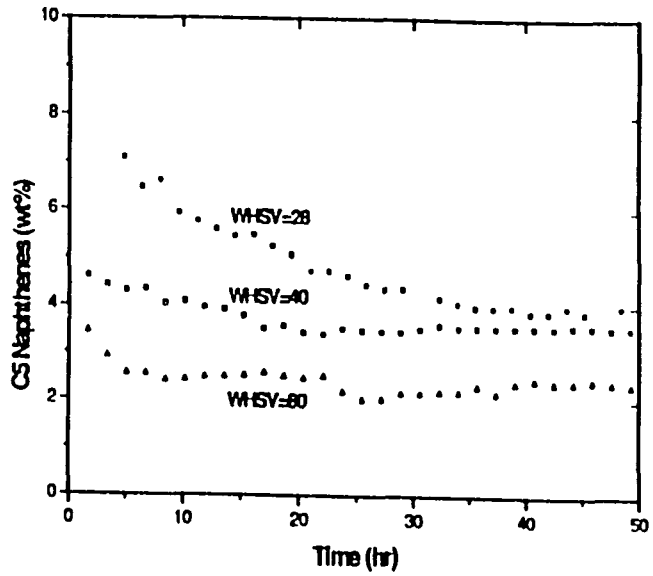

Figure 3-9

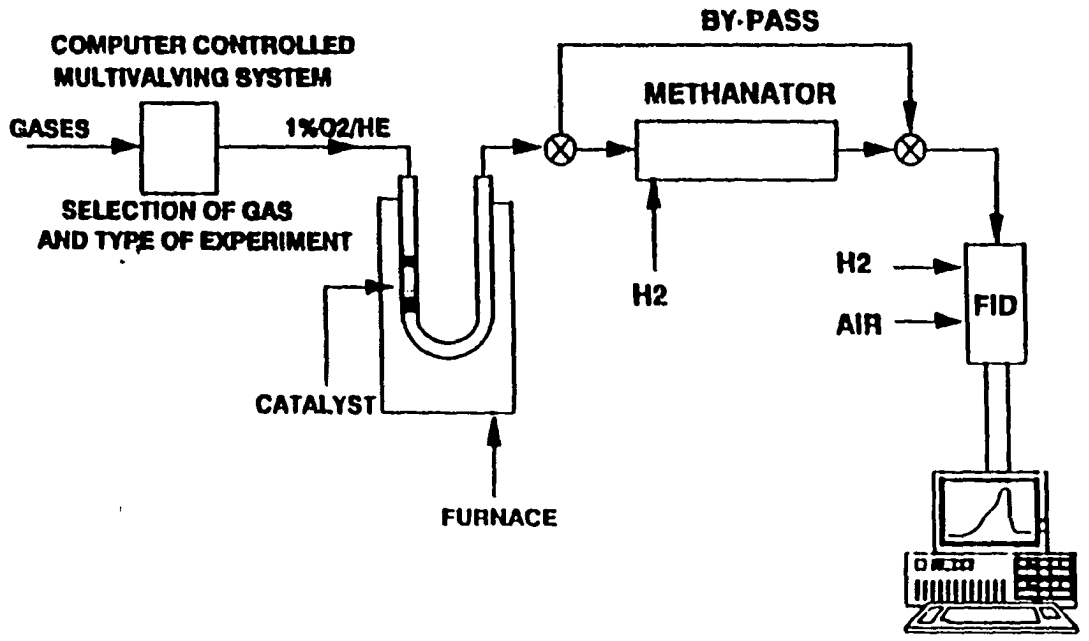

Diagram of temperature programmed oxidation unit.

Figure 3-10

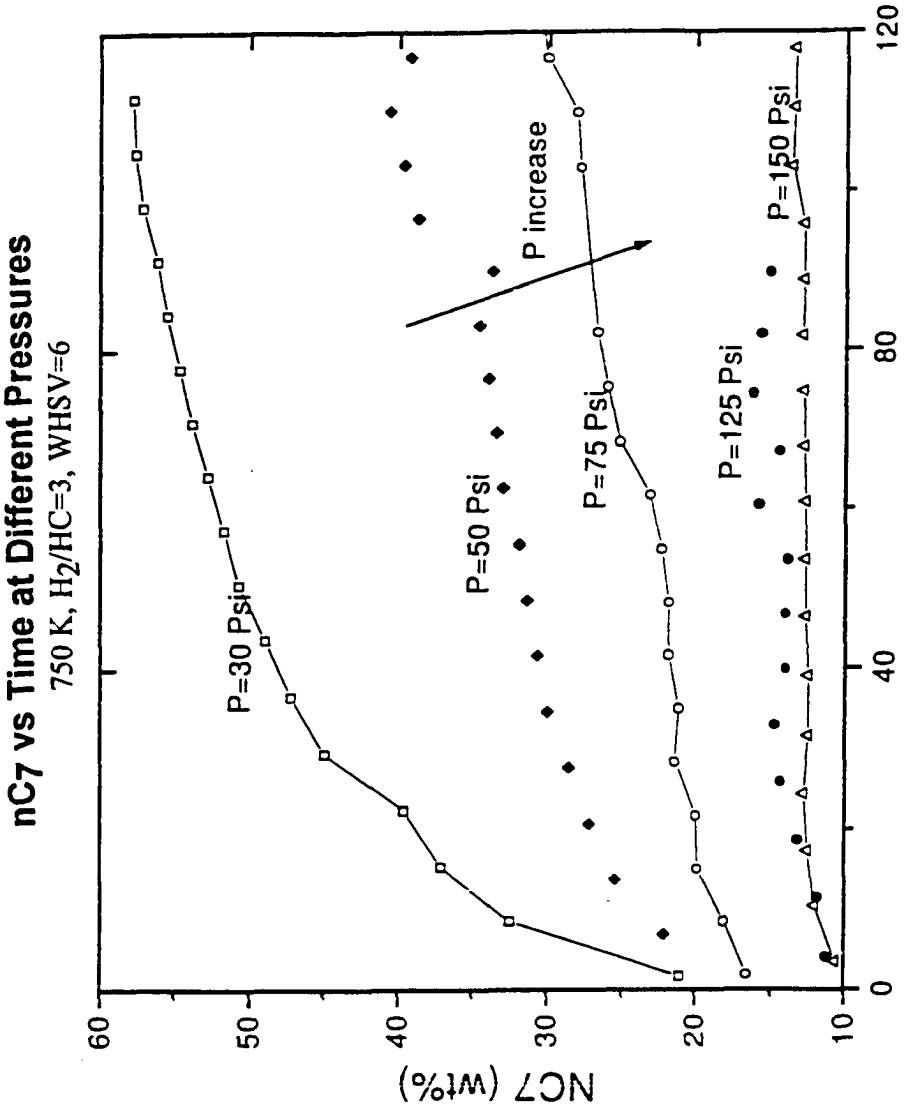

Figure 3-11

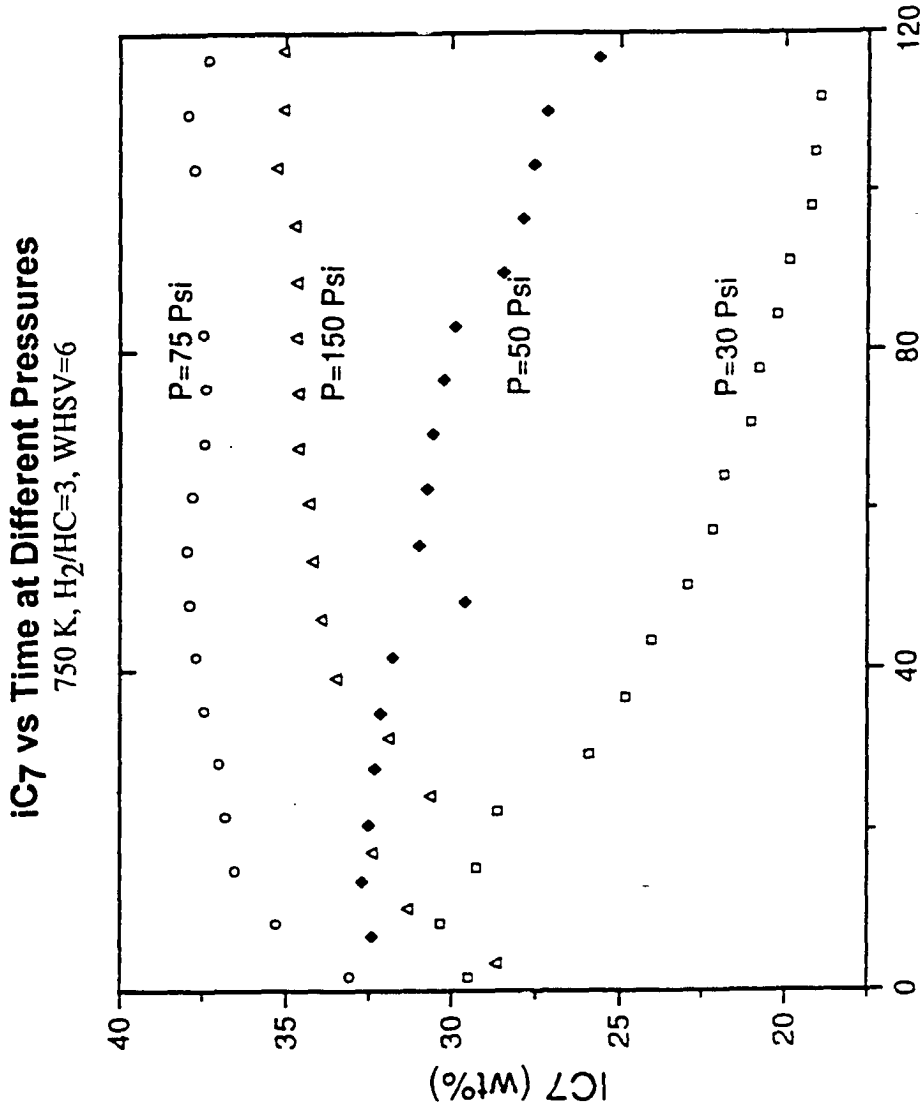

Figure 3-12

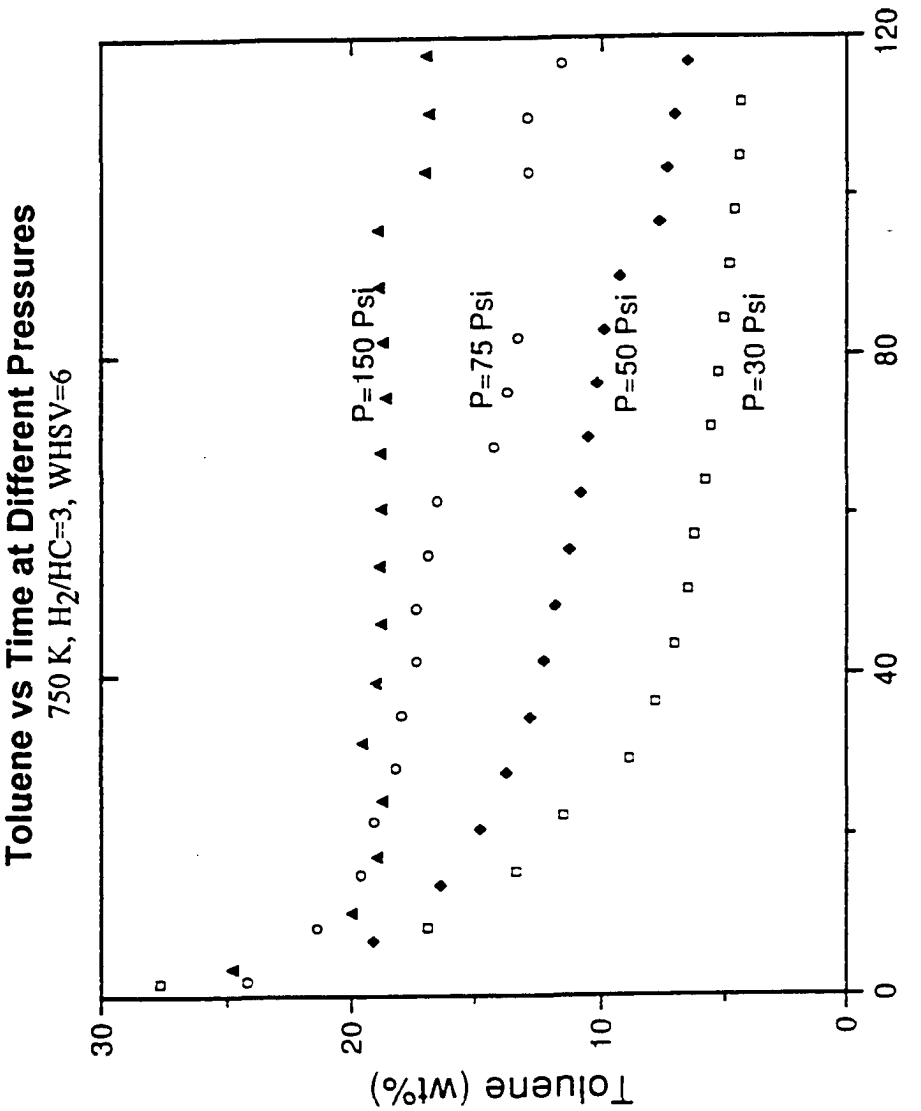

Figure 3-13

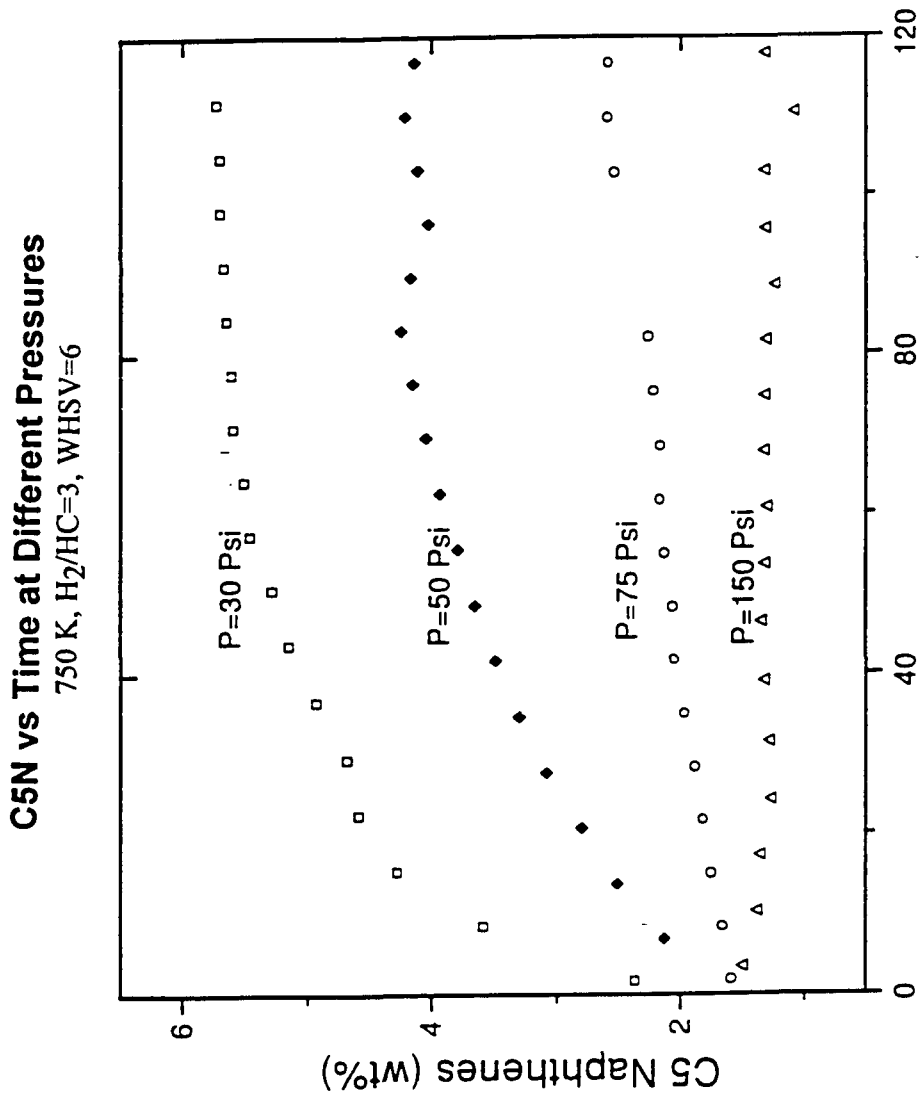

Figure 3-14

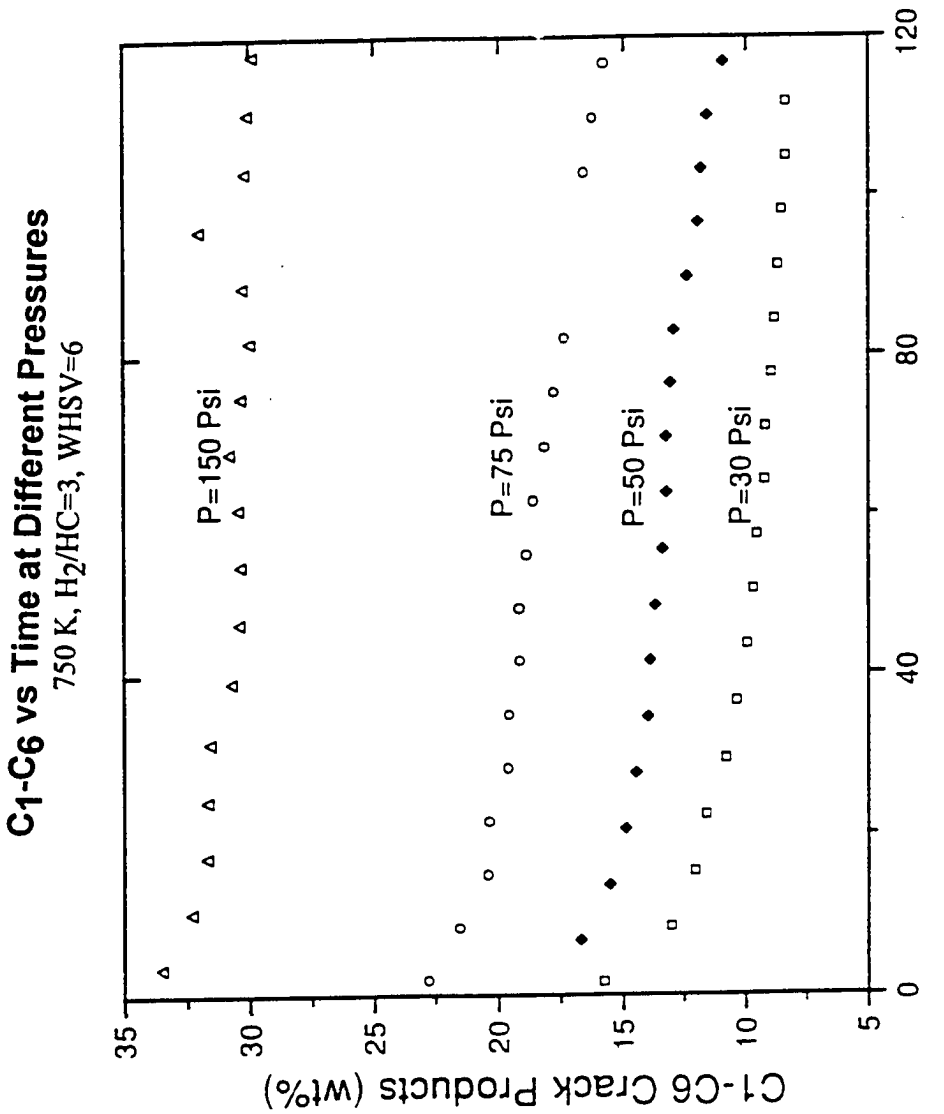

Figure 3-15

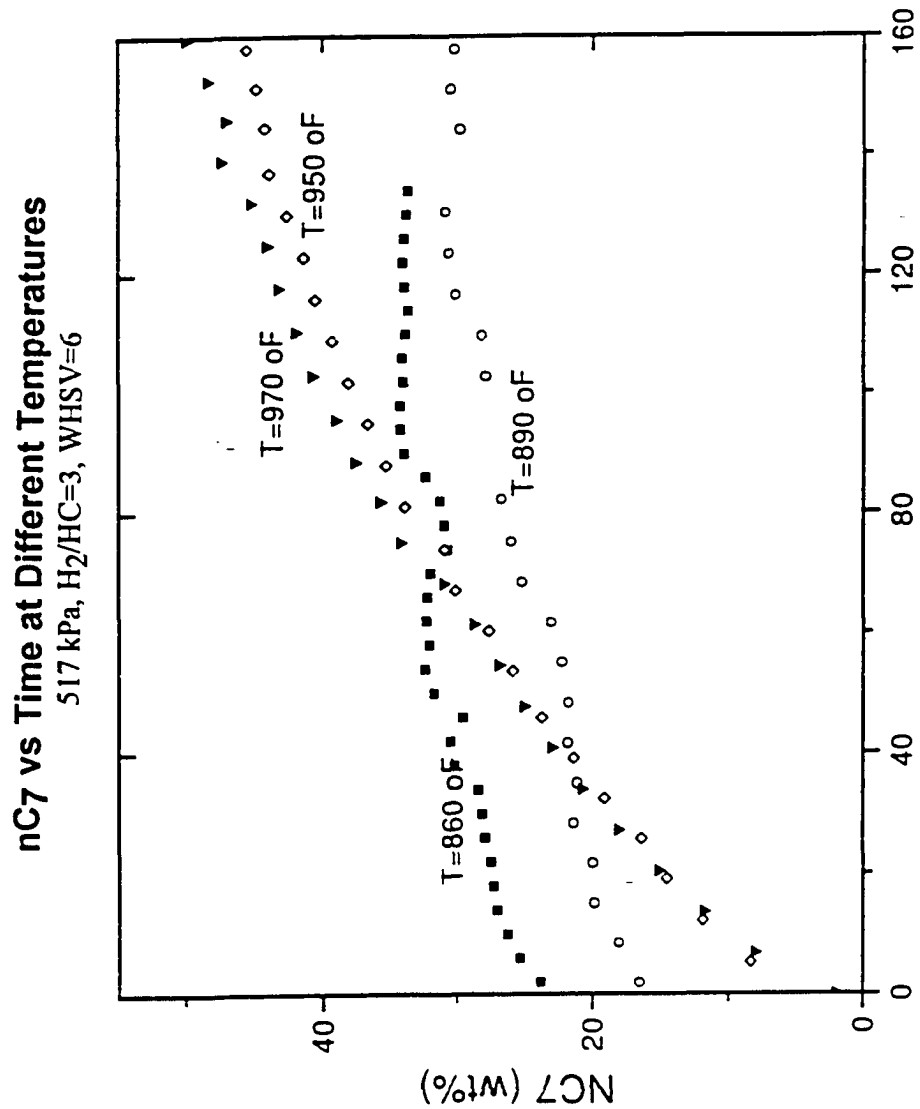

Figure 3-16

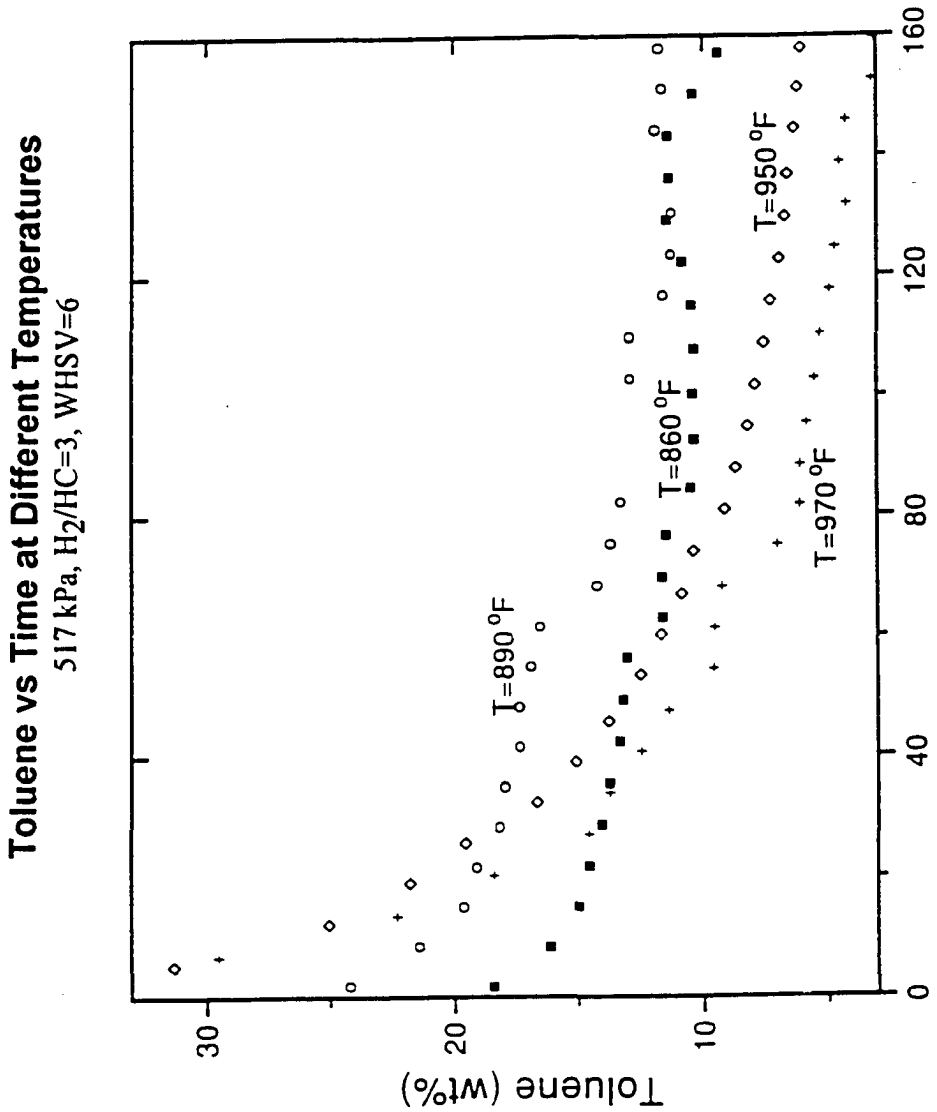

Figure 3-17

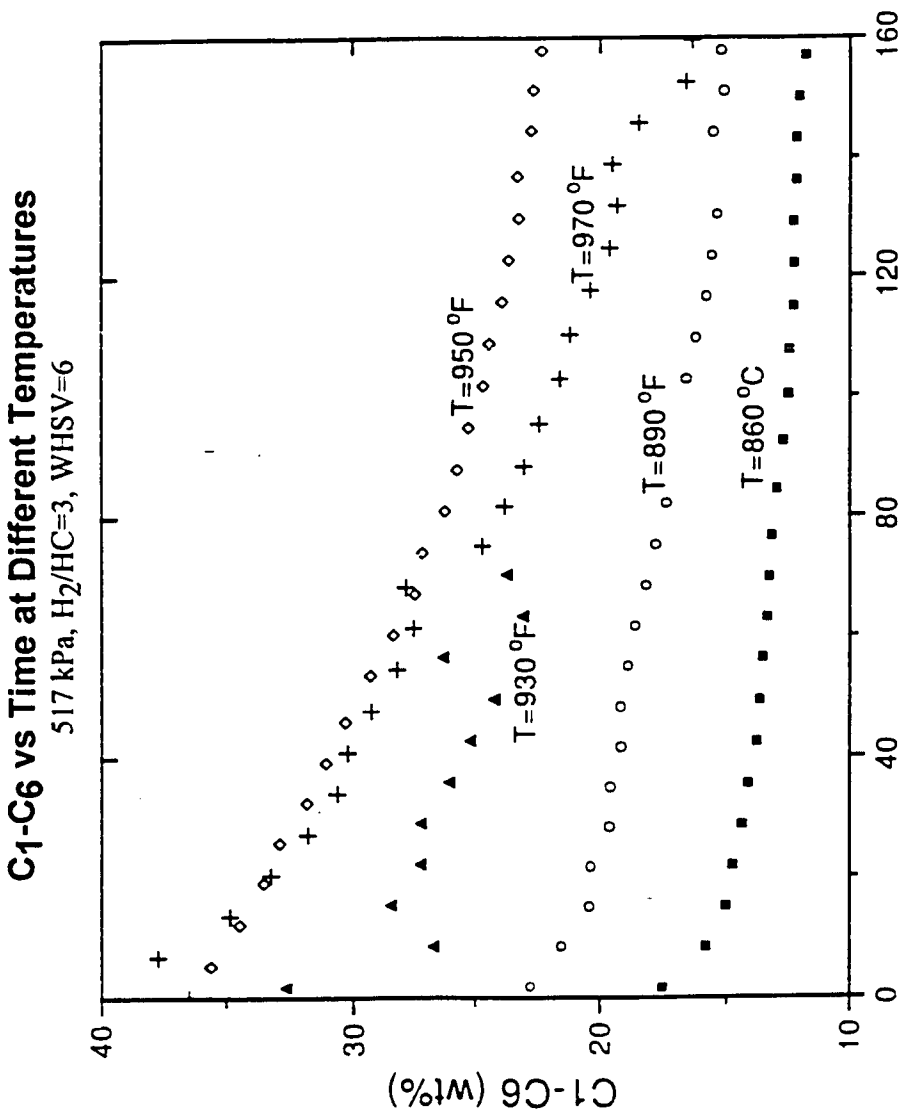

Figure 3-18

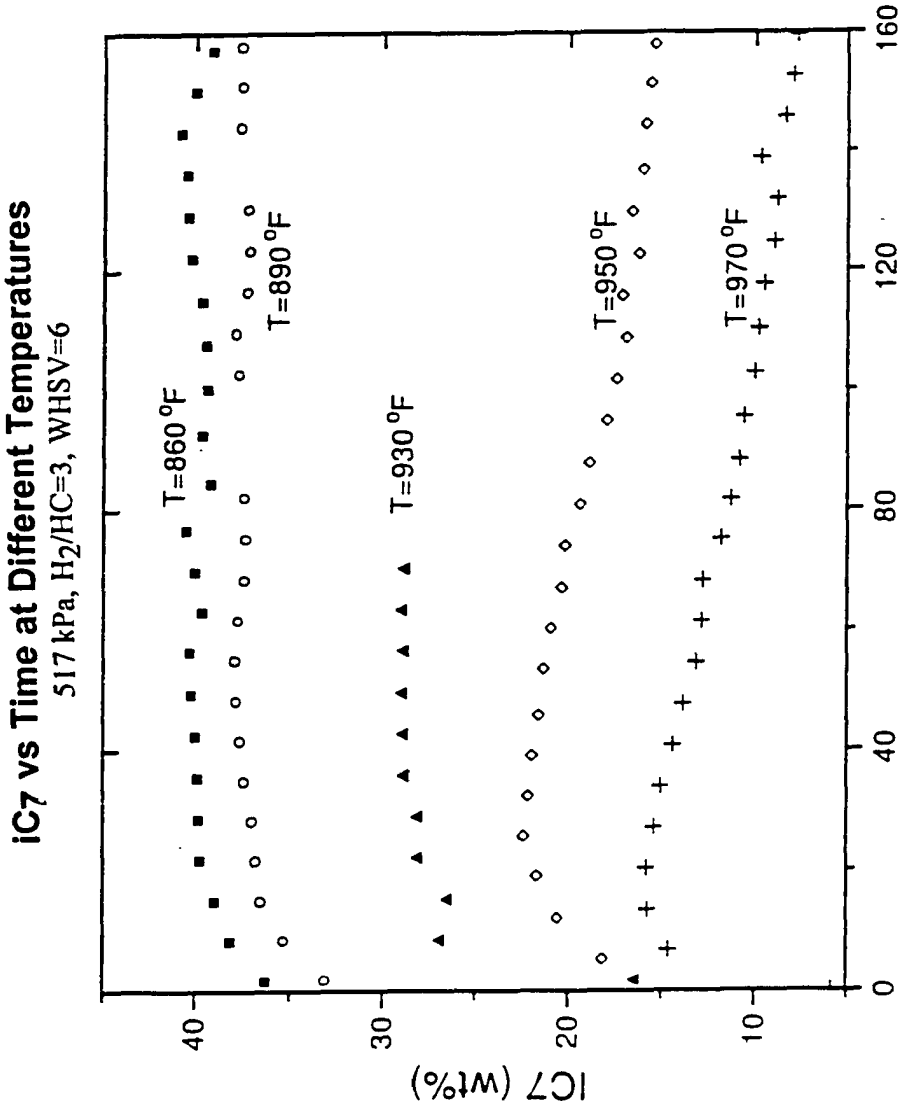

Figure 3-19

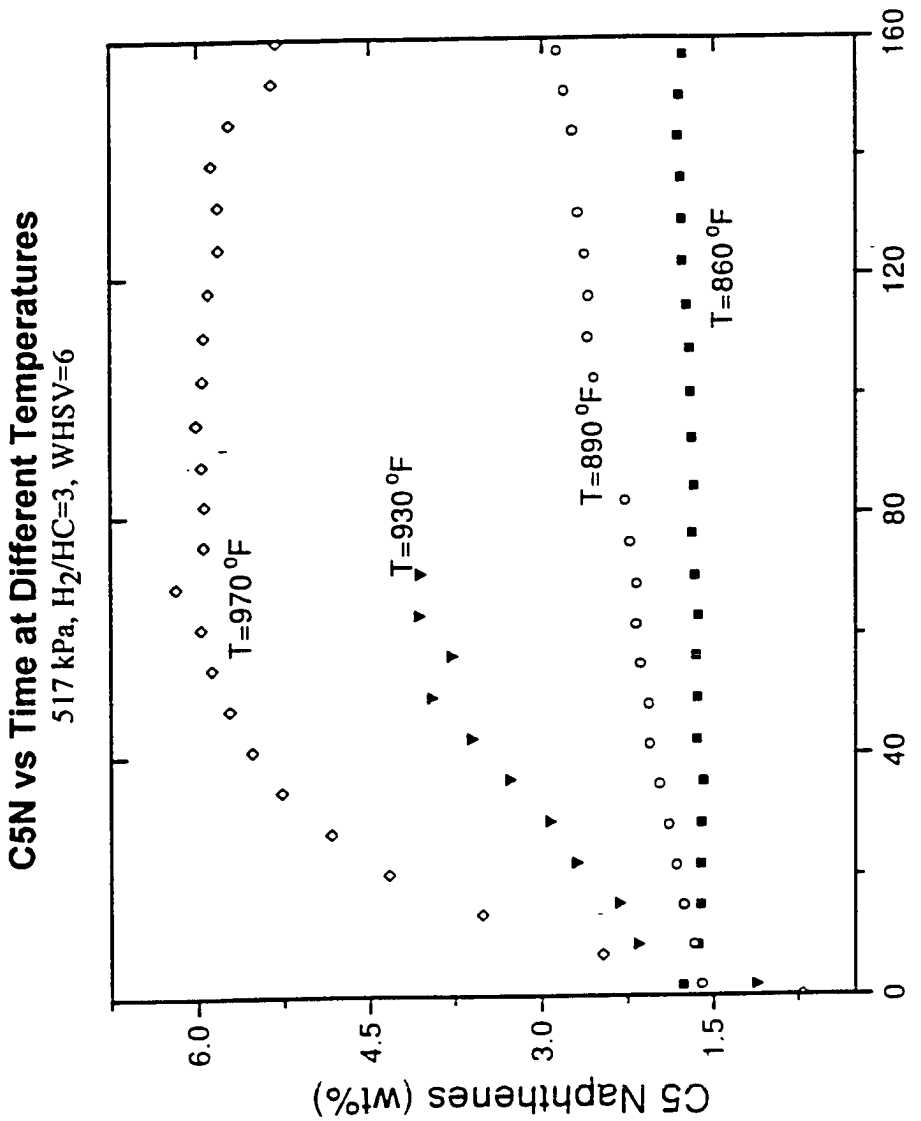

Figure 3-20

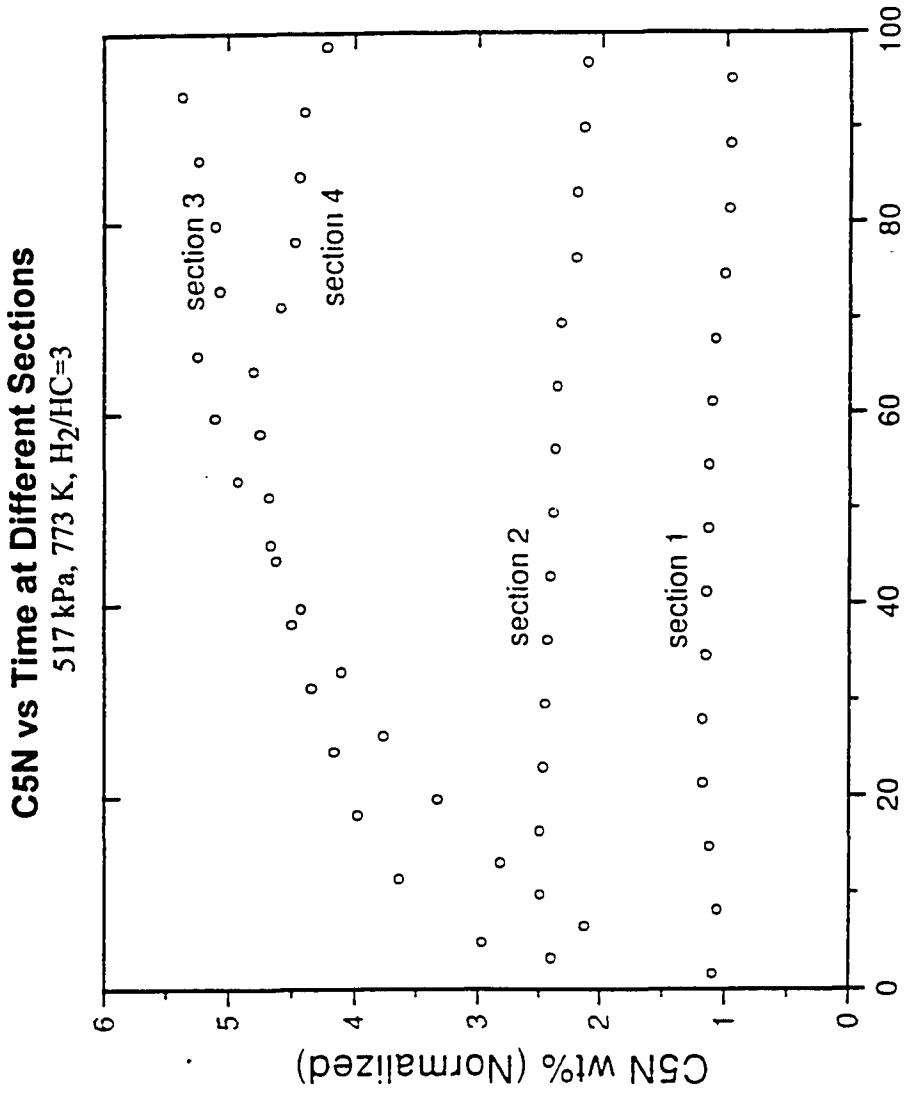

Figure 3-21

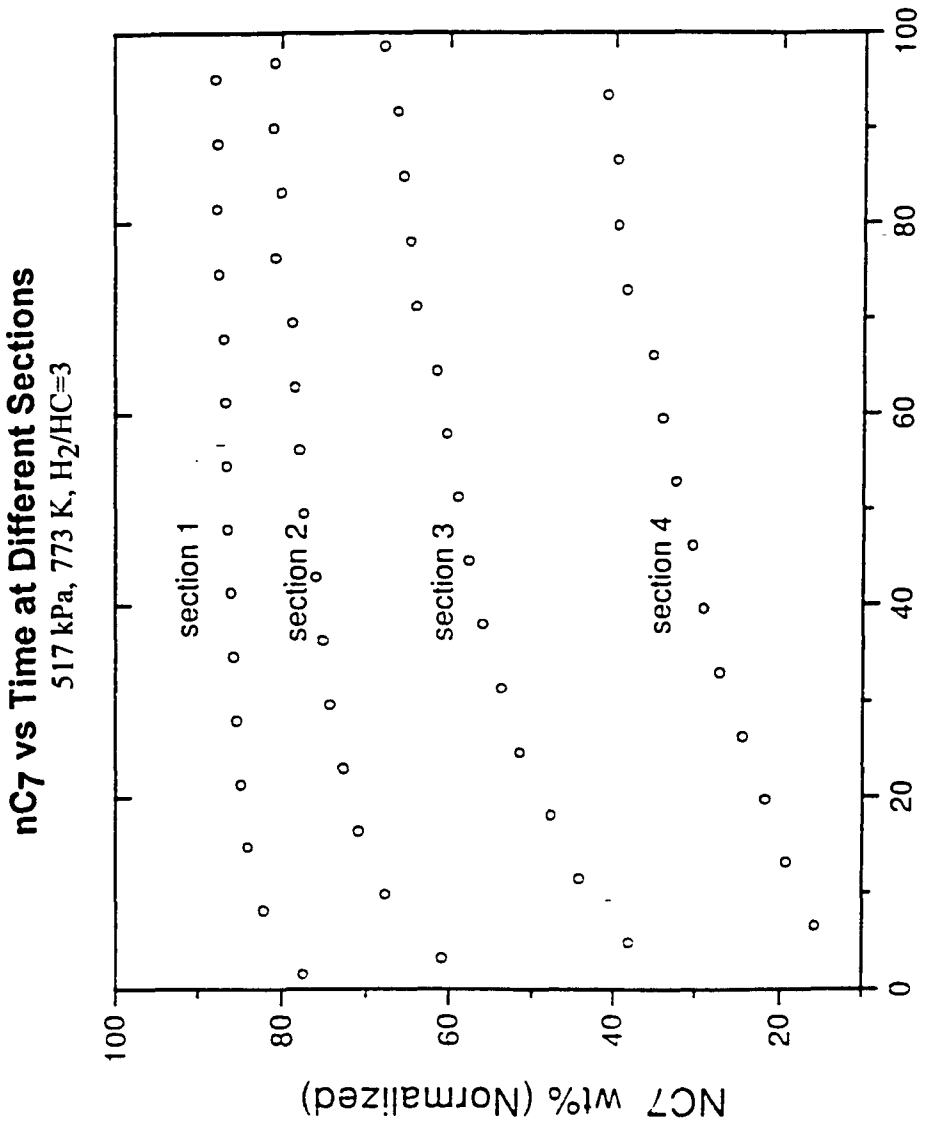

Figure 3-22

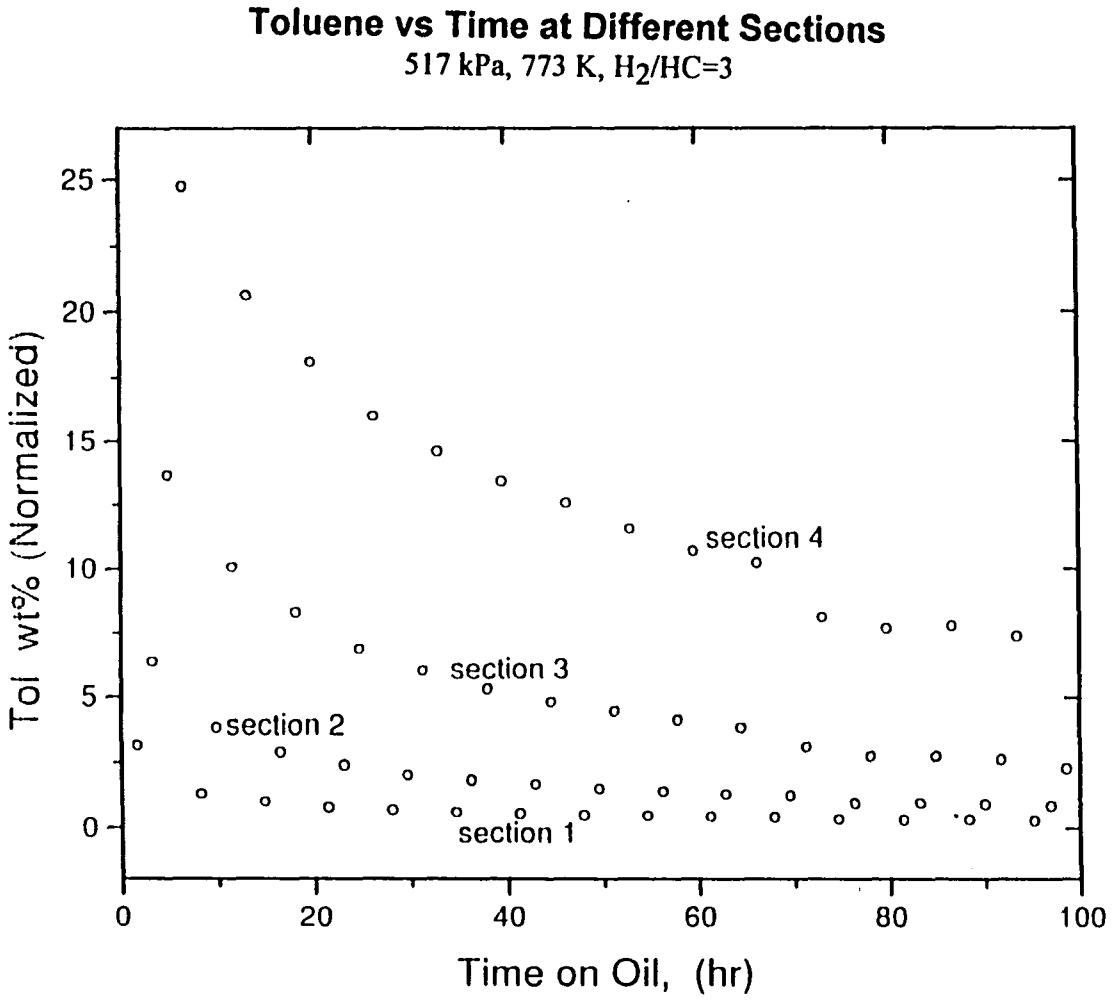

Figure 3-23

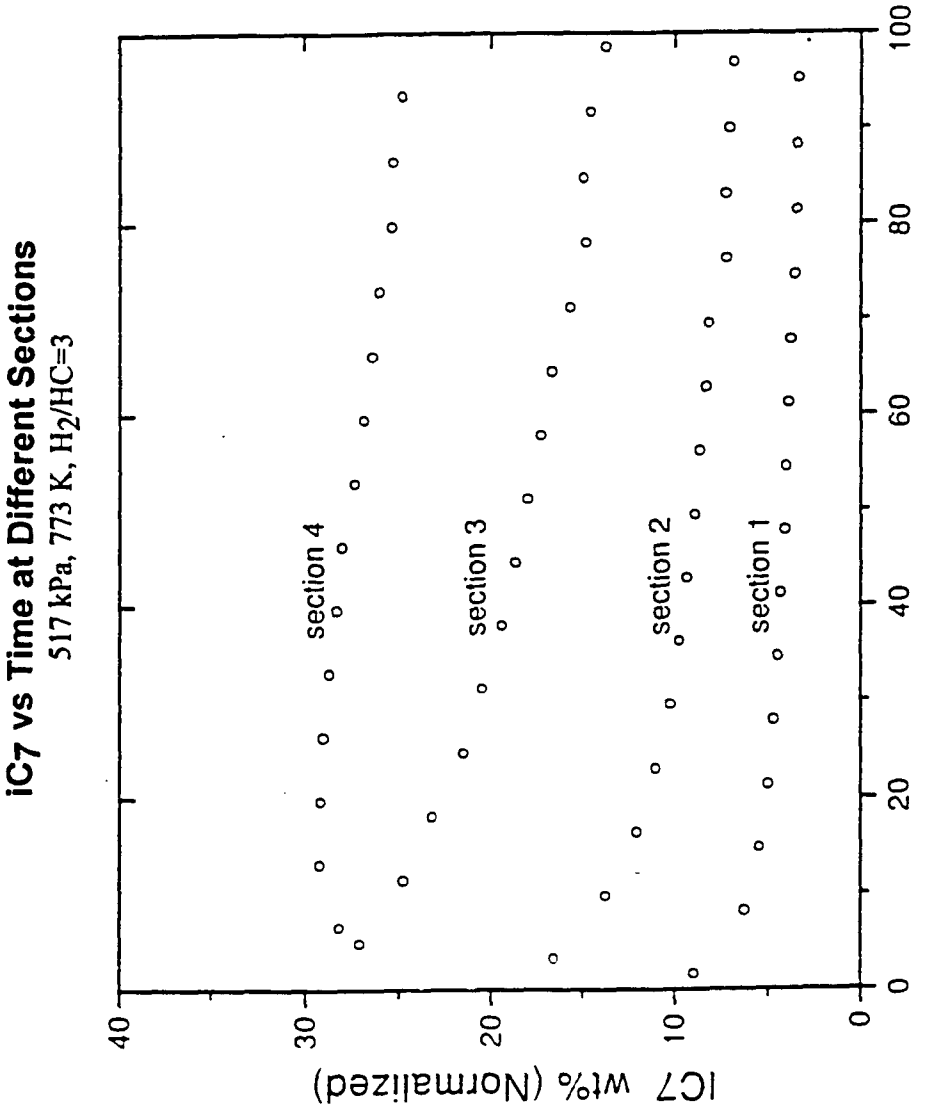

Figure 3-24

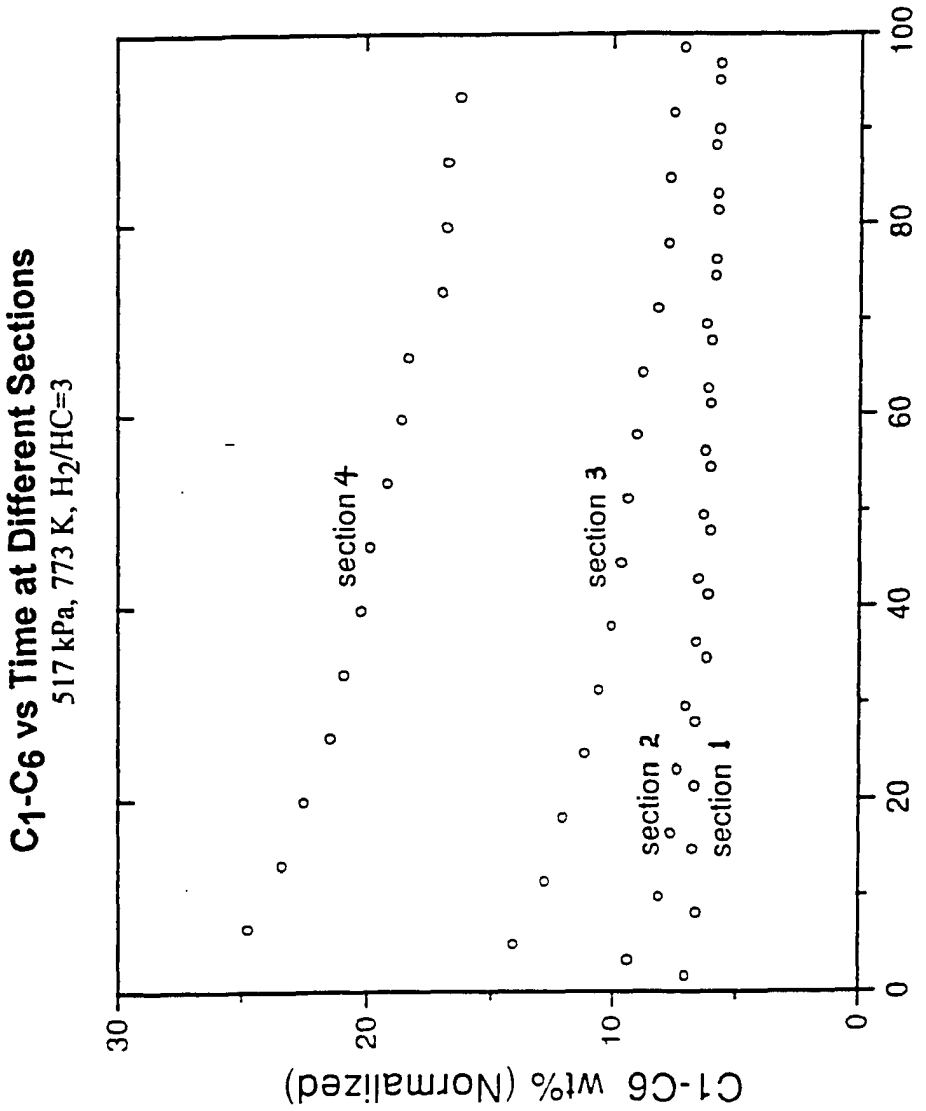

Figure 3-25

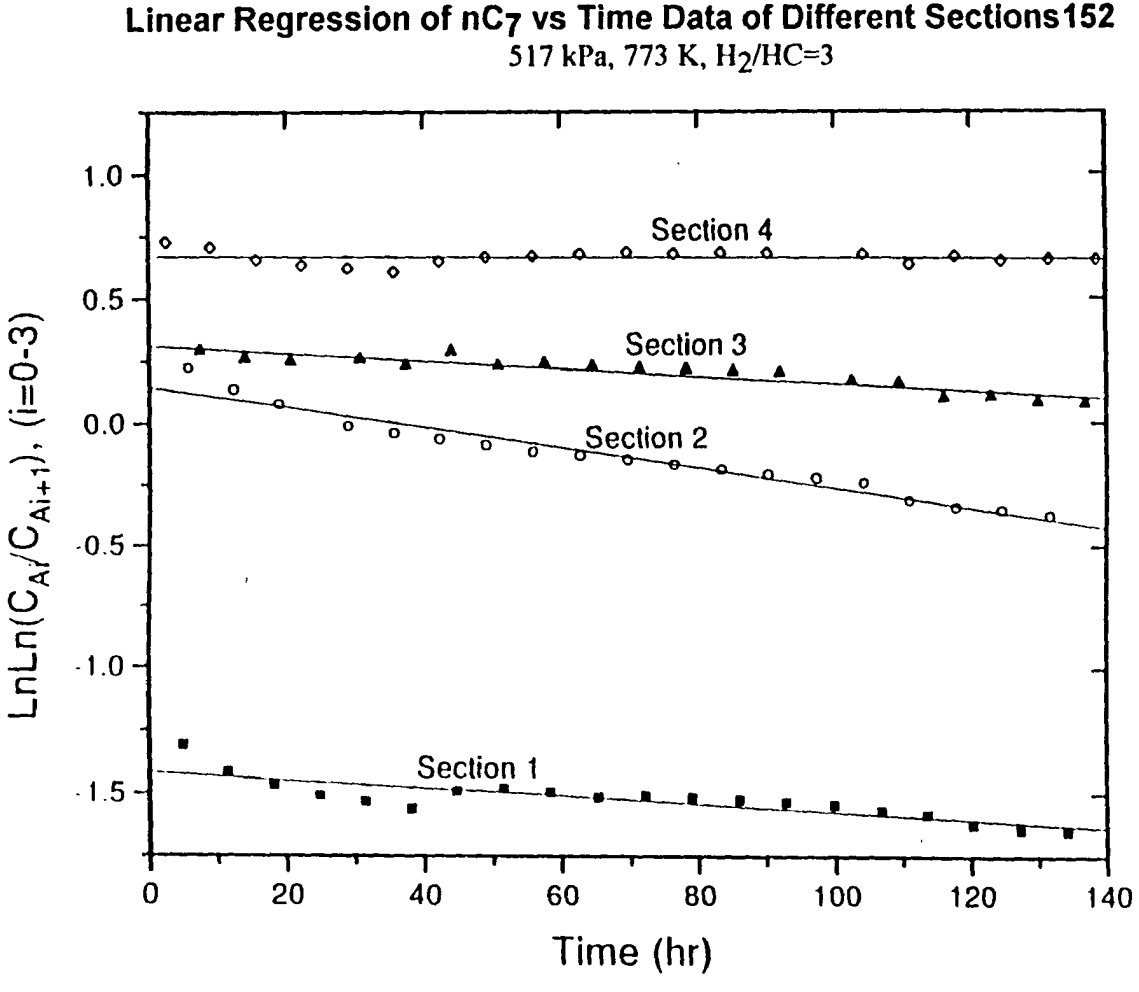

Figure 3-26

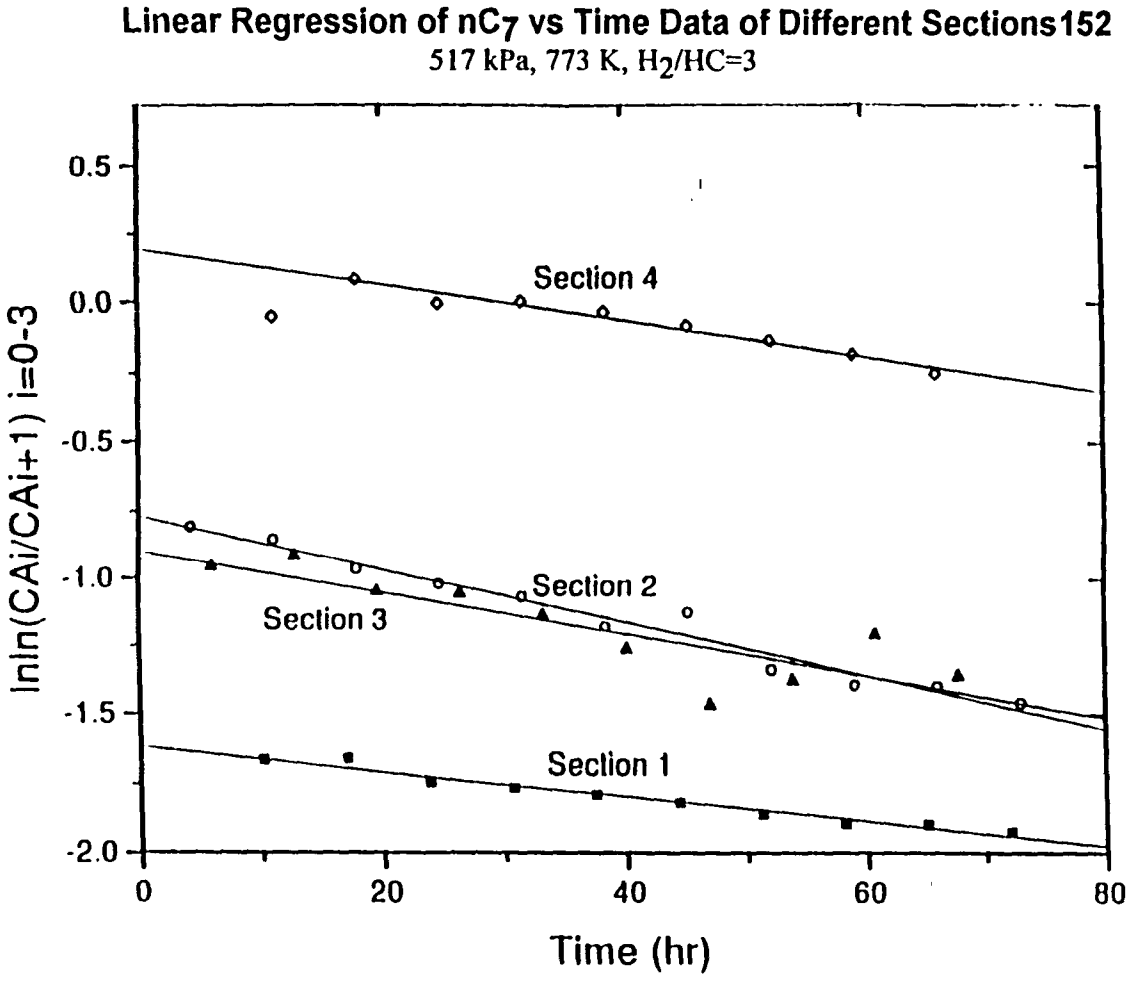

Figure 3-27

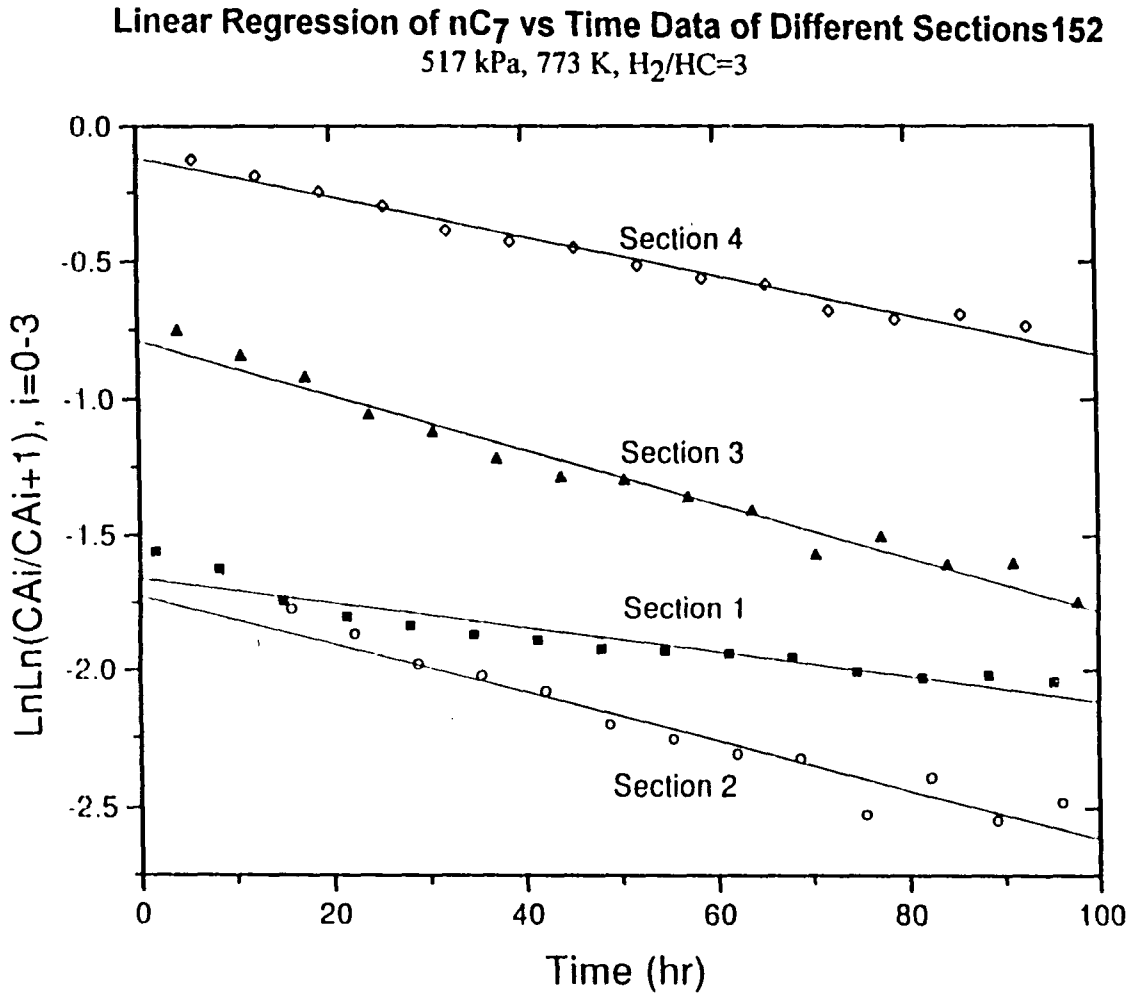

Figure 3-28

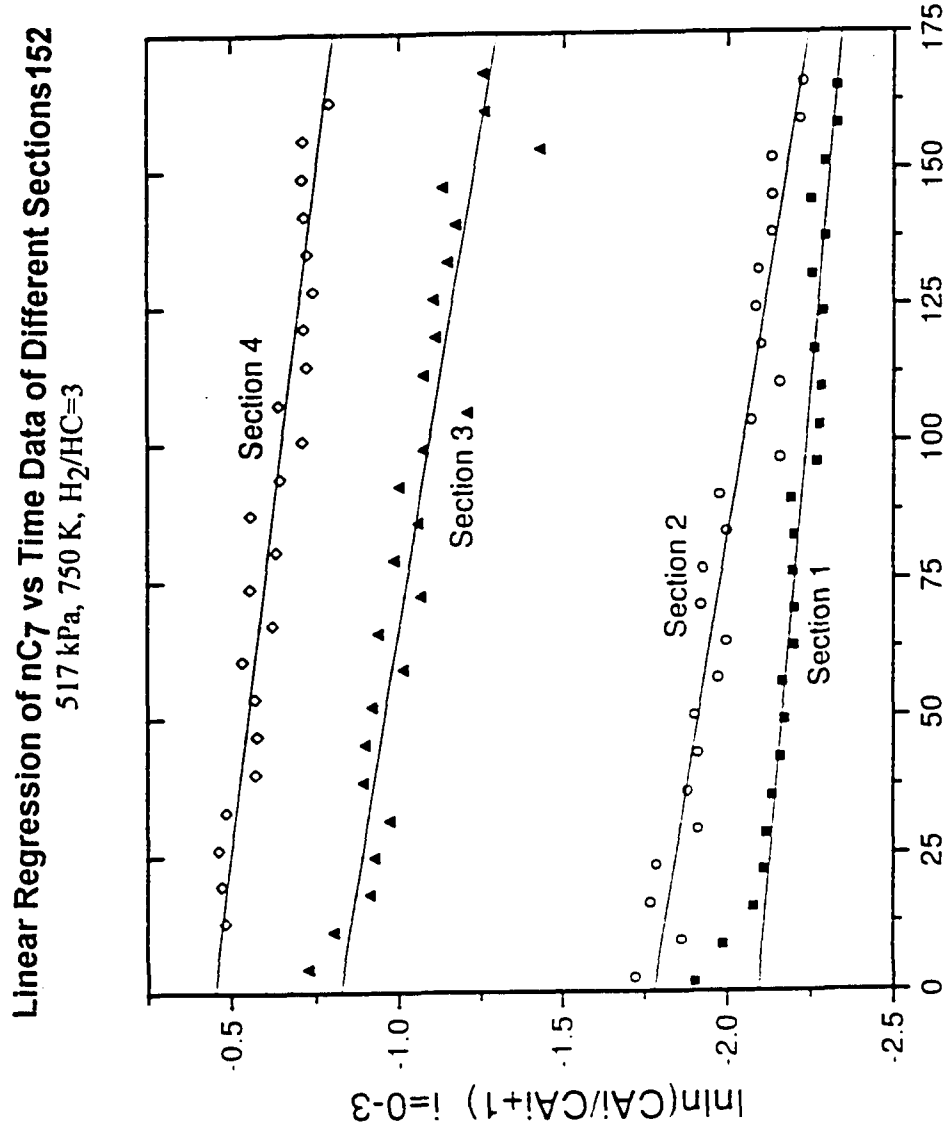

Figure 3-29

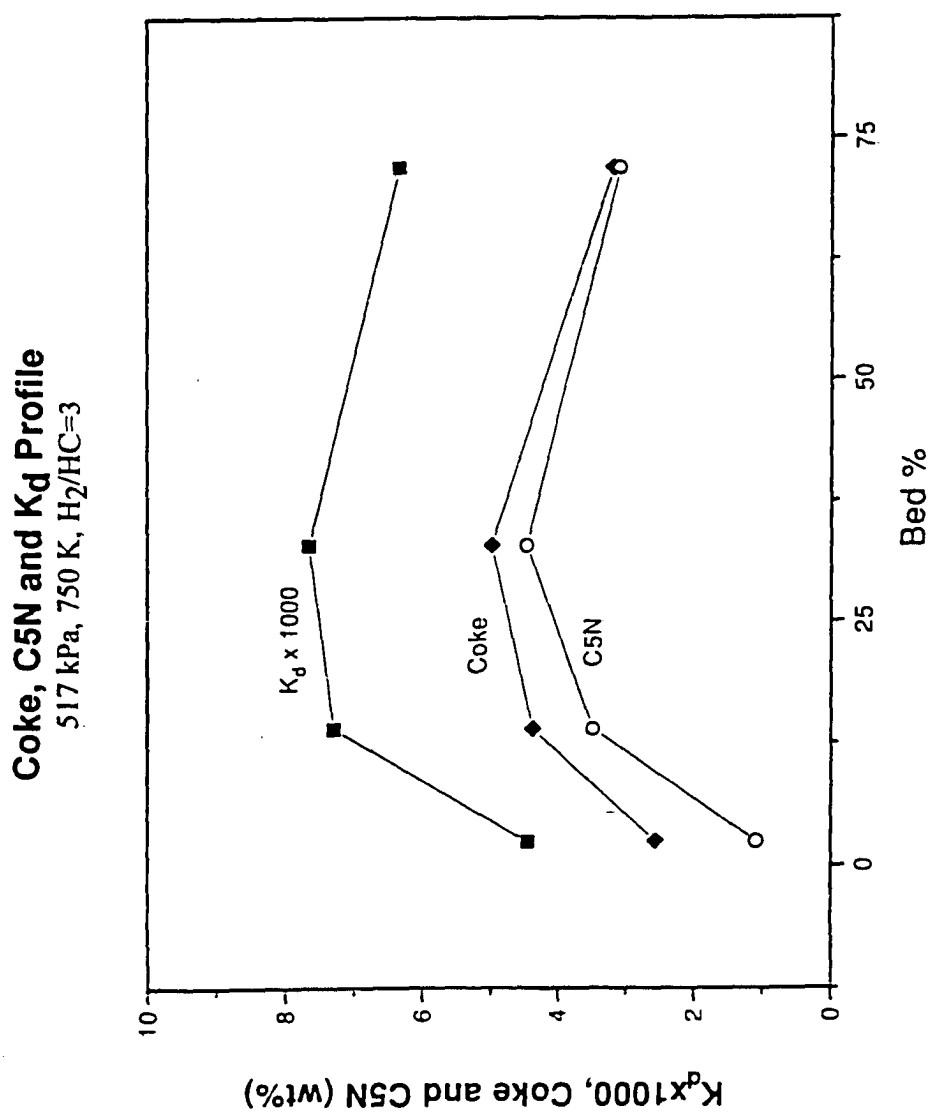

Figure 3-30

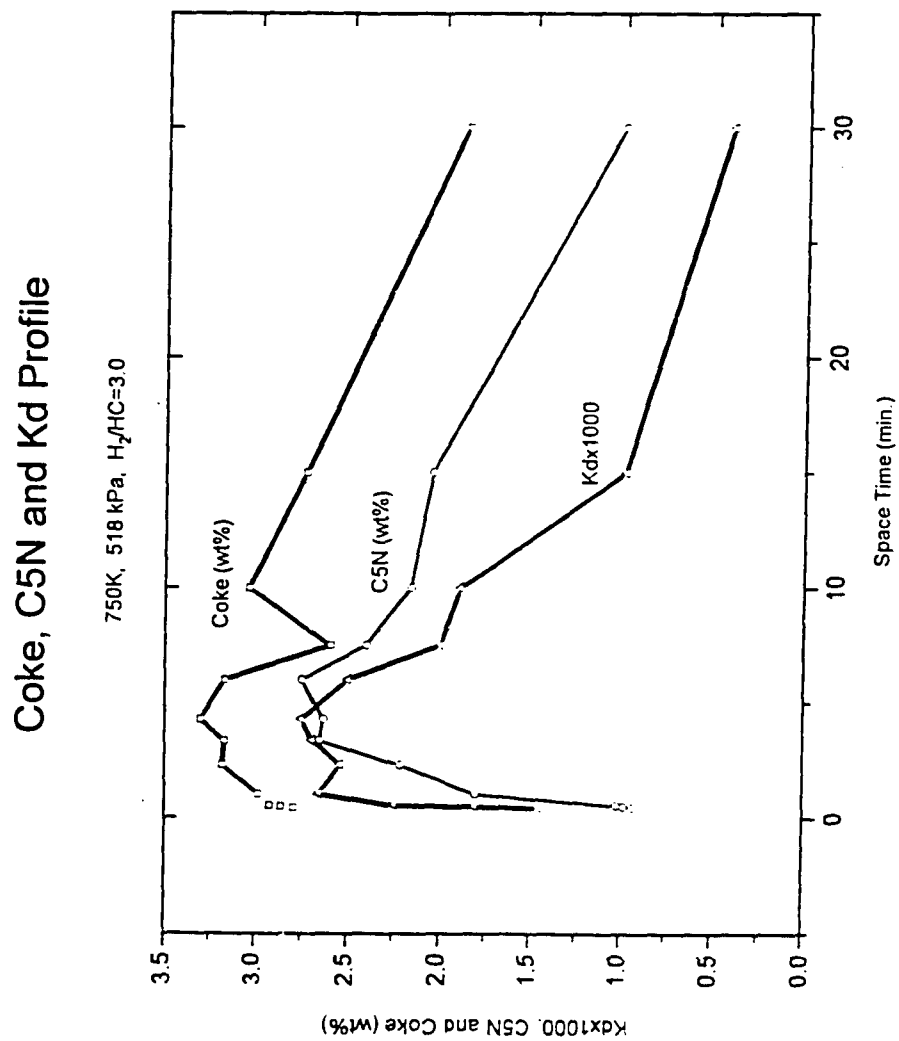

Figure 3-31

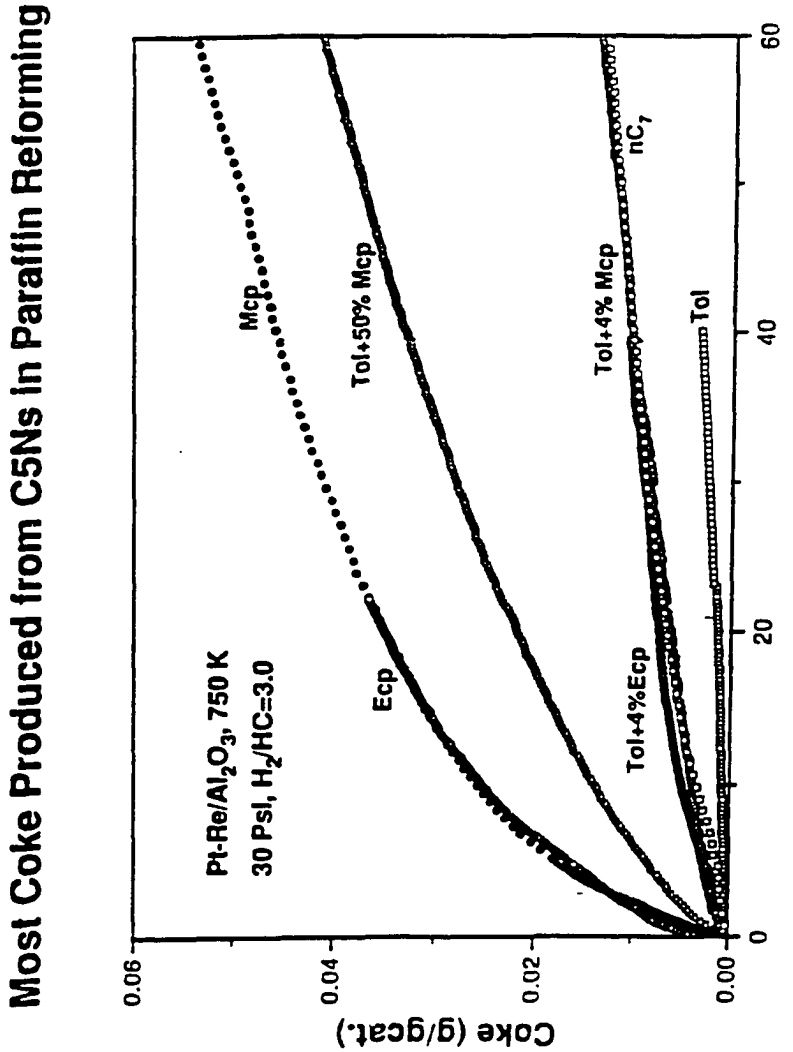

Figure 3-32

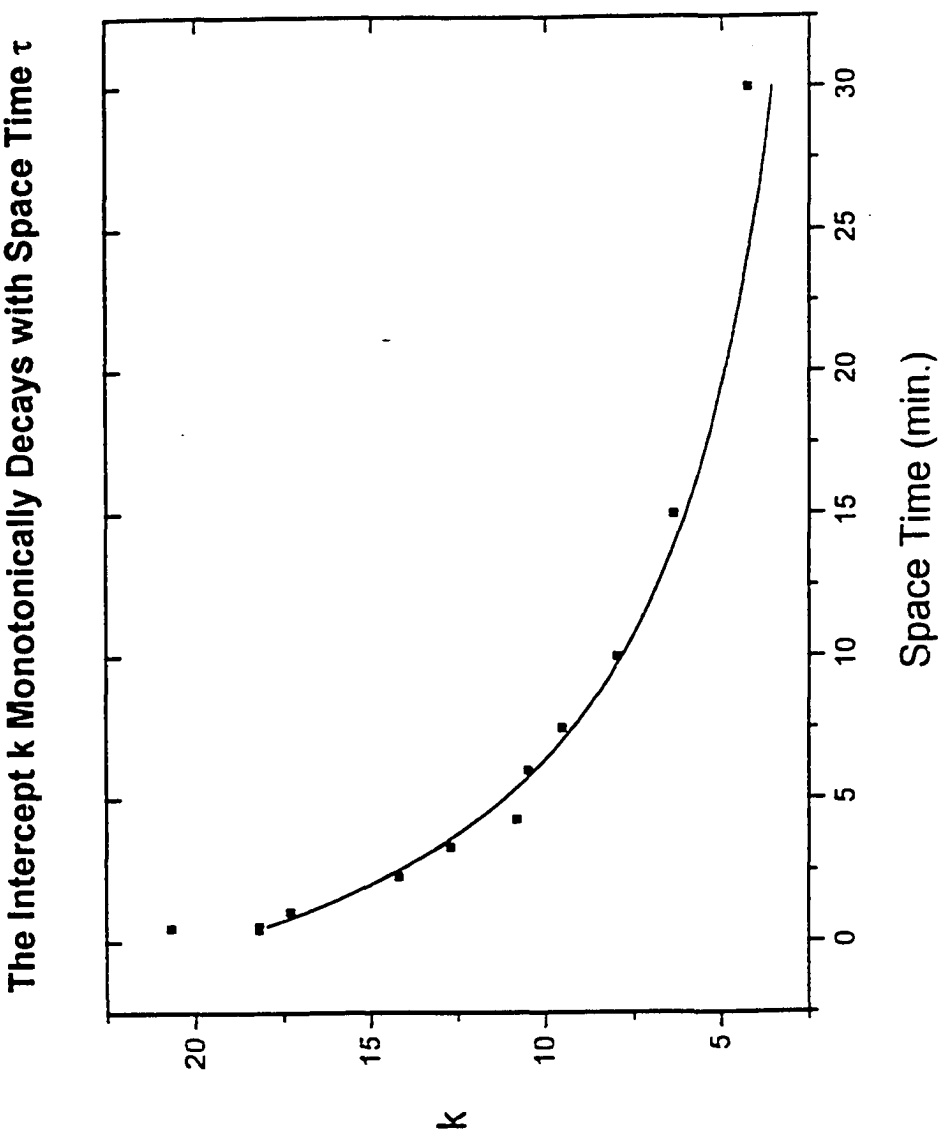

Figure 3-33

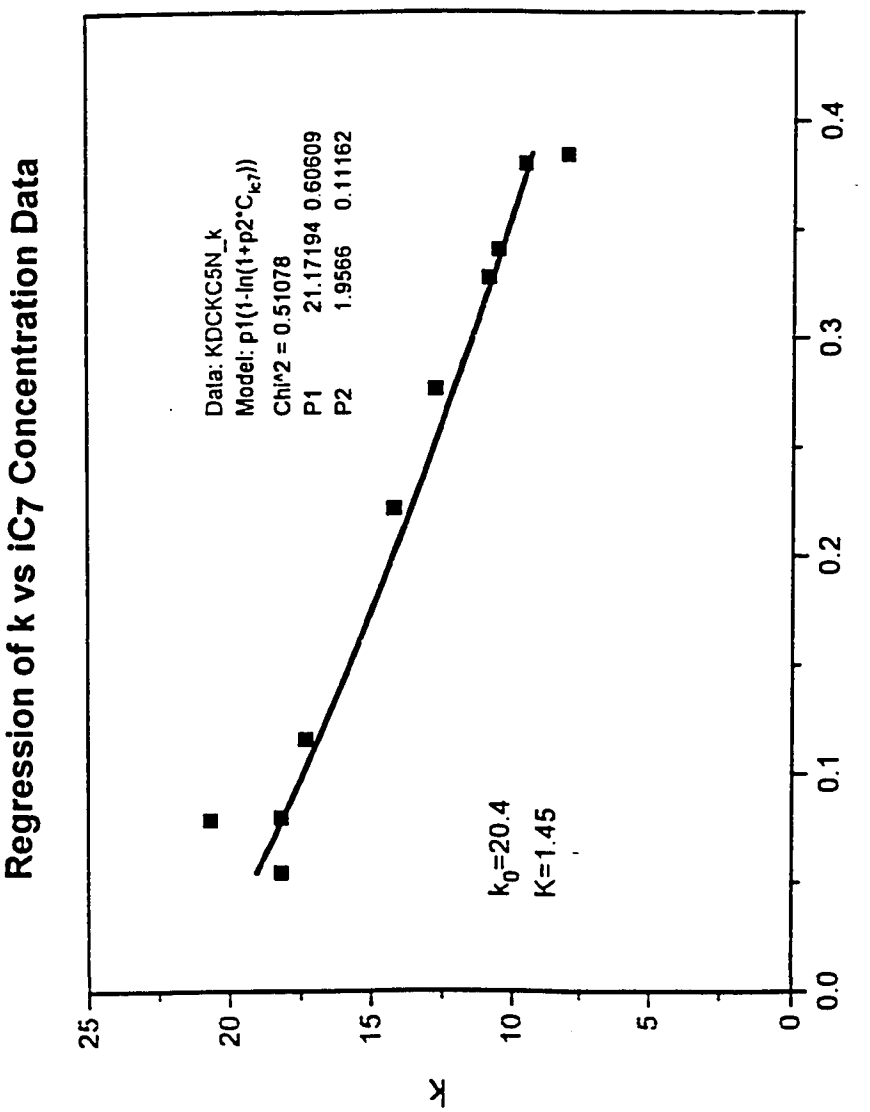

Figure 3-34

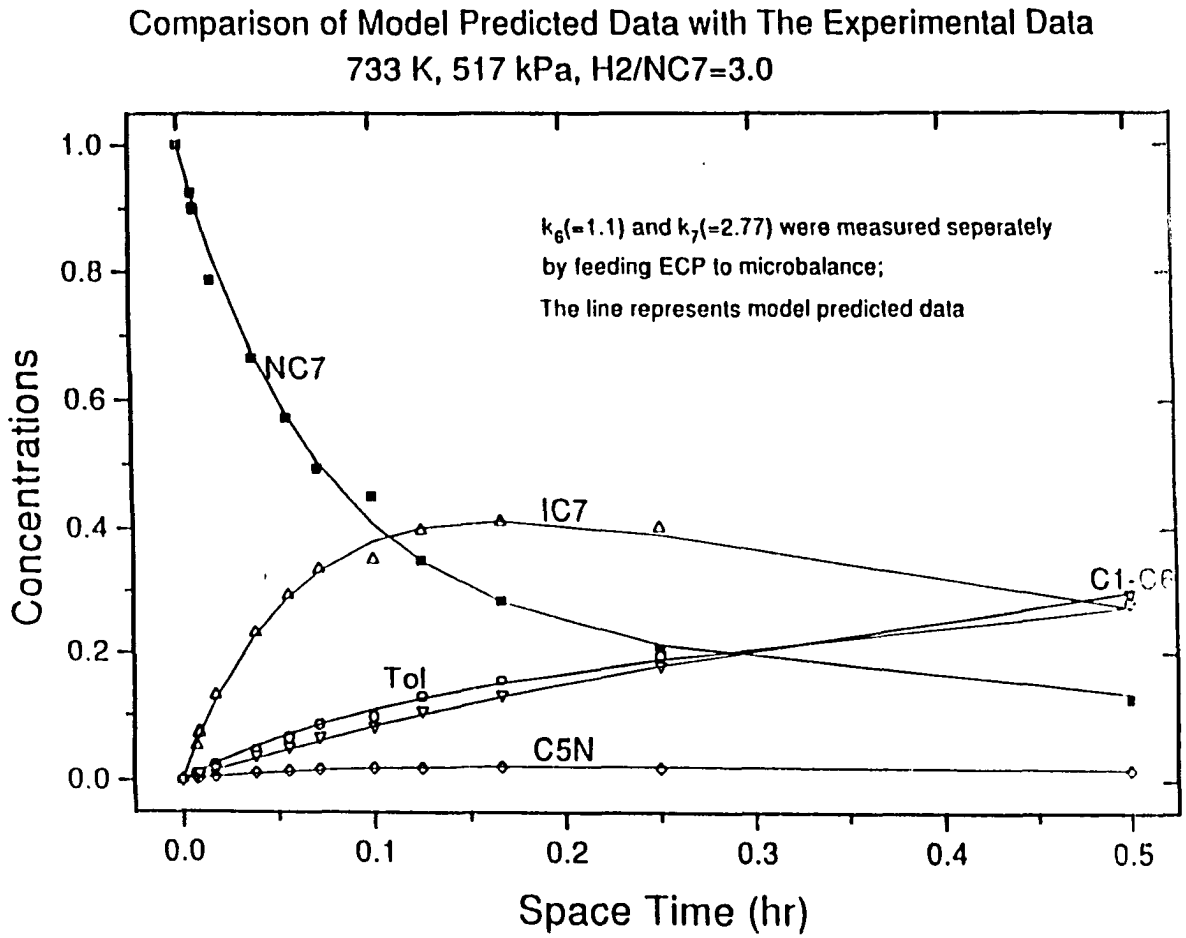

Figure 4-1

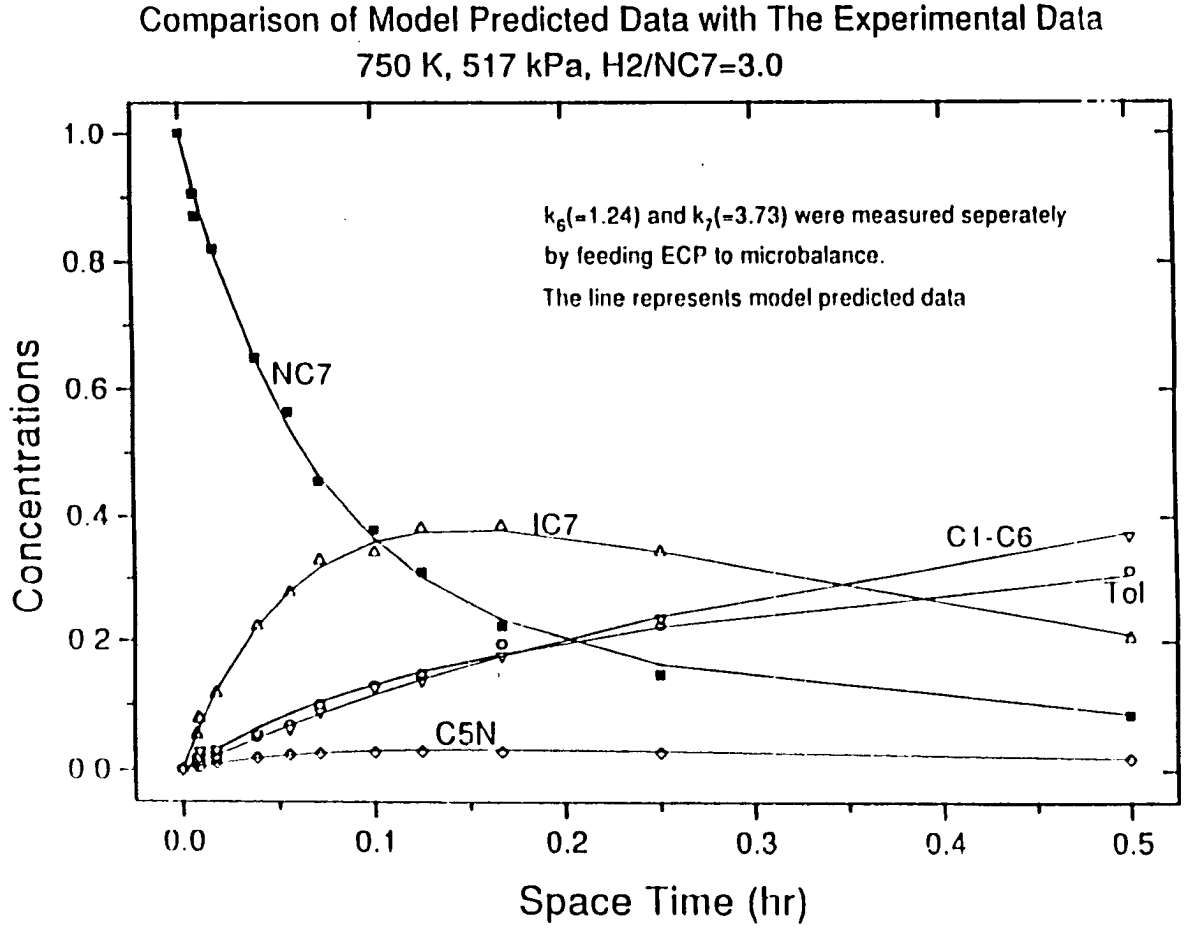

Figure 4-2

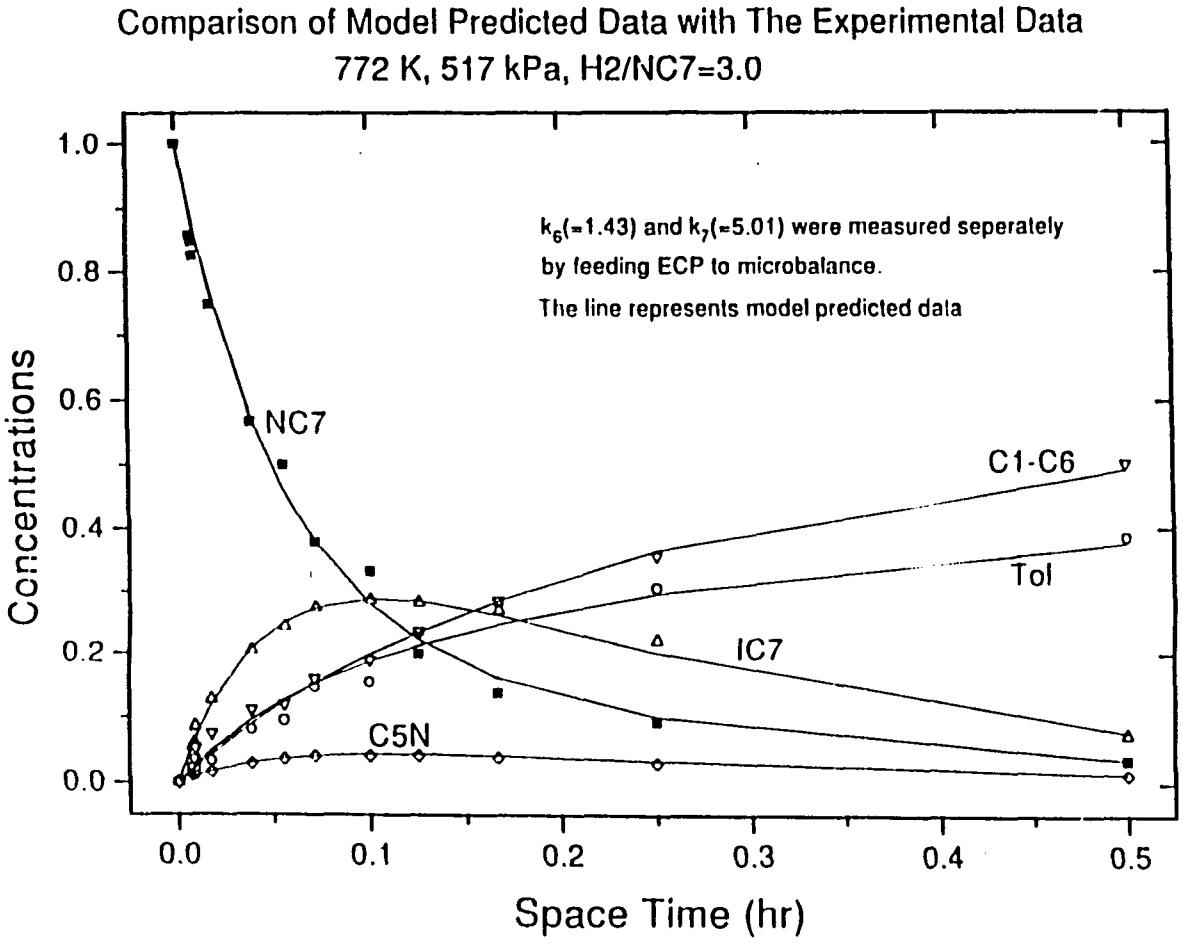

Figure 4-3

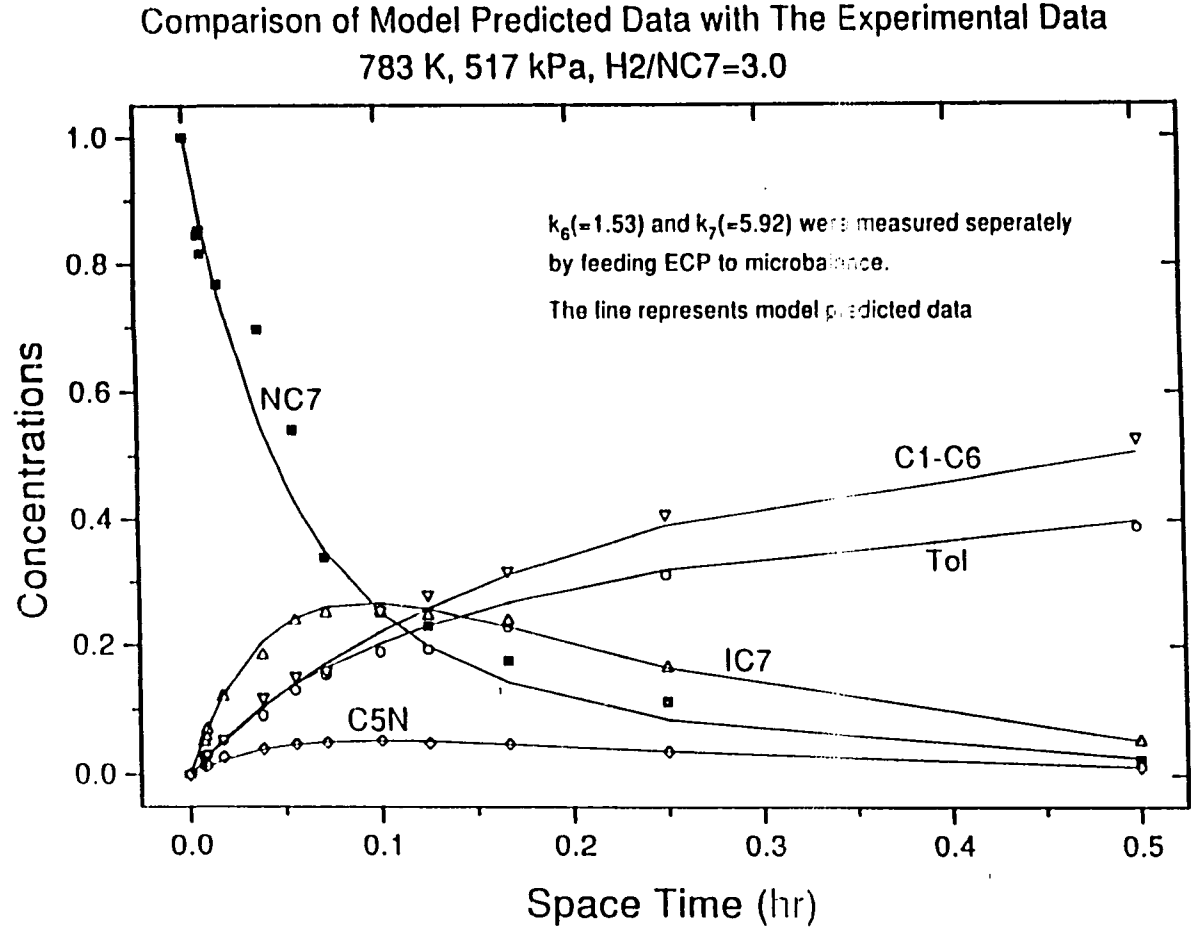

Figure 4-4

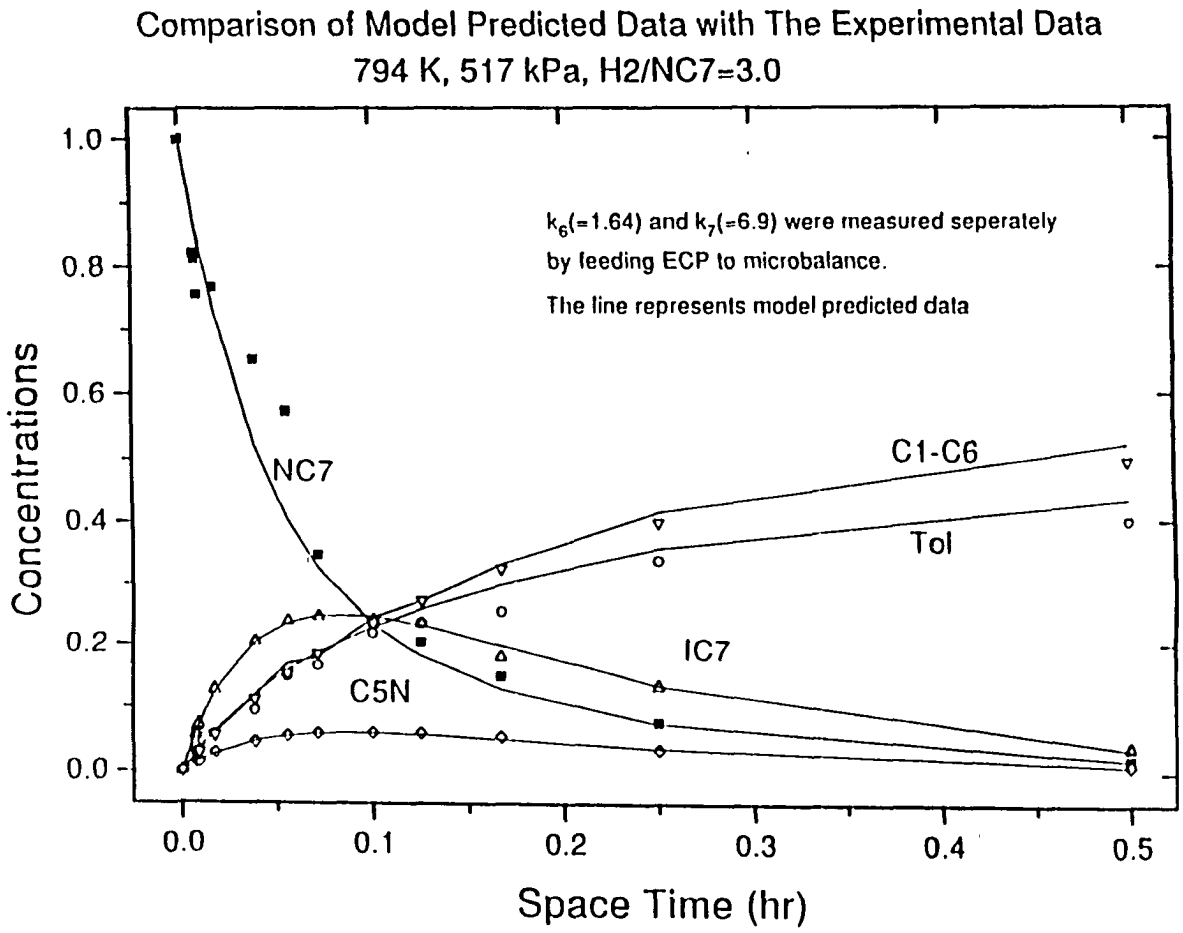

Figure 4-5

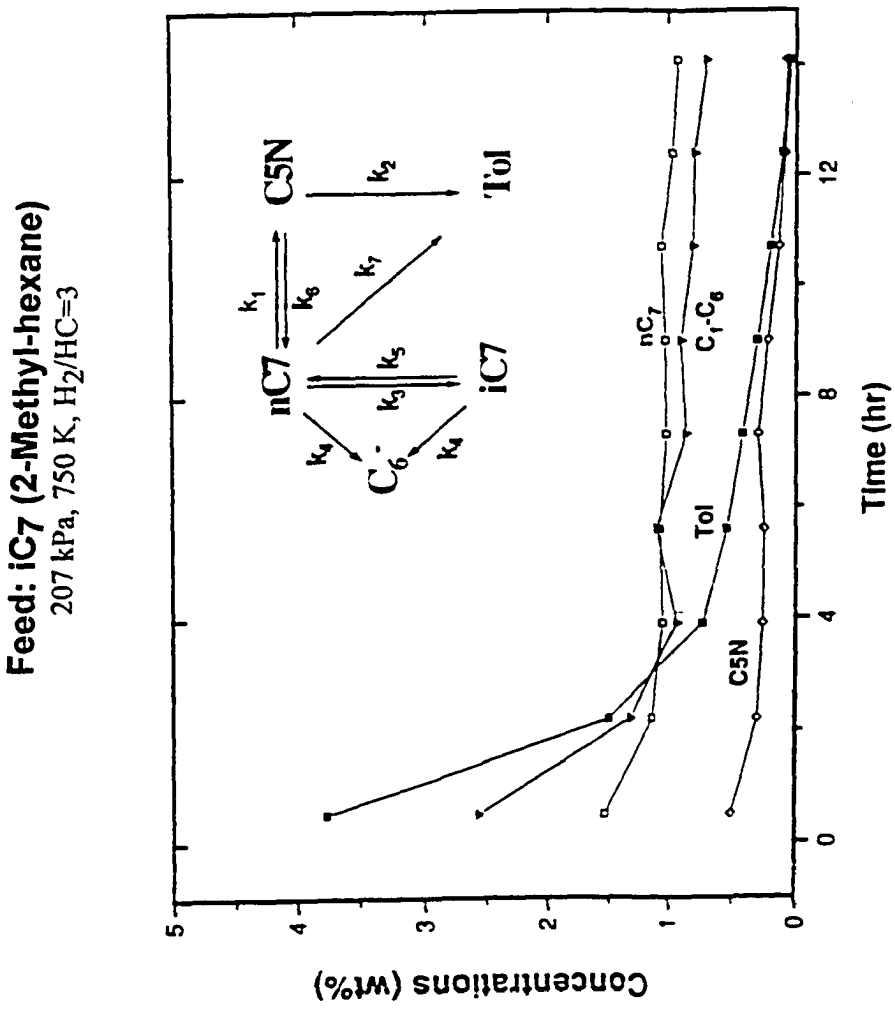

Figure 4-6

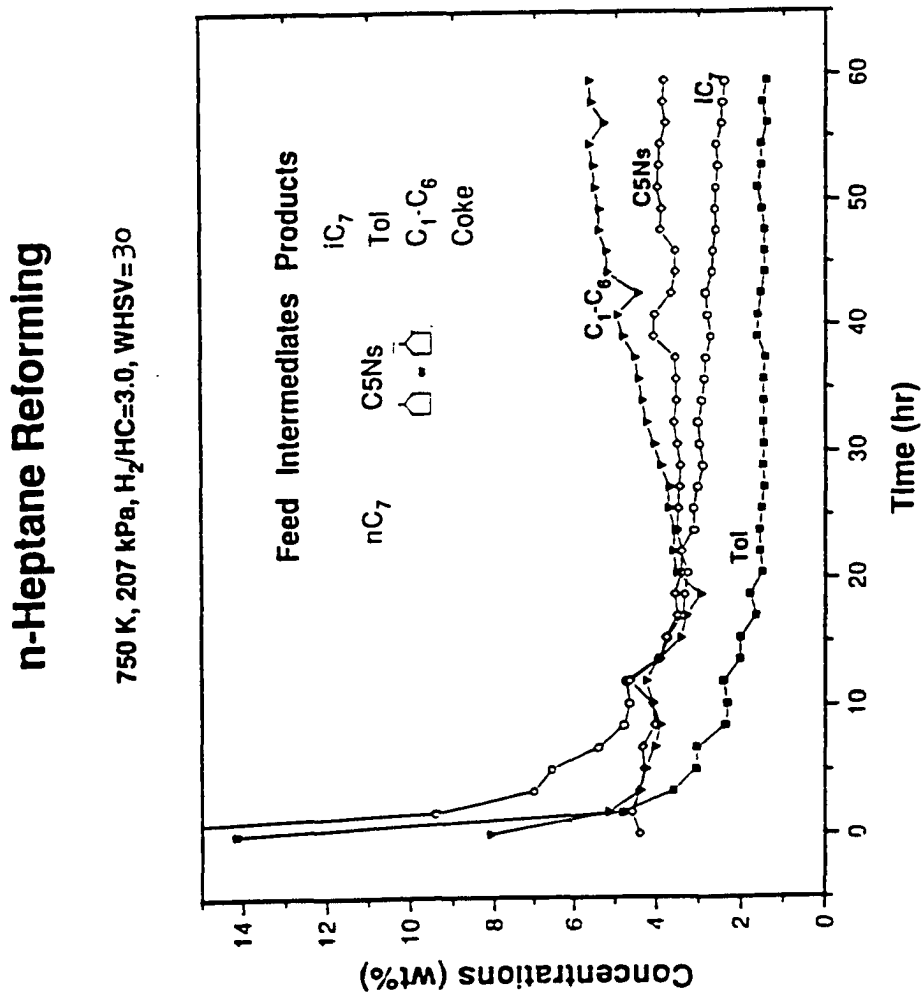

Figure 4-7

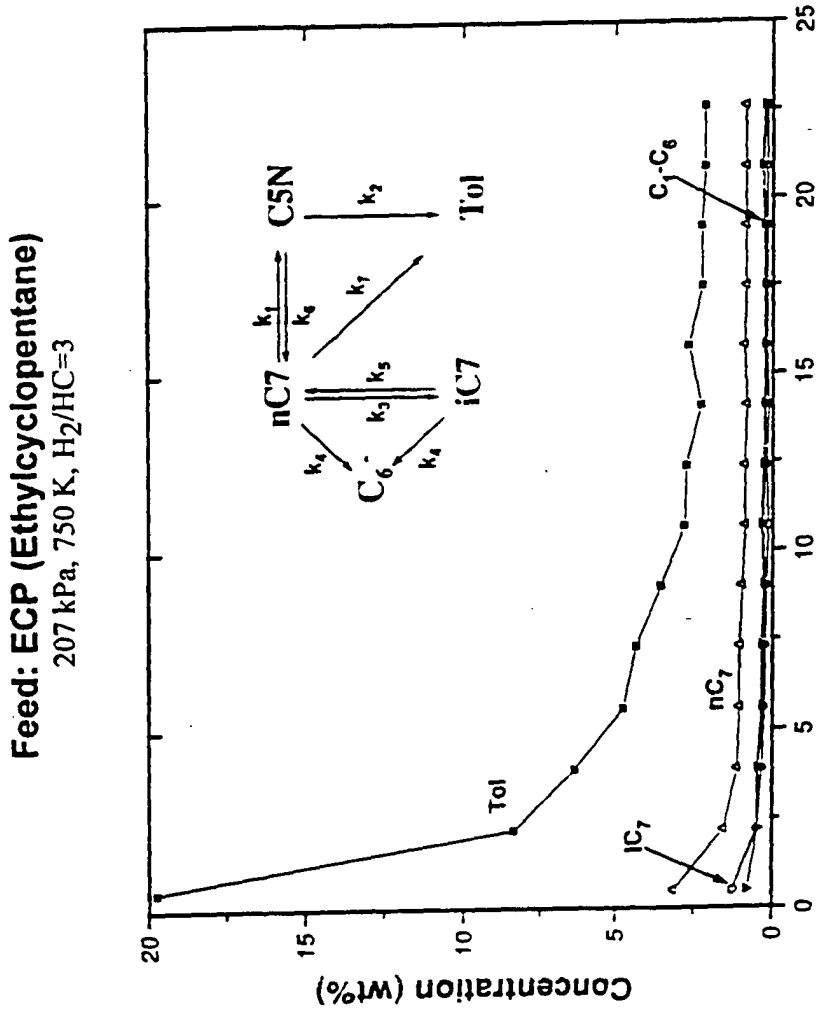

Figure 4-8

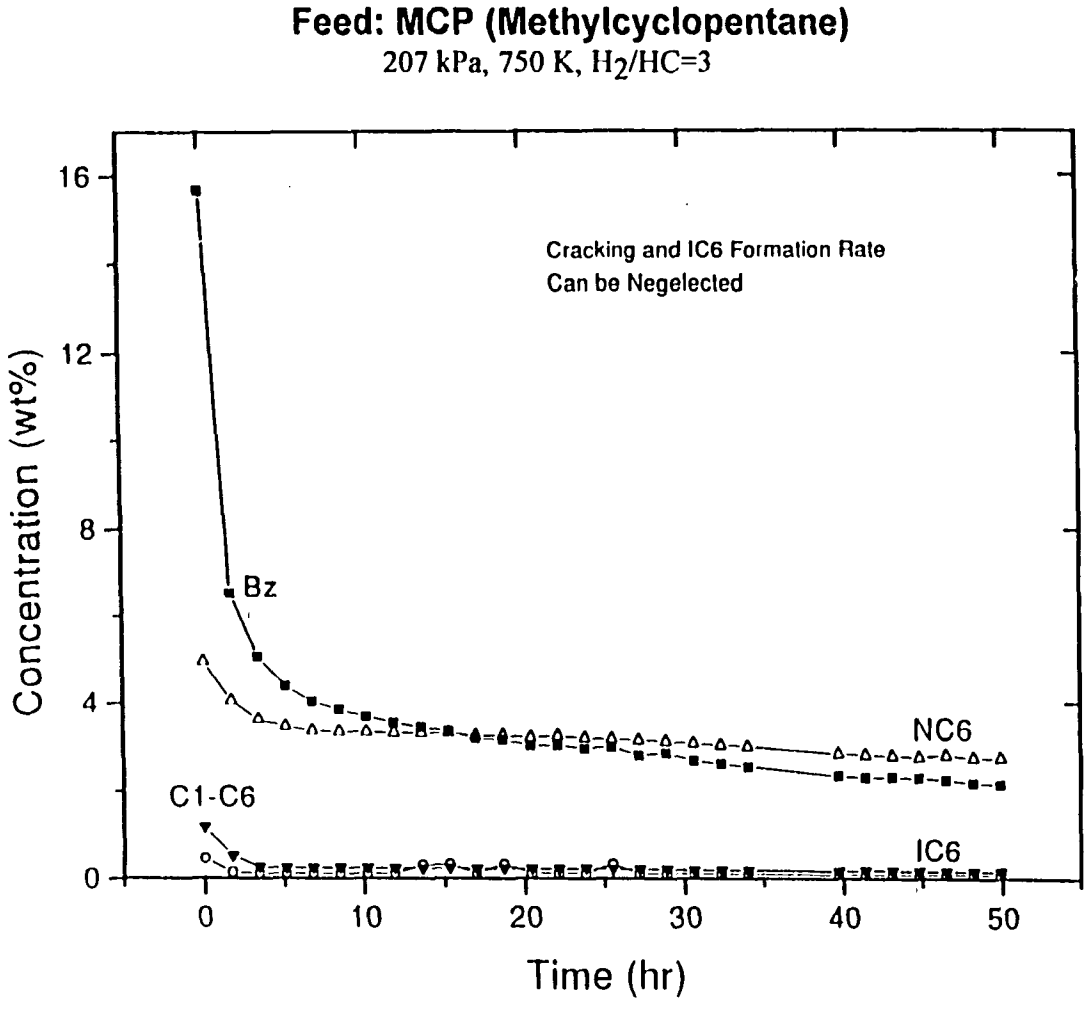

Figure 4-9

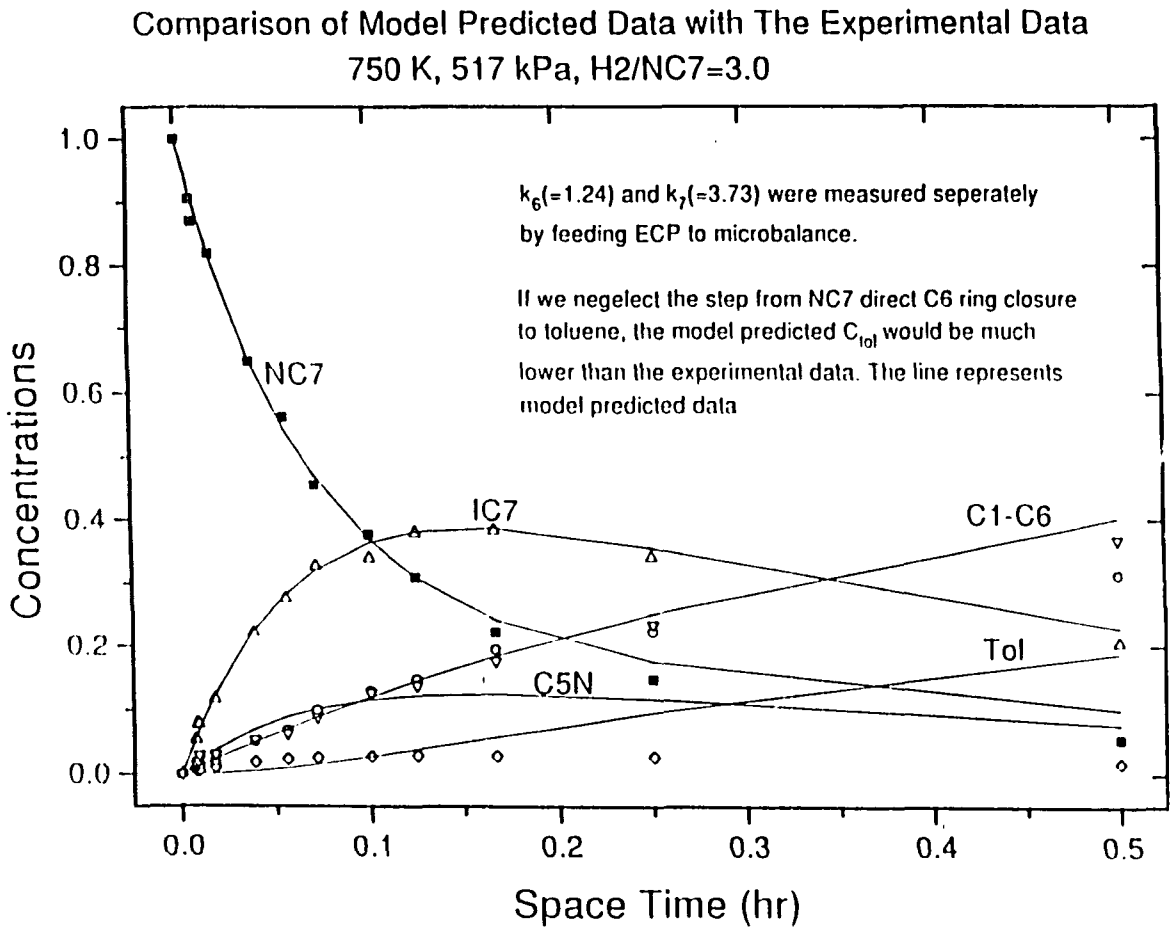

Figure 4-10a

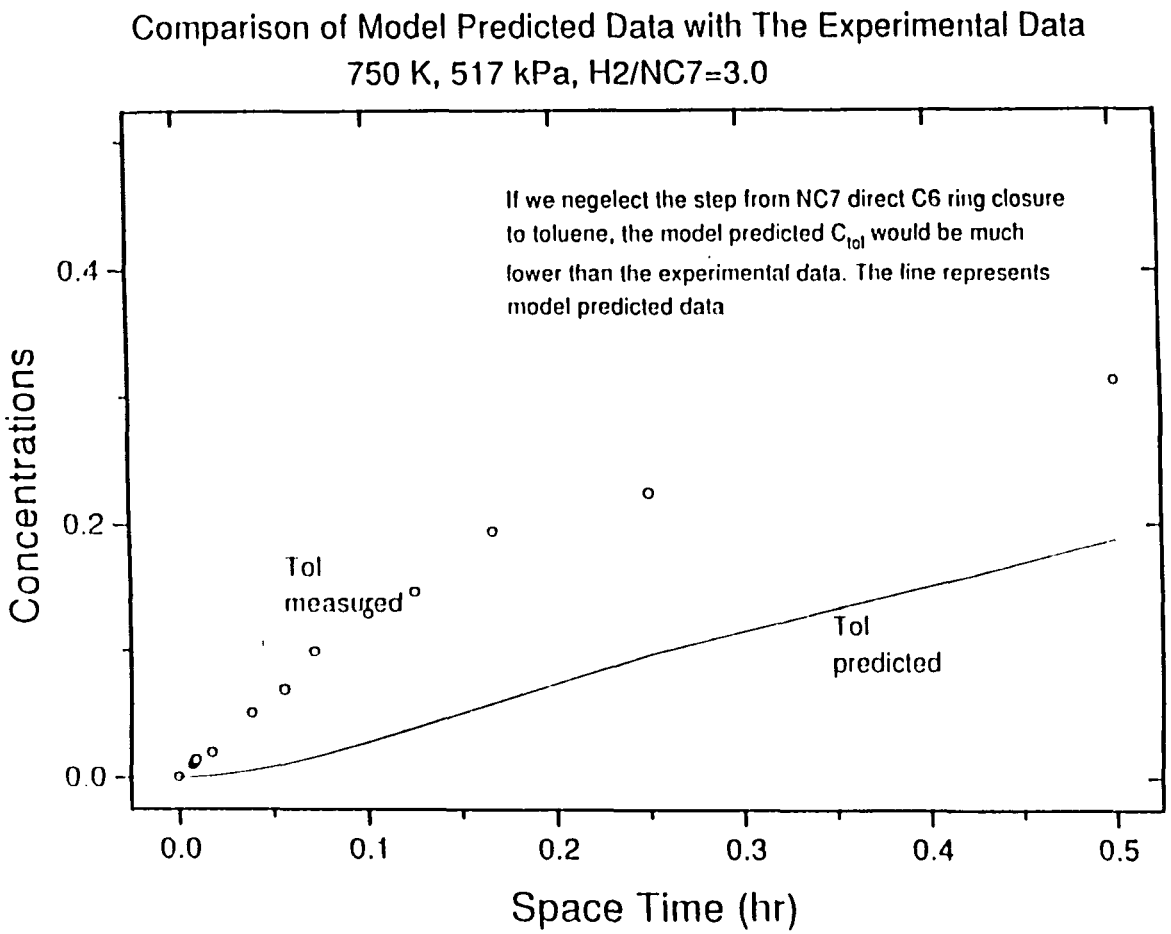

Figure 4-10b

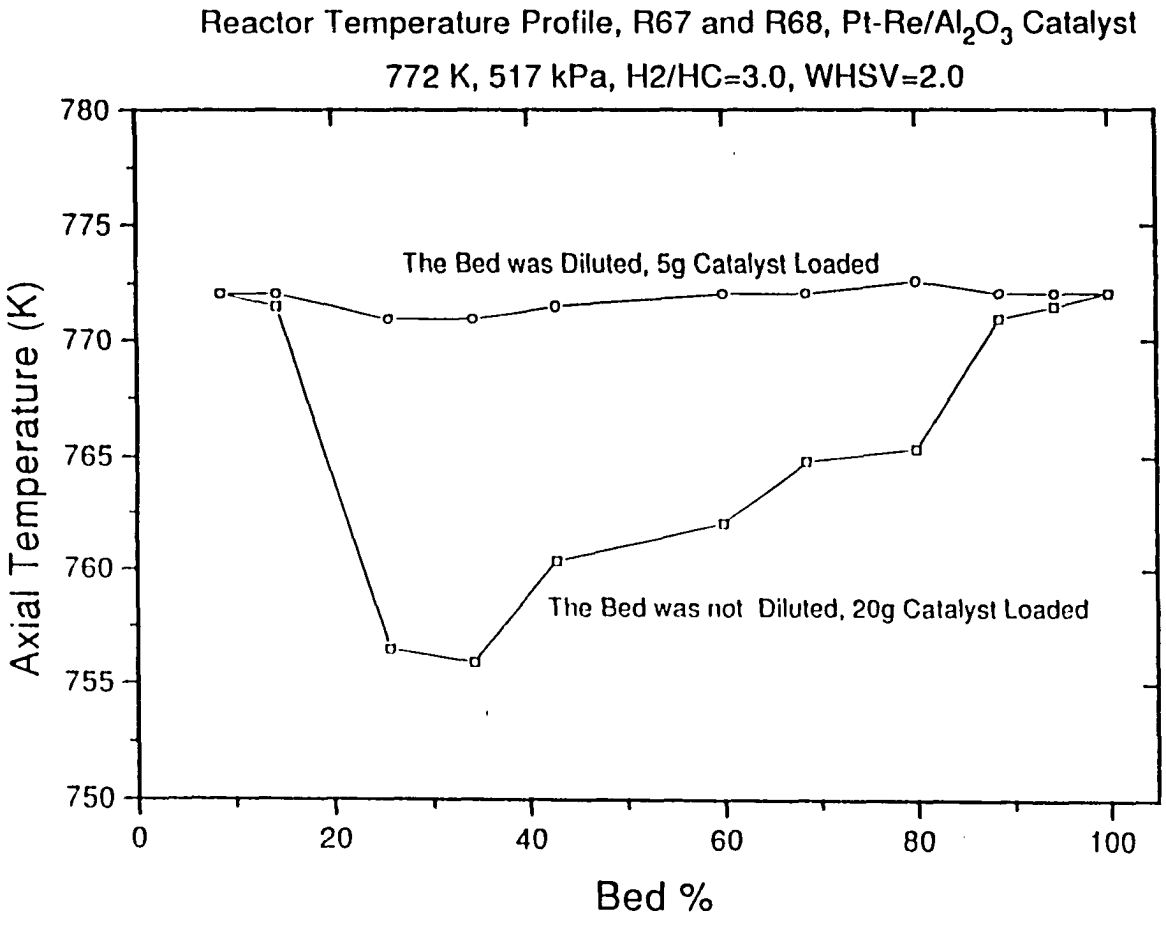

Figure 4-11

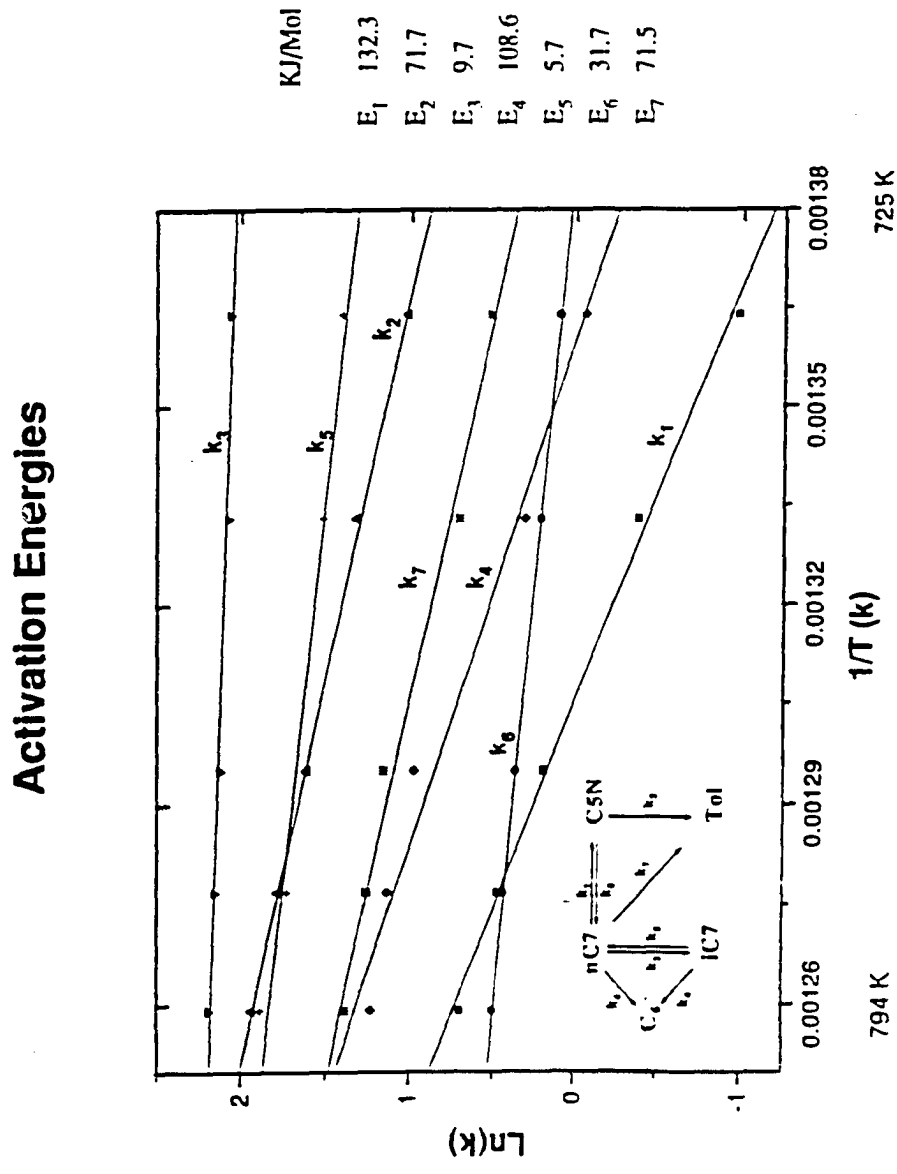

Figure 4-12

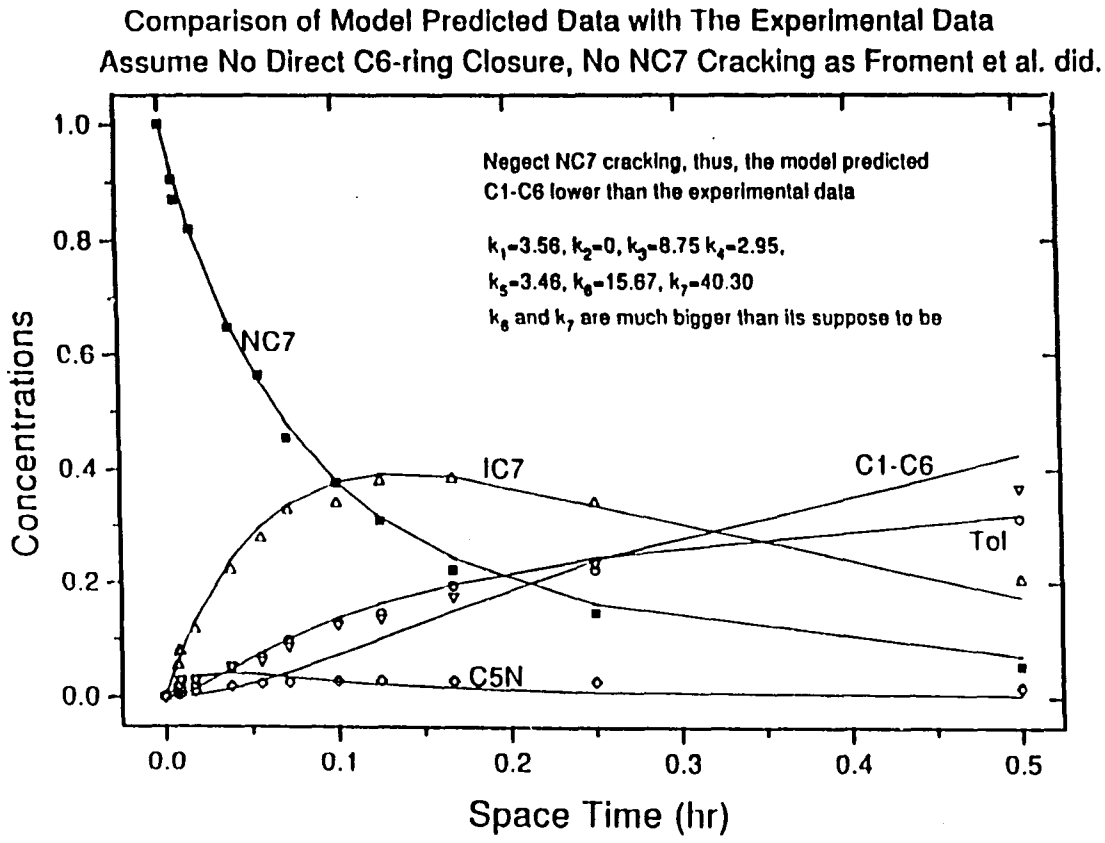

Figure 4-13

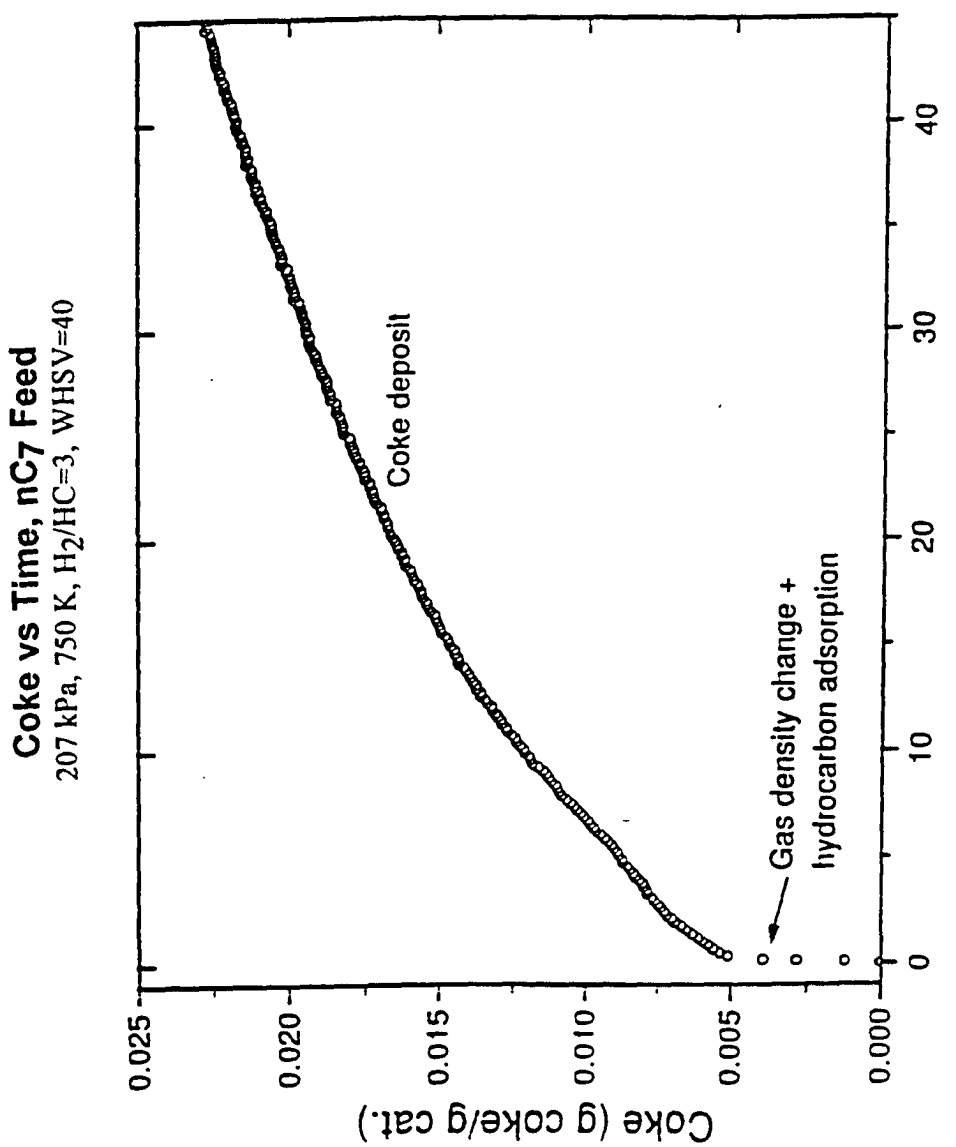

Figure 5-1

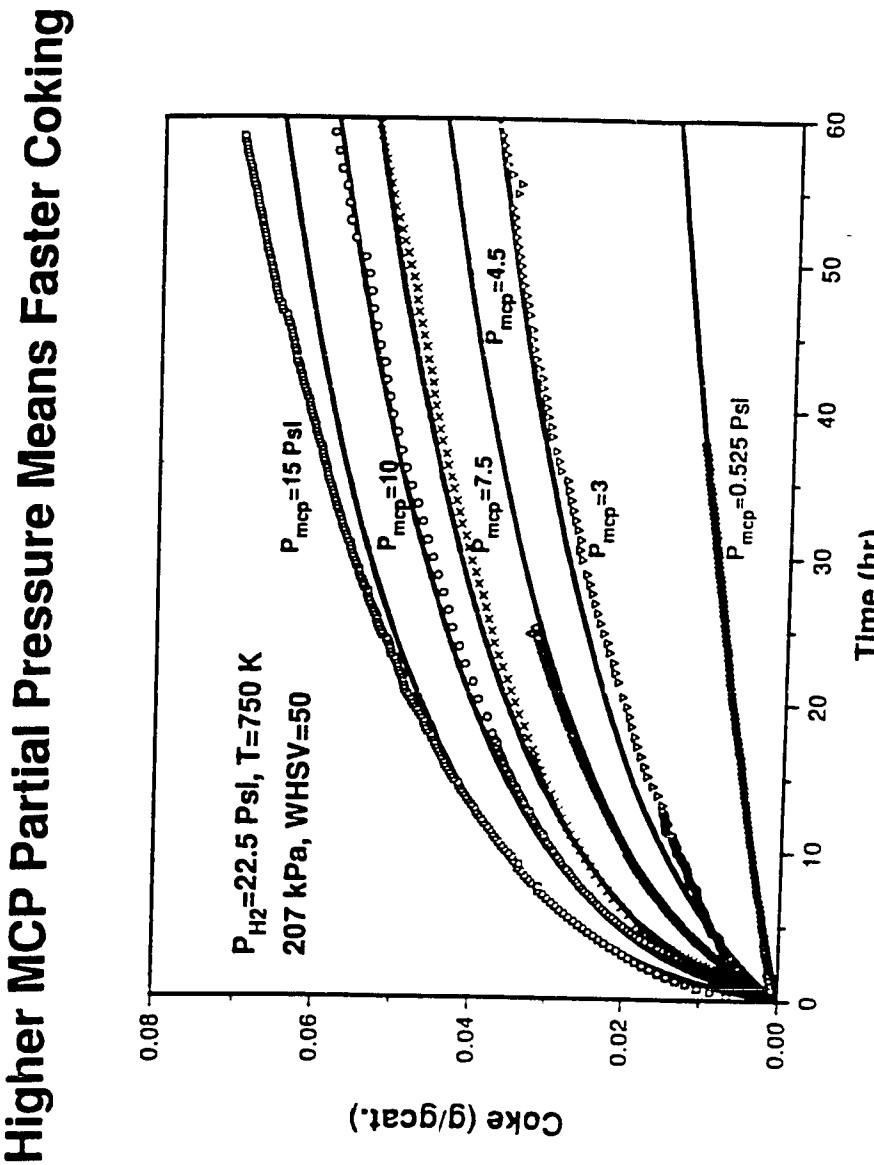

Figure 5-2

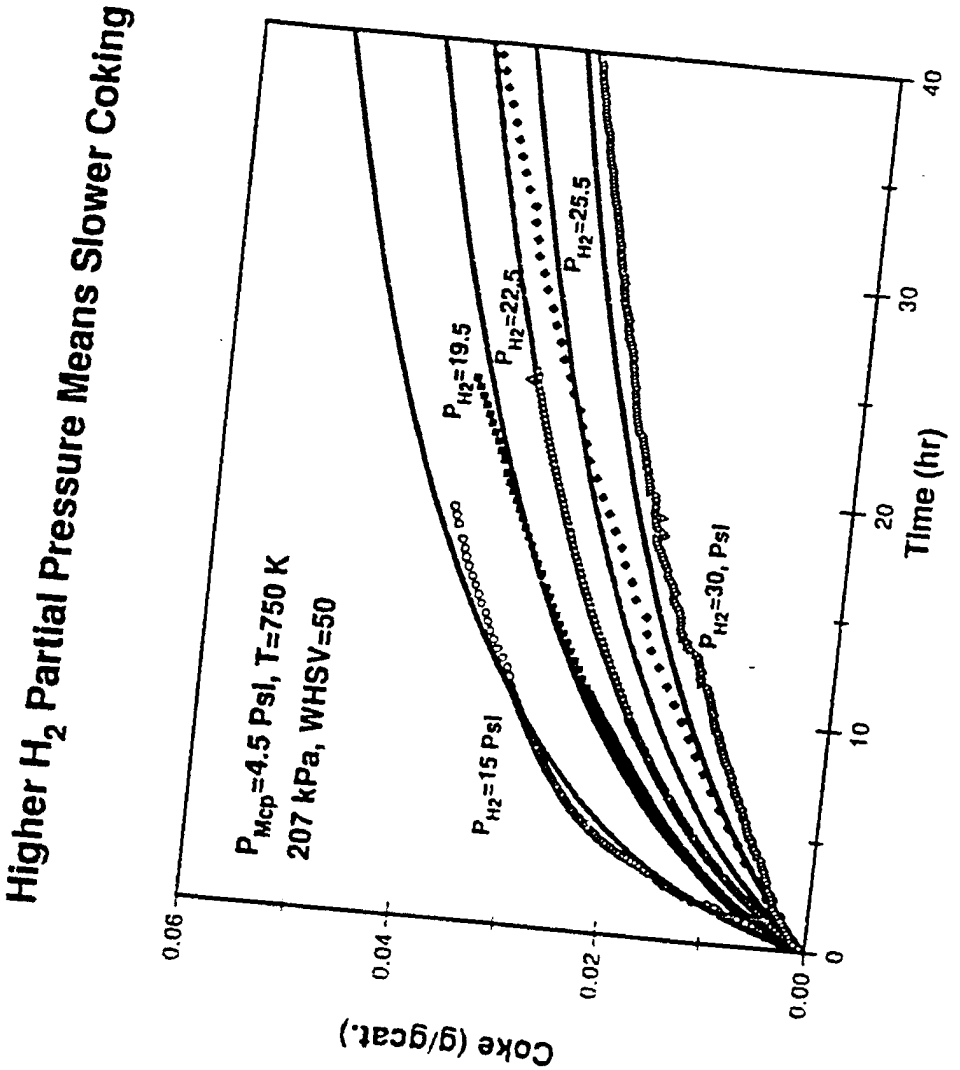

Figure 5-3

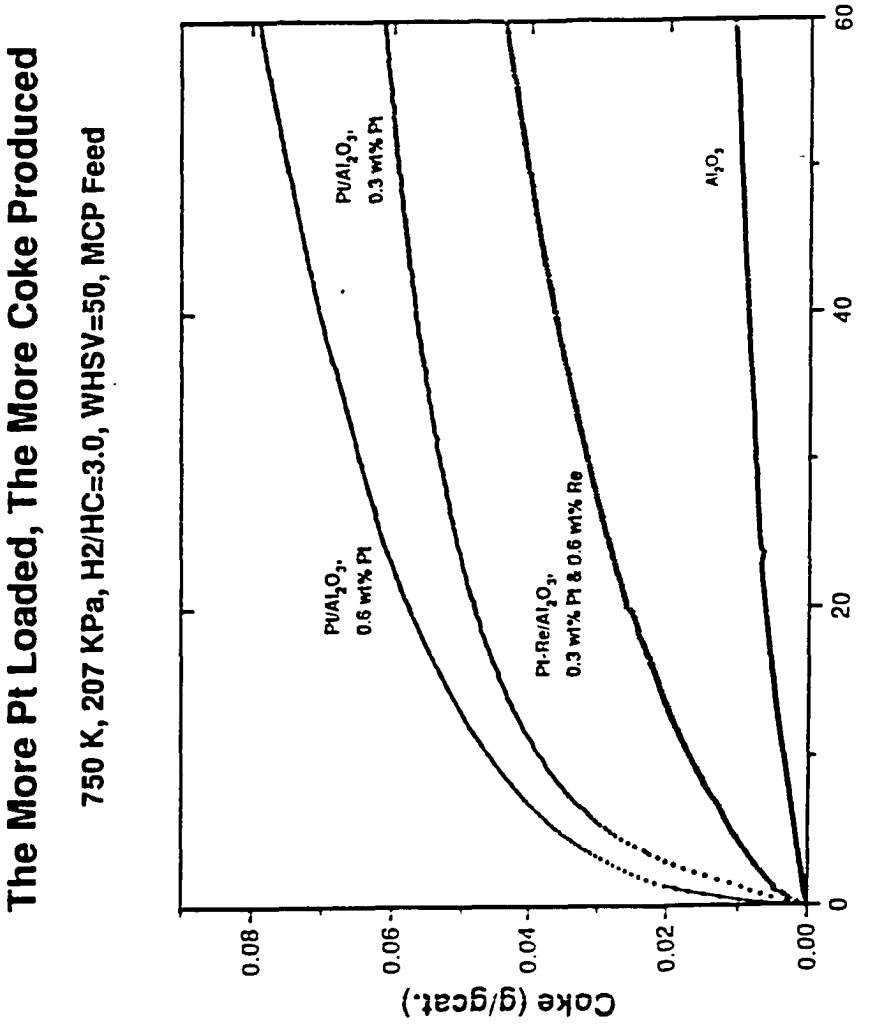

Figure 5-5

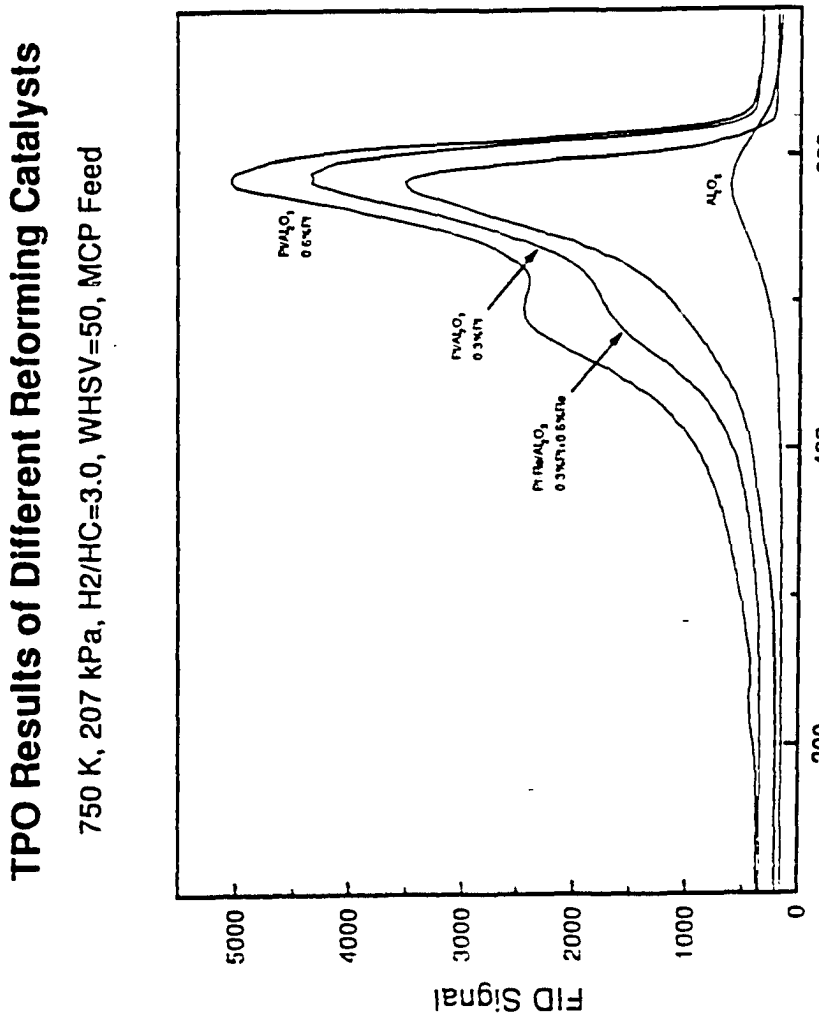

Figure 5-6

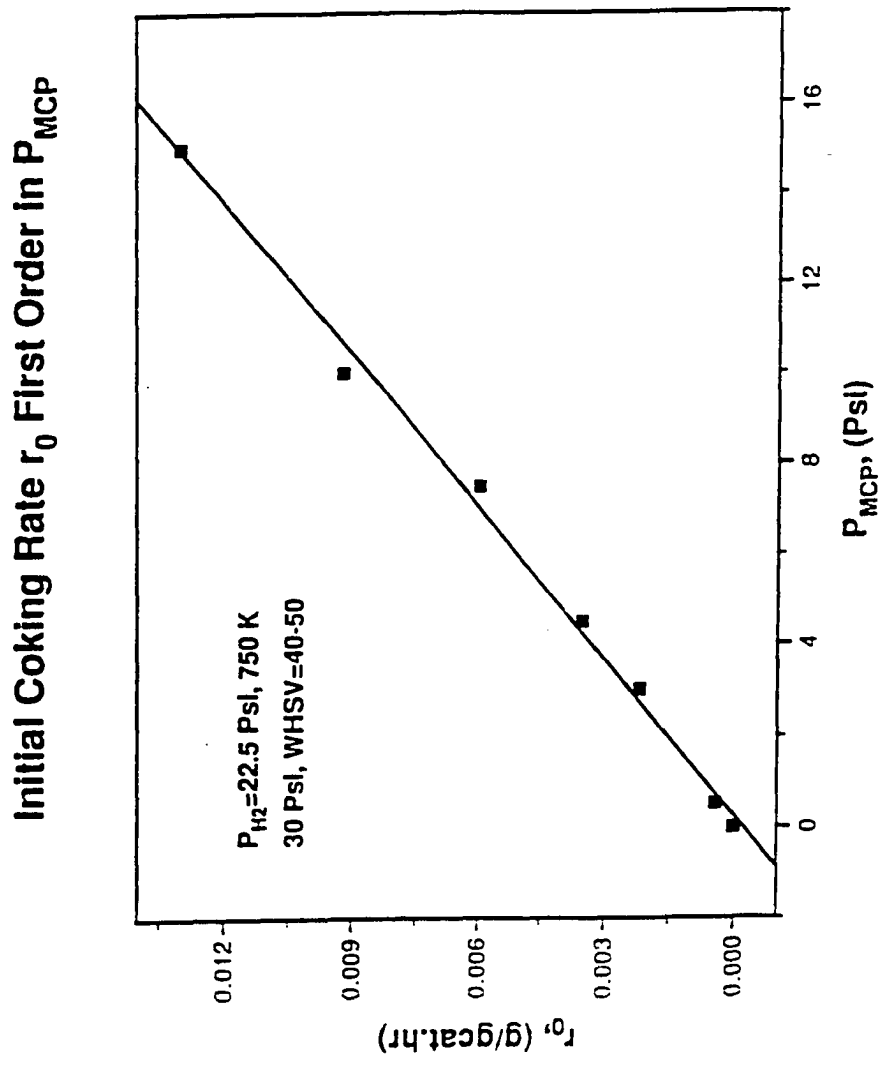

Figure 5-7

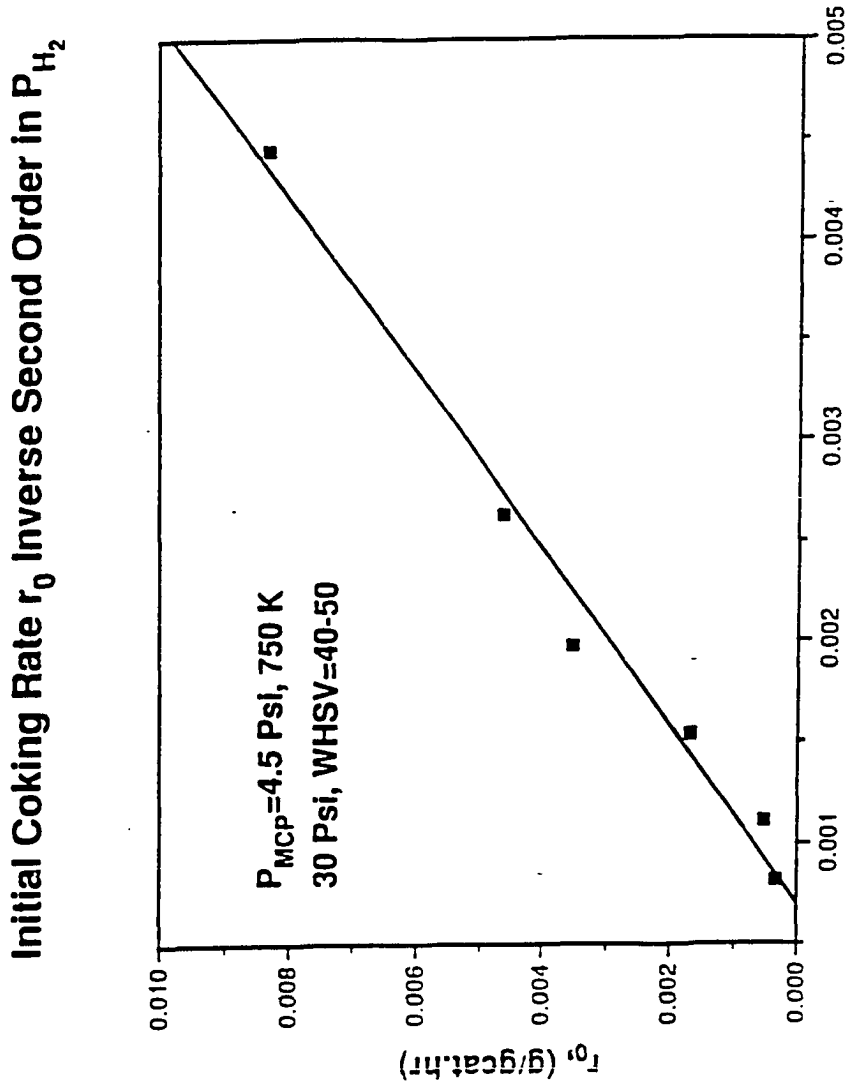

Figure 5-8

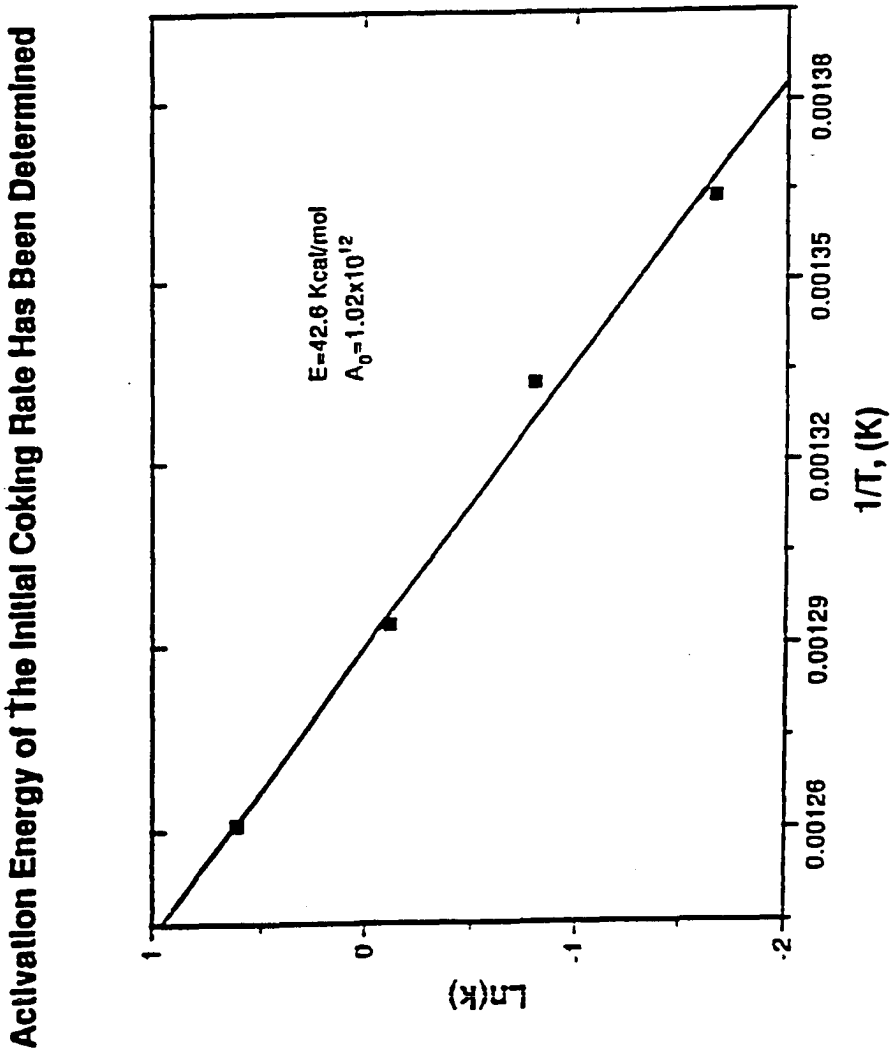

Figure 5-9

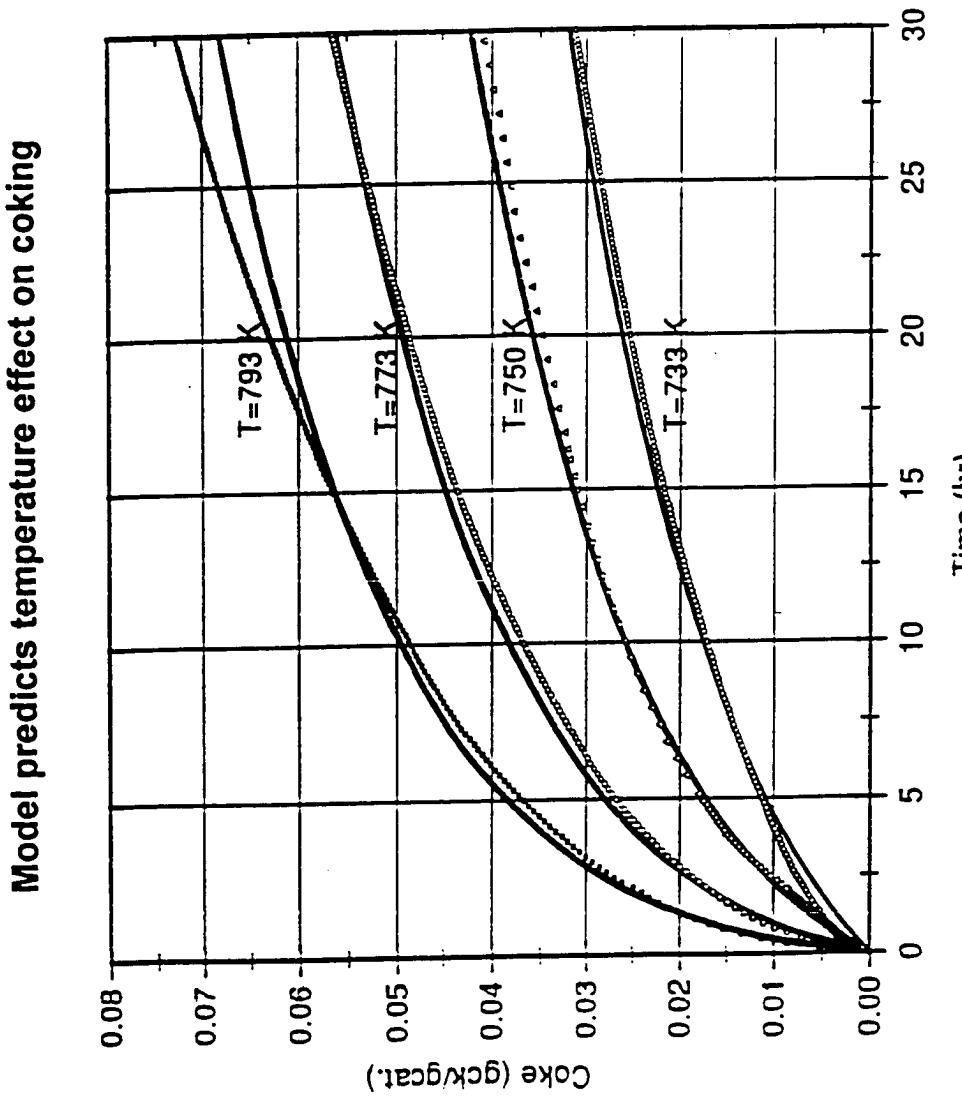

Figure 5-10

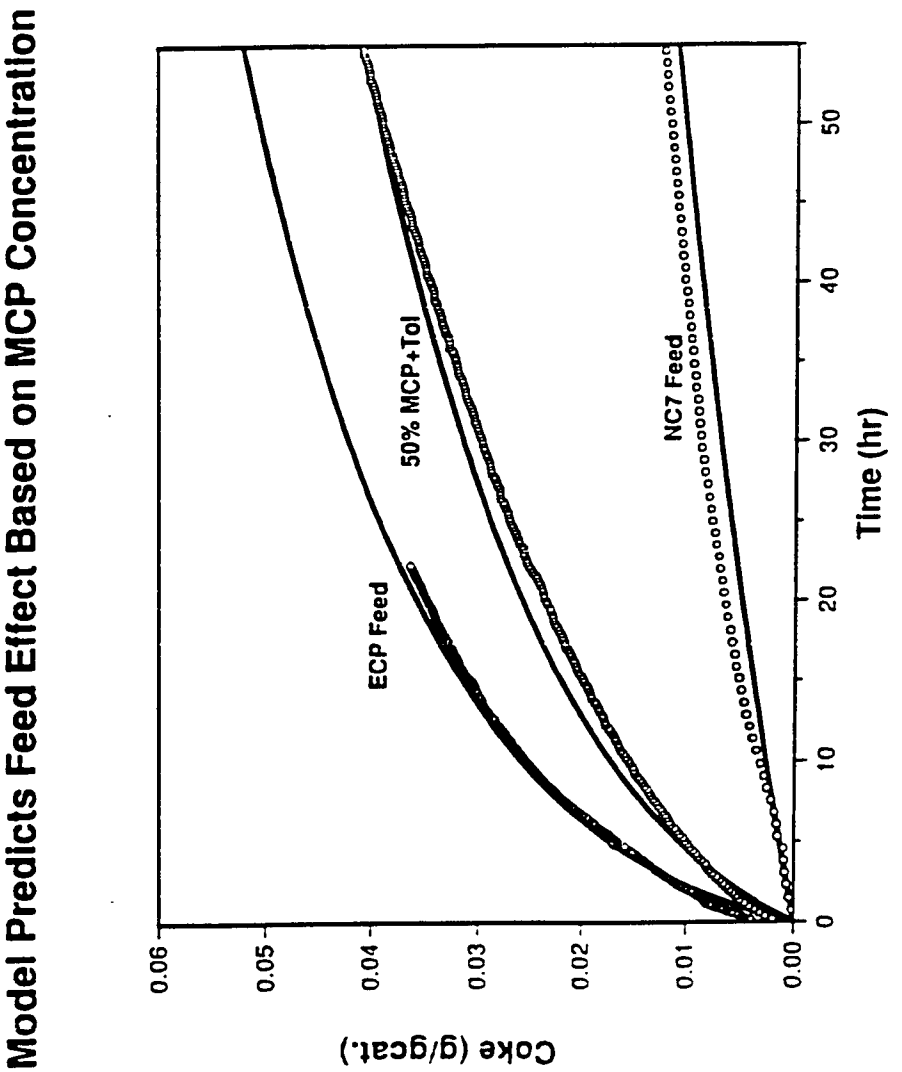

Figure 5-11

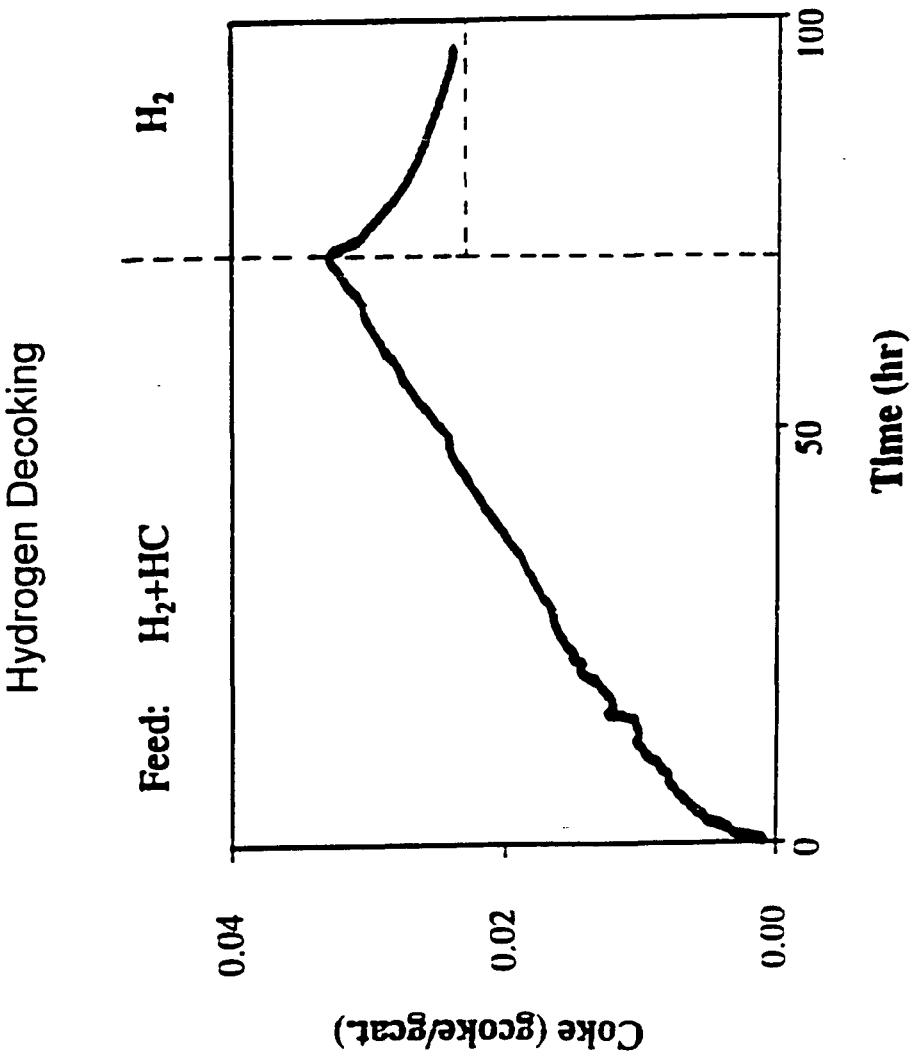

Figure 6-1

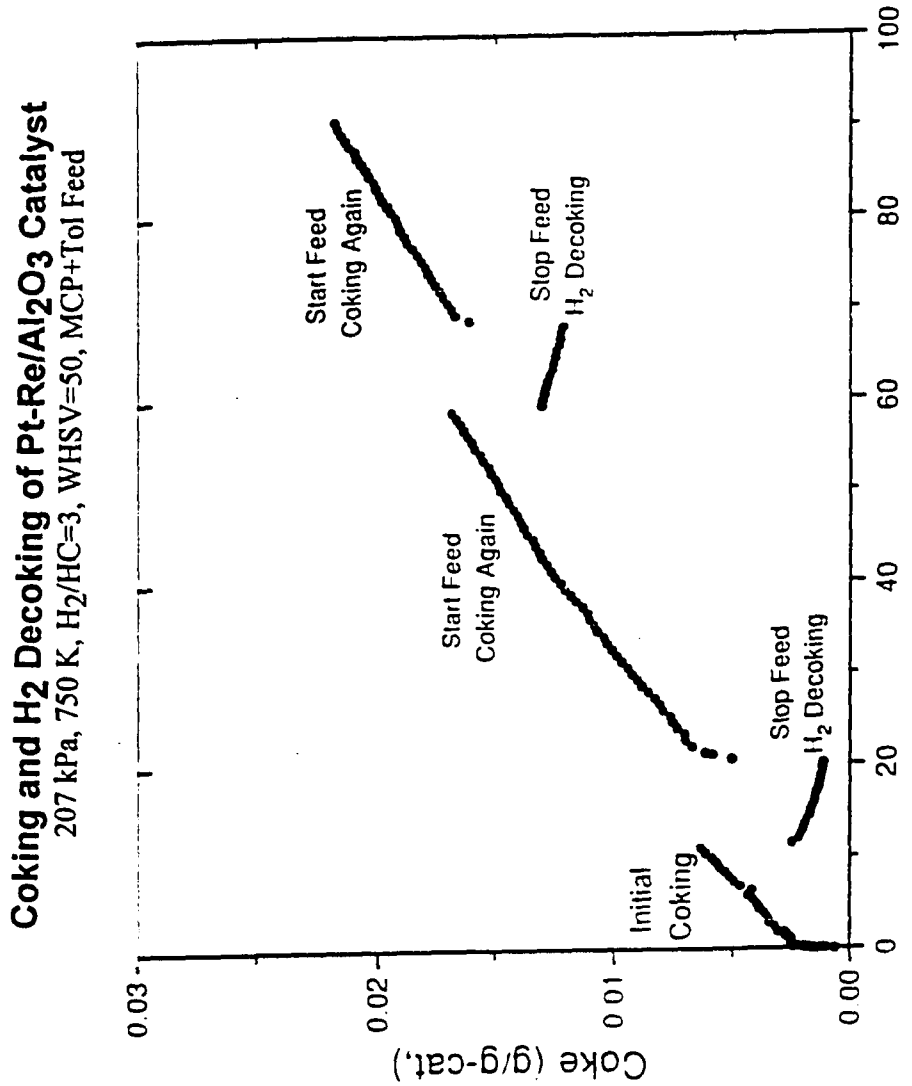

Figure 6-2

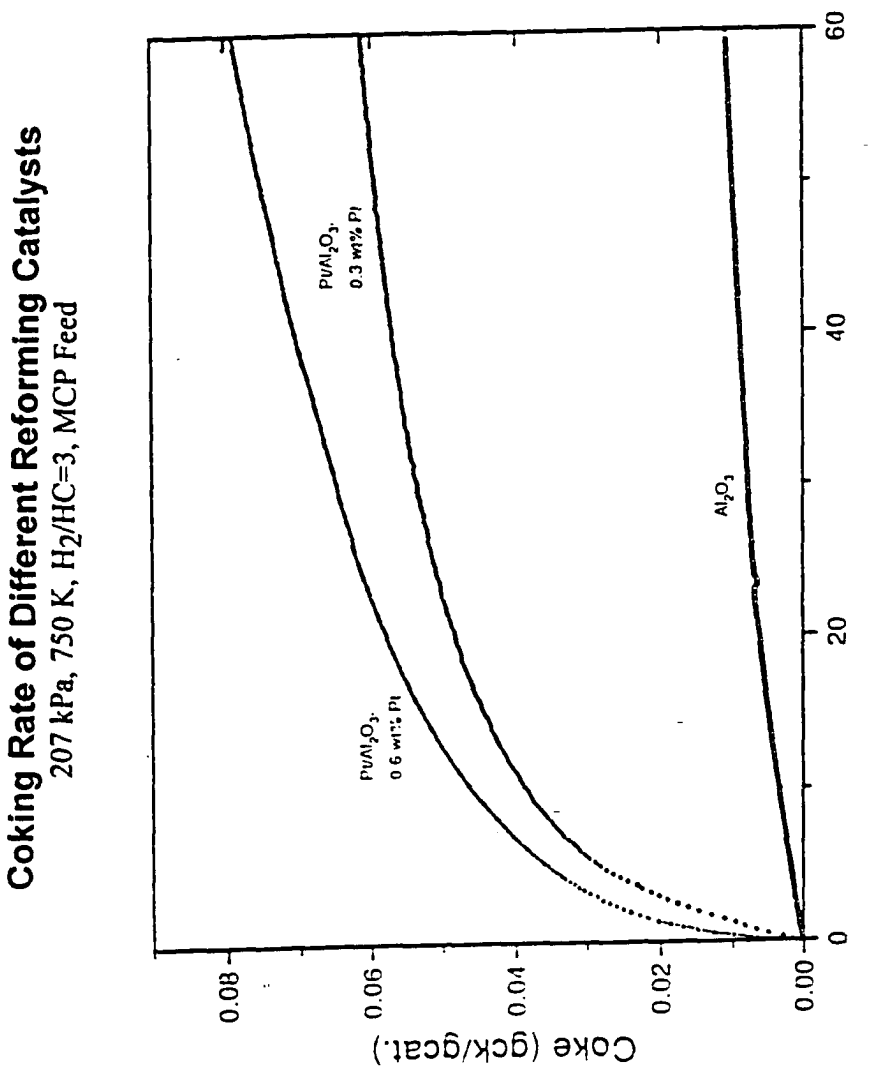

Figure 6-3a

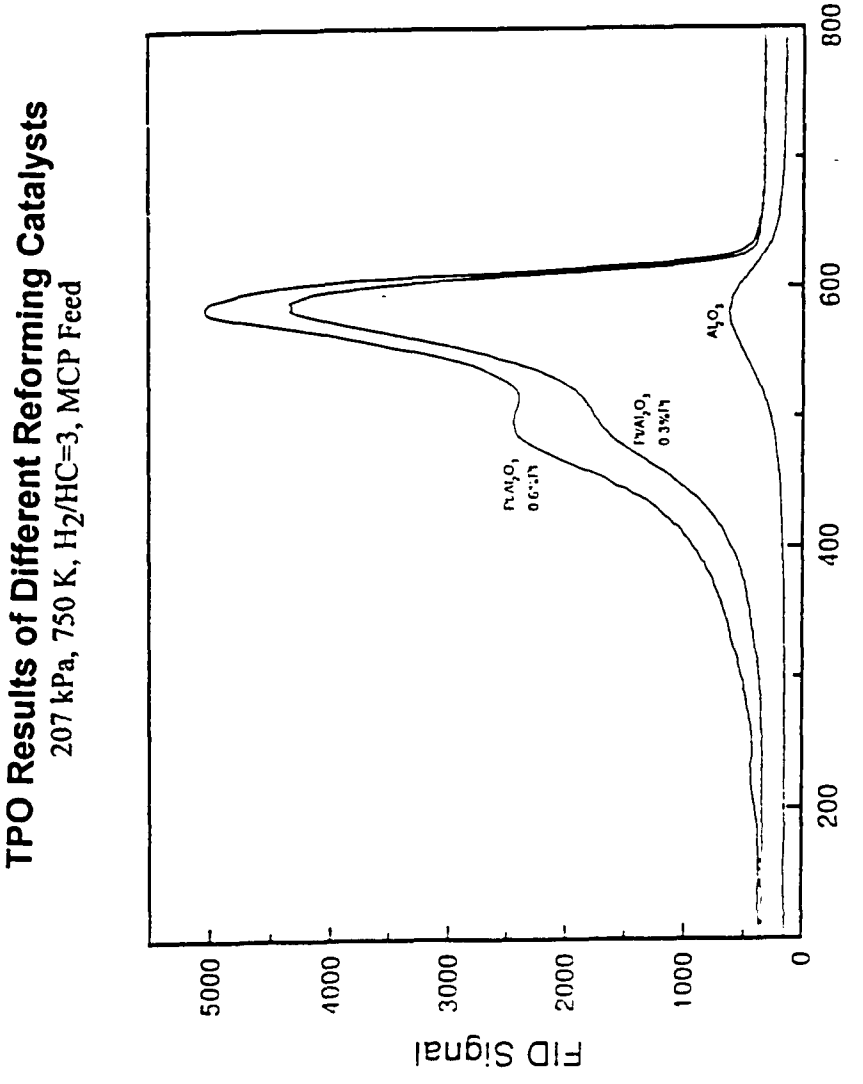

Figure 6-3b

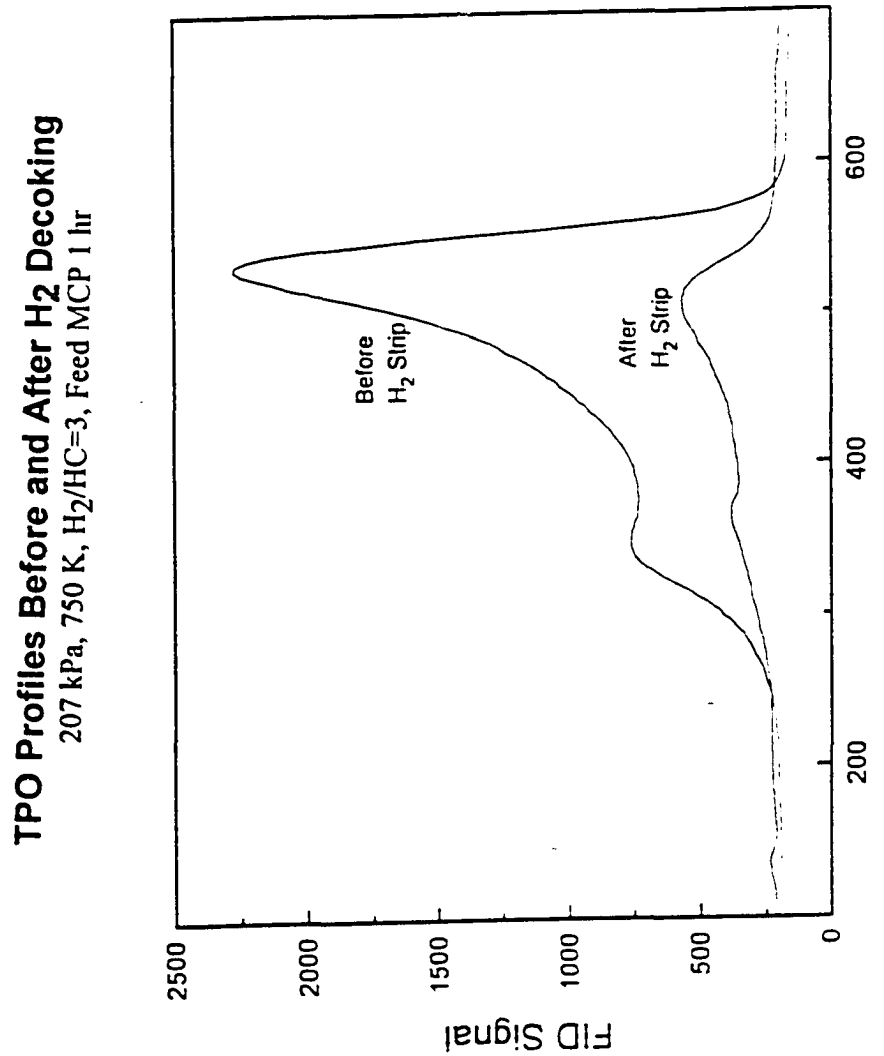

Figure 6-4

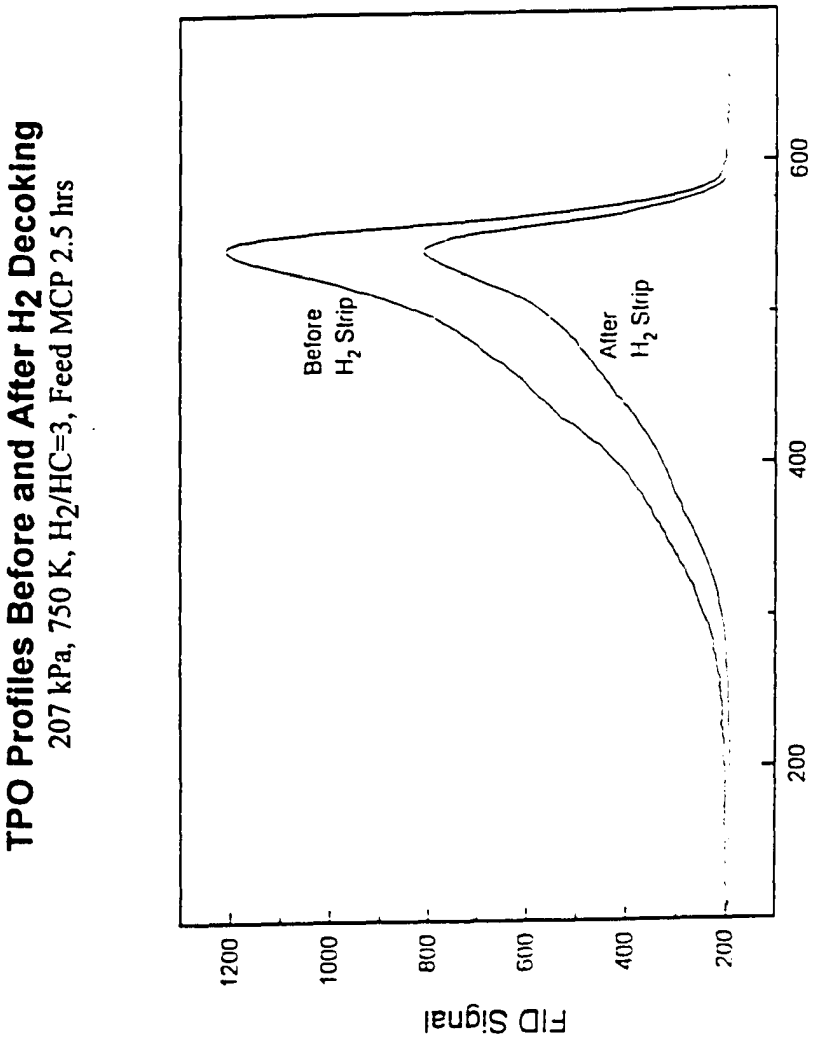

Figure 6-5

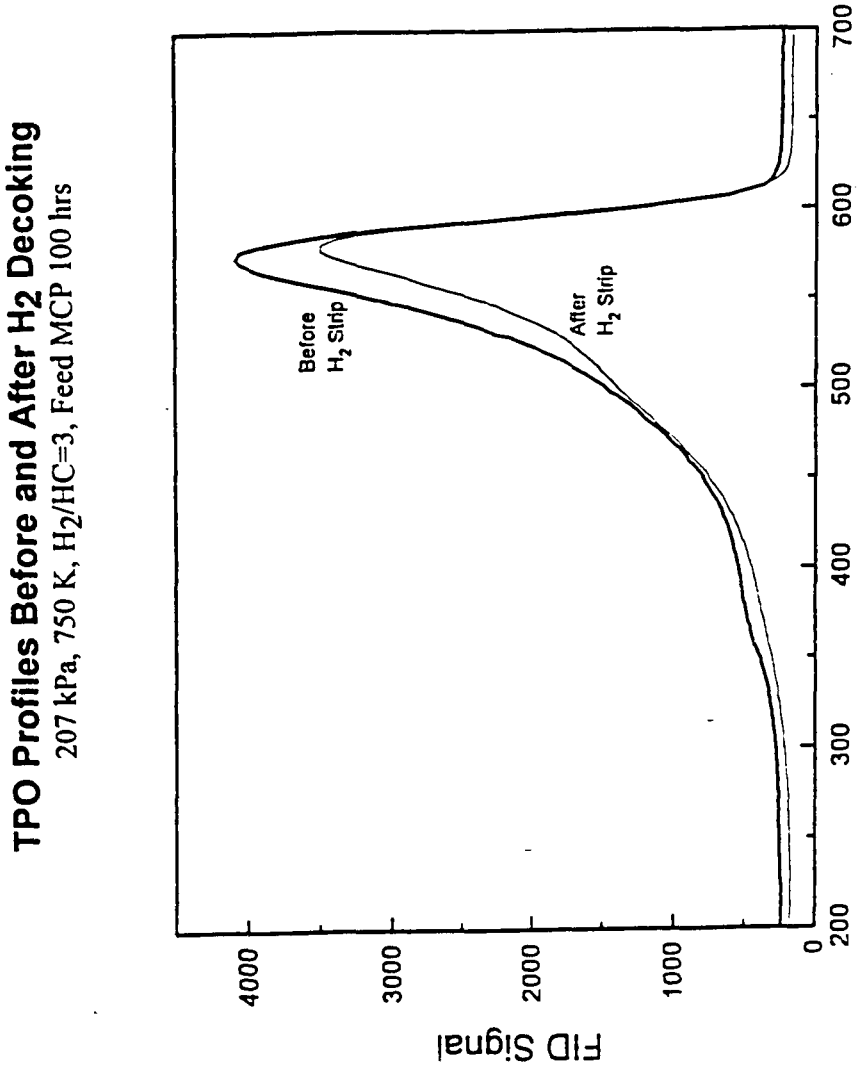

Figure 6-6

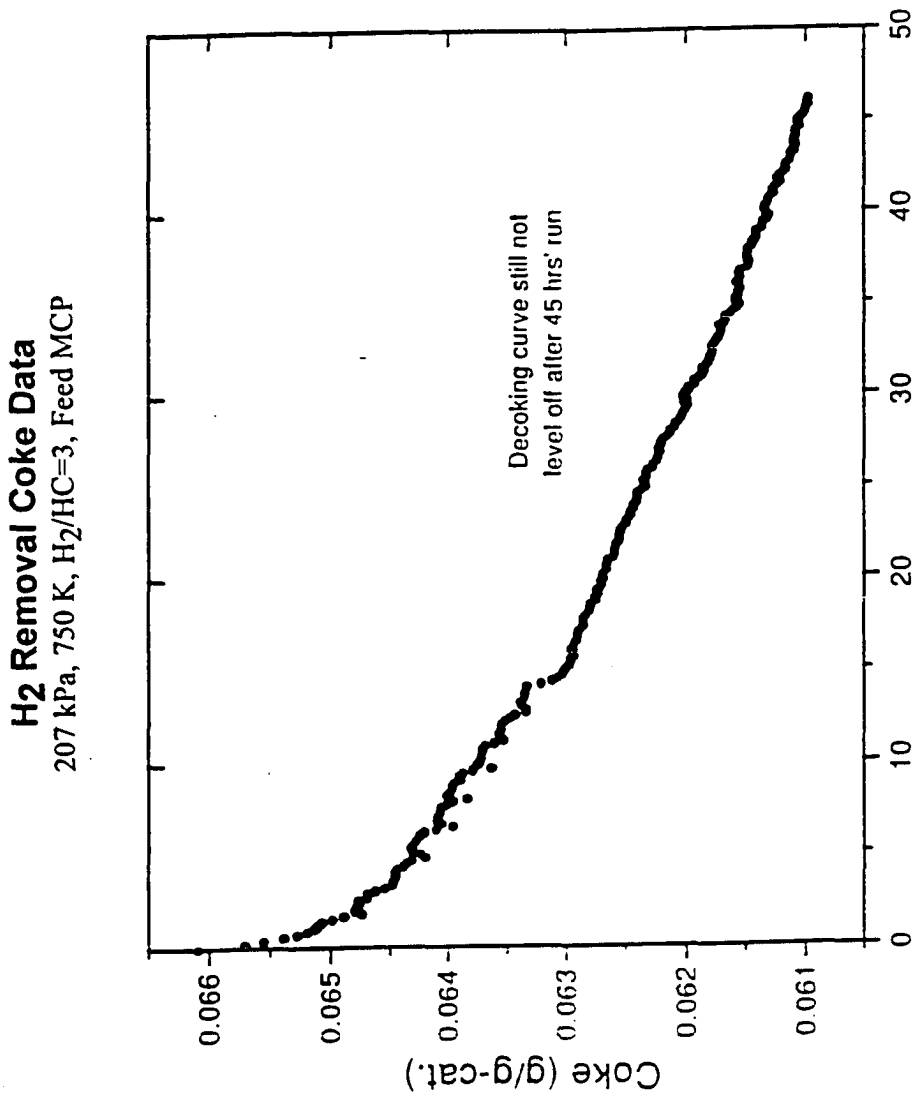

Figure 6-7

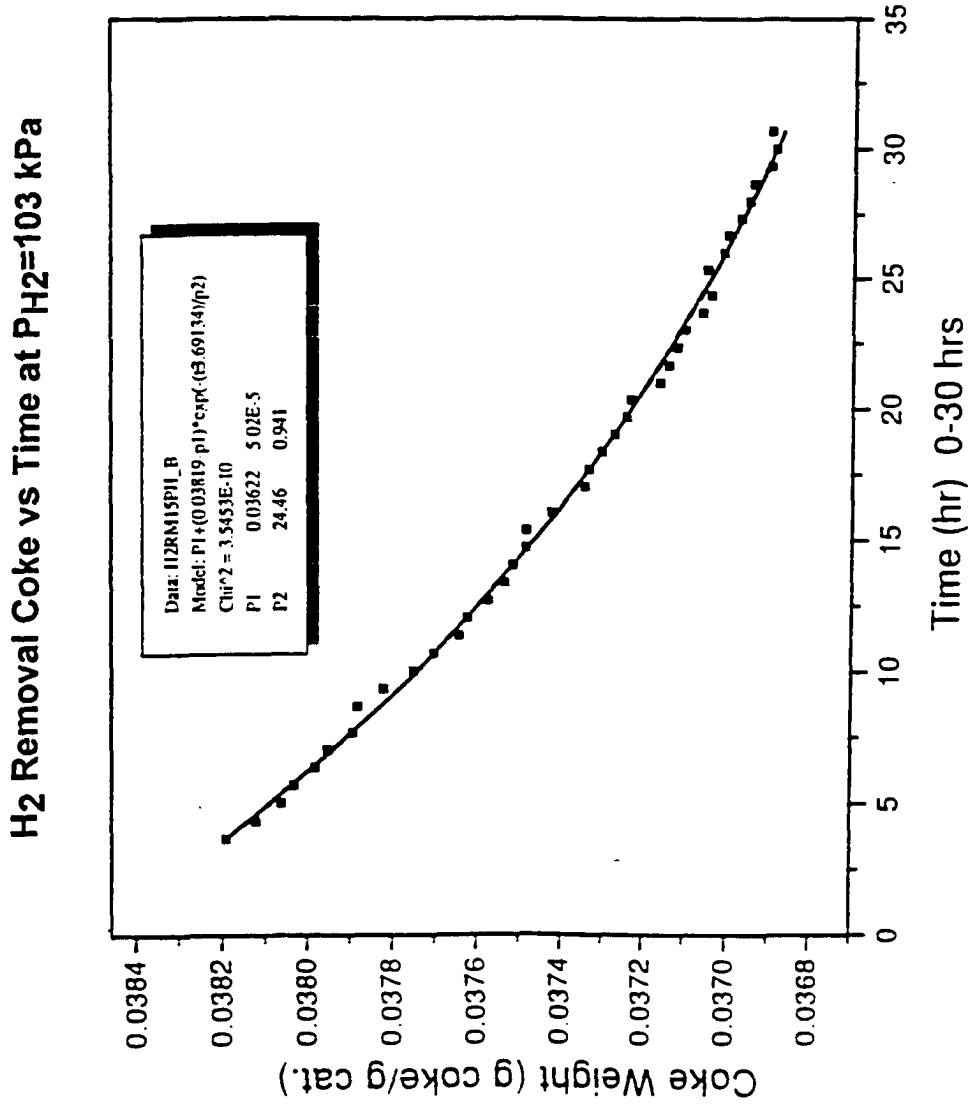

Figure 6-8

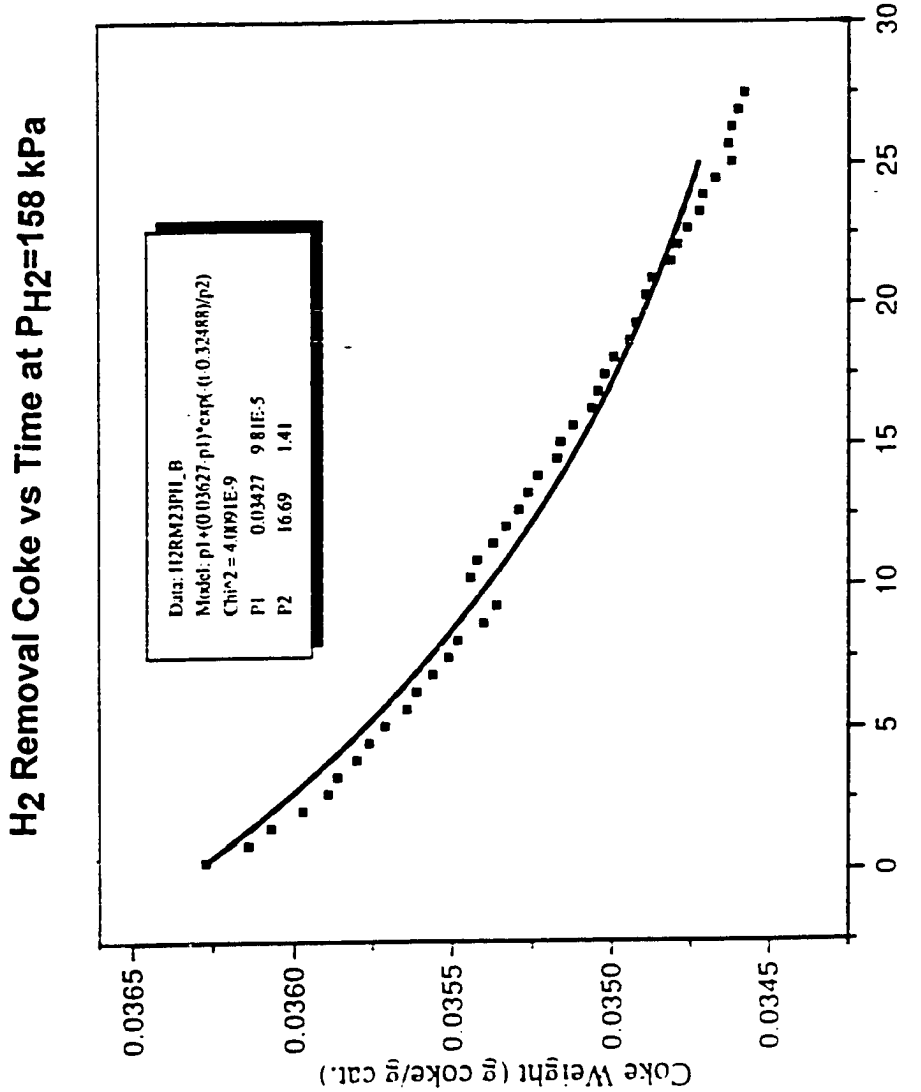

Figure 6-9

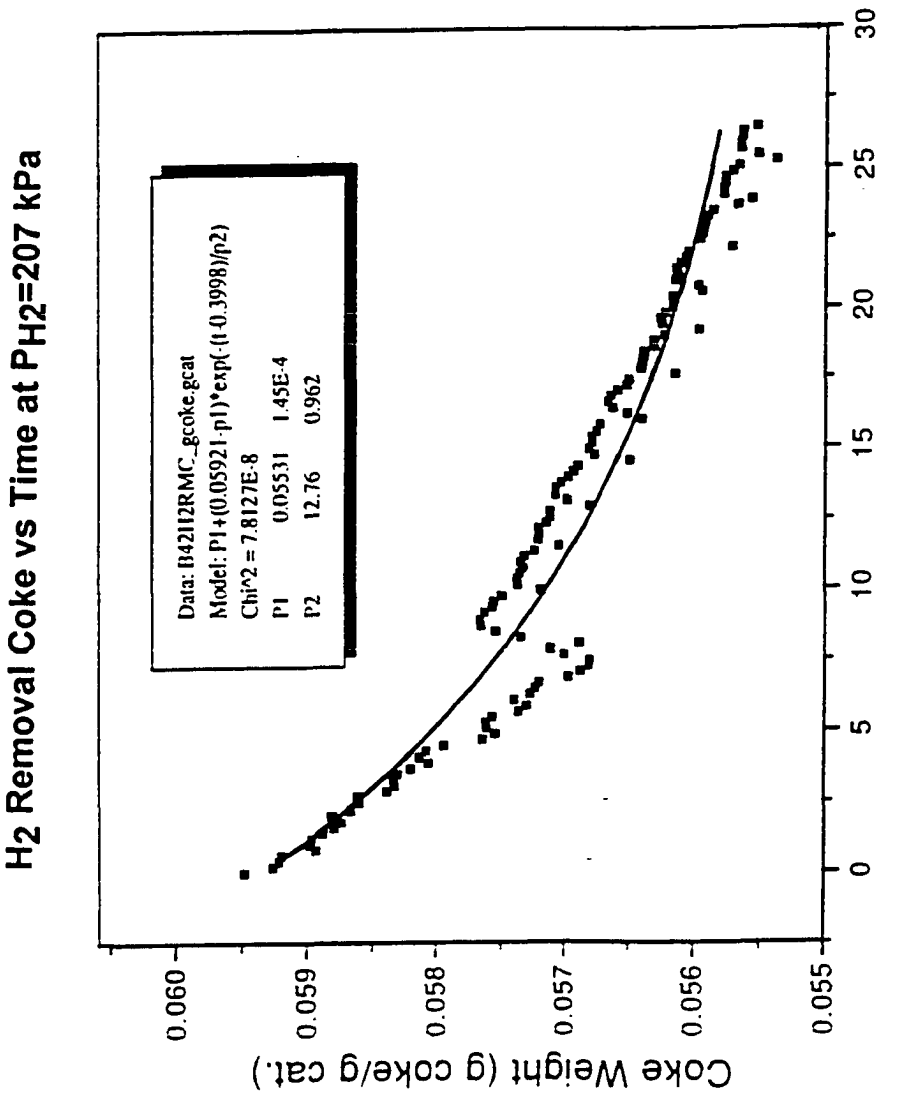

Figure 6-10

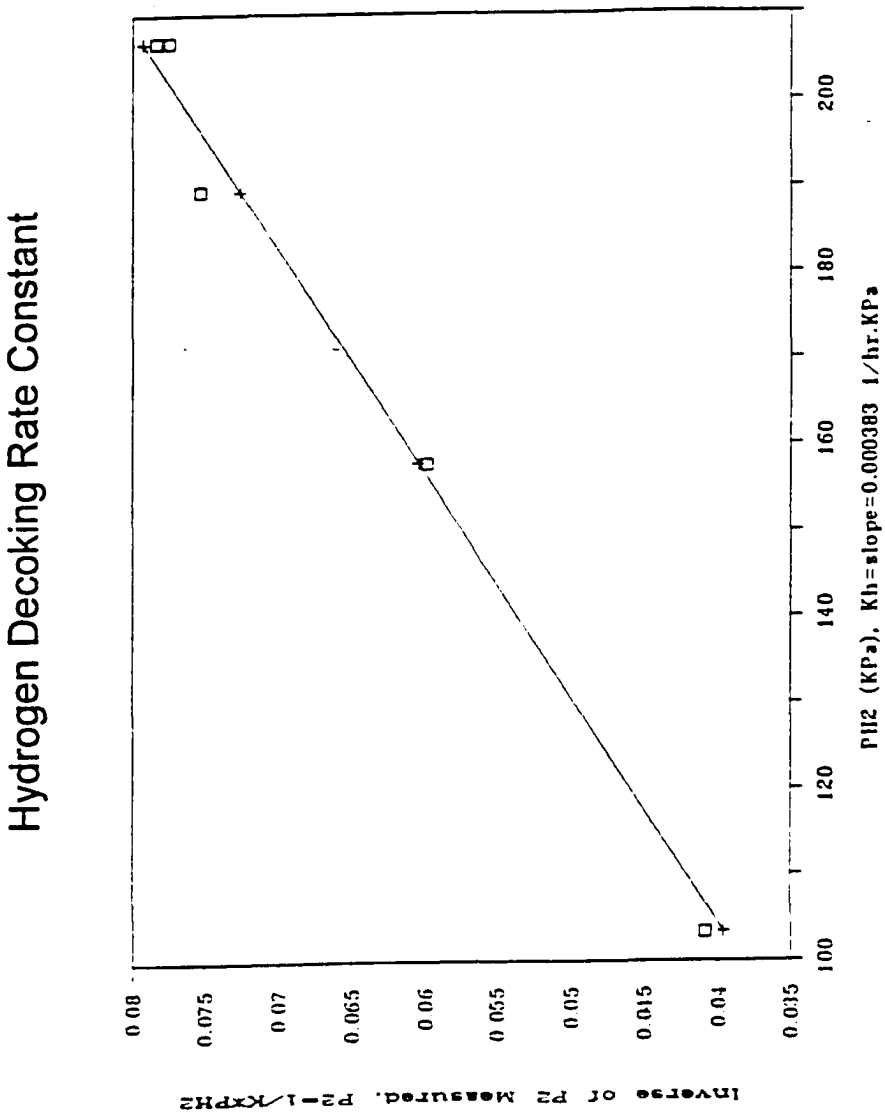

Figure 6-11

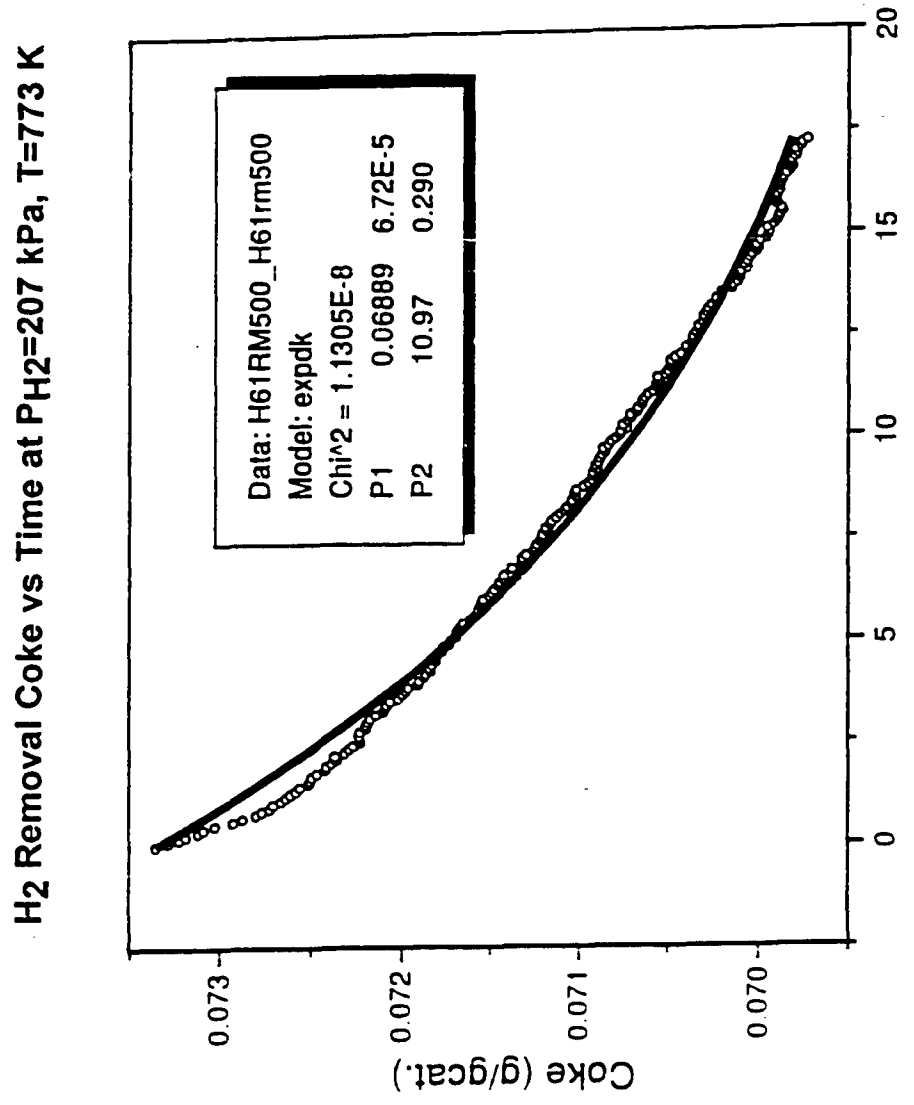

Figure 6-12

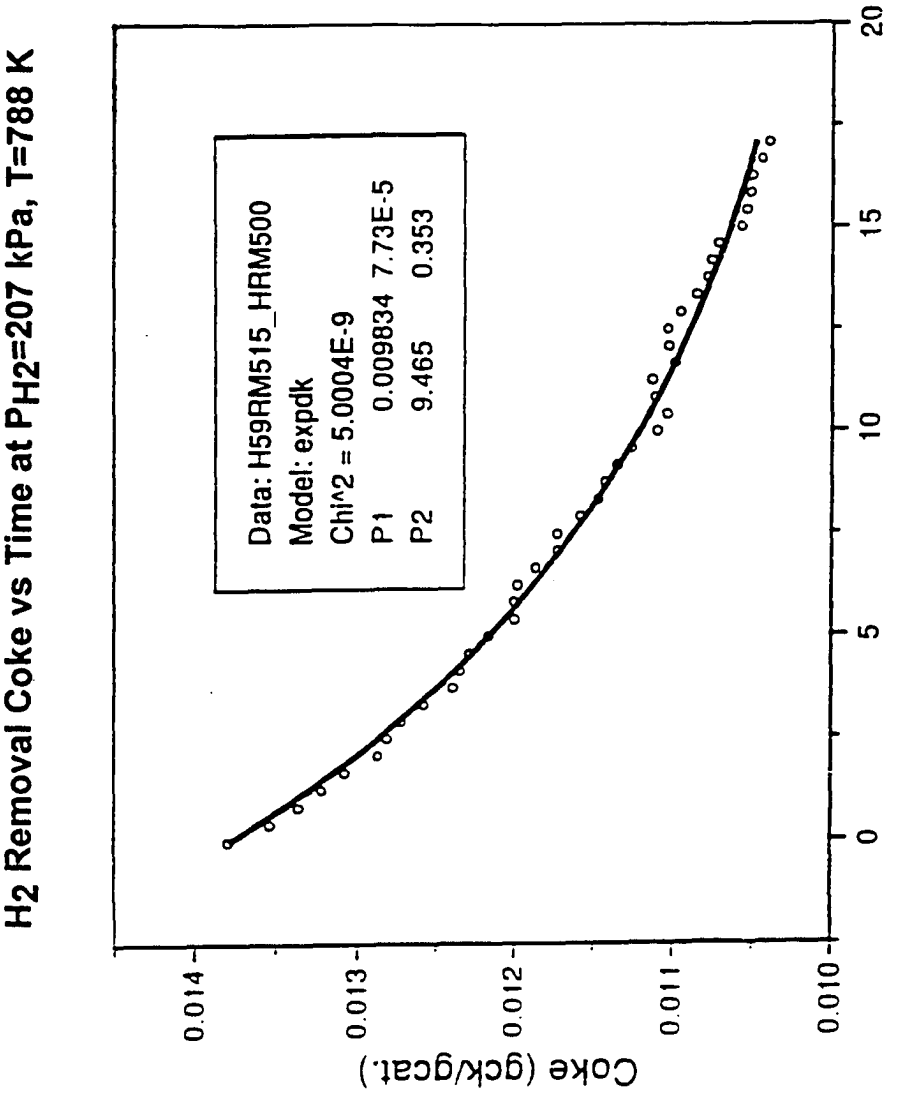

Figure 6-13

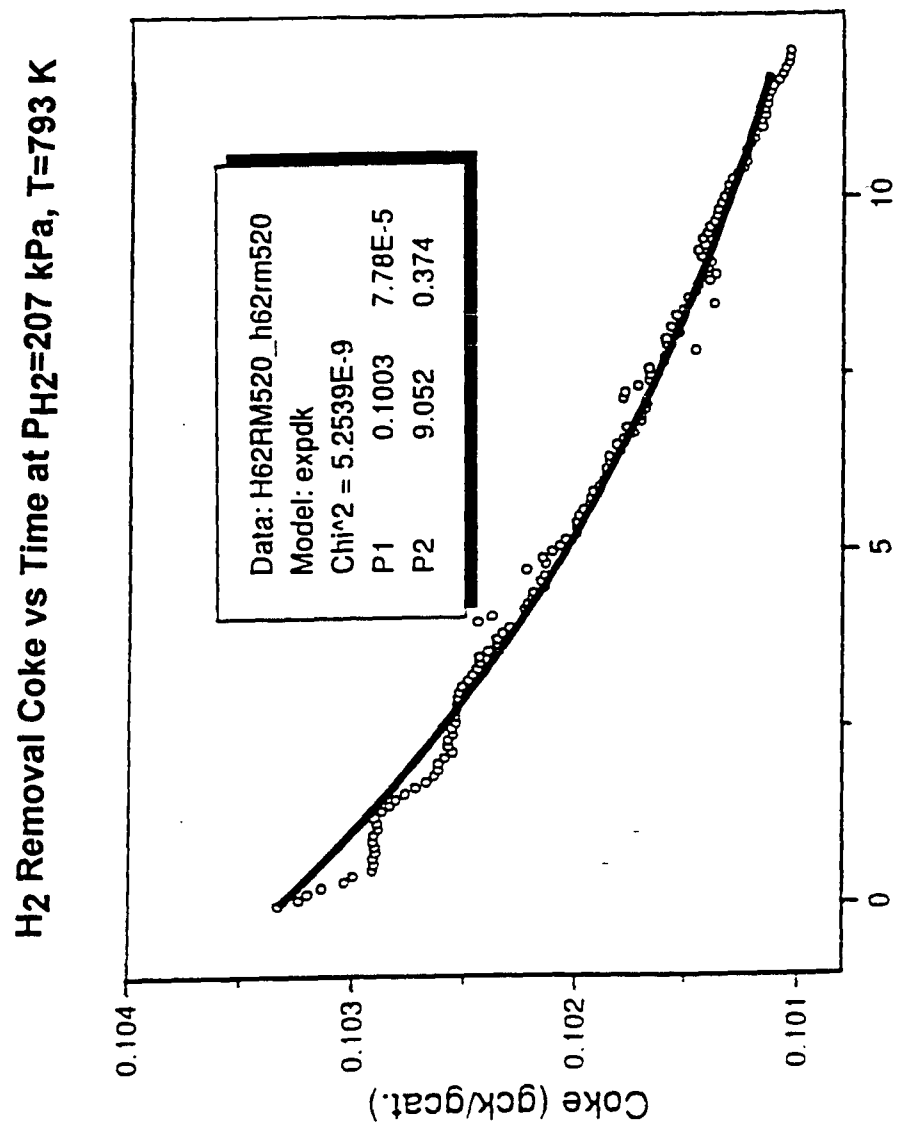

Figure 6-14

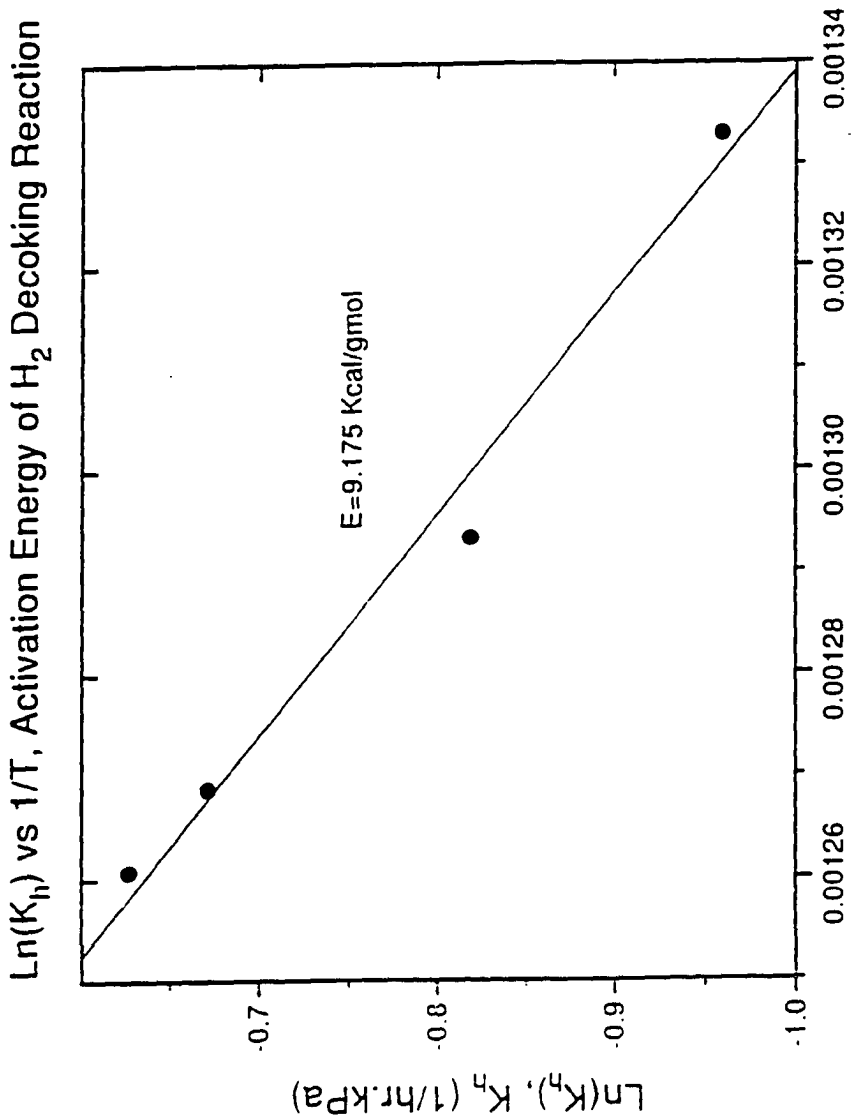

Figure 6-15

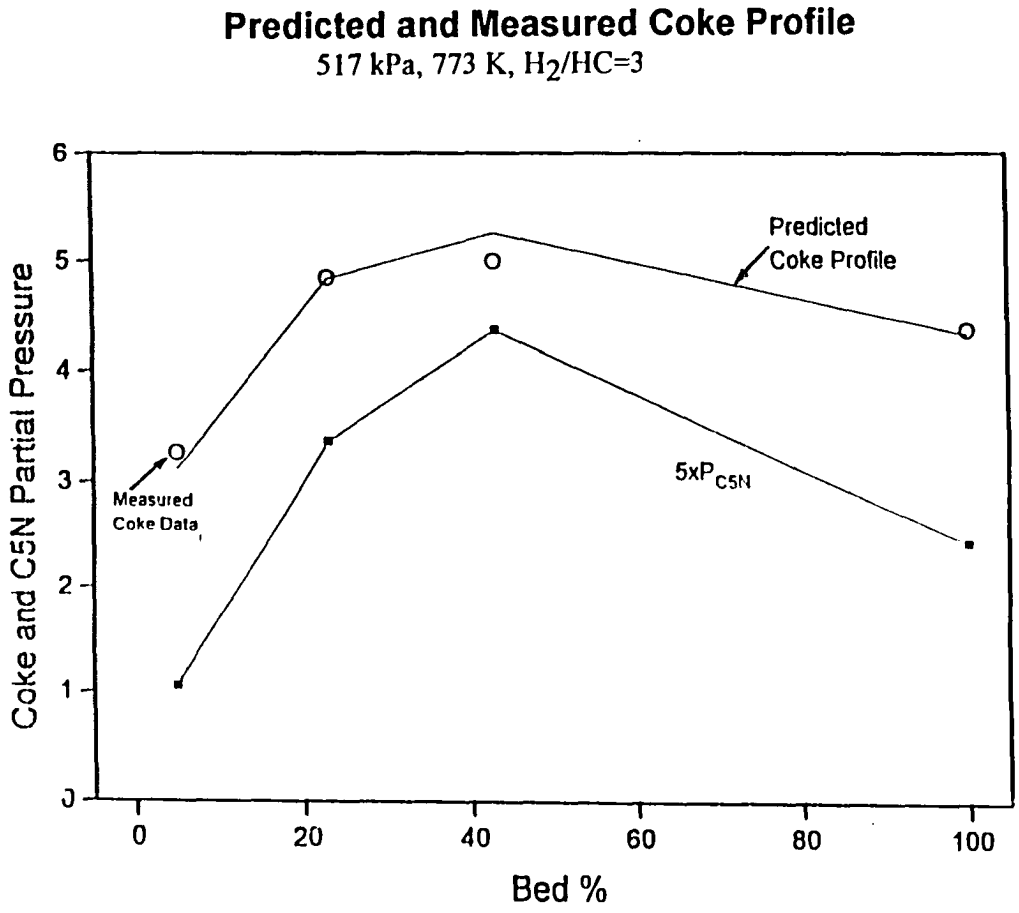

Figure 7-1a

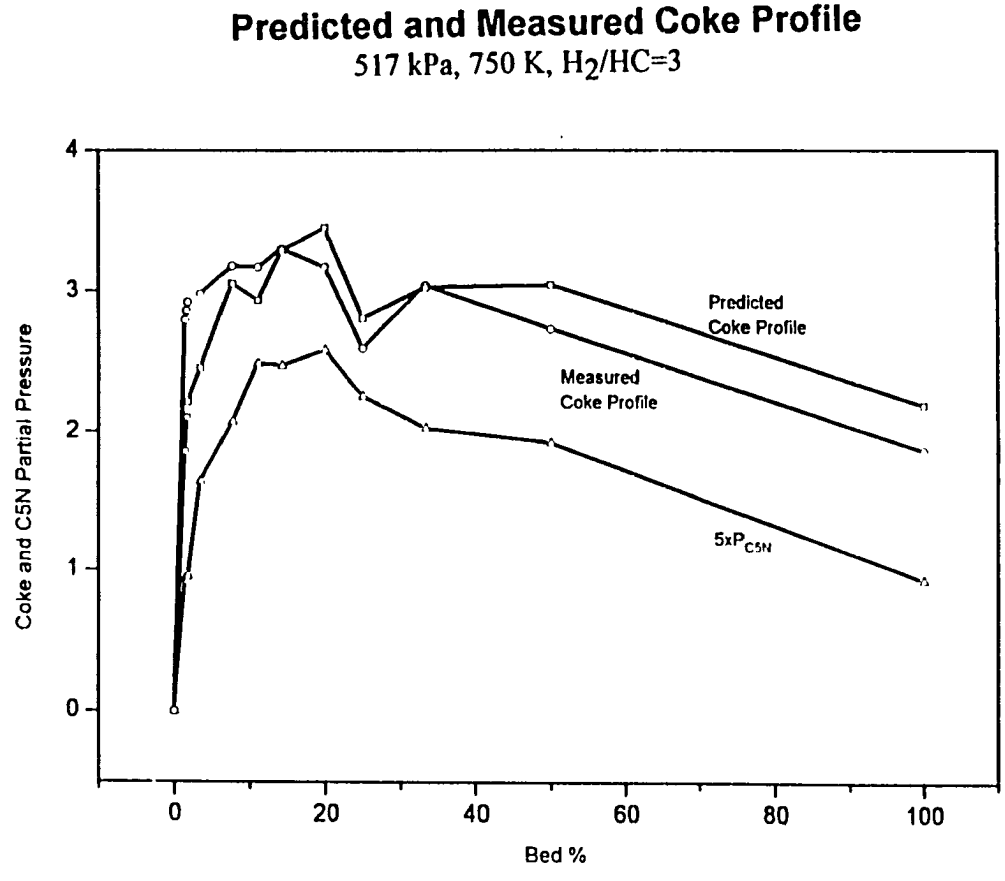

Figure 7-1b

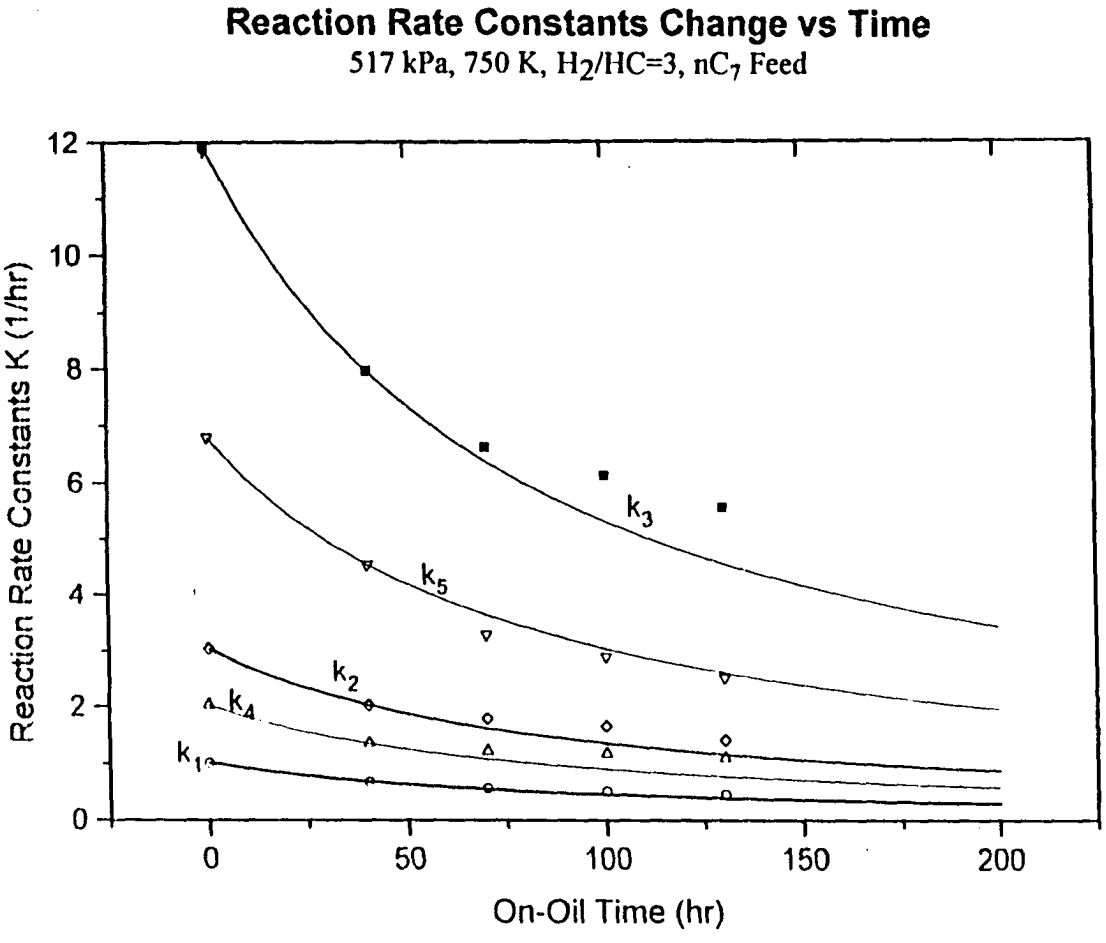

Figure 7-2

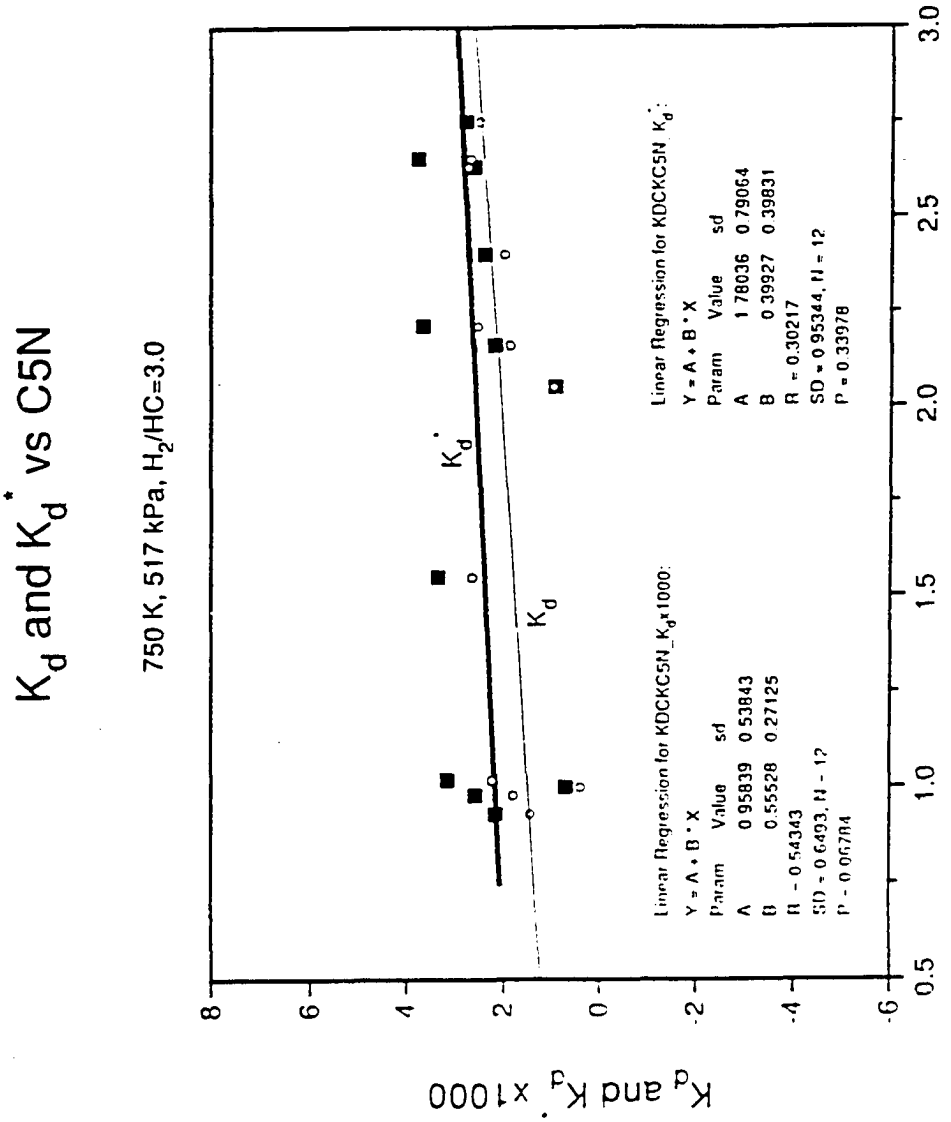

Figure 7-3a

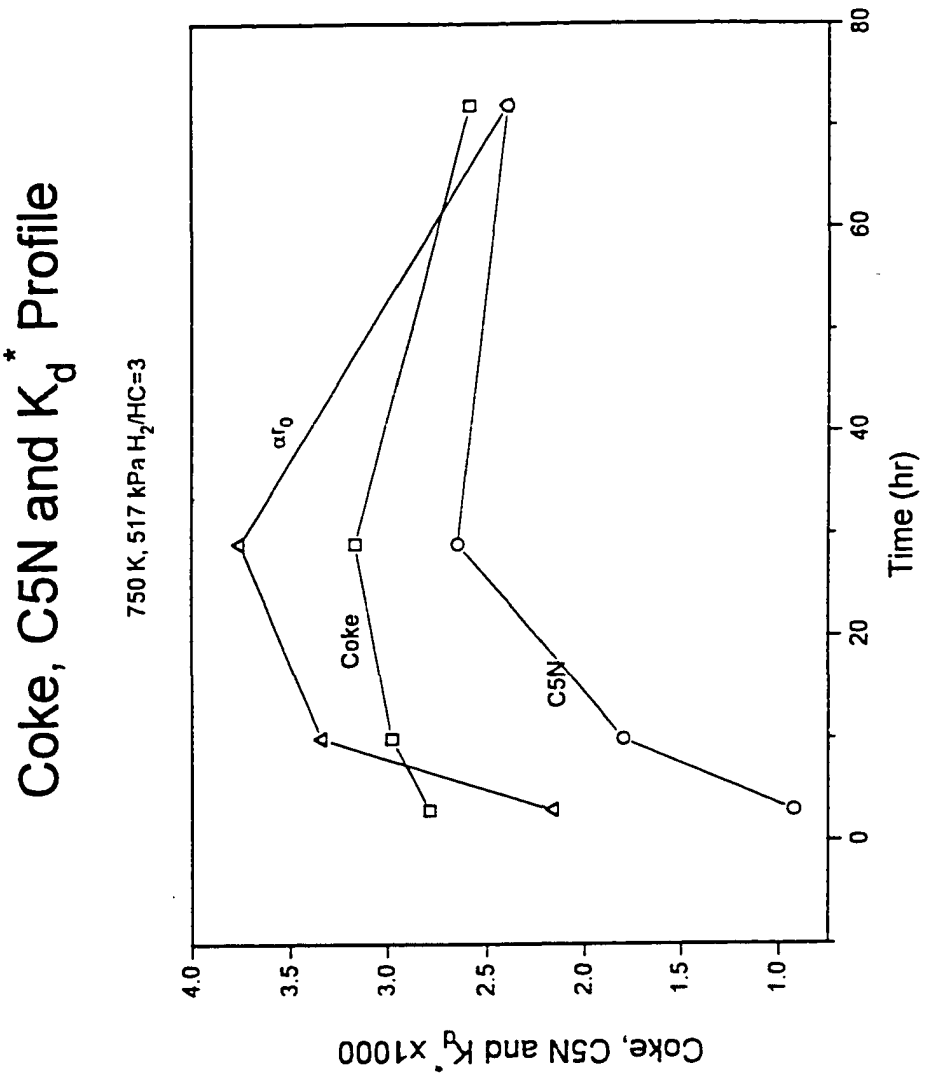

Figure 7-3b

$a=e^{-K_d t}$

Fig.2 of Shum et al, 1987

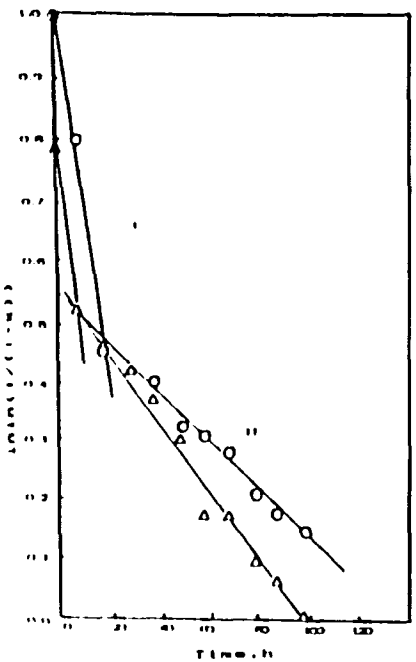

$a=1/(1+K^*_d t)$

Fit Shum et al's Data with Hyperbolic Model

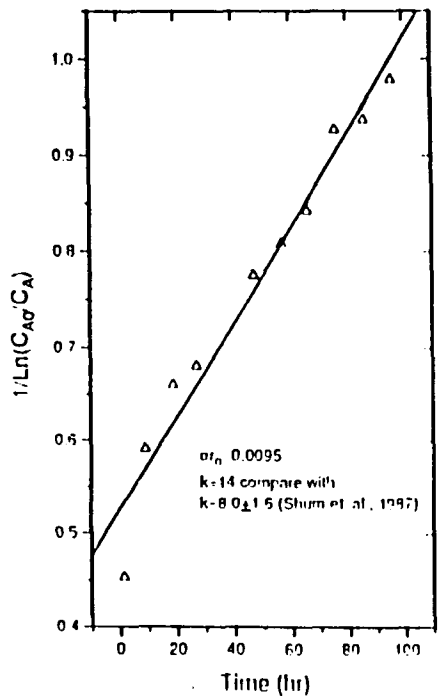

nC_6 Feed, Pt-Re/Al_2O_3(0.9wt% Cl), WHSV=7.7, P=1.5 MPa, T=770 K

Figure 7-4

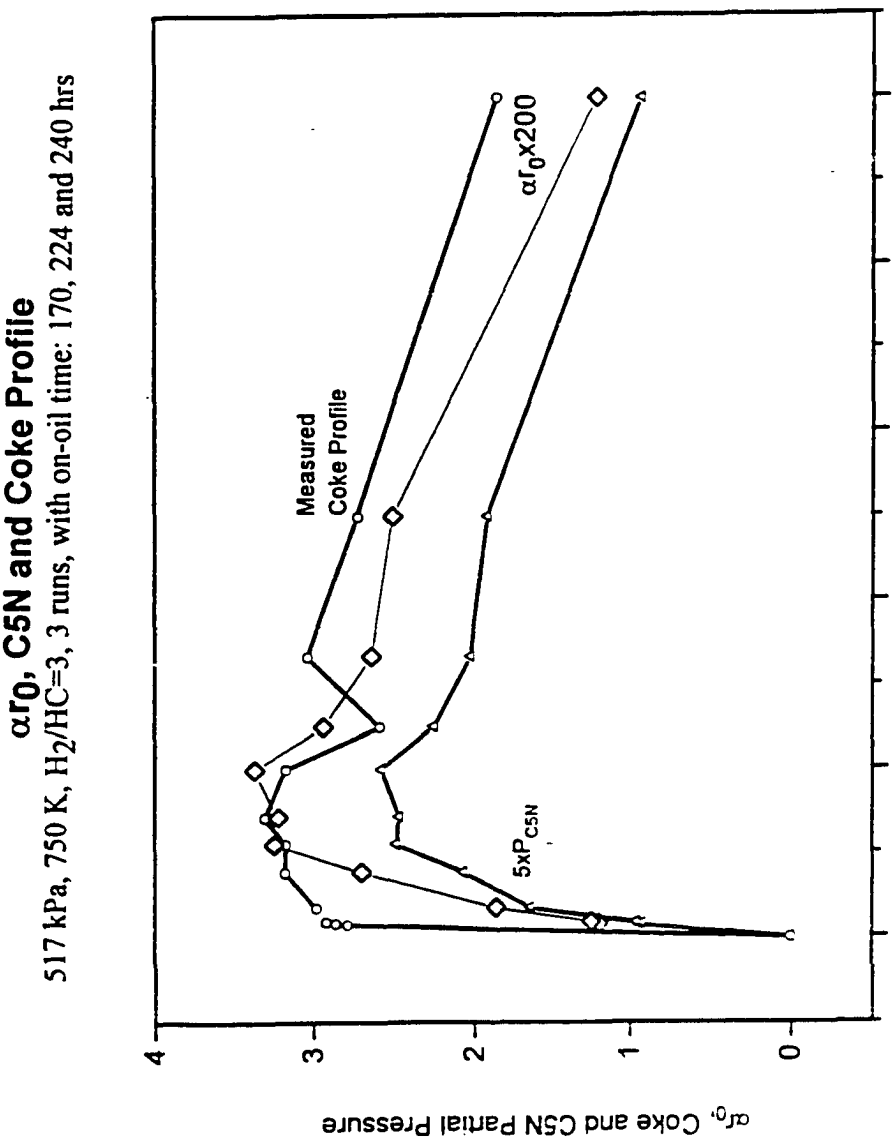

Figure 7-5

NOMENCLATURE

a= activity function,

C= concentration

C_A= nC_7 reactant concentration

C_k= total amount of coke deposited on the catalyst, gcoke/g catalyst

C5N= five carbon atom ring naphthenes

C_{6^-}= cracking products of nC_7 reforming

E= apparent activation energy of coking reaction, Kcal/mol.

ECP= ethylcyclopentane

f= fraction of the foulant on the catalyst surface.

FC= final, unremovable coke

HC= hydrocarbon

iC_7= iso-heptane

K_i= reaction equilibrium constant of MCP dehydrogenation reaction

K_d= lumped deactivation constant based on $a = e^{-K_d t}$

K_d^*= lumped deactivation constant based on $a = \frac{1}{1 + K_d^* t}$

K_h= hydrogen decoking rate constant

K_{H2}= adsorption equilibrium constant for H_2

K_{HC}= adsorption equilibrium constant for hydrocarbon

k_1-k_7= reaction rate constant as defined in the nC_7 reforming reaction scheme

m= number of active sites involved in the controlling step of the main reaction

MCP= methylcyclopentane

MCPe= methylcyclopentene

MCPde= methylcyclopentadiene

MCH= methylcyclohexane

MH= methylhexane

n= the number of H_2 molecular dehydrogenated from MCP or the reaction order

NC= new or fresh coke

nC_7= normal heptane

P= total pressure, kPa

P_{mcp}= partial pressure of MCP, kPa

P_{mcpe}= partial pressure of MCPe, kPa

P_{mcpde}= partial pressure of MCPde, kPa

P_{H2}= partial pressure of H_2, kPa

P_c= partial pressure of coke precursor such as MCPde, kPa

R= gas constant=1.987 cal/gmol K

R_A= reaction rate of component A, gmol /g catalyst hr

R_0= reaction rate of component A at time 0, gmol /g catalyst hr

R_t= reaction rate of component A at time t, gmol /g catalyst hr

S^*= number of active sites on catalyst surface

S_0= initial number of active sites on catalyst surface

r_c= rate of coke formation, gcoke/g catalyst hr

r_0= initial rate of coke formation, gcoke/g catalyst hr

r_p= rate of polymerization, g/g catalyst hr

t= time, hr

T= temperature, K

Tol= toluene

W= weight of the catalyst, g

WHSV= weight hourly space velocity, hr^{-1}

Greek letters

α= deactivation constant, g catalyst/gcoke

β= unit conversion factor, number of sites/gcoke

ϕ= deactivation function

κ_1= coking reaction rate constant of MCPe

κ_2= coking reaction rate constant of MCPde

τ= space time (hr)

BIBLIOGRAPHY

Acharya, D.R., Ghassemi, M.R., Hughes, R., Appl. Catal., 58, 53, (1990).

Allan, M.I., J. Inst. Pet., 52, 385 (1966).

Appleby, W.G., Gibson, J.W. and Good G.M., Ind. Eng. Chem. Process. Des Dev. 1, 102 (1962).

Baker, R.T.K., Sherwood, R.D. and Dumesic, J.A., J. Catal., 66, 56, (1980).

Bakulin, R.A., Levinter, M.E. and Viger, F.G., Neftekhimiya, 5, 707, (1974).

Bakulin, B.A., Author's Abstract of Candidate's Dissertation, Kuibyahev, Politekh. Inst., (1975).

Balooch, M. and Olander, D.R., J. of Chem. Phys, 63, 4772, (1975).

Barbier, J., Corro, G., Zhang, Y., Bournonville, J.P. and Franck, J.P. Appl. Catal., 16, 169, (1985).

Barbier, J., Churin, E., Marecot, P., and Menzeo, J.C., Appl. Catal., 36, 277-285, (1988).

Barbier, J., Corro, G., Zhang, Y., Bournonville, J.P. and Franck, J.P. Appl. Catal. 3, 327, (1982).

Barbier, J., Churin, E. and Marecot, P., J. of Catalysis, 126, 228-234, (1990).

Barbier, J., Corro, G., Zhang, Y., Bournonville, J.P., and Franck, J.P., Appl. Catal. 13, 245, (1985).

Barbier, J., Appl. Catal., 23, 225, (1986).

Barbier, J., Marecot, P., Martin, N., Elassal, L., and Maurel, R., " Catalyat Deactivation" (Delmon and Froment, Eds), 53, Elsevier, Amsterdam, (1980).

Beeckman, J.W., and Froment, G.F., Ind. Eng. Chem. Fundam. 18, 245, (1979).

Beltramini, J.N., Wessel, T.J. and Datta, R., AIChE J., 37 (6), 845-854, (1991).

Bernardo, C.A. and Trimm, D.L., Carbon, 17, 115, (1979).

Best, D.A. and Wojciechowski, B.W., J. Catal., 47, 11 (1977).

Biswas, J., Gray, P.G. and Do, D.D., Appl. Catal., 32, 249, (1987).

Blue, E.M., Gould, G.D., Gibson, K.R., Hughes, T.R and Ravicz, A.E., "Production of Aromatic Hydrocarbons by Low Pressure Rheniforming," NPRA Annual Meeting of the National Petroleum Refiners Association, San Antonio, Texas, March, (1976).

Bortkevich, M.I., Levinter, M.E., Zabotin, L.I. and Berkovich L.M., Kinetika i Kataliz, 16, 1, 221 (1975).

Boudart, M. Aldag, A.W. and Vannice, M.A., J. Catal., 18, 46, (1970).

Butt, J.B., Adv. Chem. Ser. 109, 259 (1972).

Butt, J., Petersen, E.E., "Activation, Deactivation and posisoning of catalyst", Academic Press, Inc. London, 1988.

Cha, B.J., Vidal, A., Huin, R. and Landeghem, H.Van, API Div. Refining, Proc. 38th Midyear Meet, Washington, D.C., Vol. 53, 138, (1973).

Christoffel, E., Fetting, F. , and Vierrath, H., "Dehydrocyclization of n-Hexane on a Bifunctional Catalyst," Journal of Catalysis, 40, 349 (1975).

Clem, Kenneth Ray, Ph.D Dissertation, Louisiana State University, (1977).

Cooper, B.J. and Trim, D.L., in "Catalyst Deactivation", B. Delmon and G.F. Froment, Eds, Elsevier, Amsterdam, 63, (1980).

Davis, B.H.,"Paraffin Dehydrocyclization: Competitive Conversion of Paraffins and Naphthenes," Journal of Catalysis, 29, 398 (1973).

Davis, S.M. and Somorjai, G.A., J. Phys. Chem., 87, 1545, (1983).

Dean, J.W., Dadyburjor, D.B., Ind. Eng. Chem. Res., 27 (10), 1754-1759, (1988).

De Pauw, R.P., Froment, G.F., Chem. Eng. Sci., 30, 789, (1975).

Dumez, F.J., Hosten, L.H., and Froment, G.F. Chem. Eng. Sci., (1976).

Dumez, F.J., and Froment, G.F. Ind. Eng. Chem. Process. Des. Dev., 15(2), 291-301, (1976).

Eisenbach, D. and Gallei, E., J. Catal., 56, 377 (1979).

Espinat, D., Thesis, Institute Francais du Petrole, (1982).

Figoli, N.S., Beltraminal, J.N., Martenelli, E.E., and Parera, J.M., J. Chem. Technol. Biotechnol., 32, 445, (1982).

Figoli, N.S., Beltramini, J.N., Barra, A.F., Martinelli, E.E. and Sad, M.R. and Parera, J.M., ACS Symp., Series 202, Washington, 1982.
Figoli, N.S., Beltramini, J.N., Martinelli, E.E. and Sad, M.R. and Parera, J.M., Appl. Catal., 5, 19, (1983).

Figueiredo, J.L. and Trimm, D.L., J. of Catal., 40, 154, (1975).

Franck, J.P. and Martino, G., Progress on Catalyst Deactivation, Figueredo, J.L. (Ed.), Nato Advanced Study Institute Series, E. - App. Sci., No. 54, M. Nijhoff Publ., The Hahue, 355, (1982).

Franck, J.P. and Martino, G., Deactivation and Poisoning of Catalysts, Marcel Dekker, New York, 205, (1885).

Froment, G.F., Proc. VI Internat. Congress on Catal., 1, 10-31, (1976).

Froment, G.F., Bishoff, K.B., Chem. Eng. Sci., 16, 189, (1961).

Froment, G.F., Bishoff, K.B., Chem. Eng. Sci., 17, 105, (1962).

Fung, S.C., Querini, C.A., McCoy, C.J., "Catalyst Deactivation 1991", (Bartholomew, C. and Butt, J., eds), Elsevier, 135, (1991).

Fung, S.C., Querini, C.A., J. of Catalysis, 138, 240-254, (1992)

Fung, S.C, Querini, C.A., Ke Liu, Rumschitzki, D.S. and Ho, T.C., "Catalyst Deactivation 1994", Stusies in Suface Science and Catalysis, Delmon, B. and Froment, G.F. (Eds), 88, 305-312, Elsevier Science B.V., (1994).

Gates, B.C., Katzer, J.R. and Schuit, G.C.A., "Chemistry of Catalytic Processes," McGraw-Hill, New York, 184-313, (1979).

Haensel, V., and Donaldson, G.R., "Platforming of Pure Hydrocarbons," Industrial and Engineering Chemistry, 43 (9), 2102 (1951).

Haensel, V., "Reforming and Hydroisomerization," ACS, Division of Petroleum Chemistry, Preprints, 6(No. 3A) A93, (1961).

Henningsen, J. and Bundgard-Neilson, M., "Catalytic Reforming," British Chemical Engineering, 15 (11), (1970).

Hershkowitz, F., Kleshgi, H.S. and Madiara, P.D. ACS, Div. Petr. Chem., 38, 619, (1993).

Hettinger, W. P., Keith, C.D., Gring, J.L. and Teter, J.W., "Hydroforming Reactions--Effect of Certain Catalyst Properties and Poisons," Industry and Engineering Chemistry, 47(4), 719 (1955).

Hougen, O.A., and Watson, K.M., Chemical Process Principles, Part III, Kinetics and Catalysts, John Wiley and Sons, New York, 1947.

Jossens, L.W. and Petersen, E.E., J. Catal., 73, 377 (1982).

Jothimurugesan, J., Nayak,A.K., Mehta, G.K., Rai, K.N., Bhatia, S. and Srivastava, R.D., AIChE J. 31, 1997, (1985).

Katzer, J.R., in "Chemistry and Chemical Engineering of Catalytic Processes" (Prins R. and Schuit G.C.A. Eds.), Sijthoff and Noordhoff, The Netherlands, (1980).

Kenneth Ray Clem, Ph.D Dissertation, Louisiana State University, (1977).

Kluksdahl, H.E., U.S. Patent, 3, 415, 737, (1969).

Krane, H. G., Groh, A.B., Schulman, B.L. and Sinfelt, J. H., "Reactions in Catalytic Reforming of Naphthas," Fifth World Petroleum Congress, Section III, 39, (1959).

Kugelmans, A.M., "What Affects Cat Reformer Yield, " Hydrocarbon Processing, January, P.95 (1976).

Levinter, M.E., Borthevich, M.I., Zabotin, L.I., Berkovich, L.M., Kinet. Catal., 16, 181, (1975).

Levitskii, I.I., Minachev, Kh.M., and Udal'tsova, E.H., Izvestia Akademi Nauk USSR, Seriya Khimichcskaya, 2, 300 (1973).

Lin, C. Park, S.W. and Hatcher, W.J., Jr., Ind. Eng. Chem. Process Des. Dev., 22(4), 609-614 (1983).

Lyster, W.N., "Kinetics of Chemical Reactions--Dehydrocyclization of n-Heptane," Ph.D. Dissertation, University of Huston, (1964).

Magnoux, P., Guisnet, M., Gnep, S., Morisset, C. and Hilaireau, P., GECAT, Mont St Odile, (1984).

Mahoney, J.A., "The use of a Gradientless Reactor in Petroleum Reaction Engineering Studies," Journal of Catalysis, 32, 247 (1974).

Marin, G.B. and Froment, G,F., "Reforming of C6 Hydrocarbons on a Pt/Al2O3 Catalyst", Chemical Engineering Science, 37 (3), 759-773 (1982).

McHeny, K.W., Bertolacini, R.J., Brennan, H.M., Wilson, J.L. and Seelig, H.S.,"The nature of the Platinum Dehydrocyclization Catalysts, " Proceedings of the Second International Congress of Catalysis, Section II, (No.117), 1 (1960).

Metzler, C.M., "NONLIN, A Computer Program For Parameter Estimation in NONLINear Situations," Technical Report 7292/69/7292/005; The UPJOHN Company, Kalamazoo, Michigan 49001, Nov. 25, (1969).

Mieville, R.L., J. Catal., 105, 536, (1987).

Mieville, R.L., J. Catal., 100, 482, (1986).

Mieville, R.L., Catalyst Deactivation 1991, Bartholomew, C.H. and Butt, J.B.(Editors), Elsevier Science Publishers B.V., Amsterdam, (1991).

Mills , G.A., Heinemann, H., Milliken, T.H. and Oblad, A.G., Ind. Eng. Chem., 45, 134, (1953).

Myers, G.A., Lang, W.H. and Weisz, P.B., Ind. Eng. Chem. 53, 299 (1961).

Nishiyama, Y. and Tamai, Y., Carbon, 14,13, (1976).

Nix, P.S. and Weisz, P.B. "Hydrocarbon Reaction Path Stusies with Fluidized Dural Function Catalyst Component Mixtures', J. of Catalysis, 3. 179 (1964).

Olander, D.R. and Balooch, M., J. Catal., 60, 41, (1979).

Pacheco, M.A. and Petersen, E.E., J. Catal., 86, 75 (1983).

Parera, J.M., Figoli, N.S. and Traffano, E.M., J. Catal., 79, 481, (1983).

Parera, J.M., Figoli, N.S., Beltramini, J.N., Churin, E.J., and Cabrol, Proc. Int. Congress on Catalysis, (Bursian et al., eds) Berlin, Vol. 2, 481, (1984).

Patashnick, H. Rupprecht, G. and Wang, J.C.F., Preprints, ACS, Div. Petr. Chem., 25,188, (1980).

Querini, C.A. and Fung, S.C., J. of Catal., 141, 389-406 (1993).

Querini, C.A., N.S. Figoli and J.M. Parera, Appl. Catal. 52, 249 (1989).

Querini, C.A., N.S. Figoli and J.M. Parera, Appl. Catal. 53, 53 (1989).

Ramage, M.P., Graziani, K.R. and Krambeck, F.J., "Development of Mobil's Kinetic Reforming Model," Chemical Engineering Science, 35, 41-49 (1980).

Ramage, M.P., Graziani, K.R., Schipper, P.H., Krambeck, F.J. and Choi, B.C., "KINPR (Mobile's Kinetic Reforming Model): A Review of Mobil's Industrial Process Modelling Philosophy," Advances in Chemical Engineering, 13, 193-266 (1987).

Rewick, K.T., Wentrcek, P.R. and Wise, H. Fuel, 53, 274, (1974).

Robell, A.J. and E. Ballou, E.V., J. Phys. Chem., 68, 2748, (1964).

Rohrer, J.C., Hurwitz, H., and Sinfelt, J.H., "Kinetics of the Catalytic Dehydrocyclization of n-Heptane," Journal of Physical Chemistry, 66, 1193 (1962).

Rossini, F.D., et al., "Selected Values of Physical and Thermodynamic Properties of Hydrocarbons and Related Compounds", Carnegie Press, Pittsburgh, PA., (1953).

Rossini, F.D., et al., "Selected Values of Physical and Thermodynamic Properties of Hydrocarbons and Related Compounds", Carnegie Press, Pittsburgh, PA., (1953).

Sachtler,J.W.A. and Somorjau, G.A., Symp. Multimetallic Catal., Div. Petro. Chem., ACS, Seattle meeting, March 20-25, (1983).

Selman, D.M., Ph.D. Thesis, Louisiana State University, 1972.

Sinfelt, J.H., Hurwitz, H., and Rohrer, J.C., "Role of Dehydrogenation Activity in the Catalytic Isomerization and Dehydrogenation of Hydrocarbons," Journal of Catalysis, 1, 481 (1962).

Sinfelt, J.H., and Rohrer, J.C., "Reactivity of Some C6-C8 Paraffins over Pt/Al2O3," Journal of Chemical Engineering Data, 8, 109 (1963).

Sinfelt, J.H., "Catalysis Science and Technology," Springer-Veriag, New York, 257, (1981).

Shum, V.K., Butt, J.B. and Sachtler, W.M.H., App. Catal., 11, 151, (1984).

Shum, V. K., Sachtler W.M.H. and John B. Butt, Ind. Eng. Chem. Res. **26**(7), 1280(1987).

Sterba, M.J., and Haensel, V., "Catalytic Reforming," Industrial and Engineering Chemistry, Product Research and Development, 15(1), 2 (1976).

Sun, S.Z., Weng, H.X., Mao, X.J. and Liu, F.Y., "Studies on Catalytic Reforming Reaction Kinetic Models: (I) Catalytic reforming reaction kinetics of C6 hydrocarbons," Chemical Reaction Engineering and Technology, 8(1), 10-17 (1992).

Sun, S.Z., Weng, H.X., Mao, X.J. and Liu, F.Y., "Studies on Catalytic Reforming Reaction Kinetic Models: (I) Catalytic reforming reaction kinetics of C7 hydrocarbons," Chemical Reaction Engineering and Technology, 8(1), 18-23 (1992).

Sutton, E.A., Greenwood, A.R. and Adams, F.H., Oil and Gas Journal, 52, May, 1972.

Svajgl, O., "The effect of Chlorine and Water on Gasoline Reforming over a Platinum Catalyst," International Chemical Engineering, 12 (1), 55 (1972).

Szepe, S. and Levenspiel, O., "Proceedings of Fourth European Symposium", Pergamon Press, London, (1971).

Tanatarov, M.A., Shaimardanov,N.M. and Levinter, M.E. "Deactivation of Bifunctional Reforming Catalysts," Kinetika i Kataliz, 16(No. 5), 1313 (1975).

Tomita, A. and Tamai, Y., J. of Catal., 27, 293, (1972).

Trimpont, P.A.Van, Marin, G.B., and Froment, G.F., "Reforming of C7 Hydrocarbons on a Sulfided Commercial Pt/Al2O3 Catalyst", Ind. Eng. Chem. Res. 27, No. 1, 51-57 (1988).

Trimpont, P.A.Van, Marin, G.B., and Froment, G.F., "Kinetics of the Reforming of C7 Hydrocarbons on a Commercial Pt-Re/Al2O3 Catalyst", Applied Catalysis, 24, 53-68 (1986).

Trimpont, P.A.Van, Marin, G.B., and Froment, G.F., Ind. Eng. Chem. Fundam., 25, 544-553 (1986).

Usov, Y.N. and IL'in, V.F., "Aromatization of Ispheptane in trhe Presence of an Alumina-Platinum Catalyst," Neftekhimiya, 14,(1), 49 (1974).

Voorhies, A. Jr., Ind. Eng. Chem. 37, 318 (1945).

Wolf, E.E. and Petersen, E.E., J. Cata., 47, 28 (1977).

Wolf, E.E. and Alfani, F., Catal. Rev. Sci. Eng. 24, 329, (1982).

Wollwebber, H., "Diels-Alder Reackeionen," George Thieme Velag, Stuttgart, 1972.

Wood, B.J. and Wise, H., J. Phys. Chem., 73, 1348, (1969).

Yang, K.H. and Hougen, O.A., Chemical Engineering Progress, 46 (3), 146, (1950).

Zhorov, Yu.M. and Panchenkov, G.M., Kinetika i Kataliz, 21(3), 776-780 (1980).